VII Curso Internacional de Ingeniería Sísmica

SISMOLOGIA Y SISMICIDAD

1 9 8 1

1. M. en I. Abraham Díaz Rodríguez
   Jefe de la Sección de Mecánica de Suelos
   División de Estudios de Posgrado
   Facultad de Ingeniería
   UNAM
   550 52 15 ext. 4490

2. Dr. Luis Esteva Maraboto
   Investigador
   Instituto de Ingeniería
   UNAM
   548 97 94

3. Dr. Octavio Rascón Chávez (Coordinador)
   Subdirector
   Instituto de Ingeniería
   UNAM
   548 54 95

4. M. en C. Jorge Prince Alfaro
   Investigador
   Instituto de Ingeniería
   UNAM
   548 11 35

5. Dr. Francisco Sánchez Sesma
   Investigador
   Instituto de Ingeniería
   UNAM
   550 52 15 ext. 3627

6. Dr. Mario Chávez G.
   Investigador
   Instituto de Ingeniería
   UNAM
   550 52 15 ext. 3628

VII CURSO INTERNACIONAL DE INGENIERIA SISMICA

SISMOLOGIA Y SISMICIDAD

1 9 8 1

FECHA	HORARIO	T E M A R I O	PROFESOR
julio 14	17:00 a 19:30 h	ORIGEN DE LOS TEMBLORES. INSTRUMENTOS PARA REGISTRAR TEMBLORES. MAGNITUD E INTENSIDAD SISMICIDAD DE LA TIERRA. PROPAGACION DE ONDAS. PREDICCION DE TEMBLORES	M. en C. Jorge Prince Alfaro
julio 14	19:45 a 21:15 h	PROPAGACION DE ONDAS: ONDAS DE CUERPO Y ONDAS SUPERFICIALES	Dr. Francisco Sánchez Sesma
julio 16	17:00 a 19:00 h	EFECTOS SISMICOS EN SUELOS GRANULARES	M. en I. Abraham Díaz Rodríguez
julio 16	19:15 a 21:15 h	RELACIONES ENTRE MAGNITUD, INTENSIDAD Y DISTANCIA FOCAL. PROPIEDADES ESTADISTICAS DE LOS TEMBLORES	Dr. Mario Chávez G.
julio 21	17:00 a 20:00 h	INFLUENCIA DE LAS CONDICIONES LOCALES. TIPOS DE TEMBLORES	Dr. Luis Esteva Maraboto
julio 21	20:15 a 21:15 h	SISMICIDAD LOCAL Y REGIONAL. REGIONALIZACION SISMICA. SISMICIDAD DE LA REPUBLICA MEXICANA. MICROREGIONALIZACION SISMICA. ELABORACION DE ESPECTROS DE DISEÑO	Dr. Luis Esteva Maraboto
julio 23	17:00 a 21:15		Dr. Luis Esteva Maraboto

DIVISION DE EDUCACION CONTINUA
FACULTAD DE INGENIERIA U.N.A.M.

VII CURSO INTERNACIONAL DE INGENIERIA SISMICA

SISMOLOGIA Y SISMICIDAD

PROPAGACION DE ONDAS ELASTICAS EN UN MEDIO SEMINFINITO

Dr Francisco Sánchez Sesma

Julio, 1981

PROPAGACION DE ONDAS ELASTICAS EN UN MEDIO SEMINFINITO

por

Francisco J Sánchez-Sesma

Instituto de Ingeniería, Universidad Nacional Autónoma de México

1. INTRODUCCION

Las ondas sísmicas se propagan desde la fuente de acuerdo con las propiedades mecánicas del medio en que viajan y, por supuesto, dependen también de las características de la fuente. La descripción del fenómeno ha podido hacerse de forma satisfactoria al recurrir a simplificaciones e hipótesis que llevan a la formulación de modelos que representan los aspectos más importantes de la propagación de ondas en la tierra. Es usual aceptar que la tierra es un medio elástico lineal, homogéneo e isotrópico. En un medio de esta naturaleza con extensión ilimitada se pueden propagar dos tipos de ondas elásticas; las ondas P o de compresión y las ondas S o de cortante. Las primeras se propagan con mayor velocidad y por eso se les suele llamar primarias mientras que las segundas reciben el nombre de secundarias. Existen diversas soluciones para las ecuaciones que gobiernan el fenómeno de propagación. Así, para una fuente puntual se podría hablar de ondas esféricas, que a grandes distancias de la fuente se pueden representar como ondas planas. En algunos casos se modela el problema de propagación como bidimensional y las soluciones para una fuente se dan en términos de ondas cilíndricas, que también a grandes distancias son aproximadamente planas. Un buen número de soluciones de las ecuaciones fundamentales puede encontrarse en el excelente texto de Ewing, Jardetzky y Press (1957).

La existencia de una superficie libre introduce reflexiones de las ondas al llegar a esta. Para estudiar la naturaleza de las reflexiones dicha superficie debe considerarse libre de esfuerzos. Dado que a grandes distancias de la fuente las ondas pueden suponerse planas y que para las longitudes de onda de interés la curvatura de la tierra es, comparativamente, pequeña se estudiará el problema de reflexión de ondas planas por la superficie de un medio elástico seminfinito. Dicha superficie se supondrá plana.

A continuación se presentan algunos aspectos de la propagación de ondas en un medio elástico de extensión ilimitada y se expresan las ecuaciones que gobiernan el fenómeno en términos de potenciales de desplazamiento. Posteriormente se discute la reflexión de ondas planas por la

Un segundo ejemplo simple se obtiene si se supone que $u = w = 0$ y que $v = v(x,t)$. De las ecs 1 se obtiene que

$$\mu \frac{\partial^2 v}{\partial x^2} = \rho \frac{\partial^2 v}{\partial t^2} \qquad (5)$$

y la solución tiene la misma forma que la ec 4 pero representa ondas que viajan con una velocidad β, donde $\beta^2 = \mu/\rho$. Debe notarse que el movimiento es perpendicular a la dirección de avance. Puede demostrarse que las soluciones de la ec 5 representan ondas de cortante, sin cambio de volumen.

Las ecuaciones de movimiento pueden resolverse de una manera más general por medio de *potenciales de desplazamiento*.

Si el vector desplazamiento se expresa como

$$\bar{u} = \nabla\phi + \nabla\times\bar{\psi}, \text{ con } \nabla\cdot\bar{\psi} = 0 \qquad (6)$$

donde ϕ es un potencial escalar y $\bar{\psi}$ es un potencial vectorial, puede demostrarse que la ec 6 representa una solución de la ec 2 (o de la ec 1 en coordenadas rectangulares) si ϕ y $\bar{\psi}$ satisfacen, respectivamente, las ecuaciones de onda:

$$\nabla^2\phi = \frac{1}{\alpha^2} \frac{\partial^2\phi}{\partial t^2} \qquad (7)$$

$$\nabla^2\bar{\psi} = \frac{1}{\beta^2} \frac{\partial^2\bar{\psi}}{\partial t^2} \qquad (8)$$

Así, por ejemplo, una solución de la ec 7 que representa una onda plana de compresión que viaja en una dirección arbitraria está dada por

$$\phi = f\left(t - \frac{x\ell + ym + zn}{\alpha}\right) \qquad (9)$$

donde ℓ, m, n = cosenos de los ángulos formados por la dirección de viaje y los tres ejes coordenados, respectivamente. Si $\bar{r} = (x, y, z)$ y $\bar{n} = (\ell, m, n)$ donde $\bar{r}$ = vector de posición y $\bar{n}$ = vector unitario que da la dirección de propagación, la ec 9 puede escribirse como

$$\phi = f(t - \bar{r}\cdot\bar{n}/\alpha) \qquad (10)$$

Es evidente que soluciones similares pueden encontrarse para los tres componentes del potencial vectorial y representarían ondas de cortante viajando con una velocidad β.

En coordenadas rectangulares la ec 6 se desarrolla como

$$\begin{aligned} u &= \frac{\partial\phi}{\partial x} + \frac{\partial\psi_z}{\partial y} - \frac{\partial\psi_y}{\partial z} \\ v &= \frac{\partial\phi}{\partial y} - \frac{\partial\psi_z}{\partial x} + \frac{\partial\psi_x}{\partial z} \\ w &= \frac{\partial\phi}{\partial z} + \frac{\partial\psi_y}{\partial x} - \frac{\partial\psi_x}{\partial y} \end{aligned} \qquad (11)$$

donde $\bar{\psi} = (\psi_x, \psi_y, \psi_z)$.

por

$$v^{(i)} = f(t + \frac{x\cos\gamma - z\,\mathrm{sen}\,\gamma}{\beta}) \qquad (13)$$

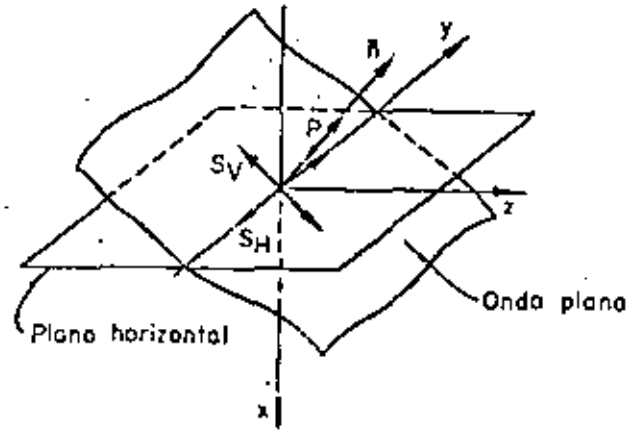

Fig 2. Nomenclatura para ondas planas

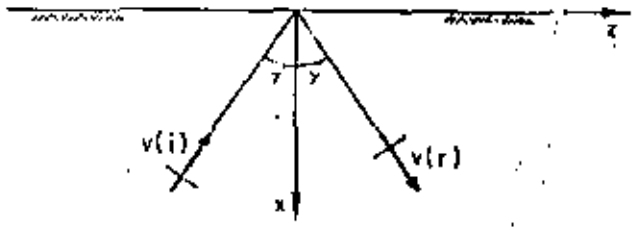

Fig 3. Ondas SH incidente y reflejada

la onda reflejada está dada simplemente por

$$v^{(r)} = f(t - \frac{x\cos\gamma + z\,\mathrm{sen}\,\gamma}{\beta}) \qquad (14)$$

aquí γ = ángulo de incidencia. Puede verificarse que $v = v^{(i)} + v^{(r)}$ satisface la ec 12 y la condición de que el plano x = 0 esté libre de esfuerzo pues los únicos esfuerzos relevantes están dados por

$$\tau_{xy} = \mu\,\frac{\partial v}{\partial x}, \quad \tau_{yz} = \mu\,\frac{\partial v}{\partial z} \qquad (15)$$

y combinando las ecs 13, 14 y 15 resulta que $\tau_{xy} = 0$ en x = 0. Debe observarse que en estas condiciones el movimiento en x = 0, la superficie libre, se puede escribir como

$$v_{x=0} = 2\,f(t - \frac{z\,\mathrm{sen}\,\gamma}{\beta}), \qquad (16)$$

por lo que el factor de amplificación es dos.

En la propagación de ondas P y SV el movimiento está en el plano xz, es decir u = u(x,z,t), w = w(x,z,t) y v = 0. En este caso las ecuaciones de onda que deben satisfacer los potenciales, si $\psi = \psi_y$, son

$$\frac{\partial^2\phi}{\partial x^2} + \frac{\partial^2\phi}{\partial z^2} = \frac{1}{\alpha^2}\,\frac{\partial^2\phi}{\partial t^2} \qquad (17)$$

que los potenciales sean finitos. Al definir k como imaginario negativo con $k = \omega/c$ se observa que el producto

$$e^{-ikz}\, e^{i\omega t} = e^{i\omega(t-z/c)} \tag{27}$$

representa una onda armónica que viaja en la dirección positiva de z con una velocidad de fase c, si c es negativa la dirección de viaje es en la dirección negativa de z. En términos de los ángulos de las figs 4 y 5 se tiene que

$$c = \frac{\alpha}{\operatorname{sen} \gamma_P} = \frac{\beta}{\operatorname{sen} \gamma_S} \tag{28}$$

Con estas definiciones M y K deben ser o reales o imaginarios pues, de las ecs 25 y 26, se tiene que

$$M^2 = k^2 - \omega^2/\alpha^2 = \omega^2(1/c^2 - 1/\alpha^2) \tag{29}$$

y

$$K^2 = k^2 - \omega^2/\beta^2 = \omega^2(1/c^2 - 1/\beta^2) \tag{30}$$

Así, para $\beta < \alpha < |c|$, M y K son imaginarios; para $\beta < |c| < \alpha$, M es real y K imaginario; para $|c| < \beta < \alpha$, M y K son reales.

Para el primer caso, $\beta < \alpha < |c|$, se tienen los potenciales

$$\phi = (A_1 e^{imx} + A_2 e^{-imx}) e^{-ikz}\, e^{i\omega t} \tag{31}$$

$$\psi = (B_1 e^{ikx} + B_2 e^{-ikx}) e^{-ikz}\, e^{i\omega t} \tag{32}$$

donde $k = \omega/c$, $m = \omega(1/\alpha^2 - 1/c^2)^{1/2}$ y $k = \omega(1/\beta^2 - 1/c^2)^{1/2}$. Si $B_1 = 0$ se tiene el caso mostrado en la fig 4 de incidencia de ondas P. En cambio si $A_1 = 0$ se tendrá incidencia de ondas SV. Sustituyendo las ecs 31 y 32 en las ecs 21 y 22, haciendo que $\sigma_x = \tau_{xz} = 0$ en $x=0$ y resolviendo el sistema de ecuaciones resultante se obtiene que

a) Para $B_1 = 0$

$$\frac{A_2}{A_1} = \frac{4 \cot \gamma_P \cot \gamma_S - (\cot^2 \gamma_S - 1)^2}{4 \cot \gamma_P \cot \gamma_S + (\cot^2 \gamma_S - 1)^2} \tag{33}$$

$$\frac{B_2}{A_1} = \frac{4 \cot \gamma_P (\cot^2 \gamma_S - 1)}{4 \cot \gamma_P \cot \gamma_S + (\cot^2 \gamma_S - 1)^2} \tag{34}$$

donde γ_P = ángulo de incidencia y de reflexión de la onda P y γ_S = ángulo de reflexión de la onda SV. Debe recordarse que la velocidad aparente está dada por

$$c = \frac{\alpha}{\operatorname{sen} \gamma_P} = \frac{\beta}{\operatorname{sen} \gamma_S} \tag{35}$$

b) Para $A_1 = 0$

$$\frac{A_2}{B_1} = -\frac{4 \cot \gamma_S (\cot^2 \gamma_S - 1)}{4 \cot \gamma_P \cot \gamma_S + (\cot^2 \gamma_S - 1)^2} \tag{36}$$

$$\frac{B_2}{B_1} = \frac{4 \cot \gamma_P \cot \gamma_S - (\cot^2 \gamma_S - 1)^2}{4 \cot \gamma_P \cot \gamma_S + (\cot^2 \gamma_S - 1)^2} \tag{37}$$

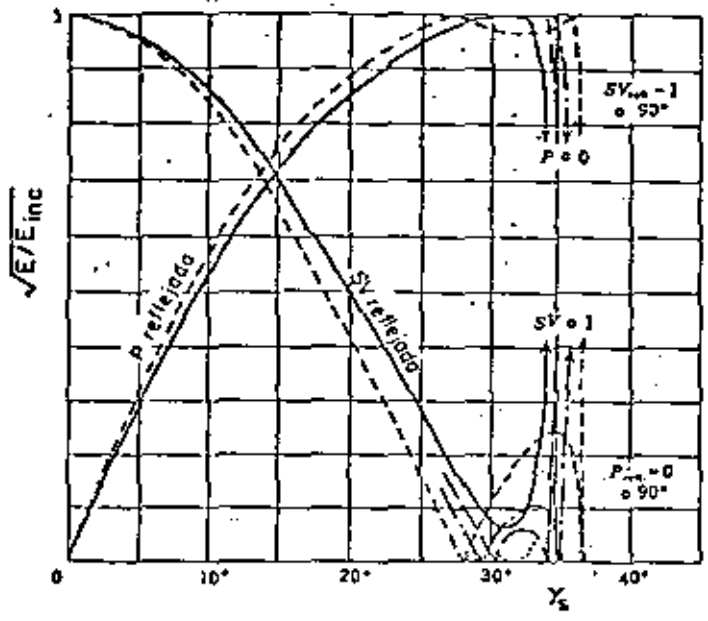

Fig 7. Raiz cuadrada de la relación de energía reflejada a energía incidente para una onda SV incidente en una superficie libre

$$\frac{A_2}{B_1} = -\frac{4\cot\gamma_S(\cot^2\gamma_S-1)}{(\cot^2\gamma_S-1)^2-4i(1-c^2/\alpha^2)^{1/2}\cot\gamma_S\ \mathrm{sgn}\,\omega} \qquad (40)$$

$$\frac{B_2}{B_1} = -\frac{(\cot^2\gamma_S-1)^2+4i(1-c^2/\alpha^2)^{1/2}\cot\gamma_S\ \mathrm{sgn}\,\omega}{(\cot^2\gamma_S-1)^2-4i(1-c^2/\alpha^2)^{1/2}\cot\gamma_S\ \mathrm{sgn}\,\omega} \qquad (41)$$

donde sgn ω =(-1 si ω<0 o 1 si ω>1). En este caso, la incidencia de ondas SV con ángulos de incidencia γ_S mayores que $\mathrm{sen}^{-1}(\beta/\alpha)$ genera ondas [illegible] que se atenuan con la profundidad.

4. ONDAS DE RAYLEIGH

Para el tercer caso, $|c| < \beta < \alpha$, se tiene que

$$\phi = A_2\, e^{-mx}\, e^{-ikz}\, e^{i\omega t} \qquad (42)$$

$$\psi = B_2\, e^{-kx}\, e^{-ikz}\, e^{i\omega t} \qquad (43)$$

donde $m = |\omega|(1/c^2 - 1/\alpha^2)^{1/2}$ y $k = |\omega|(1/c^2 - 1/\beta^2)^{1/2}$. Se han eliminado A_1 y B_1 pues no representan ondas incidentes con potenciales finitos. Las ecuaciones de esfuerzos nulos en x = 0 conducen a

$$\frac{A_2}{B_2} = \frac{2i(1-c^2/\beta^2)^{1/2}\ \mathrm{sgn}\,\omega}{2-c^2/\beta^2} \qquad (44)$$

$$\frac{A_2}{B_2} = \frac{2-c^2/\beta^2}{2i(1-c^2/\alpha^2)^{1/2}\ \mathrm{sgn}\,\omega} \qquad (45)$$

como las ecs 44 y 45 deben ser iguales se obtiene que la velocidad de fase, c, debe satisfacer la siguiente ecuación:

$$(2-\frac{c^2}{\beta^2})^2 - 4(1-\frac{c^2}{\alpha^2})^{1/2}\ (1-\frac{c^2}{\beta^2})^{1/2} = 0 \qquad (46)$$

La raiz real de esta ecuación, c_R, encontrada por vez primera por Rayleigh, da la velocidad de las llamadas ondas de Rayleigh. En la fig 8 se presentan valores de c_R para

Fig 10. Notación para un estrato sobre un semiespacio elástico

para el estrato y

$$\frac{\partial^2 v_2}{\partial x^2} + \frac{\partial^2 v_2}{\partial z^2} + k^2_{\beta_2} v_2 = 0 \qquad (48)$$

donde $k_{\beta_i} = \omega/\beta_i$, $i = 1,2$ para el semiespacio.

Haciendo uso de soluciones del tipo de las ecs 23 y 24 se puede escribir que

$$v_1 = (A\, e^{-kY_1 x} + B\, e^{kY_1 x})\, e^{ik(z-ct)} \qquad (49)$$

$$v_2 = C\, e^{-kY_2 x}\, e^{ik(z-ct)} \qquad (50)$$

donde $Y_1 = (1-c^2/\beta_1^2)^{1/2}$ y $Y_2 = (1-c^2/\beta_2^2)^{1/2}$. Se observa que si $c < \beta_2$, $v_2 \to 0$ cuando $x \to \infty$.

Las condiciones de frontera son que $v_1 = v_2$ y $(\tau_{xy})_1 = (\tau_{xy})_2$ en x=0 y que $\tau_{xy} = 0$ en $x = -H$. Estas condiciones conducen a un sistema de ecuaciones homogéneo en A, B y C. Para que se tenga solución diferente de cero el determinante del sistema debe anularse. Así, se tiene que

$$\tan k Y_1 H = \frac{\mu_2 Y_2}{\mu_1 Y_1} = \frac{\mu_2 (1 - c^2/\beta_2^2)^{1/2}}{\mu_1 (c^2/\beta_1^2 - 1)^{1/2}} \qquad (51)$$

es la ecuación para obtener la velocidad de las ondas de Love.

Si $\beta_1 < \beta_2$ la ec 51 da valores reales de c, en el intervalo $\beta_1 < c < \beta_2$, que dependen de k y H. Pueden obtenerse ondas de Love de forma general superponiendo ondas de Love del tipo de la ec 49 con diferentes k.

La dependencia de la velocidad de propagación de la frecuencia ocasiona el fenómeno de *dispersión* y, en general, este es el caso en medios estratificados.

6. BIBLIOGRAFIA

Ewing, W M, Jardetzky, W S y Press, F, *Elastic waves in layered media*, Mc Graw-Hill Book Co, Nueva York, 1957

White, J E, *Seismic waves: radiation transmission and attenuation*, Mc Graw-Hill Book Co., Nueva York, 1965

Fung, Y C, *Foundations of solid mechanics*, Prentice-Hall, Inc, Englewood Cliffs, Nueva Jersey, 1965

DIVISION DE EDUCACION CONTINUA
FACULTAD DE INGENIERIA U.N.A.M.

VII CURSO INTERNACIONAL DE INGENIERIA SISMICA

SISMOLOGIA Y SISMICIDAD

EFECTOS SISMICOS EN SUELOS GRANULARES

M en I Abraham Díaz Rodríguez

Julio, 1981

EFECTOS SISMICOS EN SUELOS GRANULARES

por

Abraham Díaz Rodríguez*

INTRODUCCION

El comportamiento adecuado de los suelos y las cimentaciones durante la ocurrencia de temblores es esencial para evitar daños severos a toda clase de estructuras.

Las condiciones bajo las cuales los suelos (como parte de la cimentación o como material de construcción) pierden una parte significativa de su resistencia, conduciendo a fallas inducidas por temblores, no son, al menos hasta la fecha (junio, 1977) completamente entendidas y constituyen un campo fertil de investigación y de gran utilidad para la práctica profesional de la Ingeniería Civil.

La importancia de los efectos que los sismos pueden inducir en los suelos granulares se debe a los graves daños que se han observado en numerosas ocasiones durante los temblores pasados.

---

* Jefe de la Sección de Mecánica de Suelos y profesor de la División de Estudios de Posgrado, Facultad de Ingeniería, UNAM

De 1881 a 1946 se ha informado de 229 deslizamientos, que causaron el desplazamiento total de 25 millones de m³ de arena. En Holanda, a orillas de los numerosos estrechos que existen, ha habido gran cantidad de deslizamientos que han provocado el rompimiento de diques y, por tanto, la inundación de grandes extensiones de terreno.

En México existen evidencias de que durante el sismo de 1959 (Marsal, 1961), un gran tramo de la margen izquierda del río Coatzacoalcos tuvo desplazamientos verticales y horizontales de importancia. Muchas instalaciones de la zona de astilleros sufrieron hundimientos bajo la cimentación y el asentamiento general fue notable después del sismo. Algunos tramos de los muelles cimentados sobre pilotes metálicos de 10 m de longitud sufrieron desplazamientos apreciables en dirección horizontal. Uno de los muelles se desplazó hacia el río más de 1/2 m. Tales movimientos se han atribuido al fenómeno de licuación en los mantos arenolimosos y limoarenosos que allí se encuentran entre 0 y 8 m de profundidad. En vista de las altas relaciones de vacíos y de la granulometría uniforme de dichos suelos, no puede descartarse esta posibilidad.

Durante el temblor de Chile, en 1960, se formaron extensas zonas de falla. La tierra fue arrastrada hacia el mar a lo largo de la costa de 600 m, llevando consigo todas las estructuras de retención; las paredes del muelle con secciones de 5 m de concreto reforzado fueron abatidas y luego arrastradas. En este mismo temblor, falló una presa debido a la licuación del suelo de cimentación.

A.3 *ESTUDIOS DE DENSIFICACION*

Es un hecho bien establecido que la aplicación de carga cíclica a una muestra de arena, da como resultado un decrecimiento progresivo de volumen, aún en el caso de arenas densas, las cuales se comportarían dilatantes bajo carga unidireccional o monotónica. Varias técnicas, tanto de laboratorio como de campo, se han desarrollado (Broms y Forsablad, 1969).

El uso de vibraciones verticales para producir la densificación de muestras de arena se ha utilizado en el pasado (D'Appolonia y D'Appolonia, 1967; Whitman y Ortigosa, 1968), estos estudios han mostrado que los cambios de peso volumétrico de las muestras son pequeños para aceleraciones menores de 1 g (figs 4 y 5).

Los cambios tanto de volumen como de características friccionantes de arenas secas inducidas por grandes aceleraciones horizontales y un gran número de ciclos de pequeña amplitud se han investigado utilizando cajas de corte colocadas sobre mesas vibradoras (Barkan, 1962; Youd, 1970), ver fig 6.

Otros estudios basados en ensayes de corte simple y mesas vibradoras, con niveles de aceleración y amplitudes de deformación semejantes a los esperados en temblores intensos, han mostrado que: la amplitud de deformación, compacidad relativa y número de ciclos de carga son los principales factores que gobiernan la densificación de suelos granulares secos o saturados bajo condiciones drenadas (Silver y Seed, 1969; Youd, 1972), ver fig 7.

Seed, Pyke y Martin (1975), realizaron una serie de ensayes de corte simple tanto en una (x) como en dos (x,y) direcciones. Se utilizaron dos patrones básicos de movimiento, en los ensayes bidireccionales.

Los resultados de los ensayes utilizando movimientos aleatorios se resumen en la fig 8, en donde se encuentra el asentamiento para 10 ciclos de carga como función de la relación, τ_h/σ_v, en donde τ_h, es el máximo esfuerzo cortante horizontal y, σ_v, es el esfuerzo vertical aplicado. Estas pruebas confirmaron las conclusiones de Silver y Seed (1971), que para un nivel de deformaciones cortantes el asentamiento inducido es independiente del esfuerzo vertical. Sin embargo, si se realiza una prueba bajo condiciones de esfuerzo controlado, las deformaciones cortantes cíclicas, y por tanto los asentamientos, se incrementan con el incremento de la relación de esfuerzos. Para un valor dado de la relación de esfuerzos se puede ver que el asentamiento causados por dos componentes de movimiento es aproximadamente igual a la suma de los asentamientos causados por cada una de los componentes.

Sobre la base de estos resultados parece razonable postular que para arenas saturadas ensayadas bajo condiciones no drenadas, el incremento de la presión de poro será aproximadamente dos veces mayor bajo dos componentes de movimiento que bajo una sola.

b) Convertir la historia de deformaciones de cortante de cada capa a un número equivalente de ciclos de deformación cortante de amplitud constante.

c) Aplicar el número de ciclos de deformación cortante, determinado en (b) a muestras de arena ensayadas bajo condiciones de corte simple y determinar las deformaciones volumétricas y a partir de éstas conocer las deformaciones verticales resultantes.

d) Repetir el procedimiento de (c) para cada capa del estrato e integrar las deformaciones verticales para obtener el asentamiento total.

El paso (b) involucra una aproximación. Martin et al (1975) ha demostrado que el efecto de una historia irregular de deformaciones de cortante depende no únicamente de la magnitud de los pulsos en el registro, como también del orden en que ellos son aplicados. El procedimiento para determinar el número equivalente de ciclos no toma en cuenta el hecho antes mencionado.

Al expresar analíticamente la relación entre deformaciones de cortante y los cambios de volumen, se pueden eliminar los pasos b, c y d como sucede con el método de Martin et al (1975), el cual es aplicable al cálculo de asentamientos de estratos de arena seca o parcialmente saturada.

A.4 PERDIDA DE RESISTENCIA DE SUELOS GRANULARES-LICUACION DE ARENAS

Probablemente uno de los efectos más costosos y espectaculares que se puedan encontrar en ingeniería sísmica se deban al fenómeno de la licuación de arenas.

El fenómeno es complejo y aún no es claro y completamente comprendido, al grado que es posible encontrar interpretaciones diferentes y aún contradictorias de los hechos experimentales existentes.

La discrepancia empieza con la propia definición del término licuación. Mientras que para Seed (1966) el término "*licuación inicial*" es la condición de una muestra de arena en la cual la presión de poro inducida por la aplicación de carga cíclica alcanza el valor de la presión de confinamiento y el término "*licuación total*" es la condición correspondiente para que la muestra alcance una amplitud de deformación del 20%; Casagrande en 1969, utiliza los términos licuación y movilidad cíclica que después modifica (Casagrande, 1976) definiendo por "*licuación real*" a la respuesta de una muestra de arena suelta y saturada cuando se le somete a deformaciones o impactos que dan como resultado una pérdida sustancial de resistencia y en casos extremos a flujo de taludes, y por "*licuación cíclica*" la respuesta de un espécimen dilatante de arena cuando se le ensaya en cámara triaxial cíclica y la presión de poro se eleva en forma incremental hasta igualar la presión de confinamiento.

d) Magnitud del esfuerzo repetido

Cualquier depósito con una relación de vacíos mayor que su e_{min} es susceptible de sufrir pérdida parcial o total de resistencia, si la excitación es de intensidad suficiente.

Evidencias de campo demuestran que depósitos de arena suelta han resistido sismos de poca intensidad (0.005 g) y se han licuado ante la acción de sismos intensos (0.16 g), (Seed e Idriss, 1971).

La resistencia a la licuación decrece al aumentar la magnitud del esfuerzo.

e) Número de ciclos de esfuerzo

Todos los estudios de laboratorio indican que en una muestra sujeta a carga repetida, con un nivel de esfuerzo o deformación prescrito, el inicio de la licuación dependerá de la aplicación de un número requerido de ciclos de esfuerzo.

Esto se confirmó en Anchorage, durante el temblor de 1964, ya que los deslizamientos ocurrieron después de 90 seg de iniciado el movimiento.

Recientes investigaciones (1973 a la fecha) han aportado nuevos datos de los factores que influyen en el fenómeno de licuación de arenas, como son:

f) Estructura

Pyke (1974), Lade (1974 y 1976) y Mulilis et al (1975), han encontrado que el método de preparación de la muestra (estructura)

afecta la relación de esfuerzos $(\frac{\sigma_{dc}}{2\sigma_3})$ que provoca la licuación hasta en un 200% .

g) Lapso de esfuerzo sostenido

Experiencias de laboratorio indican que muestras idénticas sometidas a cargas sostenidas por períodos que variaron de 0.1 a 100 días antes del ensaye, se vieron afectadas en la relación de esfuerzos hasta en un 25%. Estos resultados permiten suponer que el efecto de la edad del depósito es un factor importante. Debido a la enorme diferencia de escalas de tiempo entre laboratorio y campo se puede suponer una mayor diferencia que la del 25% mencionada arriba.

h) Historia previa de deformaciones

Este importante factor fue señalado por Finn et al en 1970, demostrando que las características de licuación de las arenas son influenciadas por la historia previa de deformaciones, él concluyó:

> *"La dependencia de la resistencia a la licuación para una arena con la historia de deformaciones conduce a la conclusión de que la resistencia de un depósito no puede ser determinada en una forma confiable mediante el ensaye de muestras formadas en el laboratorio aún y cuando se tenga la misma relación de vacíos que el depósito. Parece que la resistencia a la licuación sólo puede ser confiablemente determinada en muestras inalteradas"*

blor (atribuyendo el estado de deformaciones del suelo a la propagación de ondas de cortante).

Para un depósito de suelo con superficie horizontal, antes del sismo, el estado de esfuerzos puede ser idealizado como se muestra en la fig 13.a . Durante el sismo los esfuerzos cortantes generados superpuestos a los esfuerzos normales se muestran en la fig 13.b .

La cámara triaxial cíclica trata de simular las condiciones idealizadas descritas. Un espécimen saturado de forma cilíndrica se consolida a un esfuerzo $\bar{\sigma}_c$ y posteriormente con el drenaje cerrado se somete a un esfuerzo axial cíclico de magnitud $\pm \Delta\sigma_a$ (fig 14), este procedimiento proporciona esfuerzos cortantes cíclicos τ_{hv} en un plano a 45°.

Son varias las limitaciones de la cámara triaxial cíclica y éstas se mencionan en la literatura, siendo una de las principales la falta de entendimiento de la condición de campo que representa.

El comportamiento de las muestras de arena suelta, sometidas al ensaye con cámara triaxial cíclica, se caracteriza por un aumento gradual de la presión de poro sin que haya deformación axial apreciable, hasta que se produce el incremento que eleva la presión de poro hasta el valor de la presión confinante, momento a partir del cual la muestra se deforma súbitamente más del 20%. Las arenas en estado compacto exhiben un comportamiento similar al de las arenas sueltas, pero al llegar a la

"*licuación inicial*" no se presenta una deformación grande en forma súbita, sino que la deformación se incrementa gradualmente.

Según el concepto de Seed y Lee (1966), cualquier espécimen de arena es susceptible de licuarse no importando su compacidad relativa. Los parámetros más importantes según estos investigadores son: el número de ciclos de esfuerzo (Na), para alcanzar la condición $u = \bar{\sigma}_3$, la relación entre el esfuerzo cortante máximo y el esfuerzo confinante, $(\frac{\sigma_a}{2\sigma_c})$ y la relación de vacíos.

Castro (1969) al realizar sus ensayes en cámara triaxial cíclica observó que durante la prueba se desarrollan heterogeneidades en las muestras, de manera especial en la zona superior. Atribuye a estas heterogeneidades, inducidas por el ensaye, el que especímenes densos alcancen la condición $u = \bar{\sigma}_3$

Ensaye de corte simple cíclico

La prueba de corte simple cíclico se desarrolló con la idea de conseguir mayor aproximación a las condiciones de campo que la lograda con cámara triaxial.

Uno de los primeros aparatos de corte simple fue el desarrollado por *Swedish and Norwegian Geotechnical Institutes* (Kjellman, 1951). Sin embargo, este aparato tenía el inconveniente de utilizar muestras cilíndricas (los esfuerzos cortantes en una sección horizontal no pueden ser uniformes).

con flujos de material producidos por el incremento de la presión de poro originada por los cambios del nivel del río.

Criterio de Florin e Ivanov

Este criterio desarrollado en Rusia, en 1971, permite estimar la susceptibilidad a la licuación de suelos por medio de pruebas de campo. Se investigan los 10 m superiores de suelo haciendo explotar sucesivamente tres cargas de dinamita de 5 Kg. colocadas a una profundidad media de 4.5 m y determinando después de cada explosión, el asentamiento promedio de la superficie dentro de un radio de 4.5 m. La cantidad y profundidad a la que se coloca el explosivo se eligen de forma que no haya expulsión de suelo durante la explosión. Si el asentamiento promedio es menor de 8 a 10 cm y la relación de asentamientos entre explosiones sucesivas es menor que 0.6 se puede afirmar que ese suelo no es susceptible a licuación.

Criterio de Kishida

Este criterio está basado en el análisis de las condiciones del suelo de 3 sitios en los que ocurrió licuación, (Kishida, 1969). Bajo sismos de igual magnitud, puede ocurrir licuación si el nivel freático está cerca de la superficie, si las características granulométricas satisfacen las relaciones:

$$2mm > D_{50} > .074 \text{ mm};\ C_u < 10 \text{ y}$$

además si se cumplen las siguientes condiciones:

- El espesor del estrato de suelo no licuable, arriba del estrato, licuable es menor que 8 m.
- La relación de los espesores del estrato no licuable al

licuable es menor que 1.

Kishida también concluye que los suelos no son susceptibles a la licuación si:

- La presión efectiva de confinamiento es superior a 2 Kg/cm^2 o,
- La compacidad relativa es superior a 75%.

Criterio de Oshaki

Este criterio (Oshaki, 1969) establece que los suelos con nivel freático cercano a la superficie pueden licuarse si se presentan las siguientes características granulométricas:

$$2mm > D_{60} > 0.2 \text{ mm};\ D_{10} < 0.1 \text{ mm}$$

Adicionalmente, establece que estos suelos tendrán poca probabilidad de licuarse si el número de golpes N_{sp} en prueba de penetración estándar es mayor que 2z, en que z es la profundidad en metro.

2. Métodos simplificados. Consisten básicamente en comparar la resistencia obtenida en pruebas de laboratorio, con los esfuerzos que provocará el sismo, calculados en forma simplificada.

   En esta categoría se clasifican los métodos propuestos por Seed e Idriss (1970) y por Casagrande (1976).

Método de Seed e Idriss

Este método consiste en comparar los esfuerzos inducidos por

Los esfuerzos que provocarán la licuación en un suelo a una compacidad relativa dada, se pueden deducir en forma aproximada de los experimentos llevados a cabo por diversos investigadores, tanto en cámaras triaxiales como en aparatos de corte simple. A partir de pruebas en cámaras triaxiales se han obtenido gráficas que permiten estimar si ocurrirá licuación en un suelo sometido a un determinado número de ciclos (10 o 30 usualmente) para una relación de esfuerzos $(\frac{\sigma_{dc}}{2\sigma_c})$ dada y determinado tamaño de las partículas (representado por el D_{50}). En las figs 18 y 19 se presentan estas gráficas para una compacidad relativa de 50%.

Para determinar la relación de esfuerzos correspondiente a otra compacidad relativa se usa el hecho experimental de que la relación de esfuerzos $(\frac{\sigma_{dc}}{2\sigma_c})$ es aproximadamente proporcional a la compacidad relativa (fig 18 y 19). En las mismas figuras, se observa que el material menos resistente corresponde a un $D_{50} = 0.074$ mm.

Tomando en cuenta que el esfuerzo más significativo, en la licuación de un suelo bajo la acción de un temblor, es el esfuerzo cortante actuante en el plano horizontal; la prueba de corte simple es la que mejor asemeja las condiciones de deformación in-situ. Es por tanto importante correlacionar los resultados anteriores, obtenidos en cámaras triaxiales, con los obtenidos en pruebas de corte. Las investigaciones llevadas a cabo por Seed e Idriss, permitieron concluir que, para fines prácticos:

$(\frac{\tau_{xy}}{\sigma_y})$ corte simple $\quad C_o(\frac{\sigma_{dc}}{2\sigma_c})$ triaxial

en que C_o depende de la compacidad relativa (fig 20).

Comparando los esfuerzos producidos en el terreno por un temblor y los esfuerzos que el material es capaz de soportar, es posible determinar si el suelo presentará o no el fenómeno de licuación, para las condiciones particulares supuestas.

Seed e Idriss presentan un procedimiento simplificado que permite aplicar el método anterior en forma expedita mediante gráficas de penetración estándar contra la profundidad, elaboradas para 2 profundidades típicas del nivel freático y para 2 aceleraciones máximas del terreno (figs 21 y 22). En estas gráficas se delimitan tres zonas: una, en la cual no habrá licuación; otra, en la que podría o no presentarse licuación dependiendo de las características granulométricas del material y de la magnitud del temblor; y la tercera en la cual es muy probable que el material se licúe. Las fronteras entre las zonas anteriores se determinaron para una compacidad relativa de 50% y corresponden a condiciones extremas en cuanto al número de ciclos significativos producidos por un temblor y a la granulometría del material. La frontera a la izquierda de la cual se concluye que habrá licuación fue obtenida usando el mínimo número de ciclos razonable ($N_{sp} = 10$) combinado con la granulometría del material menos susceptible a la licuación ($D_{50} = 2$ mm); la frontera a la derecha de la cual se dice no habrá licuación se obtuvo combinando el máximo número de ciclos razonable ($N_{sp} = 30$) con

delos desarrollados en la Universidad de California, Berkeley

os modelos desarrollados en la Universidad de California, tiene
n características principales:

; Est blece l s ecuaciones de movimiento en función de esfuer-
zos totales .

) Consideran el problema de despl, zamientos pequeños.

) El comportamiento no-lineal de los suelos se trata ya sea me
diante un procedimiento lineal equivalente o media.te un cri
terio tipo Mesing, que puede ser un Ramberg- Osgood o un Mar
tin-Davidenkov.

) La generación de la presión de poro se calcula a partir de
resultados de pruebas triaxiales cíclicas consolidadas-no
drenadas (Lee y Albaese, 1974), cuyas variables son:

- σ'_o , *esfuerzo de consolidación*
- σ_{dp} , *esfuerzo desviador cíclico*
- $(u_g)_N$, *presión de poro generada para N ciclos*
- N_ℓ , *número de ciclos para provocar la licuación*

.l representar las relaciones N/N_ℓ vs $\frac{u_g}{\sigma'_o}$ se obtiene una
franja angosta de forma peculiar que se representa mediante

$$\frac{N}{N_\ell} = \left| \frac{1}{2}\left(1 - \cos \frac{u_g}{\sigma'_o}\right) \right|^\alpha$$

α es un parámetro que depende del tipo de arena y de las condiciones de prueba. Al aplicar la expresión para una historia irregular de ciclos de esfuerzos es necesario transformar dicha historia en un número de ciclos equivalentes, de amplitud constante, según el criterio descrito

por Seed et al 1975.

5) Las ecuaciones de movimiento se integran con el método del elemento finito ya sea con el criterio del método lineal equivalente o bien en forma incremental. La integración respecto al tiempo se lleva a cabo mediante un esquema que utilice el dominio de la frecuencia; o bien uno directo, paso a paso en el dominio del tiempo.

6) El amortiguamiento considerado es el lineal equivalente (Seed e Idriss, 1970) o bien el que resulta de considerar un modelo histerético.

7) La disipación de la presión de poro se calcula con base en la generación de la presión de poro conocida y la Teoría de Consolidación Unidimensional.

8) Para problemas bidimensionales la respuesta dinámica se cuantifica con el método lineal equivalente, mientras que para los problemas no lineales incrementales se considera únicamente el caso unidimensional.

El método exhibe las características de la respuesta dinámica clásica, como la de que el sistema regrese a su posición de equilibrio y no se tengan distorsiones angulares permanentes al cesar la excitación.

La solución exhibe marcados efectos de resonancia cuando el período predominante del acelerograma corresponde con el período fundamental del depósito.

G_{mo} y τ_{mo} se determina según Harden y Drnevich (1972).

Las trayectorias de descarga y recarga se describen mediante el criterio tipo Masing (Pyke, 1975)

$$\frac{\tau-\tau_r}{2} = \frac{G_{mn}(\gamma-\gamma_r)}{2} \Big/ \left(1 + \frac{G_{mn}|(\gamma-\gamma_r)|}{2\tau_{mn}}\right)$$

donde

γ_r y τ_r son la deformación cortante y esfuerzo cortante del punto donde ocurre la inversión de esfuerzo

G_{mn} y τ_{mn} son el módulo al cortante y el efuerzo cortante respectivamente para el civlo N, expresados por:

$$G_{mn} = G_{mo}\left[1 + \frac{\varepsilon_{vd}}{H_1 + H_2\,\varepsilon_{vd}}\right]\left(\frac{\sigma'_v}{\sigma'_{vo}}\right)^{1/2}$$

$$\tau_{mn} = \tau_{mo}\left[1 + \frac{\varepsilon_{vd}}{H_3 + H_4\,\varepsilon_{vd}}\right]\left(\frac{\sigma'_v}{\sigma'_{vo}}\right)^{1/2}$$

donde

ε_{vd} es la deformación volumética acumulada

H_1, H_2, H_3 y H_4 son constantes experimentales

σ'_v y σ'_{vo} son los esfuerzos verticales efectivos en el ciclo N e inicial respectivamente

4) La generación de la presión de poro se calcula mediante el cambio de volumen acumulado, obtenido experimentalmente. La expresión del incremento del cambio de volumen es:

$$\Delta\varepsilon_{vd} = C_1\,(\gamma - C_2\,\varepsilon_{vd}) + \frac{C_3\,\varepsilon_{vd}}{\gamma + C_4\,\varepsilon_{vd}}$$

C_1, C_2, C_3 y C_4 son constantes experimentales que toman en cuenta el tipo de arena y la compacidad relativa.

En condiciones no-drenadas y completa saturación, el incremento de la presión de poro durante cada intervalo de tiempo de integración se calcula mediante

$$\Delta u = \overline{E}_r\,\Delta\varepsilon_{vd}$$

donde

$\overline{E}_r$ es el módulo de recuperación elástica unidemensional

5) Las ecuaciones de movimiento se resuelven con el método de diferencias finitas y la integración se lleva a cabo con el método beta de Newmark.

6) Además del amortiguamiento histerético, se puede incluir amortiguamiento viscoso, de acuerdo con el criterio de Rayleigh.

7) La disipación de la presión de poro se calcula con base en la Teoría de la Consolidación Unidimensional.

8) El modelo es unidimensional y las ecuaciones de movimiento y las de disipación de la presión de poro se integran en forma independiente.

El modelo permite realizar análisis para tres condiciones diferentes de drenaje.

a) no permitiendo redistribución de la presión de poro
b) permitiendo redistribución pero no permitiendo disipación de la presión de poro
c) permitiendo disipación

Los resultados obtenidos muestran claramente la influencia de las condiciones de drenaje sobre el desarrollo de la presión de poro.

El método permite calcular:

a. la historia de aceleraciones ($\ddot{x}$), deformaciones de cortante (γ) y los esfuerzos cortantes (τ) en cada capa.

b) El desarrollo de la presión de poro (u).

ejemplo, el LARF (*Liquefaction analysis for radial flow*) desarrollado por Seed y Booker (1976).

REFERENCIAS

Ambraseys, N.N., 1970
"Factors controlling the earthquake response of foundation materials", Proc. Third European Symp. Earthq. Engrg., Sofia, Bulgaria, pp 309-323

Ambraseys, N.N., 1973
"*Dynamics and response of foundation materials in epicentral regions of strong earthquakes*", Proc. Fifth World Conf. Earthq. Engrg., Rome, Italy, pp CXXVI-CXLVIII

Ambraseys, N.N., and Sarma, S., 1969
"*Liquefaction of soils induced by earthquakes*", Bull. Seism. Soc. Am., 59:651-664

Barkan, D.D., 1962
"*Dynamics of Bases and Foundations*", McGraw-Hill, New York, pp 434

Bazaraa, A., 1967
"*Use of the standard penetration test for estimating settlements of shallow foundations on sand*", Doctoral thesis, Dept. of Civil Engrg., University of Illinois, Urbana, Illinois

Broms, B. B. and Forssblad, L., 1969
"*Vibratory compaction of cohesionless soils*", Proc. Specialty Session No. 2, Seventh Internl. Conf. Soil Mech. Found. Engrg., Mexico City, pp 101-118

Casagrande, A., 1936
"*Characteristics of cohesionless soils affecting the stability of slopes and earth fills*", J. of the Boston Society of Civil Engineers, January, pp 257-276

Finn, W.D.L., Bransby, P.L., and Pickering, D.J., 1970
"Effect of strain history on liquefaction of sand", Journal of the Soil Mechanics and Foundations Division, ASCE, Vol. 96, No. SM6

Finn, W.D.L., Emery, J.J., and Gupta, Y.P., 1971
"Liquefaction of Large Samples of Saturated Sand on A Shaking Table", Proc. First Canadian Conf. on Earthq. Engrg., Vancouver, Canada, pp 97-110

Finn, W.D.L. and Byrne, P.M., 1976
"Estimating Settlement in Dry Sands During Earthquakes", Canadian Geotechnical J., Vol. 13, Number 4: 355-363

Finn, W.D.L., Lee, K.W., and Martin, G.R., 1977
"An Effective Stress Model for Liquefaction", Proc. ASCE, 103 (GT6): 517-533

Florin, V.A. and Ivanov, P.L., 1973
"Liquefaction of Saturated Sandy Soils", Proc. 5th Internti. Conf. on Soil Mechanics and Foundations Engineering, Paris, France

Gibbs, H.J. and Holtz, W.G., 1957
Research on Determining the Density of Sands by Spoon Penetration Testing", Proc. Fourth Internti. Conf. Soil Mech. Found. Engrg., London, England, 1, pp 35-39

Hardin, B.O. and Drnevich, V.P., 1972a
"Shear Modulus and Damping in Soils: Measurement and Parameter Effects", Proc. ASCE, 98 (SM6): 603-624

Hardin, B.O. and Drnevich, V.P., 1972b
"Shear Modulus and Damping in Soils: Design Equation and Curves", Proc. ASCE, 98 (SM7): 667-692

Huang, Wen-Xi, 1961
"Investigations on Stability of Saturated Sand Foundations and Slopes Against Liquefaction", Proc. 5th ICSMFD, Vol. 2

Idriss, I.M. and Seed, H.B., 1968b
"Seismic Response of Horizontal Soil Layers", Proc. ASCE, 94 (SM4): 1003-1031

Ishibashi, I. and Sherif, M.A., 1974
"Soil Liquefaction by Torsional Simple Shear Device", Proc. ASCE, 100 (GT8): 871-888

Ishihara, K. and Li, S., 1972
"Liquefaction of Saturated Sand in Triaxial Torsion Shear Test" Soils and Foundations, 12(2): 19-40

Ishihara, K. and Yasuda, S., 1972
"Sand Liquefaction Due to Irregular Excitation", Soil and Foundations, Vol 12, No. 4

Ishida, H., 1970
"Characteristics of Liquefaction of Level Sandy Ground During the Tokachioki Earthquake", Soil and Foundations, 10(2): 103-111

Ladd, R.S., 1976
"Effects of Specimen Preparation on the Cyclic Structural Stability of Sands", Symposium on Soil Liquefaction, ASCE National Convention, Philadelphia

Ladd, R.S., 1977
"Specimen Preparation and Cyclic Stability of Sand", Proc. ASCE, 103 (GT6): 535-547

Lee, K.L. and Seed, H.B., 1967
"Cyclic Stress Conditions Causing Liquefaction of Sand", Proc. ASCE, 93 (SM1): 47-70

Seed, H.B., 1969
"*The Influence of Local Soil Conditions on Earthquake Damage*", Soil Dynamics Speciality Conference, VII ICSMFD, Mexico

Seed, H.B., 1970
"*Soil Problems and Soil Behavior*", In: R.L. Wiegel (Editor), Earthquake Engineering, Prentice-Hall, Englewood Cliffs, New Jersey, pp 227-252

Seed, H.B. and Lee, K.L., 1966
"*Liquefaction of Saturated Sands During Cyclic Loading*", Proc. ASCE, 92 (SM6): 105-134

Seed, H.B. and Idriss, I.M., 1967
"*An Analysis of the Soil Liquefaction in the Niigata Earthquake*", Proc. ASCE, 93 (SM3): 83-108

Seed, H.B. and Idriss, I.M., 1969
"*Influence of Soil Conditions on Ground Motions During Earthquake*", Proc. ASCE, 95 (SM1): 99-137

Seed, H.B. and Idriss, I.M., 1970b
"*A Simplified Procedure for Evaluating Soil Liquefaction Potential*", Report EERC 70-9, Earthq. Engrg. Res. Center, University of California, Berkeley, Calif.

Seed, H.B. and Idriss, I.M., 1970c
"*Soil Moduli and Damping Factors for Dynamic Response Analyses*", Report EERC 70-10, Earthq. Engrg. Res. Center, University of California, Berkeley, Calif.

Seed, H.B. and Silver, M.L., 1972
"*Settlement of Dry Sands During Earthquakes*", Proc. ASCE, 98 (SM4): 381-397

Seed, H.B., Lee, K.L., Idriss, I.M., and Makdisi, F.I., 1973
"*Analysis of the Slide in the San Fernando Dams During the Earthquake of Feb. 9, 1971*", EERC, Report No. EERC 73-2, University of California, Berkeley, Calif.

Seed, H.B., Mori, K., and Chan, C.K., 1975
"*Influence of Seismic History on the Liquefaction Characteristics of Sands*", Report No. 75-25, University of California, Berkeley, Calif.

Seed, H. B., Indress, I. M., Makdasi, F. y Banerjee, N., 1975
"*Representative of Irregular Stress Time Histories by Equivalent Uniform Stress. Series in Liquefaction Analysis*". Report No. EERC 75-29, University of California, Berkeley, Calif.

Seed, H.B., Martin, P.P., and Lysmer, J., 1975
"*The Generation and Dissipation of Pore Water Pressures During Soil Liquefaction*", Report No. EERC 75-26, University of California, Berkeley, Calif.

Seed, H.B., Arango, I., and Chan, C.K., 1975
"*Evaluation on Soil Liquefaction Potencial During Earthquakes*", Report No. EERC 75-28, University of California, Berkeley, Calif.

Seed, H.B., Pyke, R., and Martin, G.R., 1975
"*Effect of Multi-directional Shaking on Liquefaction of Sands*" Report No. EERC 75-41, University of California, Berkeley, Calif.

Seed, H.B. and Booker, J.R., 1976
"*Stabilization of Potentially Liquefiable Sand Deposits Using Gravel Drain Systems*", Report No. EERC 76-10, University of California, Berkeley, Calif.

Shannon & Wilson, Inc., and Agbabian-Jacobsen Associates. 1971
"*Soil Behavior Under Earthquake Loading Conditions*", Report Prepared for U.S.A.E.C., Contract W-7405-eng-26

Shockley, W.G. and Ahluin, R.C., 1960
"*Non-Uniform Conditions in Triaxial Test Specimens*", Research Conference on Shear Strength of Cohesive Soils, ASCE, Boulder, Colorado

Silver, M.L. and Seed, H.B., 1969
"*The Behavior of Sands Under Seismic Loading Conditions*", Report EERC 69-16, Earthq. Engrg. Res. Center, University of California, Berkeley, Calif.

Streeter, V.L., Wylie, E.B., and Richart, F.E., 1973
"*Soil Motion Computations by Characteristics Method*", ASCE, Natl. Struct. Engrg. Meeting, San Francisco, California, Preprint 1952

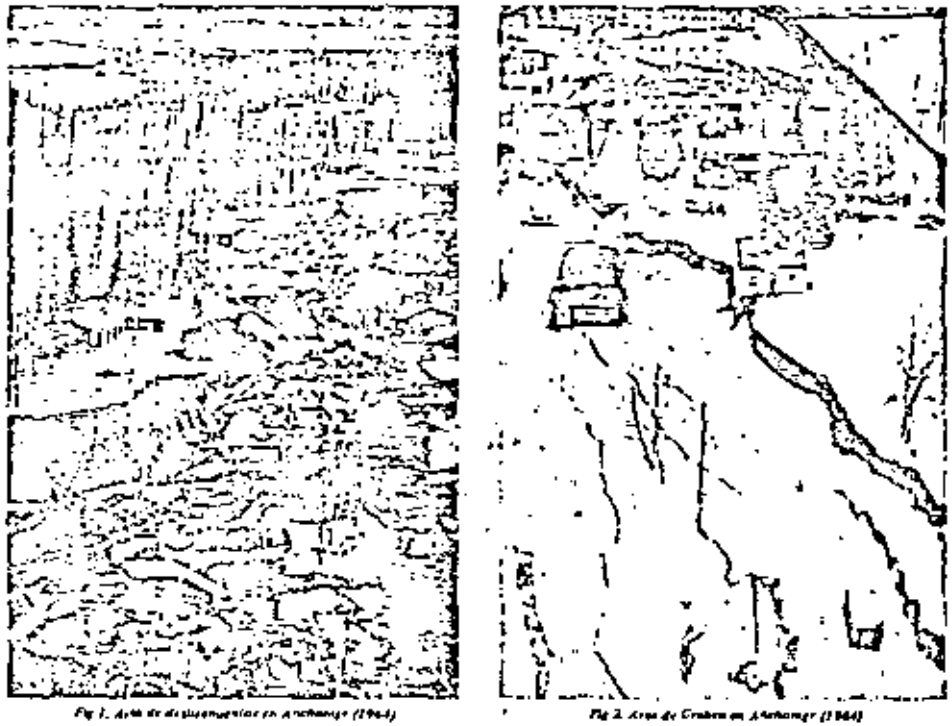

(National Geographic Magazine)

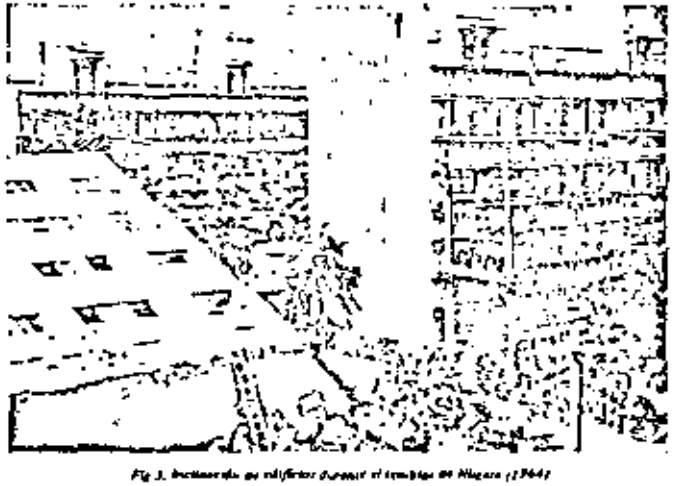

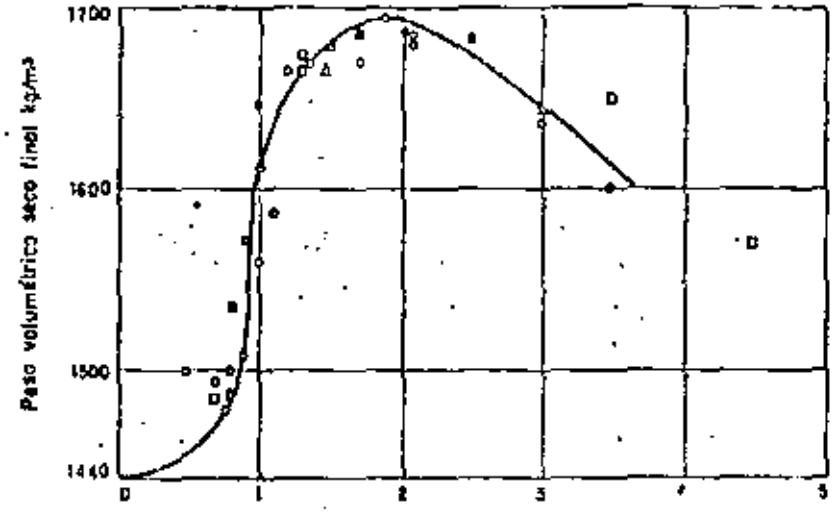

Fig 4 Efecto de la intensidad de aceleración vertical sobre la densificación de la arena en pruebas de mesa vibradora. (D'Appolonia y D'Appolonia, 1967)

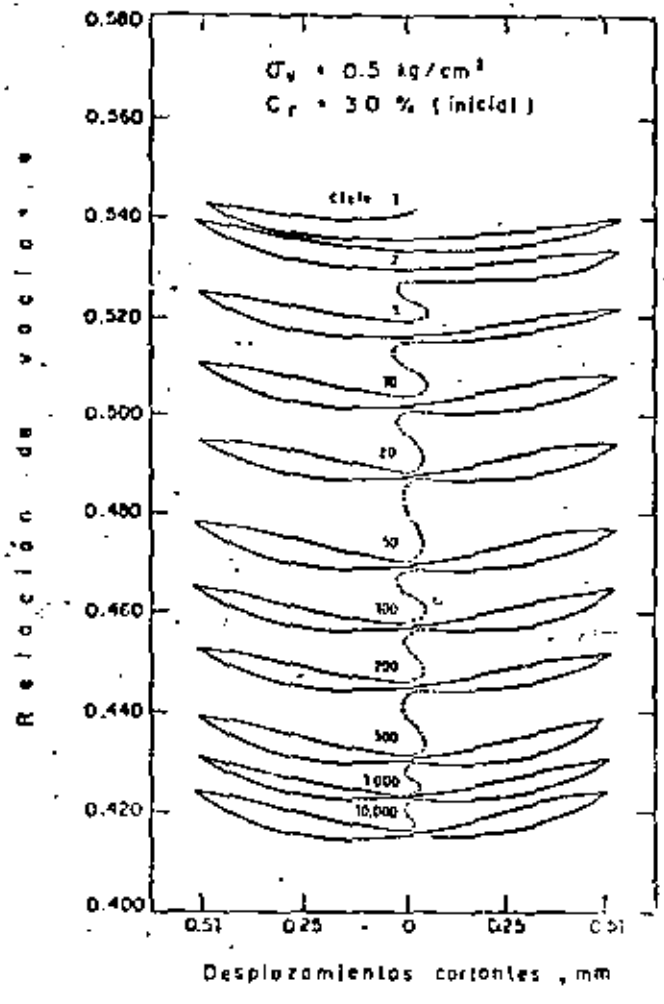

Fig 7 Compactación vs. historia esfuerzo-deformación en una prueba drenada de esfuerzo cortante cíclico sobre arena de Ottawa C-109, (Youd, 1972)

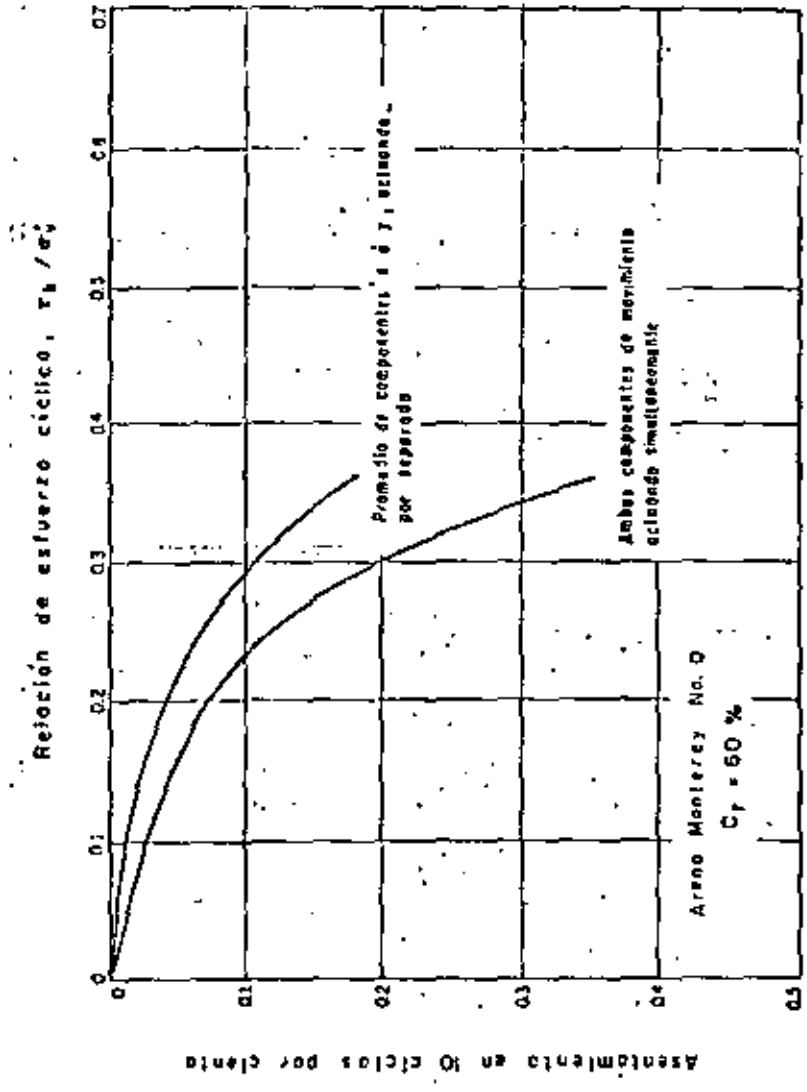

Fig 8 Asentamiento de arena seca bajo movimiento unidireccional y multidireccional, (Seed, Pyke y Martin, 1975)

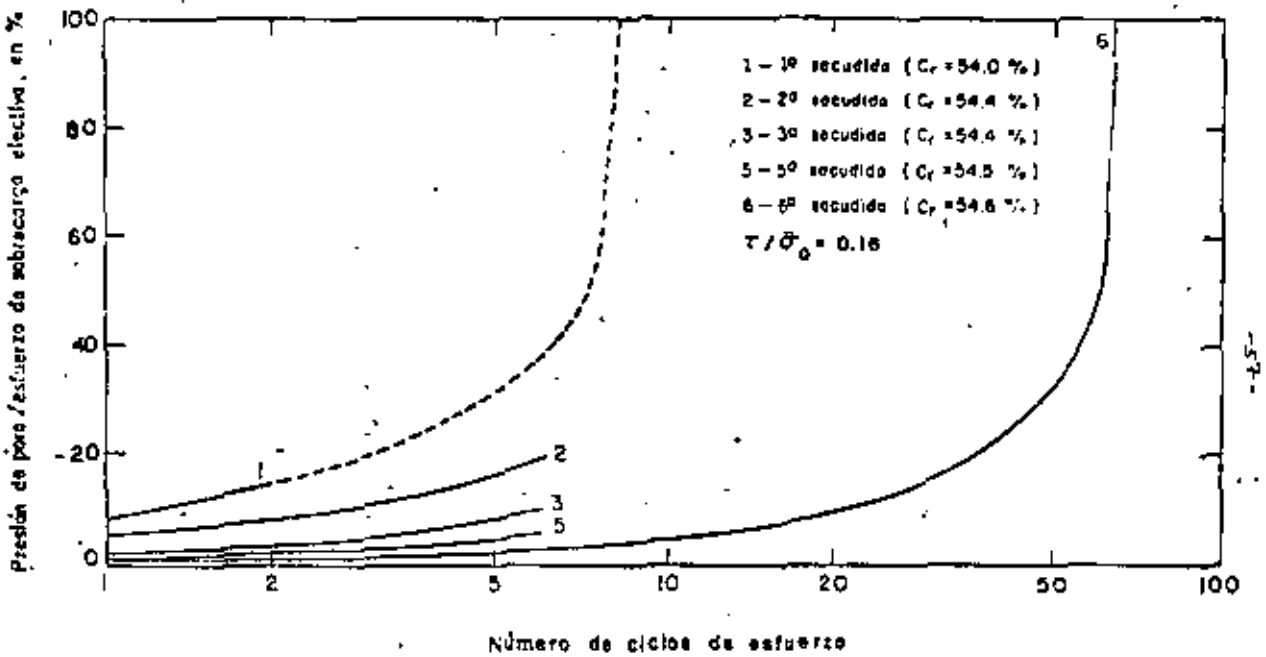

Fig 11 Efecto de la historia sísmica sobre las características de licuación de una arena

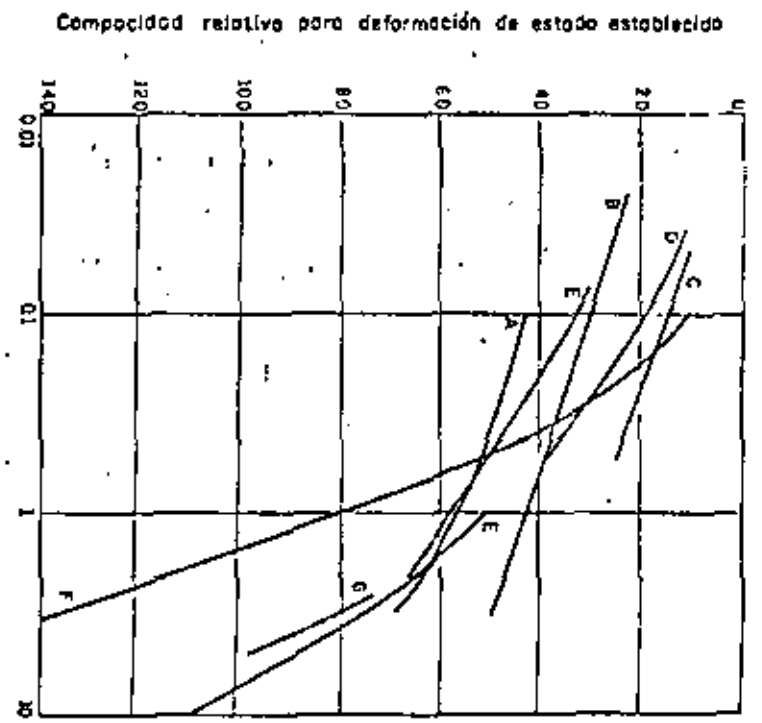

Fig 12 Curvas de estado crítico (líneas e) de arenas descritas en Castro (1972)

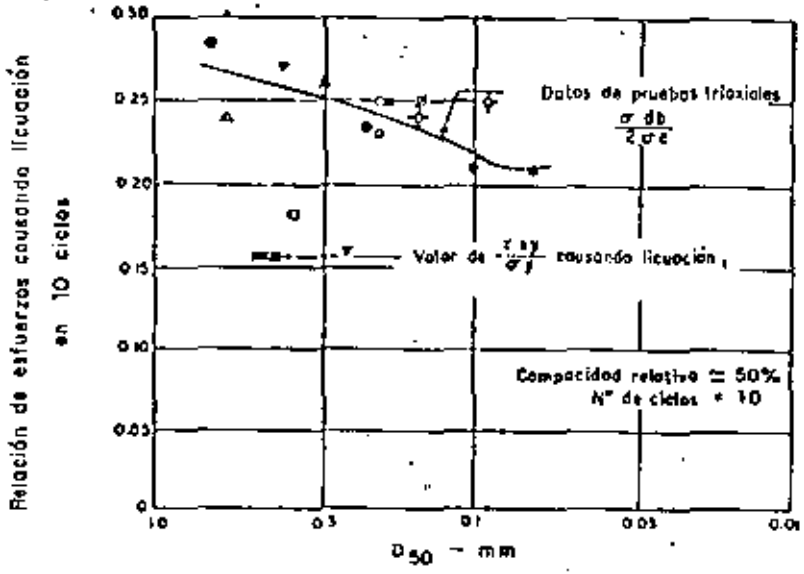

Fig 14 Condiciones de esfuerzo causando licuación de arenas en 10 ciclos

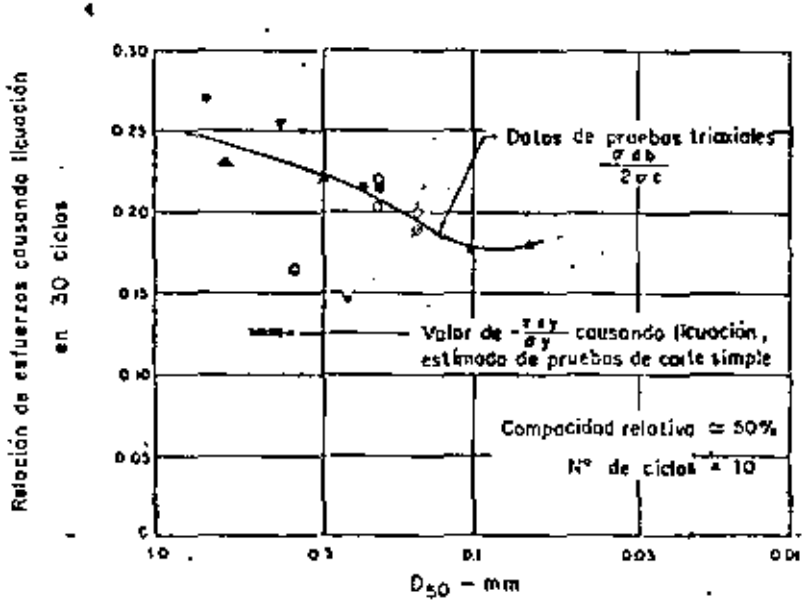

Fig 15 Condiciones de esfuerzo causando licuación de arenas en 30 ciclos

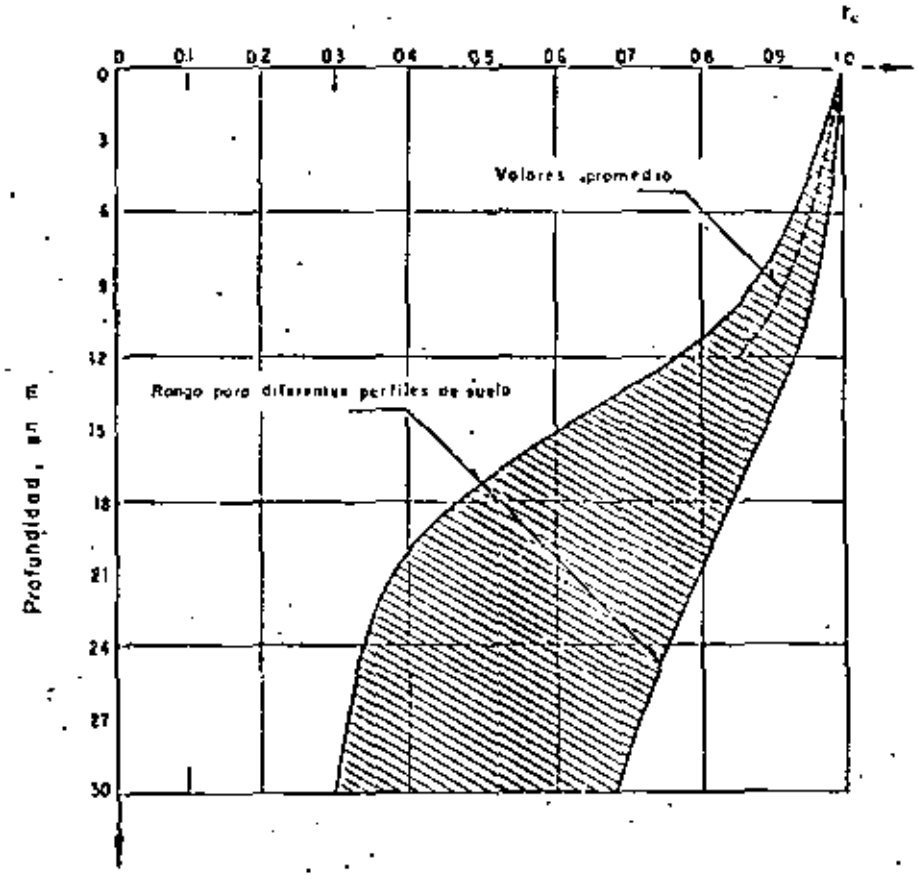

Fig 16 Rango de valores de r_d para diferentes perfiles de suelo

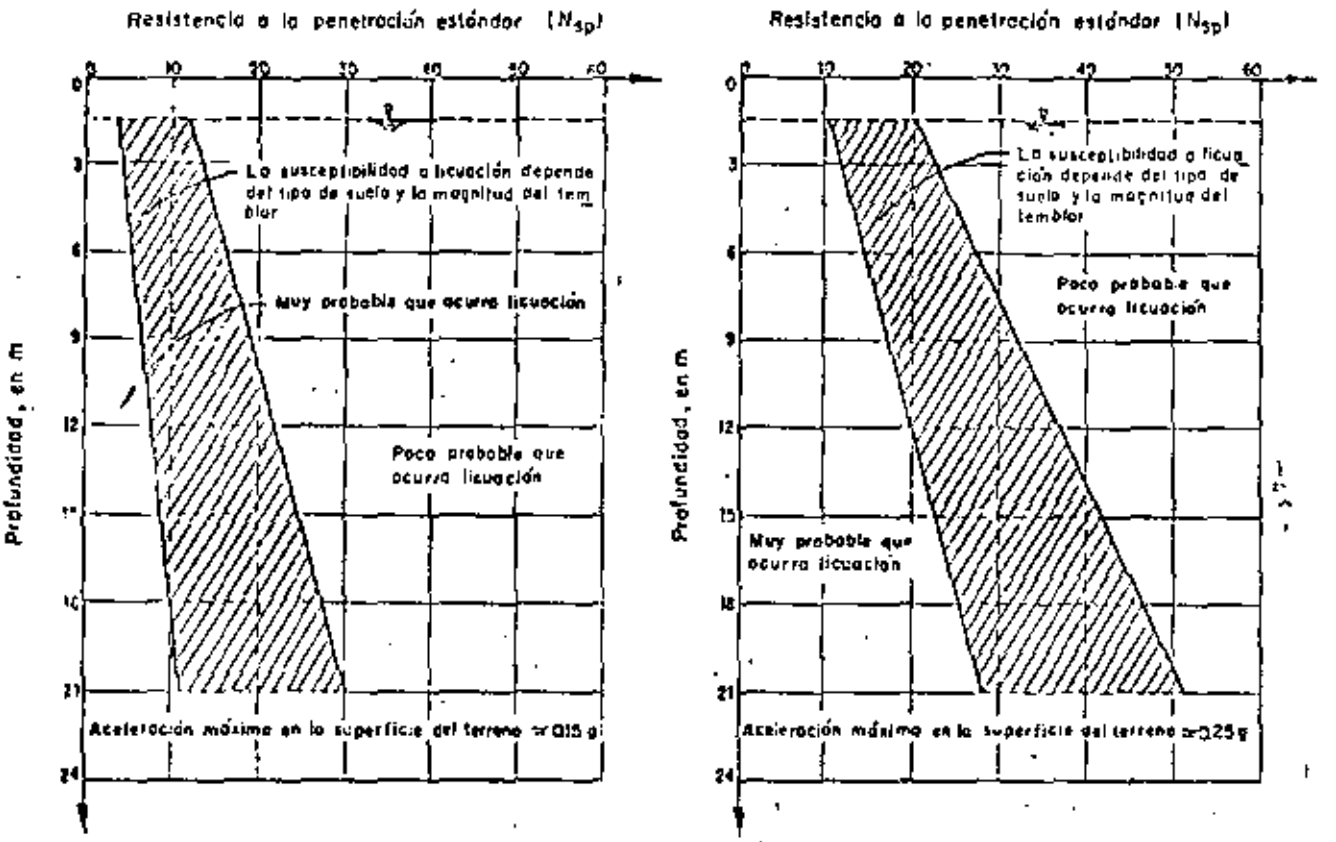

Fig 21 Gráficas para evaluar la susceptibilidad a licuación de arenas con el nivel freático a una profundidad aproximada de 1.5 m (Seed e Idress , 1970 b)

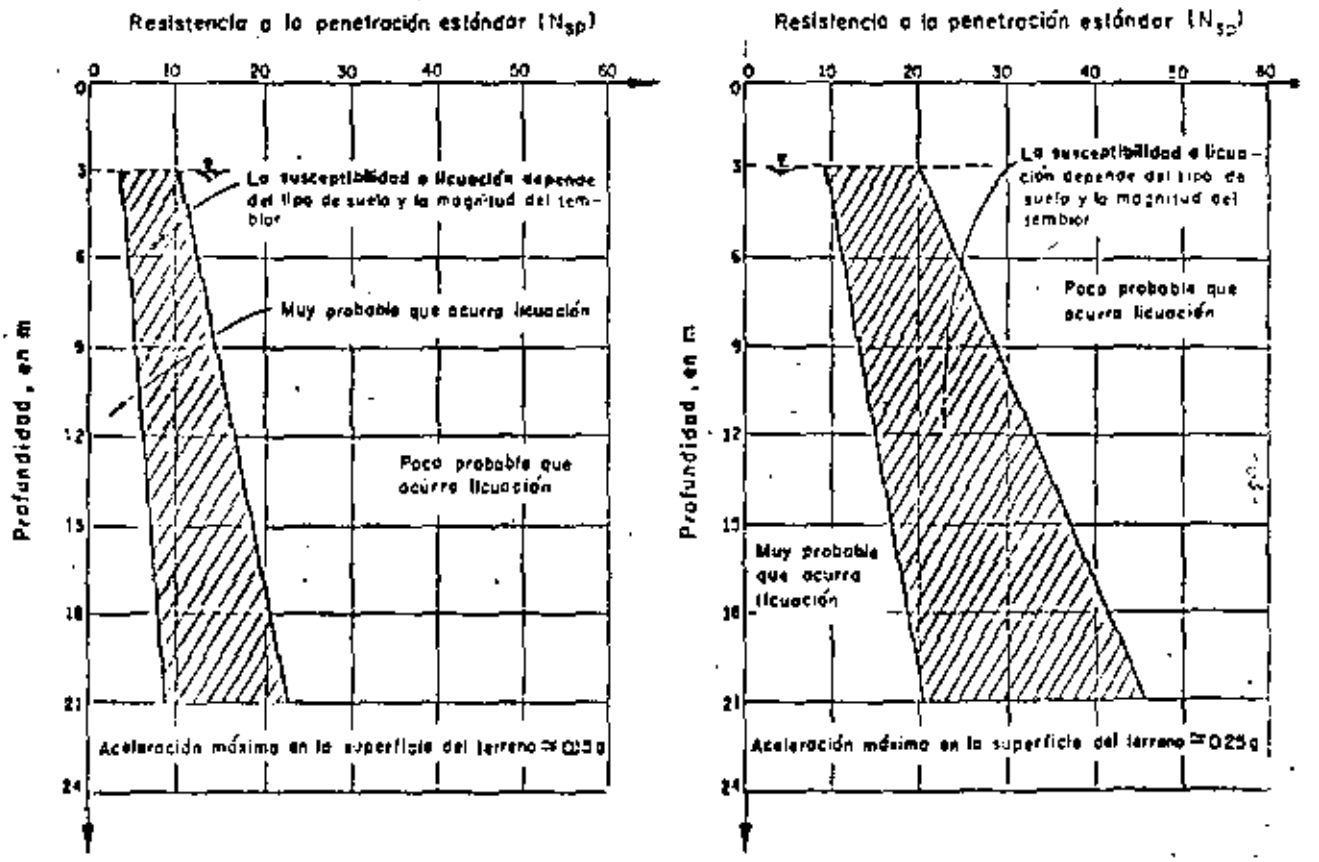

Fig 22 Gráficas para evaluar la susceptibilidad a licuación de arenas con el nivel freático a una profundidad aproximada de 3.0 m (Seed e Idress , 1970 b)

DIVISION DE EDUCACION CONTINUA
FACULTAD DE INGENIERIA U.N.A.M.

VII CURSO INTERNACIONAL DE INGENIERIA SISMICA

SISMOLOGIA Y SISMICIDAD

SISMICIDAD

Dr Luis Esteva Maraboto

Julio, 1981

Chapter 6

SEISMICITY

LUIS ESTEVA

Instituto de Ingeniería, Universidad Nacional Autónoma de México, México

6.1 ON SEISMICITY MODELS

Rational formulation of engineering decisions in seismic areas requires quantitative descriptions of seismicity. These descriptions should conform with their intended applications: in some instances, simultaneous intensities during each earthquake have to be predicted at several locations, while in others it suffices to make independent evaluations of the probable effects of earthquakes at each of those locations.

The second model is adequate for the selection of design parameters of individual components of a regional system (the structures in a region or country) when no significant interaction exists between response or damage of several such individual components, or between any of them and the system as a whole. In other words, it applies when the damage — or negative utility — inflicted upon the system by an earthquake can be taken simply as the addition of the losses in the individual components.

The linearity between monetary values and utilities implied in the second model is not always applicable. Such is the case, for instance, when a significant portion of the national wealth or of the production system is concentrated in a relatively narrow area, or when failure of life-line components may disrupt emergency and relief actions just after an earthquake. Evaluation of risk for the whole regional system has then to be based on seismicity models of the first type, that is, models that predict simultaneous intensities at several locations during each event; for the purpose of decision making, nonlinearity between monetary values and utilities can be accounted for by means of adequate scale transformations. These models are also of interest to insurance companies, when the probability distribution of the maximum loss in a given region during a given time interval is to be estimated.

Whatever the category to which a seismic risk problem belongs, it requires the prediction of probability distributions of certain ground motion characteristics (such as peak ground acceleration or velocity, spectral density, response or Fourier spectra, duration) at a given site during a single shock or of maximum values of some of those characteristics in earthquakes occurring during given time intervals. When the reference interval tends to infinity, the probability distribution of the maximum value of a given characteristic approaches that of its maximum *possible* value. Because different systems or subsystems are sensitive to different ground motion characteristics, the term *intensity characteristic* will be used throughout this chapter to mean a particular parameter or set of parameters of an earthquake motion, in terms of which the response is to be predicted. Thus, when dealing with the failure probability of a structure, intensity can be alternatively measured — with different degrees of correlation with structural response — by the ordinate of the response spectrum for the corresponding period and damping, the peak ground acceleration, or the peak ground velocity.

In general, local instrumental information does not suffice for estimating the probability distributions of maximum intensity characteristics, and use has to be made of data on subjective measures of intensities of past earthquakes, of models of *local seismicity*, and of expressions relating characteristics with magnitude and site-to-source distance. Models of local seismicity consist, at least, of expressions relating magnitudes of earthquakes generated in given volumes of the earth's crust with their return periods. More often than not, a more detailed description of local seismicity is required, including estimates of the maximum magnitude that can be generated in these volumes, as well as probabilistic (stochastic process) models of the possible histories of seismic events (defined by magnitudes and coordinates).

This chapter deals with the various steps to be followed in the evaluation of seismic risk at sites where information other than direct instrumental records of intensities has to be used: identifying potential sources of activity near the site, formulating mathematical models of local seismicity for each source, obtaining the contribution of each source to seismic risk at the site and adding up contributions of the various sources and combining information obtained from local seismicity of sources near the site with data on instrumental or subjective intensities observed at the site.

The foregoing steps consider use of information stemming from sources of different nature. Quantitative values derived therefrom are ordinarily tied to wide uncertainty margins. Hence they demand probabilistic evaluation, even though they cannot always be interpreted in terms of relative frequencies of outcomes of given experiments. Thus, geologists talk of the maximum magnitude that can be generated in a given area, assessed by looking at the dimensions of the geological accidents and by extrapolating the observations of other regions which available evidence allows to brand as similar to the one of interest; the estimates produced are obviously uncertain, and the degree of uncertainty should be expressed together with the most probable value. Following nearly parallel lines, some geophysicists estimate the energy that can be liberated by a single shock in a given area by making quantitative assumptions about source dimensions, dislocation amplitude and stress drop, consistent with tectonic models of the region and, again, with comparisons with areas of similar tectonic characteristics.

Uncertainties attached to estimates of the type just described are in gen-

eral extremely large; some studies relating fault rupture area, stress drop, and magnitude (Brune, 1968) show that, considering not unusually high stress drops, it does not take very large source dimensions to get magnitudes 8.0 and greater, and those studies are practically restricted to the simplest types of fault displacement. It is not clear, therefore, that realistic bounds can always be assigned to potential magnitudes in given areas or that, when this is feasible, those bounds are sufficiently low, so that designing structures to withstand the corresponding intensities is economically sound, particularly when occurrence of those intensities is not very likely in the near future. Because uncertainties in maximum feasible magnitudes and in other parameters defining magnitude-recurrence laws can be as significant as their mean values when trying to make rational seismic design decisions, those uncertainties have to be explicitly recognized and accounted for by means of adequate probabilistic criteria. A corollary is that geophysically based estimates of seismicity parameters should be accompanied with corresponding uncertainty measures.

Seismic risk estimates are often based only on statistical information (observed magnitudes and hypocentral coordinates). When this is done, a wealth of relevant geophysical information is neglected, while the probabilistic prediction of the future is made to rely on a sample that is often small and of little value, particularly if the sampling period is short as compared with the desirable return period of the events capable of severely damaging a given system.

The criterion advocated here intends to unify the foregoing approaches and rationally to assimilate the corresponding pieces of information. Its philosophy consists in using the geological, geophysical, and all other available non-statistical evidence for producing a set of alternate assumptions concerning a mathematical (stochastic process) model of seismicity in a given source area. An initial probability distribution is assigned to the set of hypotheses, and the statistical information is then used to improve that probability assignment. The criterion is based on application of *Bayes theorem*, also called the *theorem of the probabilities of hypotheses*. Since estimates of risk depend largely on conceptual models of the geophysical processes involved, and these are known with different degrees of uncertainty in different zones of the earth's crust, those estimates will be derived from stochastic process models with uncertain forms or parameters. The degree to which these uncertainties can be reduced depends on the limitations of the state of the art of geophysical sciences and on the effort that can be put into compilation and interpretation of geophysical and statistical information. This is an economical problem that should be handled, formally or informally, by the criteria of decision making under uncertainty.

INTENSITY ATTENUATION

Available criteria for the evaluation of the contribution of potential seismic sources to the risk at a site make use of *intensity attenuation* expressions that relate intensity characteristics with magnitude and distance from site to source. Depending on the application envisaged, the intensity characteristic to be predicted can be expressed in a number of manners, ranging from a subjective index, such as the *Modified Mercalli intensity*, to a combination of one or more quantitative measures of ground shaking (see Chapter 1).

A number of expressions for attenuation of various intensity characteristics with distance have been developed, but there is little agreement among most of them (Ambraseys, 1973). This is due in part to discrepancies in the definitions of some parameters, in the ranges of values analyzed, in the actual wave propagation properties of the geological formations lying between source and site, in the dominating shock mechanisms, and in the forms of the analytical expressions adopted a priori.

Most intensity-attenuation studies concern the prediction of earthquake characteristics on rock or firm ground, and assume that these characteristics, properly modified in terms of frequency-dependent soil amplification factors, should constitute the basis for estimating their counterparts on soft ground. Observations about the influence of soil properties on earthquake damage support the assumption of a strong correlation between type of local ground and intensity in a given shock. Attempts to analytically predict the characteristics of motions on soil given those on firm ground or on bedrock have not been too successful, however (Crouse, 1973; Hudson and Udwadia, 1973; Salt, 1974), with the exception of some peculiar cases, like Mexico City (Herrera et al., 1965), where local conditions favor the fulfillment of the assumptions implied by usual analytical models. The following paragraphs concentrate on prediction on intensities on firm ground; the influence of local soil is discussed in Chapter 4.

6.2.1 Intensity attenuation on firm ground

When isoseismals (lines joining sites showing equal intensity) of a given shock are based only on intensities observed on homogeneous ground conditions, such as *firm ground* (compact soils) or bedrock, they are roughly elliptical and the orientations of the corresponding axes are often correlated with local or regional geological trends (Figs. 6.1–6.3). In some regions — for instance near major faults in the western United States — those trends are well defined and the correlations are clear enough as to permit prediction of intensity in the near and far fields in terms of magnitude and distance to the generating fault or to the centroid of the energy liberating volume. In other regions, such as the eastern United States and most of Mexico, isoseismals seem to elongate systematically in a direction that is a function of the epi-

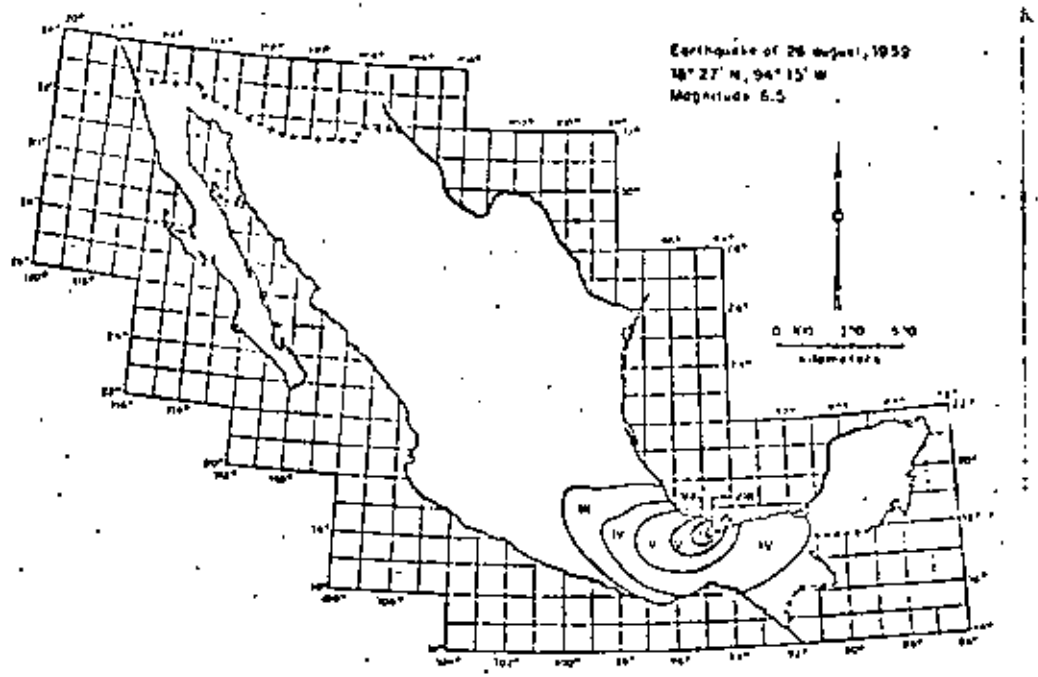

Fig. 6.1. Isoseismals of an earthquake in Mexico. (After Figueroa, 1963.)

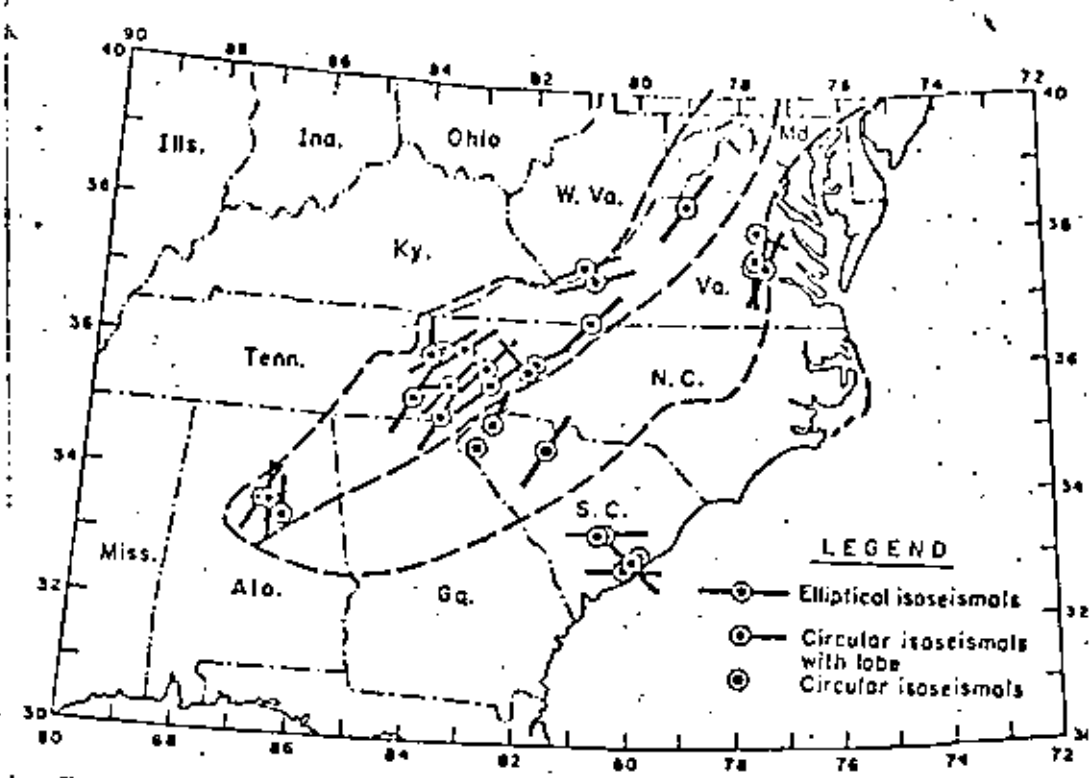

Fig. 6.2. Elongation of isoseismals in the southeastern United States. (After Bollinger, 1973.)

central coordinates (Bollinger, 1973; Figueroa, 1963). In that case, intensity should be expressed as a function of magnitude and coordinates of source and site. For most areas in the world, intensity has to be predicted in terms of simple — and cruder — expressions that depend only on magnitude and distance from site to instrumental hypocenter. This stems from inadequate knowledge of geotectonic conditions and from limited information concerning the volume where energy is liberated in each shock.

A comparison of the rates of attenuation of intensities on firm ground for shocks on western and eastern North America has disclosed systematic differences between those rates (Milne and Davenport, 1969). This is the source of a basic, but often unavoidable, weakness of most intensity-attenuation expressions, because they are based on heterogeneous data, recorded in different zones, and the very nature of their applications implies that the less is known about possible systematic deviations in a given zone, as a consequence of the meagerness of local information, the greater weight is given to predictions with respect to observations.

6.2.1.1 Modified Mercalli intensities

An analysis of the Modified Mercalli intensities on firm ground reported for earthquakes occurring in Mexico in the last few decades leads to the following expression relating magnitude M, hypocentral distance R (in kilometers) and intensity I (Esteva, 1968):

$$I = 1.45\,M - 5.7\log_{10} R + 7.9 \qquad (6.1)$$

The prediction error, defined as the difference between observed and computed intensity, is roughly normally distributed, with a standard deviation of 2.04, which means that there is a probability of 60% that an observed intensity is more than one degree greater or smaller than its predicted value.

6.2.1.2 Peak ground accelerations and velocities

A few of the available expressions will be described. Their comparison will show how cautiously a designer intending to use them should proceed.

Housner studied the attenuation of peak ground accelerations in several regions of the United States and presented his results graphically (1969) in terms of fault length (in turn a function of magnitude), shapes of isoseismals and areas experiencing intensities greater than given values (Fig. 6.4 and 6.5).

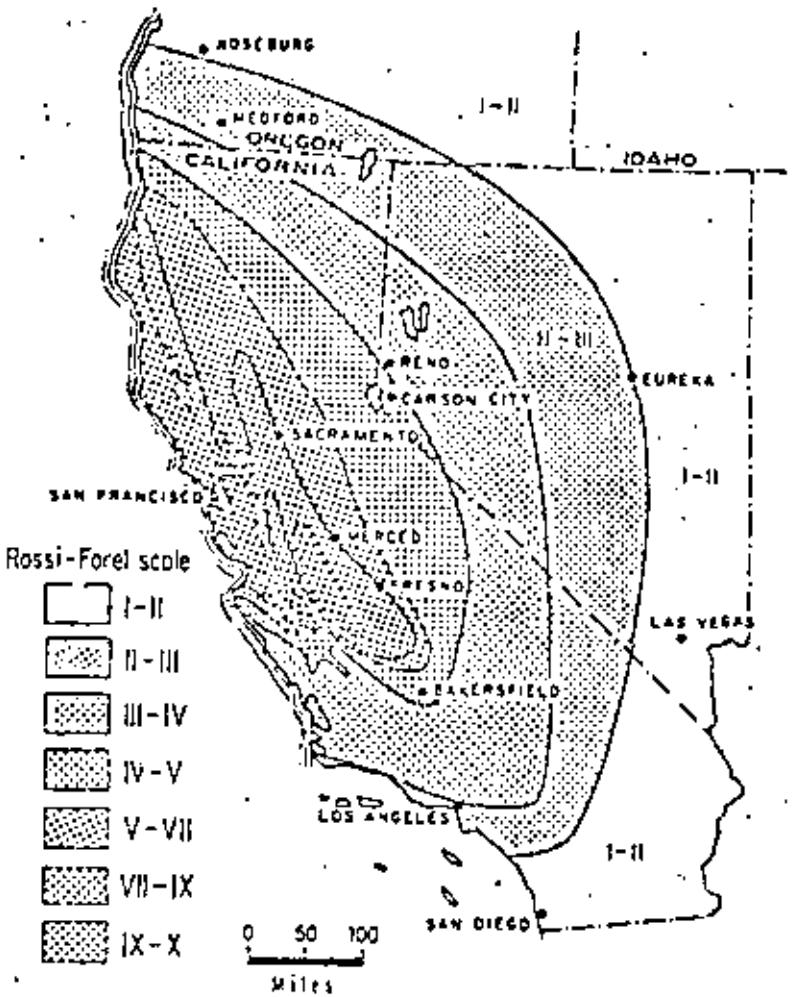

Fig. 6.3. Isoseismals in California. (After Bolt, 1970.)

He showed that intensities attenuate faster with distance on the west coast than in the rest of the country. This comparison is in agreement with Milne and Davenport (1969), who performed a similar analysis for Canada. From observations of strong earthquakes in California and in British Columbia, they developed the following expression for a, the peak ground acceleration, as a fraction of gravity:

$$a/g = 0.0069\, e^{1.6M}/(1.1\, e^{1.1M} + R^2) \qquad (6.2)$$

Here, R is epicentral distance in kilometers. The acceleration varies roughly as $e^{1.64M}R^{-2}$ for large R, and as $e^{0.54M}$ where R approaches zero. This reflects to some extent the fact that energy is released not at a single point but from a finite volume. A later study by Davenport (1972) led him

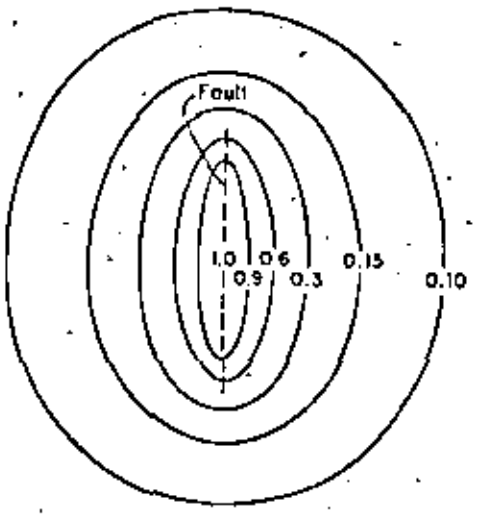

Fig. 6.4. Idealized contour lines of intensity of ground shaking. (After Housner, 1969.)

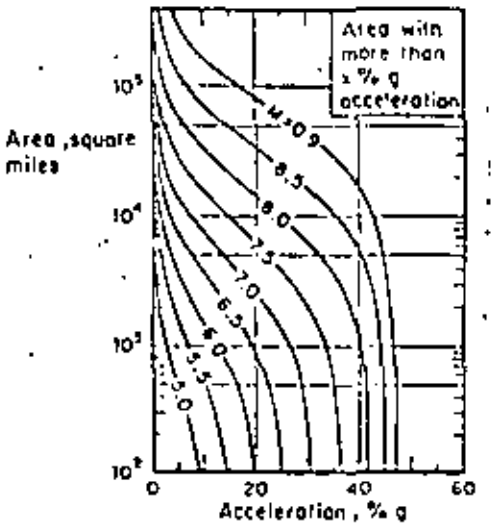

Fig. 6.5. Area in square miles experiencing shaking of x %g or greater for shocks of different magnitudes. (After Housner, 1969.)

to propose the expression:

$$a/g = 0.279\, e^{0.8M}/R^{1.64} \qquad (6.3)$$

The statistical error of this equation was studied by fitting a lognormal probability distribution to the ratios of observed to computed accelerations. A standard deviation of 0.74 was found in the natural logarithms of those ratios.

Esteva and Villaverde (1973), on the basis of accelerations reported by Hudson (1971, 1972a,b), derived expressions for peak ground accelerations and velocities, as follows:

$$a/g = 5.7\, e^{0.8M}/(R + 40)^2 \qquad (6.4)$$

$$v = 32\, e^{M}/(R + 25)^{1.7} \qquad (6.5)$$

Here v is peak ground velocity in cm/sec and the other symbols mean the same as above. The standard deviation of the natural logarithm of the ratio of observed to predicted intensity is 0.64 for accelerations and 0.74 for velocities. If judged by this parameter, eqs. 6.3 and 6.4 seem equally reliable. However, as shown by Fig. 6.6, their mean values differ significantly in some ranges.

With the exception of eq. 6.2, all the foregoing attenuation expressions are products of a function of R and a function of M. This form, which is acceptable when the dimensions of the energy-liberating source are small com-

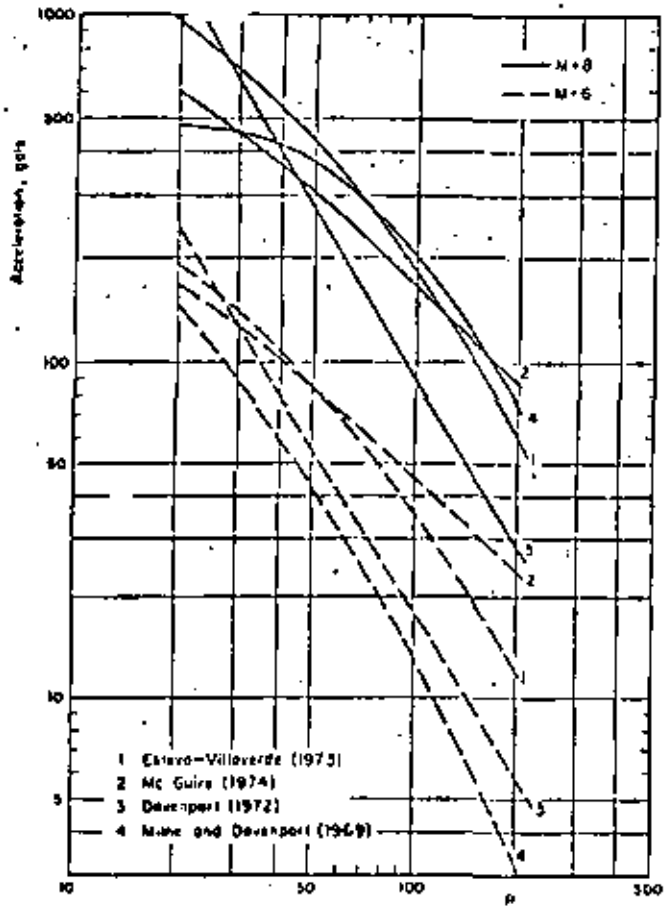

Fig. 6.6. Comparison of several attenuation expressions.

pared with R, is inadequate when dealing with earthquake sources whose dimensions are of the order of moderate hypocentral distances, and often greater than them. Although equation errors (probability distributions of the ratio of observed to predicted intensities) have been evaluated by Davenport (1972) and Esteva and Villaverde (1973), their dependence on M and R has not been analyzed. Because seismic risk estimates are very sensitive to the attenuation expressions in the range of large magnitudes and short distances, more detailed studies should be undertaken, aiming at improving those expressions in the mentioned range, and at evaluating the influence of M and R on equation error. Information on strong-motion records will probably be scanty for those studies, and hence they will have to be largely based on analytical or physical models of the generation and propagation of seismic waves. Although significant progress has been lately attained in this direction (Trifunac, 1973) the results from such models have hardly influenced the

practice of seismic risk estimation because they have remained either unknown to or imperfectly appreciated by engineers in charge of the corresponding decisions.

6.2.1.3 Response spectra

Peak ground acceleration and displacement are fairly good indicators of the response of structures possessing respectively very high and very small natural frequencies. Peak velocity is correlated with the response of intermediate-period systems, but the correlation is less precise than that tying the former parameters; hence, it is natural to formulate seismic risk evaluation and engineering design criteria in terms of spectral ordinates.

Response spectrum prediction for given magnitude and hypocentral or site-to-fault distance usually entails a two-step process, according to which peak ground acceleration, velocity and displacement are initially estimated and then used as reference values for prediction of the ordinates of the response spectrum. Let the second step in the process be represented by the operation $y_s = \alpha y_g$, where y_s is an ordinate of the response spectrum for a given natural period and damping ratio, and y_g is a parameter (such as peak ground acceleration or velocity) that can be directly obtained from the time-history record of a given shock regardless of the dynamic properties of the systems whose response is to be predicted. For given M and R, y_g is random and so is $y_s/y_g = \alpha$; the mean and standard deviation of y_s depend on those of y_g and α and on the coefficient of correlation of the latter variables. As shown above, y_g can only be predicted within wide uncertainty limits, often wider than those tied to y_s (Esteva and Villaverde, 1973). The coefficient of variation of y_s given M and R can be smaller than that of y_g only if α and y_g are negatively correlated, which is often the case: the greater the deviation of an observed value of y_g with respect to its expectation for given M and R, the lower is likely to be α. In other words, it seems that in the intermediate range of natural periods the expected values of spectral ordinates for given damping ratios can be predicted directly in terms of magnitude and focal distance with narrower (or at most equal) margins of uncertainty than those tied to predicted peak ground velocities. For the ranges of very short or very long natural periods, peak amplitudes of ground motion and spectral ordinates approach each other and their standard errors are therefore nearly equal.

McGuire (1974) has derived attenuation expressions for the conditional values (given M and R) of the mean and of various percentiles of the probability distributions of the ordinates of the response spectra for given natural periods and damping ratios. Those expressions have the same form as eqs. 6.4 and 6.5, but their parameters show that the rates of attenuation of spectral ordinates differ significantly from those of peak ground accelerations or velocities. For instance, McGuire finds that peak ground velocity attenuates in proportion to $(R + 25)^{-1.20}$, while the mean of the pseudovelocity for a

TABLE 6.1

McGuire's attenuation expressions $y = b_1\, 10^{b_2 M}(R + 25)^{-b_3}$

y	b_1	b_2	b_3	$V(y)$ = coeff. of var. of y
a gals	472.3	0.278	1.301	0.548
v cm/sec	5.64	0.401	1.202	0.696
d cm	0.393	0.434	0.885	0.683
Undamped spectral pseudovelocities				
T = 0.1 sec	11.0	0.278	1.346	0.941
0.5	3.05	0.391	1.001	0.636
1.0	0.631	0.378	0.549	0.768
2.0	0.0768	0.469	0.419	0.989
5.0	0.0834	0.564	0.897	1.344
5% damped spectral pseudovelocities				
T = 0.1 sec	10.09	0.233	1.341	0.651
0.5	5.74	0.366	1.197	0.591
1.0	0.432	0.399	0.704	0.703
2.0	0.122	0.466	0.675	0.941
5.0	0.0706	0.557	0.938	1.193

natural period of 1 sec and a damping ratio of 2% attenuates in proportion to $(R + 25)^{-0.59}$. These results stem from the way that frequency content changes with R and lead to the conclusion that the ratio of spectral velocity should be taken as a function of M and R.

Table 6.1 summarizes McGuire's attenuation expressions and their coefficients of variation for ordinates of the pseudovelocity spectra and for peak ground acceleration, velocity and displacement. Similar expressions were derived by Esteva and Villaverde (1973), but they are intended to predict only the maxima of the expected acceleration and velocity spectra, regardless of the periods associated with those maxima. No analysis has been performed of the relative validity of McGuire's and Esteva and Villaverde's expressions for various ranges of M and R.

6.3 LOCAL SEISMICITY

The term *local seismicity* will be used here to designate the degree of seismic activity in a given volume of the earth's crust; it can be quantitatively described according to various criteria, each providing a different amount of information. Most usual criteria are based on upper bounds to the magnitudes of earthquakes that can originate in a given seismic source, on the amount of energy liberated by shocks per unit volume and per unit time or on more detailed statistical descriptions of the process.

6.3.1 Magnitude-recurrence expressions

Gutenberg and Richter (1954) obtained expressions relating earthquake magnitudes with their rates of occurrence for several zones of the earth. Their results can be put in the form:

$$\lambda = \alpha e^{-\beta M} \tag{6.6}$$

where λ is the mean number of earthquakes per unit volume and per unit time having magnitude greater than M and α and β are zone-dependent constants; α varies widely from point to point, as evidenced by the map of epicenters shown in Fig. 6.7, while β remains within a relatively narrow range, as shown in Fig. 6.8. Equation 6.6 implies a distribution of the energy liberated per shock which is very similar to that observed in the process of microfracturing of laboratory specimens of several types of rock subjected to gradually increasing compressive or bending strain (Mogi, 1962; Scholz, 1968). The values of β determined in the laboratory are of the same order as those obtained from seismic events, and have been shown to depend on the heterogeneity of the specimens and on their ability to yield locally. Thus, in heterogeneous specimens made of brittle materials many small shocks precede a major fracture, while in homogeneous or plastic materials the number of small shocks is relatively small. These cases correspond to large and small β-values, respectively. No general relationship is known to the writer between β and geotectonic features of seismic provinces: complexity of crustal structure and of stress gradients precludes extrapolation of laboratory results; and statistical records for relatively small zones of the earth are not, as a rule, adequate for establishing local values of β. Figure 6.8 shows that for very high magnitudes the observed frequency of events is lower than predicted by eq. 6.6. In addition, Rosenblueth (1969) has shown that β cannot be smaller than 3.46, since that would imply an infinite amount of energy liberated per unit time. However, Fig. 6.8 shows that the values of β which result from fitting expressions of the form 6.6 to observed data are smaller than 3.46; hence, for very high values of M (above 7, approximately) the curve should bend down, in accordance with statistical evidence.

Expressions alternative to eq. 6.6 have been proposed, attempting to represent more adequately the observed magnitude-recurrence data (Rosenblueth, 1964; Merz and Cornell, 1973). Most of these expressions also fail to recognize the existence of an upper bound to the magnitude that can be generated in a given source. Although no precise estimates of this upper bound can yet be obtained, recognition of its existence and of its dependence on the geotectonic characteristics of the source is inescapable. Indeed, the prac-

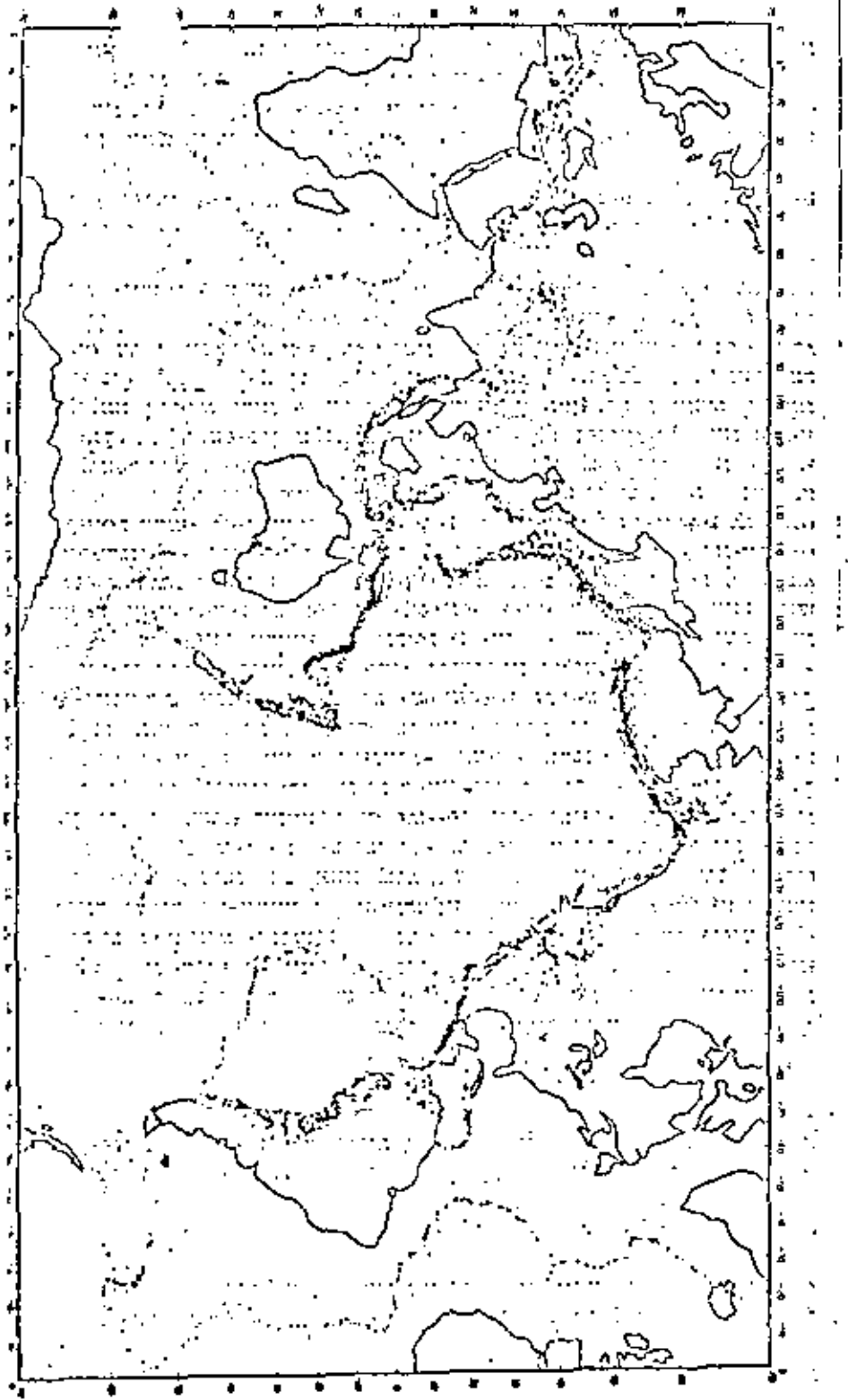

Fig. 6.7. Map showing epicenters for the interval 1961–1967. (After Newmark and Rosenblueth, 1971.)

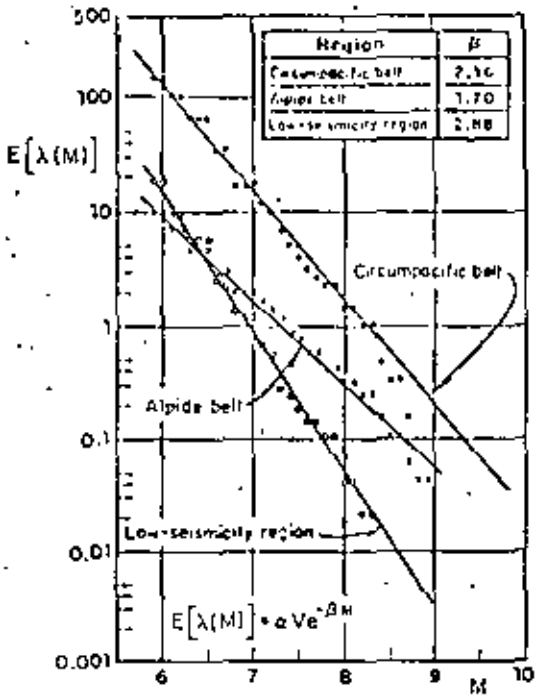

Fig. 6.8. Seismicity of macrozones. (After Esteva, 1968.)

tice of seismic zoning in the Soviet Union has been based on this concept (Gzovsky, 1962; Ananiin et al., 1968) and in many countries design spectra for very important structures, such as nuclear reactors or large dams, are usually derived from the assumption of a maximum credible intensity at a site; that intensity is ordinarily obtained by taking the maximum of the intensities that result at the site when at each of the potential sources an earthquake with magnitude equal to the maximum feasible value for that source is generated at the most unfavourable location within the same source. When this criterion is applied no attention is usually paid to the uncertainty in the maximum feasible magnitude nor to the probability that an earthquake with that magnitude will occur during a given time period. The need to formulate seismic-risk-related decisions that account both for upper bounds to magnitudes and for their probabilities of occurrence suggests adoption of magnitude recurrence expressions of the form:

$$\begin{aligned} \lambda &= \lambda_L G^{\epsilon}(M) && \text{for } M_L \leq M \leq M_U \\ &= \lambda_L && \text{for } M < M_L \\ &= 0 && \text{for } M > M_U \end{aligned} \qquad (6.7)$$

where M_L = lowest magnitude whose contribution to risk is significant, M_U

= maximum feasible magnitude, and $G^*(M)$ = complementary cumulative probability distribution of magnitudes every time that an event ($M \geq M_L$) occurs. A particular form of $G^*(M)$ that lends itself to analytical derivations is:

$$G^*(M) = A_0 + A_1 \exp(-\beta M) - A_2 \exp[-(\beta - \beta_1)M] \qquad (6.8)$$

where:

$$A_0 = A\beta_1 \exp[-\beta(M_U - M_L)]$$

$$A_1 = A(\beta - \beta_1) \exp(\beta M_L)$$

$$A_2 = A_0 \exp(-\beta_1 M_U + \beta M_L)$$

$$A = [\beta\{1 - \exp[-\beta_1(M_U - M_L)]\} - \beta_1\{1 - \exp[-\beta(M_U - M_L)]\}]^{-1}$$

As M tends to M_L from above, eq. 6.7 approaches eq. 6.6. Adoption of adequate values of M_U and β_1 permits satisfying two additional conditions: the maximum feasible magnitude and the rate of variation of λ in its vicinity. When $\beta_1 \to \infty$, eq. 6.8 tends to an expression proposed by Cornell and Vanmarcke (1969).

Yegulalp and Kuo (1974) have applied the theory of extreme values to estimating the probabilities that given magnitudes are exceeded in given time intervals. They assume those probabilities to fit an extreme type-III distribution given by:

$$F_{M_{max}}(M|t) = \exp[-C(M_U - M)^k t] \quad \text{for } M \leq M_U$$

$$= 0 \quad \text{for } M > M_U \qquad (6.9)$$

Here $F_{M_{max}}(M|t)$ indicates the probability that the maximum magnitude observed in t years is smaller than M, M_U has the same meaning as above, and C and K are zone-dependent parameters. This distribution is consistent with the assumption that earthquakes with magnitudes greater than M take place in accordance with a Poisson process with mean rate λ equal to $C(M_U - M)^k$. Equation 6.9 produces magnitude recurrence curves that fit closely the statistical data on which they are based for magnitudes above 5.2 and return periods from 1 to 50 years, even though the values of M_U that result from pure statistical analysis are not reliable measures of the upper bound to magnitudes, since in many cases they turn out inadmissibly high.

For low magnitudes, only a fraction of the number of shocks that take place is detected. As a consequence, λ-values based on statistical information lie below those computed according to eqs. 6.6 and 6.8 for M smaller than about 5.5. In addition, Fig. 6.9, taken from Yegulalp and Kuo (1974), shows that the numbers of detected shocks fit the extreme type III in eq. 6.9 better than the extreme type-I distribution implied by eq. 6.6., coupled with the assumption of Poisson distribution of the number of events. It is not

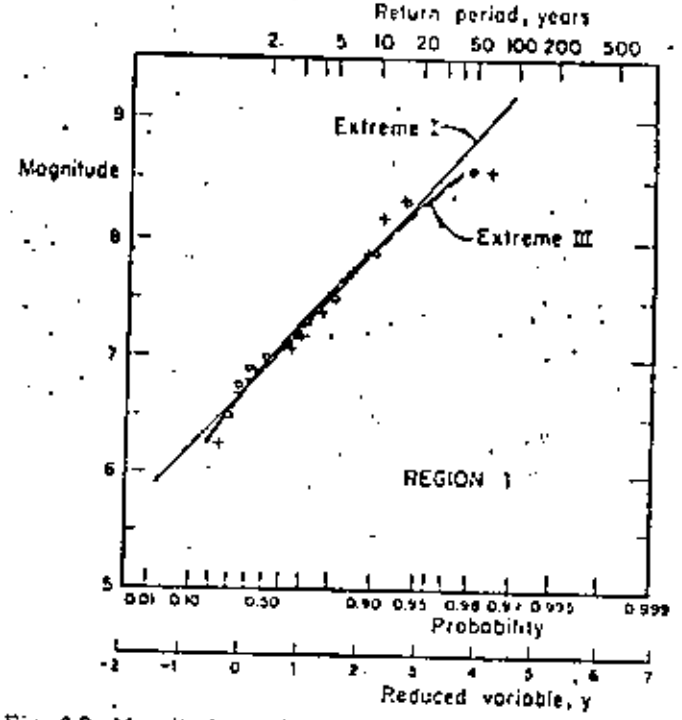

Fig. 6.9. Magnitude statistics in the Aleutian Islands region. (After Yegulalp and Kuo, 1974.)

clear what portion of the deviation from the extreme type-I distribution is due to the low values of the detectability levels and what portion comes from differences between the actual form of variation of λ with M and that given by eq. 6.6. The problem deserves attention because estimates of expected losses due to nonstructural damage may be sensitive to the values of λ for small magnitudes (say below 5.5) and because the evaluation of the level of seismic activity in a region is often made to depend on the recorded numbers of small magnitude shocks and on assumed detectability levels, i.e. of ratios of numbers of detected and occurred earthquakes (Kaila and Narain 1971; Kaila et al., 1972, 1974).

None of the expressions for λ presented in this chapter possess the desirable property that its applicability over a number of non-overlapping regions of the earth's crust implies the validity of an expression of the same form over the addition of those regions, unless some restrictions are imposed on the parameters of each λ. For instance, the addition of expressions like 6.6 gives place to an expression of the same form only if β is the same for all terms in the sum. Similar objections can be made to eq. 6.8. In what follows these forms will be preserved, however, as their accuracy is consistent with

the amount of available information and their adoption offers significant advantages in the evaluation of regional seismicity, as shown later.

6.3.2 *Variation with depth*

Depth of prevailing seismic activity in a region depends on its tectonic structure. For instance, most of the activity in the western coast of the United States and Canada consists of shocks with hypocentral depths in the range of 20–30 km. In other areas, such as the southern coast of Mexico, seismic events can be grouped into two ensembles: one of small shallow shocks and one of earthquakes with magnitudes comprised in a wide range, and with depths whose mean value increases with distance from the shoreline (Fig. 6.10). Figure 6.11 shows the depth distribution of earthquakes with magnitude above 5.9 for the whole circum-Pacific belt.

6.3.3 *Stochastic models of earthquake occurrence*

Mean exceedance rates of given magnitudes are expected averages during long time intervals. For decision-making purposes the times of earthquake occurrence are also significant. At present those times can only be predicted within a probabilistic context.

Let t_i ($i = 1, \ldots, n$) be the unknown times of occurrence of earthquakes generated in a given volume of the earth's crust during a given time interval, and let M_i be the corresponding magnitudes. For the moment it will be assumed that the risk is uniformly distributed throughout the given volume, and hence no attention will be paid to the focal coordinates of each shock.

Classical methods of time-series analysis have been applied by different researchers attempting to devise analytical models for random earthquake sequences. The following approaches are often found in the literature:

(a) Plotting of histograms of waiting times between shocks (Knopoff, 1964; Aki, 1963).

(b) Evaluation of Poisson's index of dispersion, that is of the ratio of the sample variance of the number of shocks to its expected value (Vere-Jones, 1970; Shlien and Toksöz, 1970). This index equals unity for Poisson processes, is smaller for nearly periodic sequences, and is greater than one when events tend to cluster.

(c) Determination of autocovariance functions, that is, of functions representing the covariance of the numbers of events observed in given time intervals, expressed in terms of the time elapsed between those intervals (Vere-Jones, 1970; Shlien and Toksöz, 1970). The autocovariance function of a Poisson process is a Dirac delta function. This feature is characteristic for the Poisson model since it does not hold for any other stochastic process.

(d) The hazard function $h(t)$, defined so that $h(t)\,dt$ is the conditional probability that an event will take place in the interval $(t, t + dt)$ given that

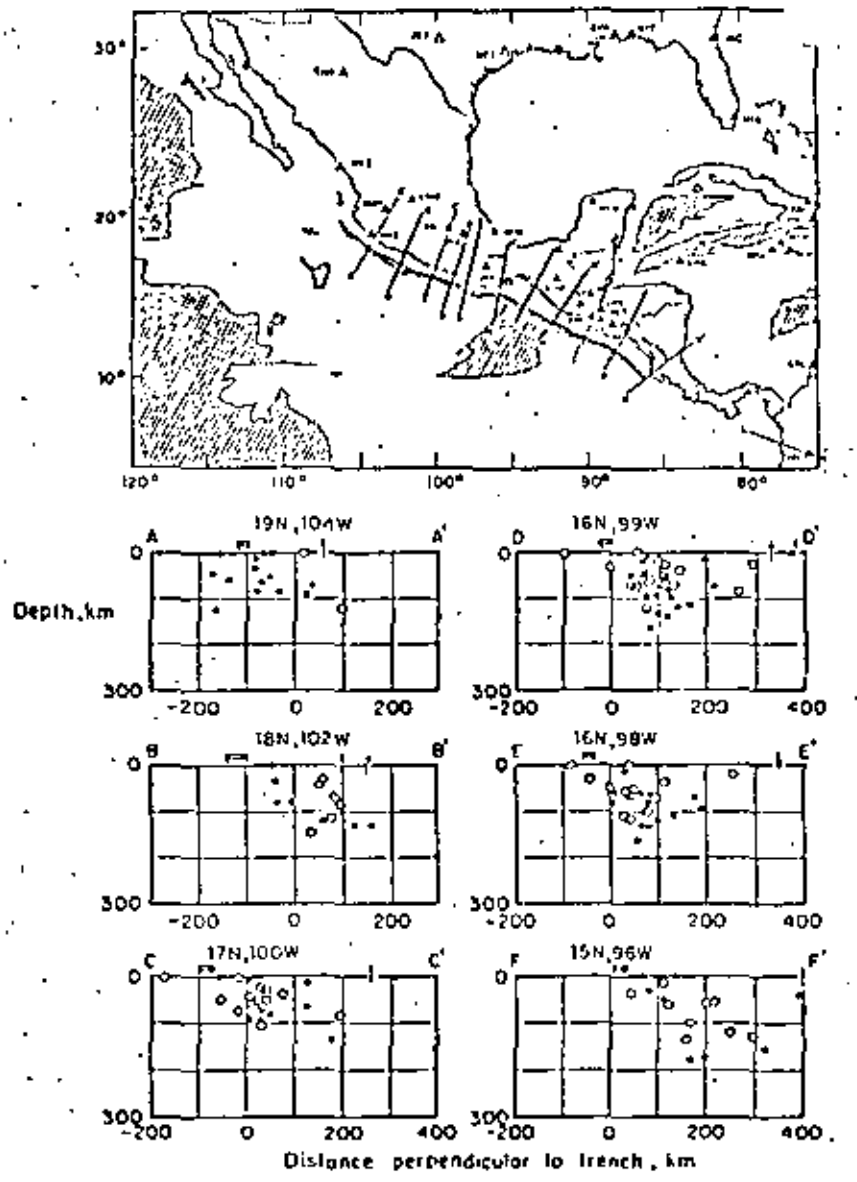

Fig. 6.10. Earthquake hypocenters projected onto a series of vertical sections through Mexico (After Molnar and Sykes, 1969.)

no events have occurred before t. If $F(t)$ is the cumulative probability distribution of the time between events:

$$h(t) = f(t)/[1 - F(t)] \qquad (6.10)$$

where $f(t) = \partial F(t)/\partial t$.

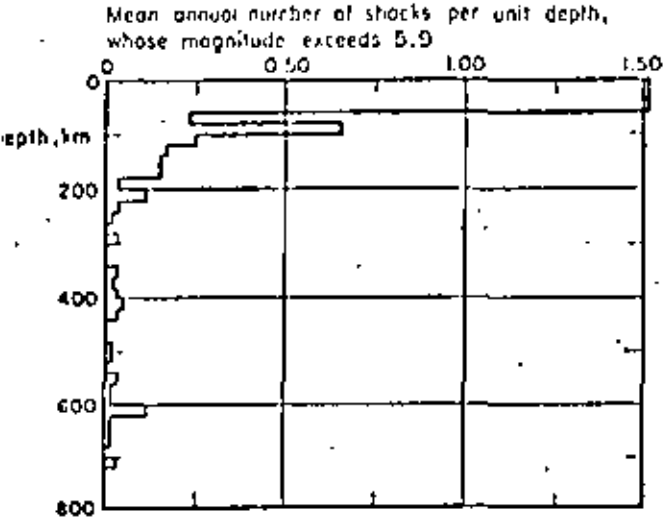

ig. 6.11. Variation of seismicity with depth. Circum-Pacific Belt. (After Newmark and osenblueth, 1971.)

For the Poisson model, $h(t)$ is a constant equal to the mean rate of the process.

6.3.3.1 Poisson model

Most commonly applied stochastic models of seismicity assume that the events of earthquake occurrence constitute a Poisson process and that the M_i's are independent and identically distributed. This assumption implies that the probability of having N earthquakes with magnitude exceeding M during time interval $(0, t)$ equals:

$$P_N = [\exp(-\nu_M t)(\nu_M t)^N]/N! \qquad (6.11)$$

where ν_M is the mean rate of exceedance of magnitude M in the given volume. If N is taken equal to zero in eq. 6.11, one obtains that the probability distribution of the maximum magnitude during time interval t is equal to $\exp(-\nu_M t)$. If ν_M is given by eq. 6.6, the extreme type-I distribution is obtained.

Some weaknesses of this model become evident in the light of statistical information and of an analysis of the physical processes involved: the Poisson assumption implies that the distribution of the waiting time to the next event is not modified by the knowledge of the time elapsed since the last one, while physical models of gradually accumulated and suddenly released energy call for a more general renewal process such that, unlike what happens in the Poisson process, the expected time to the next event decreases as time goes on (Esteva, 1974). Statistical data show that the Poisson assumption may be acceptable when dealing with large shocks throughout the world (Ben-Menahem, 1960), implying lack of correlation between seismicities of different regions; however, when considering small volumes of the earth, of the order of those that can significantly contribute to seismic risk at a site, data often contradict Poisson's model, usually because of clustering of earthquakes in time: the observed numbers of short intervals between events are significantly higher than predicted by the exponential distribution, and values of Poisson's index of dispersion are well above unity (Figs. 6.12 and 6.13). In some instances, however, deviations in the opposite direction have been observed: waiting times tend to be more nearly periodic, Poisson's index of dispersion is smaller than one, and the process can be represented by a renewal model. This condition has been reported, for instance, in the southern coast of Mexico (Esteva, 1974), and in the Kamchatka and Pamir—Hindu Kush regions (Gnisky, 1966 and 1967). The models under discussion also fail to account for clustering in space (Tsuboi, 1956; Gajardo and Lomnitz, 1960), for the evolution of seismicity with time, and for the systematic shifting of active sources along geologic accidents (Allen, Chapter 3 of this book). On account of its simplicity, however, the Poisson process model provides a valuable tool for the formulation of some seismic-risk-related decisions, particularly of those that are sensitive only to magnitudes of events having very long return periods.

6.3.3.2 Trigger models

Statistical analysis of waiting times between earthquakes does not favor the adoption of the Poisson model or of other forms of renewal processes, such as those that assume that waiting times are mutually independent with lognormal or gamma distributions (Shlien and Toksöz, 1970). Alternative models have been developed, most of them of the 'trigger type' (Vere-Jones, 1970), i.e. the overall process of earthquake generation is considered as the superposition of a number of time series, each having a different origin, where the origin times are the events of a Poisson process. In general, let N be the number of events that take place during time interval $(0, t)$, τ_m = origin time of the mth series, $W_m(t, \tau_m)$ the corresponding number of events up to instant t, and n_t the random number of time series initiated in the interval $(0, t)$. The total number of events that occur before instant t is then:

$$N = \sum_{m}^{n_t} W_m(t, \tau_m) \qquad (6.12)$$

If origin times are distributed according to a homogeneous Poisson process with mean rate ν, and all W_m's are identically distributed stochastic processes with respect to $(t - \tau_m)$, it can be shown (Parzen, 1962) that the mean and variance of N can be obtained from:

$$E(N) = \nu \int_0^t E[W(t, \tau)]d\tau \qquad (6.13)$$

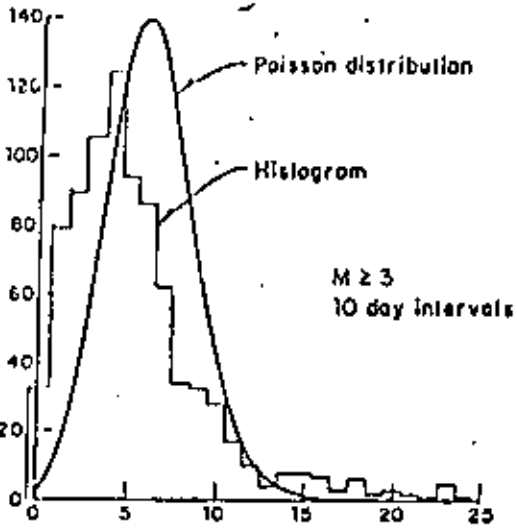

a) Including swarms

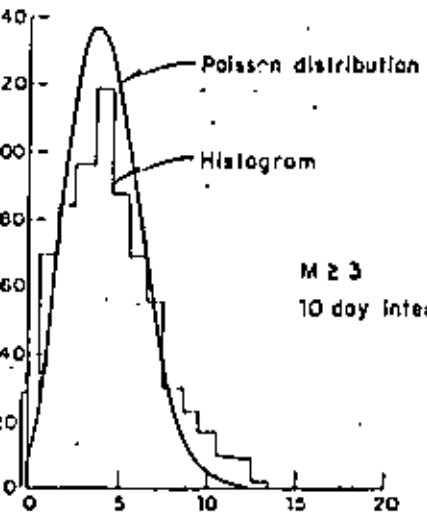

b) Eliminating swarms

Fig. 6.12. Evaluation of Poisson process assumption. (After Knopoff, 1964.)

$$\text{var}(N) = \nu \int_0^t E[W^2(t, \tau)]d\tau \qquad (6.14)$$

Parzen (1962) gives also an expression for the probability generating function $\psi_N(Z; t)$ of the distribution of N in terms of $\psi_W(Z; t, \tau)$, the generating function of each of the component processes:

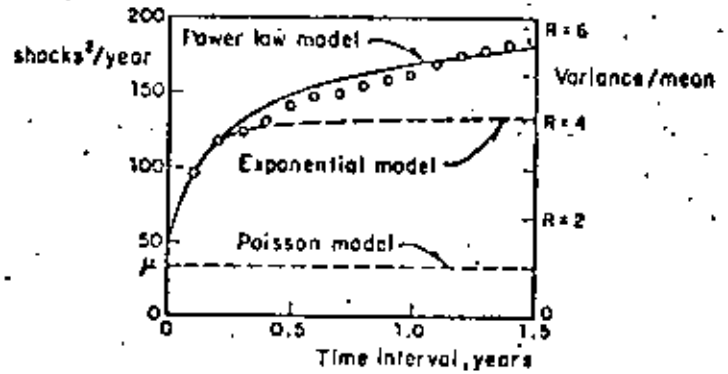

Fig. 6.13. Variance–time curve for New Zealand shallow shocks. (After Vere-Jones, 1966.)

$$\psi_N(Z; t) = \exp\left[-\nu t + \nu \int_0^t \psi_W(Z; t, \tau)d\tau\right] \qquad (6.15)$$

where:

$$\psi_W(Z; t, \tau) = \sum_{n=0}^{\infty} Z^n P\{W(t, \tau) = n\} \qquad (6.16)$$

and the probability mass function of N can be obtained from $\psi_N(Z; t)$ by recalling that:

$$\psi_N(Z; t) = \sum_{n=0}^{\infty} Z^n P\{N = n\}$$

expanding ψ_N in power series of Z, and taking $P\{N = n\}$ equal to the coefficient of Z^n in that expansion. For instance, if it is of interest to compute $P\{N = 0\}$, expansion of $\psi_N(Z; t)$ in a Taylor's series with respect to $Z = 0$ leads to:

$$\psi_N(Z; t) = \psi_N(0; t) + Z\psi'_N(0; t) + \frac{Z^2}{2!}\psi''_N(0; t) + \ldots \qquad (6.17)$$

where the prime signifies derivative with respect to Z. From the definition of ψ_N, $P\{N = 0\} = \psi_N(0; t)$.

Because the component processes of 'trigger'-type time series appear overlapped in sample histories, their analytical representation usually entails study of a number of alternative models, estimation of their parameters, and comparison of model and sample properties — often second-order properties (Cox and Lewis, 1966).

Vere-Jones models. Applicability of some general 'trigger' models to rep-

resent local seismicity processes was discussed in a comprehensive paper by Vere-Jones (1970), who calibrated them mainly against records of seismic activity in New Zealand. In addition to simple and compound Poisson processes (Parzen, 1962), he considered Neyman-Scott and Bartlett-Lewis models, both of which assume that earthquakes occur in clusters and that the number of events in each cluster is stocastically independent of its origin time. In the Neyman-Scott model, the process of clusters is assumed stationary and Poisson, and each cluster is defined by p_N, the probability mass function of its number of events, and $\Lambda(t)$, the cumulative distribution function of the time of an event corresponding to a given cluster, measured from the cluster origin. The Bartlett-Lewis model is a special case of the former, where each cluster is a renewal process that ends after a finite number of renewals. In these models the conditional probability of an event taking place during the interval $(t, t + dt)$, given that the cluster consists of N shocks, is equal to $N\lambda(t)dt$, where $\lambda(t) = \partial\Lambda(t)/\partial t$.

Because clusters overlap in time they cannot easily be identified and separated. Estimation of process parameters is accomplished by assuming different sets of those parameters and evaluating the corresponding goodness of fit with observed data.

Various alternative forms of Neyman-Scott's model were compared by Vere-Jones with observed data on the basis of first- and second-order statistics: hazard functions, interval distributions (in the form of power spectra) and variance time curves. The statistical record comprises about one thousand New Zealand earthquakes with magnitudes greater than 4.5, recorded from 1942 to 1961. Figures 6.13—6.15 show results of the analysis for shallow New Zealand shocks as well as the comparison of observed data with several alternative models. The process of cluster origins is Poisson in all cases, but the distributions of cluster sizes (N) and of times of events within clusters differ among the various instances: in the Poisson model no clustering takes place (the distribution of N is a Dirac delta function centered at $N = 1$) while in the exponential and in the power-law models the distribution of N is extremely skewed towards $N = 1$, and $\Lambda(t)$ is taken respectively as $1 - e^{-\lambda t}$

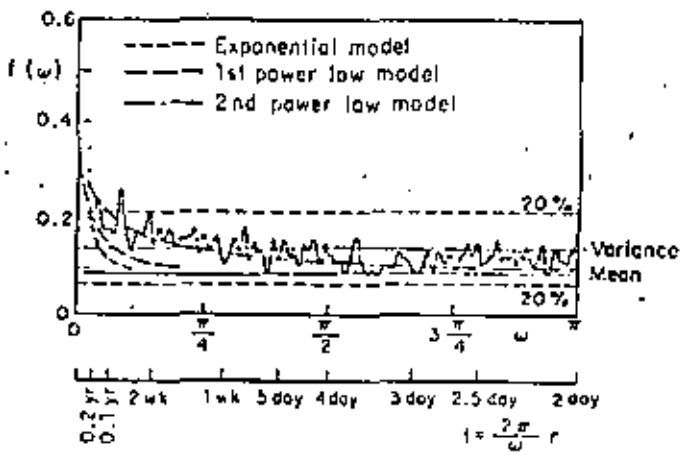

Fig. 6.14. Smoothed periodogram for New Zealand shallow shocks. (After Vere-Jones, 1966.)

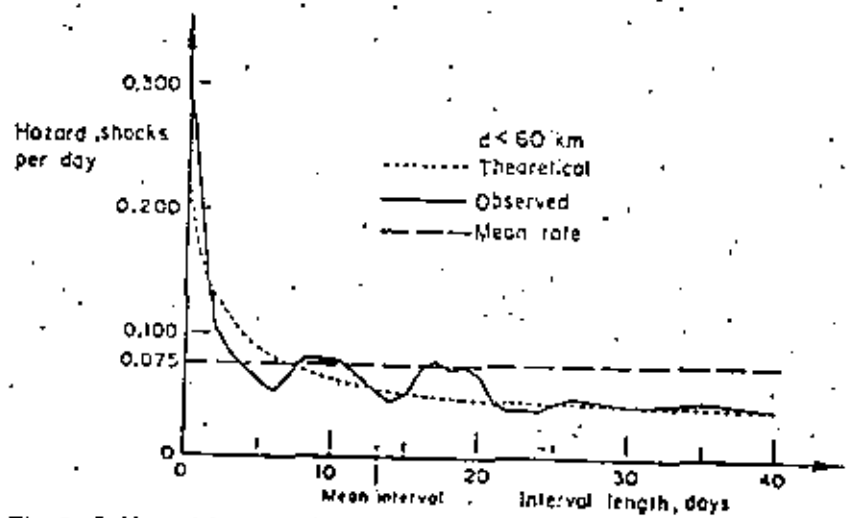

Fig. 6.15. Hazard function for New Zealand shallow shocks. (After Vere-Jones, 1970.)

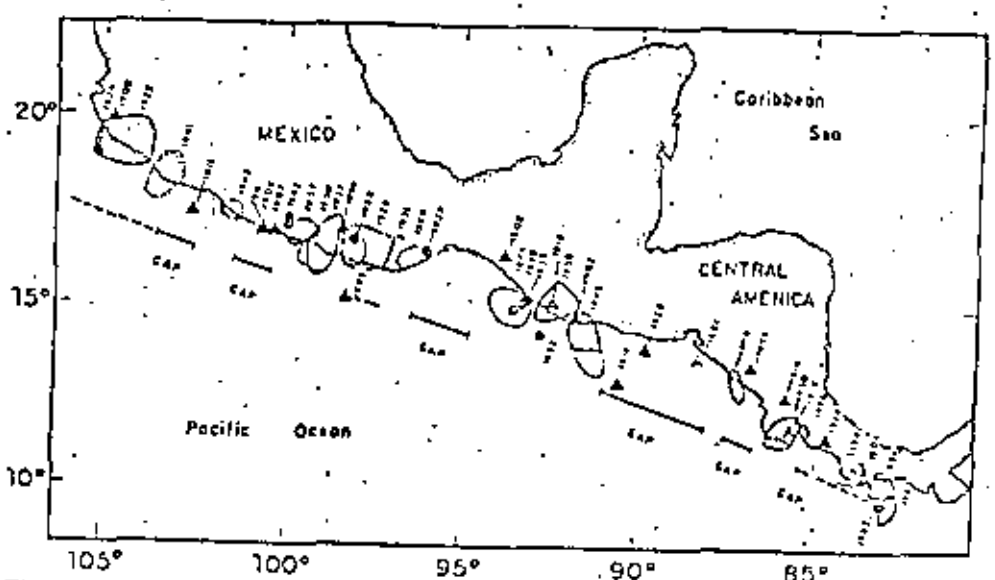

Fig. 6.16. Rupture zones and epicenters of large shallow Middle American earthquakes of this century. (After Kelleher et al., 1973.)

and $1 - [c/(c+t)]^{\delta}$ for $t \geq 0$, and as zero for $t < 0$, where λ, c, and δ are positive parameters. In Figs. 6.13–6.15, $\delta = 0.25$, $c = 2.3$ days, and $\lambda = 0.061$ shocks/day. The significance of clustering is evidenced by the high value of Poisson's dispersion index in Fig. 6.13, while no significant periodicity can be inferred from Fig. 6.14. Both figures show that the power-law model provides the best fit to the statistics of the samples. A similar analysis for New Zealand's deep shocks shows much less clustering: Poisson's dispersion index equals 2, and the hazard function is nearly constant with time.

Still, data reported by Gaisky (1967) have hazard functions that suggest models where the cluster origins as well as the clusters themselves may be represented by renewal processes. Mean return periods are of the order of several months, and hence these processes do not correspond, at least in the time scale, to the process of alternate periods of activity and quiescense of some geological structures cited by Kelleher et al. (1973), which have led to the concept of 'temporal seismic gaps', discussed below.

Simplified trigger models. Shlien and Toksöz (1970) proposed a simple particular case of the Neyman-Scott process; they lumped together all earthquakes taking place during non-overlapping time intervals of a given length and deemed them as clusters for which $\lambda(t)$ was a Dirac delta function. Working with one-day intervals, they assumed the number of events per cluster to be distributed in accordance with the discrete Pareto law and applied a maximum-likelihood criterion to the information consisting of 35 000 earthquakes reported by the USCGS from January 1971 to August 1968. The model proposed represents reasonably well both the distribution of the number of earthquakes in one-day intervals and the dispersion index. However, owing to the assumption that no cluster lasts more than one day, the model fails to represent the autocorrelation function of the daily numbers of shocks for small time lags. The degree of clustering is shown to be a regional function, and to diminish with the magnitude threshold value and with the focal depth.

Aftershock sequences. The trigger processes described have been branded as reasonable representations of regional seismic activity, even when aftershock sequences and earthquake swarms are suppressed from statistical records, however arbitrary that suppression may be. The most significant instances of clustering are related, however, to aftershock sequences which often follow shallow shocks and only rarely intermediate and deep events. Persistence of large numbers of aftershocks for a few days or weeks has propitiated the detailed statistical analysis of those sequences since last century. Omori (1894) pointed out the decay in the mean rate of aftershock occurrence with t, the time elapsed since the main shock; he expressed that rate as inversely proportional to $t + q$, where q is an empirical constant. Utsu (1961) proposed a more general expression, proportional to $(t + c)^{-\xi}$, where ξ is a constant; Utsu's proposal is consistent with the power-law expression for $\Lambda(t)$ presented above.

Lomnitz and Hax (1966) proposed a clustering model to represent aftershock sequences; it is a modified version of Neyman and Scott's model, where the process of cluster origins is non-homogeneous Poisson with mean rate decaying in accordance with Omori's law, the number of events in each cluster has a Poisson distribution, and $\Lambda(t)$ is exponential. All the results and methods of analysis described by Vere-Jones (1970) for the stationary process of cluster origins can be applied to the nonstationary case through a transformation of the time scale. Fitting of parameters to four aftershock sequences was accomplished through use of the second-order information of the sample defined on a transformed time scale. By applying this criterion to earthquake sets having magnitudes above different threshold values it was noticed that the degree of clustering decreases as the threshold value increases.

The magnitude of the main shock influences the number of aftershocks and the distribution of their magnitudes and, although the rate of activity decreases with time, the distribution of magnitudes remains stable throughout each sequence (Lomnitz, 1966; Utsu, 1962; Drakopoulos, 1971). Equation 6.6 represents fairly well the distribution of magnitudes observed in most aftershock sequences. Values of β range from 0.9 to 3.9 and decrease as the depth increases. Since values of β for regular (main) earthquakes are usually estimated from relatively small numbers of shocks generated throughout crust volumes much wider than those active during aftershock sequences, no relation has been established among β-values for series of both types of events. The parameters of Utsu's expression for the decay of aftershock activity with time have been estimated for several sequences, for instance those following the Aleutian earthquake of March 9, 1957, the Central Alaska earthquake of April 7, 1958, and the Southeastern Alaska earthquake of July 10, 1958 (Utsu, 1962), with magnitudes equal to 8.3, 7.3, and 7.9, respectively; c (in days) was 0.37, 0.40, and 0.01, while ξ was 1.05, 1.05 and 1.13, respectively. The relationship of the total number of aftershocks whose magnitude exceeds a given value with the magnitude of the main shock was studied by Drakopoulos (1971) for 140 aftershock sequences in Greece from 1912 to 1968. His results can be expressed by $N(M) = A \exp(-\beta M)$, where $N(M)$ is the total number of aftershocks with magnitude greater than M, and A is a function of M_0, the magnitude of the main shock:

$$A = \exp(3.62\,\beta + 1.1 M_0 - 3.46) \qquad (6.18)$$

Formulation of stochastic process models for given earthquake sequences is feasible once this relationship and the activity decay law are available for the source of interest. For seismic-risk estimation at a given site the spatial distribution of aftershocks may be as significant as the distribution of magnitudes and the time variation of activity, particularly for sources of relatively large dimensions.

6.3.3.3 Re[illegible] process models

The trigger models described are based on information about earthquakes with magnitudes above relatively low thresholds recorded during time intervals of at most ten years. The degrees of clustering observed and the distributions of times between clusters cannot be extrapolated to higher magnitude thresholds and longer time intervals without further study.

Available information shows beyond doubt that significant clustering is the rule, at least when dealing with shallow shocks. However, there is considerable ground for discussion on the nature of the process of cluster origins during intervals of the order of one century or longer. While lack of statistical data hinders the formulation of seismicity models valid over long time intervals, qualitative consideration of the physical processes of earthquake generation may point to models which at least are consistent with the state of knowledge of geophysical sciences. Thus, if strain energy stored in a region grows in a more or less systematic manner, the hazard function should grow with the time elapsed since the last event, and not remain constant as the Poisson assumption implies. The concept of a growing hazard function is consistent with the conclusions of Kelleher et al. (1973) concerning the theory of periodic activation of *seismic gaps*. This theory is partially supported by results of nearly qualitative analysis of the migration of seismic activity along a number of geological structures. An instance is provided by the southern coast of Mexico, one of the most active regions in the world. Large shallow shocks are generated probably by the interaction of the continental mass and the subductive oceanic Cocos plate that underthrusts it and by compressive or flexural failure of the latter (Chapter 2). Seismological data show significant gaps of activity along the coast during the present century and not much is known about previous history (Fig. 6.16). Along these gaps, seismic-risk estimates based solely on observed intensities are quite low, although no significant difference is evident in the geological structure of these regions with respect to the rest of the coast, save some transverse faults which divide the continental formation into several blocks. Without looking at the statistical records a geophysicist would assign equal risk throughout the area. On the basis of seismicity data, Kelleher et al. have concluded that activity migrates along the region, in such a manner that large earthquakes tend to occur at seismic gaps, thus implying that the hazard function grows with time since the last earthquake. Similar phenomena have been observed in other regions; of particular interest is the North Anatolian fault where activity has shifted systematically along it from east to west during the last forty years (Allen, 1969).

Conclusions relative to activation of seismic gaps are controversial because the observation periods have not exceeded one cycle of each process. Nevertheless, those conclusions point to the formulation of stochastic models of seismicity that reflect plausible features of the geophysical processes.

These considerations suggest the use of renewal-process models to represent sequences of individual shocks or of clusters. Such models are characterized because times between events are independent and identically distributed. The Poisson process is a particular renewal model for which the distribution of the waiting time is exponential. Wider generality is achieved, without much loss of mathematical tractability, if inter-event times are supposed to be distributed in accordance with a gamma function:

$$f_T(t) = \frac{\nu}{(k-1)!}(\nu t)^{k-1}\, e^{-\nu t} \qquad (6.19)$$

which becomes the exponential distribution when $k = 1$. If $k < 1$, short intervals are more frequent and the coefficient of variation is greater than in the Poisson model; if $k > 1$, the reverse is true. Shlien and Toksöz (1970) found that gamma models were unable to represent the sequences of individual shocks they analyzed; but these authors handled time intervals at least an order of magnitude shorter than those referred to in this section.

On the basis of hazard function estimated from sequences of small shocks in the Hindu-Kush, Vere-Jones (1970) deduces the validity of 'branching renewal process' models, in which the intervals between cluster centers, as well as those between cluster members, constitute renewal processes.

Owing to the scarcity of statistical information, reliable comparisons between alternate models will have to rest partially on simulation of the process of storage and liberation of strain energy (Burridge and Knopoff, 1967; Veneziano and Cornell, 1973).

6.3.4 Influence of the seismicity model on seismic risk

Nominal values of investments made at a given instant increase with time when placing them at compound interest rates, i.e. when capitalizing them. Their real value — and not only the nominal one — will also grow, provided the interest rate overshadows inflation. Conversely, for the purpose of making design decisions, nominal values of expected utilities and costs inflicted upon in the future have to be converted into present or actualized values, which can be directly compared with initial expenditures. Descriptions of seismic risk at a site are insufficient for that purpose unless the probability distributions of the times of occurrence of different intensities — or magnitudes at neighbouring sources — are stipulated; this entails more than simple magnitude-recurrence graphs or even than maximum feasible magnitude estimates.

Immediately after the occurrence of a large earthquake, seismic risk is abnormally high due to aftershock activity and to the probability that damage inflicted by the main shock may have weakened natural or man-made structures if emergency measures are not taken in time. When aftershock activity has ceased and damaged systems have been repaired, a normal risk level is attained, which depends on the probability-density functions of the waiting times to the ensuing damaging earthquakes.

For the purpose of illustration, let it be assumed that a fixed and deterministically known damage D_0 occurs whenever a magnitude above a given value is generated at a given source. If $f(t)$ is the probability-density function of the waiting time to the occurrence of the damaging event, and if the risk level is sufficiently low that only the first failure is of concern, the expected value of the actualized cost of damage is (see Chapter 9):

$$\bar{D} = D_0 \int_0^\infty e^{-\gamma t} f(t) dt \qquad (6.20)$$

where γ is the discount (or compound interest) coefficient and the overbar denotes expectation. If the process is Poisson with mean rate ν, then $f(t)$ is exponential and $\bar{D} \simeq D_0\ \nu/\gamma$; however, if damaging events take place in clusters and most of the damage produced by each cluster corresponds to its first event, the computation of $\bar{D}$ should make use of the mean rate ν corresponding to the clusters, instead of that applicable to individual events. Table 6.II shows a comparison of seismic risk determined under the alternative assumptions of a Poisson and a gamma model ($k = 2$), both with the same mean return period, k/ν (Esteva, 1974). Three descriptions of risk are presented as functions of the time t_0 elapsed since the last damaging event: T_1, the expected time to the next event, measured from instant t_0; the expected value of the present cost of failure computed from eq. 6.20, and the hazard function (or mean failure rate). Since clustering is neglected, risk of aftershock occurrence must be either included in D_0 or superimposed on that displayed in the table.

This table shows very significant differences among risk levels for both processes. At small values of t_0, risk is lower for the gamma process, but it grows with time, until it outrides that for the Poisson process, which remains constant. The differences shown clearly affect engineering decisions.

TABLE 6.II

Comparison of Poisson and gamma processes

$t_0\ \nu/k$	$\bar{T}_1\ \nu/k$	Poisson process, $k = 1$		hk/ν	$T_1\ \nu/k$	Gamma process, $k = 2$		hk/ν
		D/D_0				D/D_0		
		$\gamma k/\nu = 10$	$\gamma k/\nu = 100$			$\gamma k/\nu = 10$	$hk/\nu = 100$	
0					1.0	0.0278	0.0004	0
0.1					0.92	0.0511	0.0036	0.367
0.2					0.86	0.0675	0.0050	0.667
0.5					0.75	0.0973	0.0100	1.333
1	1.0	0.0909	0.0099	1.0	0.67	0.120	0.0132	2.000
2					0.60	0.139	0.0158	2.667
5					0.54	0.154	0.0179	3.333
10					0.52	0.160	0.0187	3.633
					0.50	0.167	0.0196	4.000

6.4 ASSESSMENT OF LOCAL SEISMICITY

Only exceptionally can magnitude-recurrence relations for small volumes of the earth's crust and statistical correlation functions of the process of earthquake generation be derived exclusively from statistical analysis of recorded shocks. In most cases this information is too limited for that purpose and it does not always reflect geological evidence. Since the latter, as well as its connection with seismicity, is beset with wide uncertainty margins, information of different nature has to be evaluated, its uncertainty analyzed, and conclusions reached consistent with all pieces of information. A probabilistic criterion that accomplishes this is presented here: on the basis of geotectonic data and of conceptual models of the physical processes involved, a set of alternate assumptions can be made concerning the functions in question (magnitude recurrence, time, and space correlation) and an initial probability distribution assigned thereto; statistical information is used to judge the likelihood of each assumption, and a posterior probability distribution is obtained. How statistical information contibutes to the posterior probabilities of the alternate assumptions depends on the extent of that information and on the degree of uncertainty implied by the initial probabilities. Thus, if geological evidence supports confidence in a particular assumption or range of assumptions, statistical information should not greatly modify the initial probabilities. If, on the other hand, a long and reliable statistical record is available, it practically determines the form and parameters of the mathematical model selected to represent local seismicity.

6.4.1 Bayesian estimation of seismicity

Bayesian statistics provide a framework for probabilistic inference that accounts for prior probabilities assigned to a set of alternate hypothetical models of a given phenomenon as well as for statistical samples of events related to that phenomenon. Unlike conventional methods of statistical inference, Bayesian methods give weight to probability measures obtained from samples or from other sources; numbers, coordinates and magnitudes of earthquakes observed in given time intervals serve to ascertain the probable validity of each of the alternative models of local seismicity that can be postulated on the grounds of geological evidence. Any criterion intended to weigh information of different nature and different degrees of uncertainty should lead to probabilistic conclusions consistent with the degree of confidence attached to each source of information. This is accomplished by Bayesian methods.

Let H_i ($i = 1, \ldots, n$) be a comprehensive set of mutually exclusive assumptions concerning a given, imperfectly known phenomenon and let A be the observed outcome of such a phenomenon. Before observing outcome A we assign an initial probability $P(H_i)$ to each hypothesis. If $P(A|H_i)$ is the probability of A in case hypothesis H_i is true, then Bayes' theorem (Raiffa and Schlaifer, 1968) states that:

$$P(H_i|A) = P(H_i)\frac{P(A|H_i)}{\sum_j P(H_j)P(A|H_j)} \tag{6.21}$$

The first member in this equation is the (posterior) probability that assumption H_i is true, given the observed outcome A.

In the evaluation of seismic risk, Bayes' theorem can be used to improve initial estimates of $\lambda(M)$ and its variation with depth in a given area as well as those of the parameters that define the shape of $\lambda(M)$ or, equivalently, the conditional distribution of magnitudes given the occurrence of an earthquake. For that purpose, take $\lambda(M)$ as the product of a rate function $\lambda_L = \lambda(M_L)$ by a shape function $G^c(M,B)$, equal to the conditional complementary distribution of magnitudes given the occurrence of an earthquake with $M \geq M_L$, where M_L is the magnitude threshold of the set of statistical data used in the estimation, and B is the vector of (uncertain) parameters $B_1, \ldots, B_r$ that define the shape of $\lambda(M)$. For instance, if $\lambda(M)$ is taken as given by eq. 6.8, B is a vector of three elements equal respectively to β, β_1, and M_0; if eq. 6.9 is adopted, B is defined by b and M_0.

The initial distribution of seismicity is in this case expressed by the initial joint probability density function of λ_L and B: $f(\lambda_L, B)$. The observed outcome A can be expressed by the magnitudes of all earthquakes generated in a given source during a given time interval. For instance, suppose that N earthquakes were observed during time interval t and that their magnitudes were $m_1, m_2, \ldots, m_N$. Bayes' expression takes the form:

$$f''(\lambda_L, B|m_1, \ldots, m_N; t) = f(\lambda_L, B)\frac{P[m_1, m_2, \ldots, m_N; t|\lambda_L, B]}{\int\int P[m_1, m_2, \ldots, m_N; t|l, b]f(l,b)\,dl\,db} \tag{6.22}$$

where $f''(.)$ is the posterior probability density function, and l and b are dummy variables that stand for all values that may be taken by λ_L and B, respectively. Estimation of λ_L can usually be formulated independently of that of the other parameters. The observed fact is then expressed by N_L, the number of earthquakes with magnitude above M_L during time t, and the following expression is obtained, as a first step in the estimation of $\lambda(M)$:

$$f''(\lambda_L|N_L; t) = f(\lambda_L)\frac{P(N_L; t|\lambda_L)}{\int P(N_L; t|l)f(l)\,dl} \tag{6.23}$$

6.4.1.1 Initial probabilities of hypothetical models

Where statistical information is scarce, seismicity estimates will be very sensitive to initial probabilities assigned to alternative hypothetical models; the opinions of geologists and geophysicists about probable models, about the parameters of these models, and the corresponding margins of uncertainty should be adequately interpreted and expressed in terms of a function f', as required by equations similar to 6.22 and 6.23. Ideally, these opinions should be based on the formulation of potential earthquake sources and on their comparison with possibly similar geotectonic structures. This is usually done by geologists, more qualitatively than quantitatively, when they estimate M_0. Initial estimates of λ_L are seldom made, despite the significance of this parameter for the design of moderately important structures (see Chapter 9).

Analysis of geological information must consider local details as well as general structure and evolution. In some areas it is clear that all potential earthquake sources can be identified by surface faults, and their displacements in recent geological times measured. When mean displacements per unit time can be estimated, the order of magnitude of creep and of energy liberated by shocks and hence of the recurrence intervals of given magnitudes can be established (Wallace, 1970; Davies and Brune, 1971), the corresponding uncertainty evaluated, and an initial probability distribution assigned. The fact that magnitude-recurrence relations are only weakly correlated with the size of recent displacements is reflected in large uncertainties (Petrushevsky, 1966).

Application of the criterion described in the foregoing paragraph can be unfeasible or inadequate in many problems, as in areas where the abundance of faults of different sizes, ages, and activity, and the insufficient accuracy with which focal coordinates are determined preclude a differentiation of all sources. Regional seismicity may then be evaluated under the assumption that at least part of the seismic activity is distributed in a given volume rather than concentrated in faults of different importance. The same situation would be faced when dealing with active zones where there is no surface evidence of motions. Hence, consideration of the overall behavior of complex geological structures is often more significant than the study of local details.

Not much work has been done in the analysis of the overall behavior of large geological structures with respect to the energy that can be expected to be liberated per unit volume and per unit time in given portions of those structures. Important research and applications should be expected, however, since, as a result of the contribution of plate-tectonics theory to the understanding of large-scale tectonic processes, the numerical values of some of the variables correlated with energy liberation are being determined, and can be used at least to obtain orders of magnitude of expected activity along plate boundaries. Far less well understood are the occurrence of shocks in apparently inactive regions of continental shields and the behavior of complex continental blocks or regions of intense folding, but even there some

progress is expected in the study of accumulation of stresses in the crust.

Knowledge of the geological structure can serve to formulate initial probability distributions of seismicity even when quantitative use of geophysical information seems beyond reach. Initial probability distributions of local seismicity parameters λ_{t_0}, b in the small volumes of the earth's crust that contribute significantly to seismic risk at a site, can be assigned by comparison with the average seismicity observed in wider areas of similar tectonic characteristics, or where the extent and completeness of statistical information warrant reliable estimates of magnitude-recurrence curves (Esteva, 1969). In this manner we can, for instance, use the information about the average distribution of the depths of earthquakes of different magnitudes throughout a seismic province to estimate the corresponding distribution in an area of that province, where activity has been low during the observation interval, even though there might be no apparent geophysical reason to account for the difference. Similarly, the expected value and coefficient of variation of λ_{t_0} in a given area of moderate or low seismicity (as a continental shield) can be obtained from the statistics of the motions originated at all the supposedly stable or aseismic regions in the world.

The significance of initial probabilities in seismic risk estimates, against the weight given to purely statistical information, becomes evident in the example of Fig. 6.16: if Kelleher's theory about activation of seismic gaps is true, risk is greater at the gaps than anywhere else along the coast; if Poisson models are deemed representative of the process of energy liberation, the extent of statistical information is enough to substantiate the hypothesis of reduced risk at gaps. Because both models are still controversial, and represent at most two extreme positions concerning the properties of the actual process, risk estimates will necessarily reflect subjective opinions.

6.4.1.2 Significance of statistical information

Estimation of λ_{t_0}. Application of eq. 6.23 to estimate λ_{t_0} independently of other parameters will be first discussed, because it is a relatively simple problem and because λ_{t_0} is usually more uncertain than M_0 and much more so than β.

A model as defined by eq. 6.19 will be assumed to apply. If the possible assumptions concerning the values of λ_{t_0} constitute a continuous interval, the initial probabilities of the alternative hypotheses can be expressed in terms of a probability-density function of λ_{t_0}. If, in addition, a certain assumption is made concerning the form of this probability-density function, only the initial values of $E(\lambda_{t_0})$ and $V(\lambda_{t_0})$ have to be assumed. It is advantageous to assign to $\nu = k/E(T)$ a gamma distribution. Then, if ρ and μ are the parameters of this initial distribution of ν, if k is assumed to be known, and if the observed outcome is expressed as the time t_n elapsed during $n+1$ consecutive events (earthquakes with magnitude $\geq M_0$), application of eq. 6.23 leads to the conclusion that the posterior probability function of ν is

also gamma, now with parameters $\rho + nk$ and $\mu + t_n$. The initial and the posterior expected values of ν are respectively equal to ρ/μ, and to $(\rho + nk)/(\mu + t_n)$. When initial uncertainty about ν is small, ρ and μ will be large and the initial and the posterior expected values of ν will not differ greatly. On the other hand, if only statistical information were deemed significant, ρ and μ should be given very small values in the initial distribution, and $E(\nu)$, and hence λ_{t_0}, will be practically defined by n, k, and t_n. This means that the initial estimates of geologists should not only include expected or most probable values of the different parameters, but also statements about ranges of possible values and degrees of confidence attached to each.

In the case studied above only a portion of the statistical information was used. In most cases, especially if seismic activity has been low during the observation interval, significant information is provided by the durations of the intervals elapsed from the initiation of observations to the first of the $n+1$ events considered, and from the last of these events until the end of the observation period. Here, application of eq. 6.23 leads to expressions slightly more complicated than those obtained when only information about t_n is used.

The particular case when the statistical record reports no events during at least an interval $(0, t_0)$ comes up frequently in practical problems. The probability-density function of the time T_1 from t_0 to the occurrence of the first event must account for the corresponding shifting of the time axis. Furthermore, if the time of occurrence of the last event before the origin is unknown, the distribution of the waiting time from $t = 0$ to the first event coincides with that of the *excess life* in a renewal process at an arbitrary value of t that approaches infinity (Parzen, 1962). For the particular case when the waiting times constitute a gamma process, T_1 is measured from $t = 0$, T is the waiting time between consecutive events, and it is known that $T_1 \geq t_0$, the conditional density function of $\tau_1 = (T_1 - t_0)/E(T)$ is given by eq. 6.24 (Esteva, 1974), where $u_0 = t_0/E(T)$:

$$f_{\tau_1}(u|T_1 \geq t_0) = \frac{\sum_{m=1}^{k} \frac{k}{(m-1)!} [k(u+u_0)]^{m-1}}{\sum_{m=1}^{k} \sum_{n=1}^{m} \frac{1}{(n-1)!} (ku_0)^{n-1}} e^{-ku} \qquad (6.24)$$

Consider now the implications of Bayesian analysis when applied to one of the seismic gaps in Fig. 6.16, under the conditions implicit in eq. 6.24. An initial set of assumptions and corresponding probabilities was adopted as described in the following. From previous studies referring to all the southern coast of Mexico, local seismicity in the gap area (measured in terms of λ for $M \geq 6.5$) was represented by a gamma process with $k = 2$. An initial

probability density function for ν was adopted such that the expected value of $\lambda(6.5)$ for the region coincided with its average throughout the complete seismic province. Two values of ρ were considered: 2 and 10, which correspond to coefficients of variation of 0.71 and 0.32, respectively. Values in Table 6.III were obtained for the ratio of the final to the initial expected values of ν, in terms of u_0.

The last two columns in the table contain the ratios of the computed values of $E''(T_1)$ and $E''(T)$ when ν is taken as equal respectively to its initial or to its posterior expected value. This table shows that, for $\rho = 10$, that is, when uncertainty attached to the geologically based assumptions is low, the expected value of the time to the next event keeps decreasing, in accordance with the conclusions of Kelleher et al. (1973). However, as time goes on and no events occur, the statistical evidence leads to a reduction in the estimated risk, which shows in the increased conditional expected values of T_1. For $\rho = 2$, the geological evidence is less significant and risk estimates decrease at a faster rate

TABLE 6.III

Bayesian estimates of seismicity in one seismic gap

$u_0 = t_0/E'(T)$	$E''(\nu)/E'(\nu)$		$E''(T_1 \mid T_1 > t_0)/E'(T)$	
	$\rho = 2$	$\rho = 10$	$\rho = 2$	$\rho = 10$
0	1.0	1.0	0.75	0.75
0.1	0.95	0.99	0.76	0.74
0.5	0.75	0.94	0.91	0.71
1	0.58	0.87	1.14	0.73
5	0.20	0.54	3.11	1.05
10	0.11	0.36	5.47	1.55
20	0.06	0.22	10.50	2.48

6.4.1.3 Bayesian estimation of jointly distributed parameters

In the general case, estimation of B will consist in the determination of the posterior Bayesian joint probability function of its components, taking as statistical evidence the relative frequencies of observed magnitudes. Thus, if event A is described as the occurrence of N shocks, with magnitudes $m_1, \ldots, m_N$, and b_i ($i = 1, \ldots, r$) are values that may be adopted by the components of vector B being estimated, eq. 6.21 becomes:

$$f''_B(b_1, \ldots, b_r|A) = \frac{f'_B(b_1, \ldots, b_r)P(A|b_1, \ldots, b_r)}{\int \ldots \int f'_B(u_1, \ldots, u_r)P(A|u_1, \ldots, u_r)du_1, \ldots, du_r} \tag{6.25}$$

where $P(A|u_1, \ldots, u_r)$ is proportional to:

$$\prod_{i=1}^{N} g(m_i|u_1, \ldots, u_r)$$

and $g(m) = -\partial G^*(m)/\partial m$.

Closed-form solutions for f'' as given by eq. 6.25 are not feasible in general. For the purpose of evaluating risk, however, estimates of the posterior first and second moments of f'' can be obtained from eq. 6.25, making use of available first-order approximations (Benjamin and Cornell, 1970; Rosenblueth, 1975). Thus, the posterior expected value of B_i is given by $\int f''_{B_i}(u)\, u\, du$, where $f''_{B_i}(u_i) = \int \ldots \int f''_B(u_1, \ldots, u_r)\, du_1, \ldots, du_r$ and the multiple integral is of order $r - 1$, because it is not extended to the dominion of B_i. Hence:

$$E''(B_i) = \frac{E'_B[B_i P(A|B_1, \ldots, B_r)]}{E'_B[P(A|B_1, \ldots, B_r)]} \tag{6.26}$$

where E' and E'' stand for initial and posterior expectation, and subscript B means that expectation is taken with respect to all the components of B. Likewise, the following *posterior moments* can be obtained:

Covariance of B_i and B_j

$$\mathrm{Cov}''(B_i, B_j) = \frac{E'_B[B_i B_j P(A|B_1, \ldots, B_r)]}{E'_B[P(A|B_1, \ldots, B_r)]} - E''(B_i)E''(B_j) \tag{6.27}$$

Expected value of $\lambda(M)$

$$E''[\lambda(M)] = E''(\lambda_1)E''[G^*(M; B)] = E''(\lambda_1)\frac{E'_B[G^*(M; B)P(A|B_1, \ldots, B_r)]}{E'_B[P(A|B_1, \ldots, B_r)]} \tag{6.28}$$

Marginal distributions. The posterior expectation of $\lambda(M)$ is in some cases all that is required to describe seismicity for decision-making purposes. Often, however, uncertainty in $\lambda(M)$ must also be accounted for. For instance, the probability of exceedance of a given magnitude during a given time interval has to be obtained as the expectation of the corresponding probabilities over all alternative hypotheses concerning $\lambda(M)$. In this manner it can be shown that, if the occurrence of earthquakes is a Poisson process and the Bayesian distribution of λ_L is gamma with mean $\bar{\lambda}_L$ and coefficient of variation V_L, the marginal distribution of the number of earthquakes is negative binomial with mean $\bar{\lambda}_L$. In particular, the marginal probability of zero events during time interval t — equivalently, the complementary distribution function of the waiting time between events — is equal to $(1 + t/t^*)^{-r^*}$, where $r^* = V_L^{-2}$ and $t^* = r^*/\bar{\lambda}_L$. The marginal probability-density function of the waiting time, that should be substituted in eq. 6.20, is $\bar{\lambda}_L(1 + t/t^*)^{-r^*-1}$, which tends to the exponential probability function as r^* and t^* tend to infinity (and $V_L \to 0$) while their ratio remains equal to $\bar{\lambda}_L$.

Bayesian uncertainty tied to the joint distribution of all seismicity parameters (λ_L, B_1, ..., B_r) can be included in the computation of the probability of occurrence of a given event Z by taking the expectation of that probability with respect to all parameters:

$$P(Z) = E_{\lambda_L, B}[P(Z); \lambda_L, B_1, ..., B_r)] \tag{6.29}$$

When the joint distribution of λ_L, B stems from Bayesian analysis of an initial distribution and an observed event, A, this equation adopts the form:

$$P''(Z) = \frac{E'_{\lambda_L, B}[P(Z|\lambda_L, B)P(A|\lambda_L, B)]}{E'_{\lambda_L, B}[P(A|\lambda_L, B)]} \tag{6.30}$$

where ' and " stand for initial and posterior, respectively.

Spatial variability. Figure 6.17 shows a map of geotectonic provinces of Mexico, according to F. Mooser. Each province is characterized by the large-scale features of its tectonic structure, but significant local perturbations to the overall patterns can be identified. Take for instance zone 1, whose seismotectonic features were described above, and are schematically shown in Fig. 6.18 (Singh, 1975): the Pacific plate underthrusts the continental block and is thought to break into several blocks, separated by faults transverse to the coast, that dip at different angles. The continental mass is also

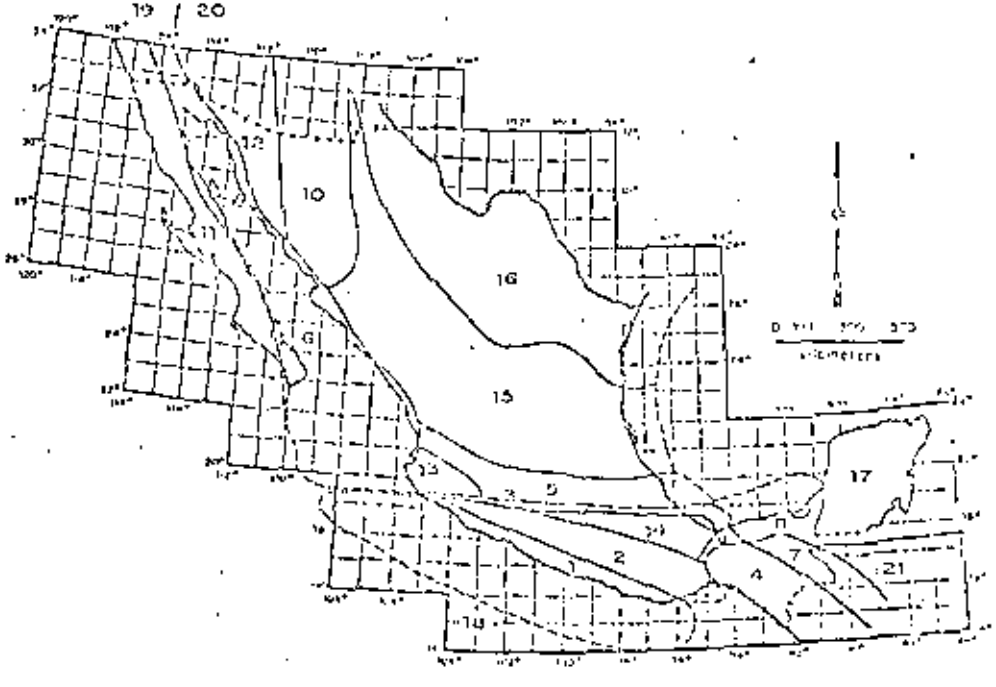

Fig. 6.17. Seismotectonic provinces of Mexico. (After F. Mooser.)

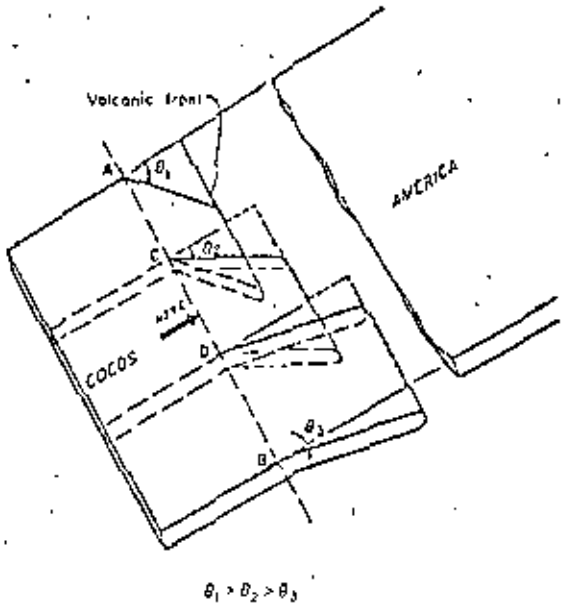

Fig. 6.18. Schematic drawing of the segmenting of Cocos plate as it subducts below American plate. (After Singh, 1974.)

made up of several large blocks. Seismic activity at the underthrusting plate or at its interface with the continental mass is characterized by magnitudes that may reach very high values and by the increase of mean hypocentral depth with distance from the coast; small and moderate shallow shocks are generated at the blocks themselves. Variability of statistical data along the whole tectonic system was discussed above and is apparent in Fig. 6.10. Bayesian estimation of local seismicity averaged throughout the system is a matter of applying eq. 6.21 or any of its special forms (eqs. 6.22 and 6.23), taking as statistical evidence the information corresponding to the whole system. However, seismic risk estimates are sensitive to values of local seismicity averaged over much smaller volumes of the earth's crust; hence the need to develop criteria for probabilistic inference of possible patterns of space variability of seismicity along tectonically homogeneous zones.

On the basis of seismotectonic information, the system under consideration can first be subdivided into the underthrusting plate and the subsystem of shallow sources; each subsystem can then be separately analyzed. Take for instance the underthrusting plate and subdivide it into s sufficiently small equal-volume subzones. Let ν_L be the rate of exceedance of magnitude M_L throughout the main system, ν_{L_i} the corresponding rate at each subzone, and define p_i as ν_{L_i}/ν_L, with ν_i independent of ν_L (p_i is equal to the probability that an earthquake known to have been generated in the overall system originated at subzone i). Initial information about possible space variability of

ν_{L_i} can be expressed in terms of an initial probability distribution of p_i and of the correlation among p_i and p_j for any i and j. Because $\Sigma\nu_{L_i} = \nu_L$, one obtains $\Sigma p_i = 1$. This imposes two restrictions on the initial joint probability distribution of the p_i's: $E'(p_i) = 1$, $\text{var}'\ \Sigma p_i = 0$. If all p_i's are assigned equal expectations and all pairs p_i, p_j, $i \neq j$ are assumed to possess the same correlation coefficient $\rho_{ij} = \rho'$, the restrictions mentioned lead to $E'(p_i) = 1/s$ and $\rho' = -1/(s-1)$. Posterior values of $E(p_i)$ and ρ_{ij} are obtained according to the same principles that led to eqs. 6.25–6.28. Statistical evidence is in this case described by N, the total number of earthquakes generated in the system, and n_i ($i = 1, \ldots, s$) the corresponding numbers for the subzones. Given the p_i's, the probability of this event is the multinomial distribution:

$$P[A|p_1, \ldots, p_s] = \frac{N!}{n_1! \ldots n_s!}\, p_1^{n_1} \ldots p_s^{n_s} \tag{6.31}$$

If the correlation coefficients among seismicities of the various subzones can be neglected, each p_i can be separately estimated. Because p_i has to be comprised between 0 and 1, it is natural to assign it a beta initial probability distribution, defined by its parameters n_i' and N_i', such that $E'(p_i) = n_i'/N_i'$ and $\text{var}'(p_i) = n_i'(N_i' - n_i')/[N_i'^2(N_i' + 1)]$ (Raiffa and Schlaifer, 1968). The parameters of the posterior distribution will be:

$$n_i'' = n_i' + n_i, N_i'' = N_i' + N$$

Take for instance a zone whose prior distribution of λ_L is assumed gamma with expected value λ_L' and coefficient of variation V_L'. Suppose that, on the basis of geological evidence and of the dimensions involved, it is decided to subdivide the zone into four subzones of equal dimensions; a-priori considerations lead to the assignment of expected values and coefficients of variation of p_i for those subzones, say $E'(p_i) = 0.25$, $V'(p_i) = 0.25$ ($i = 1, \ldots, 4$). From previous considerations for $s = 4$ take $\rho_{ij}' = -1/3$ for $i \neq j$. Suppose now that, during a given time interval t, ten earthquakes were observed in the zone, of which 0, 1, 3, and 6 occurred respectively in each subzone. If the Poisson process model is adopted, λ_L' and V_L' can be expressed in terms of a fictitious number of events $n' = V_L'^{-2}$ occurred during a fictitious time interval $t' = n'/\lambda_L'$; after observing n earthquakes during an interval t, the Bayesian mean and coefficient of variation of λ_L will be $\lambda_L'' = (n' + n)/(t' + t)$, $V_L'' = (n' + n)^{-1/2}$ (Esteva, 1968). Hence:

$$\lambda_L'' = (V_L'^{-2} + 10)/(V_L'^{-2}\lambda_L'^{-1} + t), \quad V_L'' = (V_L'^{-2} + 10)^{-1/2}$$

Local deviations of seismicity in each subzone with respect to the average λ_L can be analyzed in terms of p_i ($i = 1, \ldots, 4$); Bayesian analysis of the proportion in which the ten earthquakes were distributed among the subzones proceeds according to:

$$E''(p_i|A) = \frac{E'[p_i P(A|p_1, \ldots, p_4)]}{E'[P(A|p_1, \ldots, p_4)]} \tag{6.32}$$

The expectations that appear in this equation have to be computed with respect to the initial joint distribution of the p_i's. In practice, adequate approximations are required. For instance, Benjamin and Cornells' (1970) first-order approximation leads to $E''(p_1) = 0.226$, $E''(p_4) = 0.294$.

If correlation among subzone seismicities is neglected, and statistical information of each subzone is independently analyzed, when the p_i's are assigned beta probability-density functions with means and coefficients of variation as defined above, one obtains $E''(p_1) = 0.206$, $E''(p_4) = 0.311$, which are not very different from those formerly obtained; however, when $E'(p_i) = 0.25$ and $V'(p_i) = 0.5$, the first criterion leads to $E''(p_1) = 0.206$, $E''(p_4) = 0.314$, while the second produces 0.131 and 0.416, respectively. Part of the difference may be due to neglect of ρ_{ij}', but probably a significant part stems from inaccuracies of the first-order approximation to the expectations that appear in eq. 6.32; alternate approximations are therefore desirable.

Incomplete data. Statistical information is known to be fairly reliable only for magnitudes above threshold values that depend on the region considered, its level of activity, and the quality of local and nearby seismic instrumentation. Even incomplete statistical records may be significant when evaluating some seismicity parameters; their use has to be accompanied by estimates of detectability values, that is, of ratios of the numbers of events recorded to total numbers of events in given ranges (Esteva, 1970; Kaila and Narain, 1971).

6.5 REGIONAL SEISMICITY

The final goal of local seismicity assessment is the estimation of regional seismicity, that is, of probability distributions of intensities at given sites, and of probabilistic correlations among them. These functions are obtained by integrating the contributions of local seismicities of nearby sources, and hence their estimates reflect Bayesian uncertainties tied to those seismicities. In the following, regional seismicity will be expressed in terms of mean rates of exceedance of given intensities; more detailed probabilistic descriptions would entail adoption of specific hypotheses concerning space and time correlations of earthquake generation.

6.5.1 Intensity-recurrence curves

The case when uncertainty in seismicity parameters is neglected will be discussed first. Consider an elementary seismic source with volume dV and local seismicity $\lambda(M)$ per unit volume, distant R from a site S, where intensity-recurrence functions are to be estimated. Every time that a magnitude M shock is generated at that source, the intensity at S equals:

$$Y = \epsilon Y_p = \epsilon b_1 \cdot \quad ^{b_2 M} g(R) \tag{6.33}$$

(see eqs. 6.4 and 6.5), where ϵ is a random factor and Y and Y_p stand for actual and predicted intensities, b_1 and b_2 are given constants, and $g(R)$ is a function of hypocentral distance. The probability that an earthquake originating at the source will have an intensity greater than y is equal to the probability that $\epsilon Y_p \geq y$. If Y_p is expressed in terms of M and randomness in ϵ is accounted for, one obtains:

$$\nu(y) = \int_{a_U}^{a_L} \nu_p(y/u) f_\epsilon(u) du \tag{6.34}$$

where ν and ν_p are respectively mean rates at which actual and predicted intensities exceed given values, $a_U = y/y_U$, $a_L = y/y_L$, y_U, and y_L are the predicted intensities that correspond to M_U and M_L, and f_ϵ the probability-density function of ϵ. If eq. 6.33 is assumed to hold:

$$\nu_p(y) = K_0 + K_1 y^{-r_1} - K_2 y^{-r_2} \tag{6.35}$$

where:

$$K_i = [b_1 g(R)]^{r_i} \lambda_1 \lambda_2 \, dV \quad (i = 0, 1, 2) \tag{6.36}$$

$$r_0 = 0, \quad r_1 = \beta/b_2, \quad r_2 = (\beta - \beta_1)/b_2 \tag{6.37}$$

Substitution of eq. 6.35 into 6.34, coupled with the assumption that $\ln \epsilon$ is normally distributed with mean m and standard deviation σ leads to:

$$\nu(y) = c_0 K_0 + c_1 K_1 y^{-r_1} - c_2 K_2 y^{-r_2} \tag{6.38}$$

where:

$$c_i = \exp(Q_i) \left[\phi\left(\frac{\ln a_L - u_i}{\sigma}\right) - \phi\left(\frac{\ln a_U - u_i}{\sigma}\right) \right] \tag{6.39}$$

ϕ is the standard normal cumulative distribution function, $Q_i = 1/2\ \sigma^2 r_i^2 + m r_i$, and $u_i = m + \sigma^2 r_i$. Similar expressions have been presented by Merz and Cornell (1973) for the special case of eq. 6.8 when $\beta_1 \to \infty$ and for a quadratic form of the relation between magnitude and logarithm of exceedance rate. Closed-form solutions in terms of incomplete gamma functions are obtained when magnitudes are assumed to possess extreme type-III distributions (eq. 6.9).

Intensity-recurrence curves at given sites are obtained by integration of the contributions of all significant sources. Uncertainties in local seismicities can be handled by describing regional seismicity in terms of means and variances of $\nu(y)$ and estimating these moments from eq. 6.34 and suitable first- and second-moment approximations. Influence of these uncertainties in design decisions has been discussed by Rosenblueth (in preparation).

6.5.2 *Seismic probability maps*

When intensity-recurrence functions are determined for a number of sites with uniform local ground conditions the results are conveniently represented by sets of seismic probability maps, each map showing contours of intensities that correspond to a given return period. For instance, Figs. 6.19 and 6.20 show peak ground velocities and accelerations that correspond to 100 years return period on firm ground in Mexico. These maps form part of a set that was obtained through application of the criteria described in this chapter. Because the ratio of peak ground accelerations and velocities does not remain constant throughout a region, the corresponding design spectra will not only vary in scale but also in shape (frequency content); in other words, seismic risk will usually have to be expressed in terms of at least the values of two parameters (for instance, as in this case, peak ground accelerations and velocities that correspond to various risk levels (return periods)).

6.5.3 *Microzoning*

Implicit in the above criteria for evaluation of regional seismicity is the adoption of intensity attenuation expressions valid on firm ground. Scatter of actual intensities with respect to predicted values was ascribed to differences in source mechanisms, propagation paths, and local site conditions; at least the latter group of variables can introduce systematic deviations in the

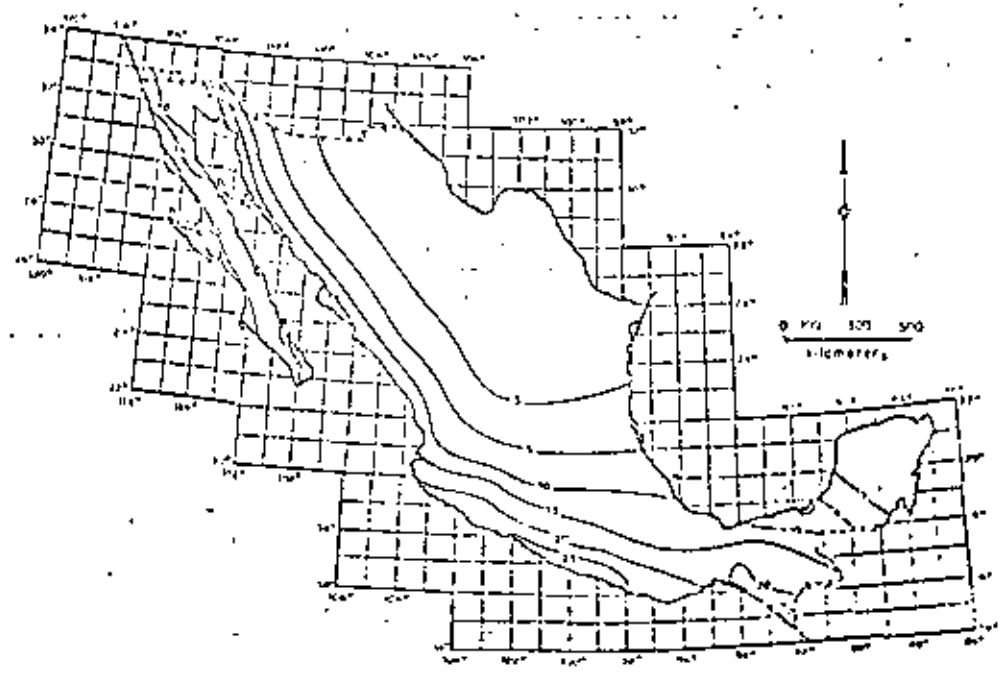

Fig. 6.19. Peak ground velocities with return period of 100 years (cm/sec).

trying to fi[illegible]t boundary for the purpose of predicting the motion at t[illegible] top of a hill or the slope stability of a high cliff (Rukos, 1974).

It can be concluded that rational formulation of microzoning for seismic risk is still in its infancy and that new criteria will appear that will probably require intensity attenuation models which include the influence of local systematic perturbations. Whether these models are available or the two-step process described above is acceptable, intensity-recurrence expressions can be obtained as for the unperturbated case, after multiplying the second member of eq. 6.34 by an adequate intensity-dependent corrective factor.

REFERENCES

Aki, K., 1963. *Some Problems in Statistical Seismology.* University of Tokyo, Geophysical Institute.

Allen, C.R., 1969. Active faulting in northern Turkey. *Calif. Inst. Tech., Div. Geol. Sci., Contrib.* 1577.

Allen, C.R., St. Amand, P., Richter, C.F. and Nordquist, J.M., 1965. Relationship between seismicity and geologic structure in the southern California region. *Bull. Seismol. Soc. Am.*, 55 (4): 753–797.

Ambraseys, N.N., 1973. Dynamics and response of foundation materials in epicentral regions of strong earthquakes. *Proc. 5th World Conf. Earthquake Eng.: Rome.*

Ananiin, I.V., Bune, V.I., Vvedenskaia, N.A., Kirilluva, I.V., Reisner, G.I. and Sholpo, V.N., 1968. *Methods of Compiling a Map of Seismic Regionalization on the Example of the Caucasus.* O. Yu. Schmidt Institute of the Physics of the Earth, Academy of Sciences of the USSR, Moscow.

Benjamin, J.R. and Cornell, C.A., 1970. *Probability, Statistics and Decision for Civil Engineers.* McGraw-Hill, New York.

Ben-Menahem, A., 1960. Some consequences of earthquake statistics for the years 1918–1955. *Gerlands Beitr. Geophys.*, 69: 65–72.

Bollinger, G.A., 1973. Seismicity of the southeastern United States. *Bull. Seismol. Soc. Am.*, 63: 1785–1808.

Bolt, B.A., 1970. Causes of earthquakes. In: R.L. Wiegel (editor), *Earthquake Engineering.* Prentice-Hall, Englewood Cliffs.

Brune, J.N., 1968. Seismic moment, seismicity and rate of slip along major fault zones. *J. Geophys. Res.*, 73: 777–784.

Burridge, R. and Knopoff, L., 1967. Model and theoretical seismicity. *Bull. Seismol. Soc. Am.*, 57: 341–371.

Cornell, C.A. and Vanmarcke, E.H., 1969. The major influences on seismic risk. *Proc. 4th World Conf. Earthquake Eng. Santiago.*

Crouse, C.B., 1973. Engineering studies of the San Fernando earthquake. *Calif. Inst. Technol., Earthquake Eng. Res. Lab.* Rep. 73-04.

Cox, D.F. and Lewis, P.A.W., 1966. *The Statistical Analysis of Series of Events.* Methuen, London.

Davenport, A.G., 1972. A statistical relationship between shock amplitude, magnitude and epicentral distance and its application to seismic zoning. *Univ. Western Ontario, Faculty Eng. Sci.*, BLWT-4-72.

Davies, G.F. and Brune, J.N., 1971. Regional and global fault slip rates from seismicity. *Nature*, 229: 101–107.

Drakopoulos, J.C., 1971. A statistical model on the occurrence of aftershocks in the area of Greece. *Bull. Int. Inst. Seismol. Earthquake Eng.*, 8: 17–39.

Esteva, L., 1968. Bases para la formulación de decisiones de diseño sísmico. *Natl. Univ. Mexico, Inst. Eng. Rep.* 182.

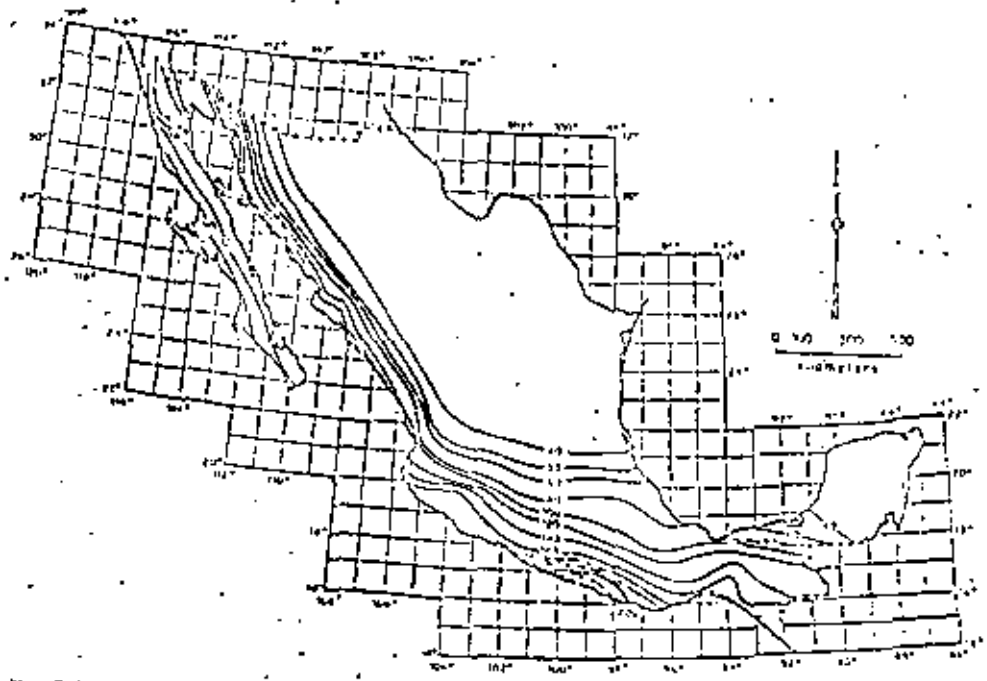

Fig. 6.20. Peak ground accelerations with return period of 100 years (cm/sec^2).

atio of actual to predicted intensities; and geological details may significantly alter local seismicity in a small region, as well as energy radiation patterns, and hence regional seismicity in the neighbourhood. These systematic deviations are the matter of microzoning, that is, of local modification of risk maps similar to Figs. 6.19 and 6.20.

Most of the effort invested in microzoning has been devoted to study of the influence of local soil stratigraphy on the intensity and frequency content of earthquakes (see Chapter 4). Analytical models have been practically limited to response analysis of stratified formations of linear or nonlinear soils to vertically traveling shear waves. The results of comparing observed and predicted behavior have ranged from satisfactory (Herrera et al., 1965) to poor (Hudson and Udwadia, 1972). Topographic irregularities, as hills or slopes of firm ground formations underlying sediments, may introduce significant systematic perturbations in the surface motion, as a consequence of wave focusing or dynamic amplification. The latter effect was probably responsible for the exceptionally high accelerations recorded at the abutment of Pacoima dam during the 1971 San Fernando earthquake.

Present practice of microzoning determines seismic intensities or design parameters in two steps. First the values of those parameters on firm ground are estimated by means of suitable attenuation expressions and then they are amplified according to the properties of local soil; but this implies an arbitrary decision to which seismic risk is very sensitive: selecting the boundary between soil and firm ground. A specially difficult problem stems when

Esteva, L., 1969. Seismicity prediction: a bayesian approach. *Pro[illegible] World Conf. Earthquake Eng. Santiago.*

Esteva, L., 1970. Consideraciones prácticas en la estimación bayesiana de riesgo sísmico. *Natl. Univ. Mexico, Inst. Eng., Rep.* 248.

Esteva, L., 1974. Geology and probability in the assessment of seismic risk. *Proc. 2nd Int. Congr. Int. Assoc. Eng. Geol., Sao Paulo.*

Esteva, L. and Villaverde, R., 1973. Seismic risk, design spectra and structural reliability. *Proc. 5th World Conf. Earthquake Eng., Rome*, pp. 2586–2597.

Figueroa, J., 1963. Isosistas de macrosismos mexicanos. *Ingeniería*, 33 (1): 45–68.

Gaisky, V.N., 1966. The time distribution of large, deep earthquakes from the Pamir–Hindu-Kush. *Dokl. Akad. Nauk Tadjik S.S.R.*, 9 (8): 18–21.

Gaisky, V.N., 1967. On similarity between collections of earthquakes, the connections between them, and their tendency to periodicity. *Fiz. Zemli*, 7: 20–28 (English transl., pp. 432–437).

Gajardo, E. and Lomnitz, C., 1960. Seismic provinces of Chile. *Proc. 2nd World Conf. Earthquake Eng., Tokyo*, pp. 1529–1540.

Gutenberg, B. and Richter, C.F., 1954. *Seismicity of the Earth.* Princeton University Press, Princeton.

Gzovsky, M.G., 1962. Tectonophysics and earthquake forecasting. *Bull. Seismol. Soc. Am.*, 52 (3): 485–505.

Herrera, I., Rosenblueth, E. and Rascón, O.A., 1965. Earthquake spectrum prediction for the Valley of Mexico. *Proc. 3rd Int. Conf. Earthquake Eng., Auckland and Wellington*, 1: 61–74.

Housner, G.W., 1969. Engineering estimates of ground shaking and maximum earthquake magnitude. *Proc. 4th World Conf. Earthquake Eng., Santiago.*

Hudson, D.E., 1971. *Strong Motion Instrumental Data on the San Fernando Earthquake of February 9, 1971.* California Institute of Technology, Earthquake Engineering Research Laboratory.

Hudson, D.E., 1972a. Local distributions of strong earthquake ground shaking. *Bull. Seismol. Soc. Am.*, 62 (6).

Hudson, D.E., 1972b. *Analysis of Strong Motion Earthquake Accelerograms. III, Response Spectra, Part A.* California Institute of Technology, Earthquake Engineering Research Laboratory.

Hudson, D.E. and Vidwadia, F.E., 1973. Local distribution of strong earthquake ground motions. *Proc. 5th World Conf. Earthquake Eng., Rome*, pp. 691–700.

Kaila, K.L. and Narain, H., 1971. A new approach for preparation of quantitative seismicity maps as applied to Alpide Belt–Sunda Arc and adjoining areas. *Bull. Seismol. Soc. Am.*, 61 (5): 1275–1291.

Kaila, K.L., Gaur, V.K. and Narain, H., 1972. Quantitative seismicity maps of India. *Bull. Seismol. Soc. Am.*, 62 (5): 1119–1132.

Kaila, K.L., Rao, N.M. and Narain, H., 1974. Seismotectonic maps of southwest Asia region comprising eastern Turkey, Caucasus, Persian Plateau, Afghanistan and Hindu-kush. *Bull. Seismol. Soc. Am.*, 64 (3): 657–669.

Kelleher, J., Sykes, L. and Oliver, J., 1973. Possible criteria for predicting earthquake locations and their application to major plate boundaries of the Pacific and the Caribbean. *J. Geophys. Res.*, 78 (14): 2547–2585.

Knopoff, L., 1964. The statistics of earthquakes in southern California. *Bull. Seismol. Soc. Am.*, 54: 1871–1873.

Lomnitz, C., 1966. Magnitude stability in earthquake sequences. *Bull Seismol. Soc. Am.*, 56: 247–249.

Lomnitz, C. and Hax, A., 1966. Clustering in aftershock sequences. In: J.S. Steinhart and T. Jefferson Smith (editors), *The Earth Beneath the Continents.* Am. Geophys. Union, pp. 502-508.

McGuire, R.K., 1974. Seismic structural response risk analysis incorporating peak response regressions on earthquake magnitude and distance. *Mass. Inst. Technol., Dep. Civ. Eng.*, R74-51.

Merz, H.A. and Cornell, C.A., 1973. Seismic risk analysis based on a quadratic magnitude–frequency law. *Bull. Seismol. Soc. Am.*, 63 (6): 1999–2006.

Milne, W.G. and Davenport, A.G., 1969. Earthquake probability. *Proc. 4th World Conf. Earthquake Eng., Santiago.*

Mogi, K., 1962. Study of elastic shocks caused by the fracture of heterogeneous materials and its relations to earthquake phenomena. *Bull. Earthquake Res. Inst. Tokyo*, 40: 125–173.

Molnar, P. and Sykes, L.R., 1969. Tectonics of the Caribbean and Middle America regions from focal mechanisms and seismicity. *Geol. Soc. Am. Bull.*, 80: 1639.

Newark, N.M. and Rosenblueth, E., 1971. *Fundamentals of Earthquake Engineering.* Prentice-Hall, Englewood Cliffs.

Omori, F., 1894. On the aftershocks of earthquakes. *J. Coll. Sci. Imp. Univ. Tokyo*, 7: 111–200.

Parzen, E., 1962. *Stochastic Processes.* Holden Day, San Francisco.

Petrushevsky, B.A., 1966. *The Geological Fundamentals of Seismic Zoning.* Scientific Translation Service, order 5032, Ann Arbor, USA.

Raiffa, H. and Schlaifer, R., 1968. *Applied Statistical Decision Theory*, MIT Press.

Rosenblueth, E., 1964. Probabilistic design to resist earthquakes. *Am. Soc. Civ. Eng., J. Eng. Mech. Div.*, 90 (EM5): 189–249.

Rosenblueth, E., 1969. Seismicity and earthquake simulation. *Rep. NSF-UCEER Conf. Earthquake Eng. Res., Pasadena*, pp. 47-64.

Rosenblueth, E., 1975. *Point Estimates for Probability Moments.* National University of Mexico, Institute of Engineering, Mexico City.

Rosenblueth, E., in preparation. Optimum design for infrequent disturbances.

Rukos, E., 1974. *Análysis dinamico de la margen izquierda de Chicoasén.* National University of Mexico, Institute of Engineering, Mexico City.

Salt, P.E., 1974. Seismic site response. *Bull. N. Z. Natl. Soc. Earthquake Eng.*, 7 (2): 63–77.

Scholz, C.H., 1968. The frequency–magnitude relation of microfracturing and its relation to earthquakes. *Bull. Seismol. Soc. Am.*, 58: 399–417.

Shlien, S. and Toksöz, M.N., 1970. A clustering model for earthquake occurrences. *Bull. Seismol. Soc. Am.*, 60 (6): 1765–1787.

Singh, S.K., 1975. *Mexican Volcanic Belt: Some Comments on a Model Proposed by F. Mooser.* National University of Mexico, Institute of Engineering, Mexico City.

Trifunac, M.D., 1973. Characterization of response spectra by parameters governing the gross nature of earthquake source mechanisms. *Proc. 5th World Conf. Earthquake Eng., Rome*, pp. 701–704.

Tsuboi, C., 1958. Earthquake province, Domain of sympathetic seismic activities. *J. Phys. Earth.*, 6 (1): 35–49.

Utsu, T., 1961. A statistical study on the occurrence of aftershocks. *Geophys. Mag., Tokyo*, 30: 521–605.

Utsu, T., 1962. On the nature of three Alaska aftershock sequences of 1957 and 1958. *Bull. Seismol. Soc. Am.*, 52: 179–297.

Veneziano, D. and Cornell, C.A., 1973. Earthquake models with spatial and temporal memory for engineering seismic risk analysis. *Mass. Inst. Technol., Dep. Civ. Eng.*

Vere-Jones, D., 1970. Stochastic models for earthquake occurrence. *J. R. Stat. Soc.*, 32 (1): 1–45.

Wallace, R.E., 1970. Earthquake recurrence intervals on the San Andreas Fault. *Geol. Soc. Am. Bull.*, 81: 2875–2890.

Yegulalp, T.M. and Kuo, J.T., 1974. Statistical prediction of the occurrences of maximum magnitude earthquakes. *Bull. Seismol. Soc. Am.*, 64 (2): 393–414.

Accelerograph Location. Completely adequate definition of input ground motions and structural response would require a large number of accelerographs at carefully selected points. For major projects, in highly seismic regions, detailed studies of the optimum number and location of accelerographs would be expected for the special conditions of the particular site. For minimum recommendations, however, questions of location are secondary to the prime object of ensuring that at least some information of engineering value will be obtained for all strong shaking.

For this purpose, it is recommended that not fewer than four strong motion accelerographs be installed. Two of these should be located to record earthquake motions in the foundation, and two to measure structural response. For dams, the foundation instruments can often be mounted on abutments, or at an appropriate site in the immediate vicinity of the dam that is not obviously influenced in a major way by local geologic structural features. The instruments to measure dam response can usually be mounted at two different locations on the crest, or in upper galleries should they exist; they should not be mounted on special superstructures that may introduce localized dynamic behavior.

The purpose of requiring two instruments for each function is to give some indication of the uniformity of conditions, and to ensure some useful information in the event of instrument malfunction.

Accelerograph Installation and Maintenance. It is essential that the instruments be well protected from such environmental conditions as flooding or excessive summer temperatures, and from tampering or vandalism. The accelerograph, which is about 20 centimeters by 20 centimeters by 30 centimeters in size, can often be conveniently installed in the corner of a basement office, storage room, or gallery of a dam. If no space of this type is available near a suitable site, an insulated metal enclosure sealed against weather and interference can usually be provided by the instrument manufacturer at a reasonable cost. The accelerograph should be firmly bolted down to a concrete foundation, as specified by the instructions of the instrument manufacturer.

Checking, maintenance, and servicing of the accelerographs should be carried out on a regular schedule according to the instructions of the instrument manufacturer. Routine maintenance can usually be carried out by a regular member of the technical staff, if he is given a small degree of special training. Similarly, instructions in the proper preservation of records and their transmittal for data processing can be given, so that they are not lost during or after an earthquake.

Accelerograph Cost Estimates. Accelerographs meeting the necessary requirements are commercially available at 1978 prices in the $2,000 to $2,500 range. A suitable protective housing can usually be provided, if necessary, for $500 to $1,000. The only additional cost of installation will be the provision of standard electric lines or solar panels for battery trickle charging. The total 1978 cost of a typical recommended system will thus be about $12,000.

Local Seismograph Networks

Network Requirements. Sensitive seismographs to measure local earthquakes are sometimes advisable in the vicinity of projects such as large dams and nuclear reactors before major construction begins. The purposes of such instrumentation are to (1) determine the frequency of local earthquakes (if any); (2) determine the location of seismic activity and its depth; (3) determine the magnitude and some indication of focal mechanisms of the earthquakes; (4) allow prediction of the course of earthquake occurrence.

Reasonably precise location of an earthquake focus requires that the onset of P waves (and also S waves where feasible) be recorded to an accuracy of ±0.1 second or better, at a minimum of four nearby seismographs. There must be a common time base for all seismographs, and they should ideally surround the region of earthquake activity. For dams, the overall aims can be accomplished in two stages. In the preclosure stage, where the main purpose is to establish if any local earthquakes at all occur normally, a minimum network of three short-period vertical-component seismometers may be sufficient. With such a network a rough but adequate assessment of background earthquake frequency, location (using P and S waves), and magnitude can be made. If local earthquakes are prevalent the network should be expanded to at least four seismographs with the additional seismometer as near as possible to the active area.

After dam closure, it is advisable, at the least, to operate a four-station network for a period extending some years beyond the time when maximum impounding is complete. If a sequence of earthquakes does occur, then the network should be densified. Such studies of reservoir induced seismicity usually warrant special research. The requirement then is to obtain an accuracy in the location of earthquake foci of about 1 kilometer, so that correlations with geological faults can be made.

landes connections. Power is needed at the individual seismometers for the amplifiers and voltage-controlled oscillators. At the recording station, additional power is needed for the signal discriminators, amplifiers, and drum and tape recorders. The system is costlier than System A because of the cost of land lines. Its great advantage is the centralization of recording at one convenient accessible location. Maintenance personnel would rarely need to visit the seismometers in the field. Components of the telemetered system are now all commercially available.

Network Operation and Analysis. Operation of either network A or B should not require instrumentation specialists or a staff seismologist. The critical requirements in all such studies of seismicity are continuity of operation and minimum system adjustments.

For either system, an operator would need to change the paper records each day of the week at about the same hour. He would need to mark the date and location on each seismogram. Any absolutely essential changes in system characteristics would need to be logged. It may be necessary, from time to time, to readjust and calibrate the seismometers in accord with the procedures specified by the equipment manufacturers.

For the telemetry system B, the discriminators, radio, clock, and recording drums can usually be located in a small room in the engineering quarters. The ac power is usually available. Seismograms can often be examined and stored in the same facility. All seismographic instrumentation should be bolted to the building structure to prevent movement and damage in the case of an earthquake.

The analysis side of the high-gain system often requires some seismological expertise. Special arrangements are not needed, of course, if no or very few local earthquakes are recorded. However, if the region is seismic or, at a dam, if the local seismicity increases on closure, or both, it is recommended that some special advice be obtained on analysis from a consultant seismologist.

Cost Estimates. The components in systems A and B are now commonly available and widely used by seismologists. At 1975 prices, the seismometers in System A cost about $1,000. A complete portable recording system can be obtained for $4,000. A suitable solar cell unit is about $500 or $600. The total cost of a four-station network of System A type is thus about $20,000. No cost is included for preparation of pits or housing.

The cost of installation of the preferred System B is somewhat higher. The seismometer-amplifier-oscillator package at each site is

Network Location. The selection of sites for the sensitive seismographs often depends on practical considerations such as accessibility and avoidance of construction work. However, several general considerations should govern the configuration to the greatest extent practically possible. First, the sites should be uniformly spread in azimuth around the project.

The interstation distance should not be more than about 30 kilometers or less than 3 kilometers. Individual site selection should depend upon the local tectonic structures. It is best to locate the instruments on outcrops of basement rock, and they should be as remote as possible from construction activities, streams, quarrying, spillways, and so on. Normally, sites should be chosen so that they do not have to be shifted throughout the life of the project. It is also helpful to make field surveys of the relative background microseismic noise at prospective sites, with the use of a portable seismographic recorder before locations are finalized.

It has been found adequate to place the seismometers in shallow pits (about 1 meter deep) in the surficial rock. A generally adequate housing is a steel drum, with a watertight cover, that is set on concrete poured at the bottom of the pit.

Seismographic Characteristics. A variety of suitable components for a reliable high-gain seismographic system is now commercially available. Thus numerous systems can be designed to meet the aims previously established. The following two alternative systems—A and B—meet the minimum requirement and have been field tested. In both, the response of the overall seismographic system should be between 5 hertz and 50 hertz.

Seismographic System A. The system makes use of available portable seismometers and visual recording units. The network stations are not connected, and depend on separate crystal clocks at each recorder. Recording is normally on smoked paper and the paper records must be changed every day. This can be done by a member of the maintenance staff without special training.

The portable system for each site is in four parts: (1) seismometer; (2) waterproof single-package d recording unit with batteries (size approximately 30 centimeters by 30 centimeters by 25 centimeters); (3) radio receiver; (4) power source such as solar battery charger.

Seismographic System B. This system telemeters the signals from individual seismometers of the network to a central recording room by

listed at about $1,800 in 1978. At the central recording facility, each discriminator-amplifier-recorder package costs about $2,500. A suitable crystal clock is about $1,500 and a WWV radio receiver $500. The estimated total cost of the instrumentation at current prices is thus again about $20,000. In addition, however, there is the cost of the overland telemetry lines. In some areas commercial telephone lines may be available for rental. (In certain locations, RF radio telemetry links may be suitable.)

DIVISION DE EDUCACION CONTINUA
FACULTAD DE INGENIERIA U.N.A.M.

VII CURSO INTERNACIONAL DE INGENIERIA SISMICA

SISMOLOGIA Y SISMICIDAD

GEOLOGY AND PROBABILITY IN THE ASSESSMENT OF SESISMIC RISK

Dr Luis Esteva Maraboto

Julio, 1981

GEOLOGY AND PROBABILITY IN THE ASSESSMENT OF SEISMIC RISK

by

LUIS ESTEVA
INSTITUTE OF ENGINEERING
NATIONAL UNIVERSITY OF MEXICO

presented at the

2nd INTERNATIONAL CONGRESS OF THE INTERNATIONAL ASSOCIATION OF ENGINEERING GEOLOGY
SAO PAULO, BRASIL, AUGUST 1974

assumptions about source dimensions, dislocation amplitude and stress drop, consistent with tectonic models of the region and, again, with comparisons with areas of similar tectonic characteristics. Statisticians, on the other hand, are prone to base their predictions of the future exclusively on the basis of observations on a sample, however scanty that sample may be.

None of these approaches, by itself, suffices to provide a satisfactory answer to the requirements of decision makers: purely statistical analysis is unacceptable because it neglects a wealth of relevant information, and it is not clear that bounds can always be assigned to magnitudes in given areas, or that, when this is feasible, those bounds are sufficiently low that designing for them is economically sound, even if they are not very likely to occur in the near future. In fact, some studies relating source dimensions, stress drop and magnitude show that, considering not unusually high stress drops, it does not take very large source dimensions to get magnitudes 8.0 and greater.

A criterion for combining the above approaches in the probabilistic assessment of seismic risk is presented in this paper. Its philosophy consists in using the geological, geophysical or any other non-statistical evidence for producing a set of alternate assumptions concerning a mathematical (stochastic process) model of seismicity in a given source area. An initial, or prior, probability is assigned to each hypothesis, and the statistical information is then used for improving that probability assignment. The criterion is based on application of Bayes theorem, also called the theorem of the probabilities of the hypotheses. A previous formulation (1) has evolved through the interaction of multidisciplinary groups in the development of seismic risk studies performed in the last few years in Mexico (2-4). Since estimates of risk depend on conceptual models of the geophysical process involved, and these are little known at present, more questions are raised here than solutions given.

2. MEASURES OF SEISMIC RISK

Let y be a measure of earthquake intensity. According to the problem at hand, y may be peak ground acceleration, velocity, spectral ordinate for a given natural period, or, shortly, any variable that determines the response of the system under study. This means that a relation can be established between the intensity of a given earthquake and the corresponding loss $D(y)$.

A currently applied criterion assumes that seismic risk should be measured by the highest intensity that can be caused at the site by the largest-magnitude earthquake that can be generated at any of the potential seismic sources in the vicinity. However, engineering systems cannot always be designed for the worst possible condition to be expected. Instead, decisions have to be based on cost-benefit studies. When designing for earthquakes, a significant cost term is made of the value of the expected actualized cost of damage or failure, as given by the following equation:

$$E[F] = \int_0^\infty \delta_t e^{-rt} dt \qquad (1)$$

$$y = b_1 e^{b_2 M} R'^{-b_3} \qquad (4)$$

where $R' = h + R_0$; R must be given in kilometers and b_1, b_2, b_3 and R_0 are given in Table 1, which also shows the mean m and the standard deviation σ of the natural logarithm of the ratio of observed to computed intensities.

TABLE 1. EXPRESSIONS RELATING MAGNITUDE, INTENSITY AND HYPOCENTRAL DISTANCE

Expression for:	b_1	b_2	b_3	R_0	m	σ
v (cm/sec)	37	1.0	1.7	25	0.12%	0.7%
a (cm/sec²)	5 600	0.8	2.0	40	0.0%	0.6%
$\bar{V}$ (cm/sec)	250	1.0	1.7	25	0.05%	0.5%
$\bar{I}$ (cm/sec²)	85 600	0.8	2.0	70	0	0.7%

The significant dispersion of these expressions, implied by the high values of σ, is due mainly to their having been obtained from data of earthquakes originating in different sources and having different mechanisms and propagation paths. The form of Eq 4 gives place, moreover, to a faster variation of intensities with respect to magnitudes in the near field than what occurs in nature because the liberation of energy is distributed throughout volumes whose dimensions can be significant with respect to the site-to-source distance. This relatively low sensitivity of y with respect to M in the near-field has been verified in practice at least for earthquakes produced by a strike-slip mechanism (10, 11). This effect can be represented by expressions of the type of Eq 4, if b_2 is taken, for instance, of the form $b_2 = A + B/(C + R)$.

For wide areas in the earth's crust, $\lambda(M)$, the average value of $\lambda_i(M)$ over long time intervals, can be approximated as follows,

$$\lambda(M) = \alpha_1 e^{-\beta_1 M} \quad \text{for } M \leq M_1$$
$$\lambda(M) = \alpha_2 e^{-\beta_2 M} \quad \text{for } M > M_1 \qquad (5)$$

where $\beta_2 > \beta_1$, M_1 is a magnitude beyond which there is a higher rate of decrease of $\lambda(M)$ with magnitude; continuity at M_1 requires that α_2 equal $\alpha_1 \exp[(\beta_2 - \beta_1) M_1]$.

As a result of the statistical dispersion in the expressions relating M, X and y, Eq 3 has to be changed to the following:

$$\nu(y) = \int_{vol} \lambda[M(y,X)] \varphi(y, X)\, dV \qquad (6)$$

where $\varphi(y, X)$ is a corrective function that can be computed as described in Ref 21.

4. ANALYTICAL MODELS OF SEISMICITY.

As has been pointed out, when engineering decisions concerning construction in seismic areas have to be made, it does not suffice to express local seismicity in terms of an upper bound for magnitudes, the probability of whose exceedance is arbitrarily assumed to be negligibly small. Instead, it should be expressed in terms of the probability distribution of the maximum magnitude that can be generated at given sources during given time periods. These probabilities depend on the following factors:

a) Frequency-magnitude relations for small volumes of the earth's crust
b) Statistical correlation functions of the processes of earthquake generation in time and space.

particularly in small areas or for large magnitudes. After consideration of the geophysical processes in play it is reasonable to conclude, however, that if strain energy stored in a region grows in a more or less systematic manner, the risk function should grow with the time elapsed since the last event. Preliminary statistical analysis of the waiting times between earthquakes with magnitudes 6.5 or 7.0 and greater in some seismic provinces in the southern coast of Mexico shows that if shocks occurred in the same seismic province within a few months of each other are lumped together as single events, the resulting distribution of waiting times can be approximated by a gamma function with k = 2. However, results have not been uniform. Reliable evaluations of alternate assumptions concerning k will have to rest partially on prediction of the process of storage and liberation of strain energy.

According to Eqs 1 and 2, the actualized value of the expected cost of damage or failure is a function of $\nu_t(y)$, which is a function not only of $\lambda(x)$ in the neighbouring seismic sources, but also of the probability distribution of $T/E(T)$. The possible significance of the value of k in the variables that affect seismic design decisions can be inferred from Table 2, which compares the initial and the conditional expected values of the time to next event, as well as the actualized values of the expected cost of failure for the Poisson and the gamma processes. These quantities were computed by means of the expressions developed in the appendix. The actualized value of the expected cost of failure was obtained from the expression that follows.

$$\frac{E[F]}{D} = \int_0^\infty f_{t_1}(t+t_0 \mid T > t_0)\, e^{-\nu t}\, dt \qquad (12)$$

This expression is consistent with the assumptions that a structure fails when a given intensity with return period E(T) is exceeded, that the cost of that failure is D, and that the system is not rebuilt after failure. k was taken as 2, and two values of $\gamma E(T)$ were considered: 10 and 100.

TABLE 2. COMPARISON OF POISSON AND GAMMA PROCESSES

t_0	GAMMA PROCESS, k = 2				POISSON PROCESS		
	$E(t \mid T>t_0)$	$E(T_1 \mid T>t_0)$	$E(F)/D$ $\gamma E(T)=10$	$E(F)/D$ $\gamma E(T)=100$	$E(t \mid T>t_0) = E(T_1 \mid T>t_0)$	$E(F)/D$ $\gamma E(T)=10$	$E(F)/D$ $\gamma E(T)=100$
0	1.0	0.75	0.0278	0.0004			
0.1	0.92	0.73	0.0211	0.0036			
0.2	0.86	0.71	0.0175	0.0059			
0.5	0.75	0.67	0.0093	0.0100			
1	0.67	0.63	0.120	0.0132	1.0	0.0909	0.0099
2	0.60	0.58	0.139	0.0156			
5	0.54	0.54	0.154	0.0179			
10	0.52	0.52	0.160	0.0187			
00	0.50	0.50	0.167	0.0196			

This table shows very significant differences between the expected cost of failure for both processes. At small values of t_0, E(F)/D for the Poisson process is greater than that for the gamma process, but as time goes on and no earthquakes occur, E(F)/D grows gradually for the gamma process, until the actualized risk for the latter becomes nearly twice that for the Poisson process. Clearly, the problem is significant when making engineering decisions.

tones where surface evidence of motions does not exist. Hence, consideration of the overall behaviour of complex geological structures is in general more significant than the study of local details.

To the authors's knowledge, not much work has been done in the analysis of the overall behaviour of large geological structures with respect to the energy that can be expected to be liberated per unit volume and per unit time in given portions of those structures. Important research and applications should be expected, however, since, as a result of the contribution of modern plate tectonics theory to the understanding of large scale tectonic processes, the numerical values of some of the variables correlated with energy liberation are being determined, and can be used at least to obtain orders of magnitude of expected activity along plate boundaries. Far less understood are the occurrence of shocks in apparently inactive regions of continental shields and the behaviour of complex continental blocks or regions of intense folding, but even there some progress is contemplated in the study of accumulation of stresses in the crust (15).

Knowledge of the geological structure can serve to formulate initial probability distributions of seismicity even when quantitative use of geophysical information seems beyond reach. Initial probability distribution of local seismicity parameters α, β, M_1 (Eq 5) of the relatively small volumes of the earth's crust that contribute significantly to the seismic risk at a site can be assigned by comparison with the average seismicity observed in wider areas of similar tectonic characteristics or where the extent and completeness of

statistical information warrant reliable estimates of frequency-magnitude curves (1). In this manner we can, for instance, use the information about the average distribution of the depths of earthquakes of different magnitudes throughout a seismic province in order to estimate the corresponding distribution in an area of that province where activity has been low during the observation interval even though there might be no apparent geophysical reason for the difference. Likewise, the expected value and the coefficient of variation of $\lambda(M)$ in a given area of moderate or low seismicity (like a continental shield) can be obtained from the statistics of the motions originated at all the supposedly stable or aseismic regions in the world (16).

Fig. 1 illustrates the kind of concepts that one has to consider when trying to use all available information for the quantitative probabilistic analysis of seismic risk. The southern coast of Mexico is one of the regions of highest activity in the world. Large shallow shocks are produced by the interaction of the continental mass and the ocean bottom's plate (Cocos plate) that underthrusts it. Seismological data shows significant gaps of activity along the coast during the present century and not much is known about previous history. At points along these gaps seismic risk estimates based on observed intensities would be quite low. No significant difference is evident in the geological structure of these regions with respect to the rest of the coast, with the exception of some faults transverse to the coast, that divide the continental formation into several blocks. An analysis of the locations of previous [illegible] along

are the parameters of this initial distribution of ν, if k is assumed to be known, and if the observed outcome is expressed as the time t_n elapsed between n + 1 consecutive events (earthquakes with magnitude > M), application of Eq 13 leads to the conclusion that the posterior probability function of ν is also gamma, now with parameters $\rho + nk$ and $\mu + t_n$. The initial and the posterior expected values of ν are respectively equal to ρ/μ, and to $(\rho + nk)/(\mu + t_n)$. When initial uncertainty about ν is small ρ and μ will be relatively large and the initial and the posterior expected values of ν will not differ greatly. On the other hand, if only statistical information were deemed significant, ρ and μ should be given very small values in the initial distribution, and E(ν), and hence λ(M), would be practically defined by n, k and t_n. This means that the initial estimates of geologists should not only include expected or most probable values of the different parameters, but also statements about ranges of possible values and degrees of confidence attached to each.

In the case studied above only a portion of the statistical information was used. In most cases, especially if seismic activity has been low during the observation interval, significant information is provided by the durations of the intervals elapsed from the initiation of observations to the first of the n + 1 events considered and from the last of these events until the end of the observation period. Here, application of Eq 13 leads to expressions slightly more complicated than those obtained when only information about t_n is used.

The particular case when the statistical record reports no events during time t_0 comes up frequently in practical problems. Expressions applicable to

that situation are presented in the appendix. Here, consider their application to one of the seismic gaps in Fig 1. An initial set of assumptions and corresponding probabilities was adopted as described in the following. From previous studies referring to all the southern coast of Mexico, local seismicity in the gap area (measured in terms of λ for M > 6.5) was represented by a gamma process with k = 2. An initial probability density function for ν was adopted in such a manner that the expected value of λ(6.5) for the region coincided with its average throughout the complete seismic province. Two values of ρ were considered: 2 and 10, which correspond to coefficients of variation of 0.71 and 0.32, respectively. The values in Table 3 were obtained for the ratio of the final to the initial expected values of ν, in terms of u_0, the ratio of the length of the observation interval to the initial expected value of the return period, E(T).

TABLE 3. BAYESIAN ESTIMATES OF SEISMICITY IN ONE SEISMIC GAP

$u_0 = t_0/E(T)$	$E''(\nu)/E'(\nu)$		$E''(\tau_1 \mid T_1 > t_0)$	
	ρ = 2	ρ = 10	ρ = 2	ρ = 10
0	1.0	1.0	0.75	0.75
0.1	0.85	0.99	0.76	0.74
0.5	0.75	0.94	0.91	0.71
1	0.58	0.87	1.14	0.73
5	0.20	0.54	3.11	1.05
10	0.11	0.36	5.47	1.55
20	0.06	0.22	10.50	2.48

The last two columns of the table contain the ratios of the computed values of $E(T_1)$ and E(T) when ν is taken equal respectively to its initial or to its

4. J. L. Trigos and L. Esteva, Riesgo sísmico en El Sombrero (México), *Institute of Engineering*, National University of Mexico (1973)

5. N. N. Ambraseys, Dynamics and response of foundation materials in epicentral regions of strong earthquakes, *Proc., 5th World Conference on Earthquake Engineering*, Rome (1973)

6. D. E. Hudson, Analysis of strong motion earthquake accelerograms, Vol. III, Response spectra, part A, *EERL, Caltech*, Pasadena, Calif. (1972)

7. D. E. Hudson, Ed., Strong motion instrumental data on the San Fernando earthquake of February 9, 1971, *EERL, Caltech*, Pasadena, Calif. (1971)

8. D. E. Hudson, Strong motion earthquake accelerograms, digitized and plotted data, Vol. III, corrected accelerograms and integrated ground velocity and displacement curves, Part A, *EERL, Caltech*, Pasadena, Calif. (1971)

9. L. Esteva and R. Villaverde, Seismic risk, design spectra and structural reliability, *Proc., 5th World Conference on Earthquake Engineering*, Rome (1973)

10. J. H. Dietrich, A deterministic near-field source model, *Proc., 5th World Conference on Earthquake Engineering*, Rome (1973)

11. M. I. Todorovska, Characterization of response spectra by parameters governing the gross nature of the earthquake source mechanism, *Proc., 5th World Conference on Earthquake Engineering*, Rome (1973)

12. R. E. Wallace, Earthquake recurrence intervals on the San Andreas Fault, *Bull. Geological Society of America*, Vol. 81 (oct 1970)

13. G. F. Davies and J. N. Brune, Regional and global fault slip rates from seismicity, *Nature Physical Science*, Vol. 229, No 4 (jan 1971)

14. B. A. Petrushevsky, The geological fundamentals of seismic zoning, *Scientific Translation Service*, order 5032, Ann Arbor, Mich (1966)

15. E. Artyushkov (Institute of Physics of the Earth, USSR Academy of Sciences), personal communication.

16. L. Esteva, Bases para la formulación de decisiones de diseño sísmico, *Institute of Engineering*, National University of Mexico (1968)

17. H. Raiffa and R. Schlaifer, Applied statistical decision theory, *MIT Press*, Cambridge, Mass (1969)

18. E. Parzen, Stochastic processes, *Holden Day*, San Francisco (1962)

19. E. Rosenblueth, Optimum design for infrequent disturbances, *Submitted for publication to ASCE* (1974)

The corresponding conditional probability density function for T_1 is

$$f_{\tau_1}(u|T_1 > t_o) = \frac{\sum_{n=1}^{k} (n^{-k} - 1)! \, [k(u+t_o)]^{n-1}}{\sum_{n=1}^{k} \sum_{i=1}^{n} \frac{1}{(n-1)!} (k\,t_o)^{n-i}} \, e^{-k t_o} \qquad (A4)$$

where $\tau_1 = (T_1 - t_o)/E(T)$.

The conditional expectations of T and T_1 can be obtained from weighting of T and T_1 with respect to the probability density functions of Eqs A3 and A4:

$$E(\tau \mid T > t_o) = (A - Bt_o)/B \qquad (A5)$$

$$E(\tau_1 | T_1 > t_o) = (A_1 - B_1 t_o)/B \qquad (A6)$$

where

$$A = \sum_{n=1}^{k+1} \frac{1}{(n^{-1} - 1)!} (k t_o)^{n-1} e^{-k t_o} \qquad (A7)$$

$$B = \sum_{n=1}^{k} \frac{1}{(n^{-1} - 1)!} (k t_o)^{n-1} e^{-k t_o} \qquad (A8)$$

$$A_1 = \frac{1}{k} \sum_{n=1}^{k} \sum_{i=1}^{n+1} \frac{n}{(n-1)!} (k t_o)^{n-1} e^{-k t_o} \qquad (A9)$$

$$B_1 = \frac{1}{k} \sum_{n=1}^{k} \sum_{i=1}^{n} \frac{1}{(n-1)!} (k t_o)^{n-1} e^{-k t_o} \qquad (A10)$$

APPENDIX 2. BAYESIAN ESTIMATION OF ν WHEN $T_1 > t_o$

Suppose that the initial probability density function of ν in a given area is gamma with parameters ρ and μ, and that no events have occurred in the area for t_o years. The probability of this outcome given ν is equal to the probability that $T_1 > t_o$. From integration of Eq A1 one obtains,

$$P(T_1 > t \mid \nu, k) = \frac{1}{k} \sum_{n=1}^{k} \sum_{i=1}^{n} \frac{1}{(n-1)!} (\nu t_o)^{n-1} e^{-\nu t_o} \qquad (A11)$$

Application of Eq 13 in this case can be expressed as

$$f''(\nu \mid T_1 > t_o) = \frac{f'(\nu) \, P(T_1 > t_o | \nu, k)}{\int f'(\nu) \, P(T_1 > t_o | \nu, k) \, d\nu} \qquad (A12)$$

Here, f' and f'' stand for the initial and posterior probability density functions of ν and f'(ν) adopts the form of a gamma function with parameters ρ and μ. After performing all substitutions and integrations, the following is obtained:

$$f''(\nu \mid T_1 > t_o) = K^{-1} \sum_{n=1}^{k} \sum_{i=1}^{n} B_n \, E_n(\nu) \qquad (A13)$$

Here,

$$K = \sum_{n=1}^{k} \sum_{i=1}^{n} B_n \qquad (A14)$$

DIVISION DE EDUCACION CONTINUA
FACULTAD DE INGENIERIA U.N.A.M.

VII CURSO INTERNACIONAL DE INGENIERIA SISMICA

SISMOLOGIS Y SISMICIDAD

ORIGEN DE LOS TEMBLORES

* The Interior of the earth
* The Plastic layer of the earth's mantle
* The confirmation of continental drift
* The San Andreas Fault

M en C Jorge Prince Alfaro

Julio, 1981

THE INTERIOR OF THE EARTH

K. E. BULLEN
[illegible]

Each year 10 or more major earthquakes shake the earth. The smallest of them releases about a thousand times more energy than an atomic bomb; the Assam earthquake of August, 1950, had about 100,000 times that energy. The waves set up by these convulsions travel through the whole interior of the earth, including the core, and their paths are bent and shaped by the [illegible] of the earth's internal structure. Thus the waves [illegible] clues of the regions [illegible] from the [illegible] they tell when they are received at seismological stations on the surface it is possible to form a picture of the interior. In effect the seismologist X-rays the earth, even if at times [illegible] cloudily.

Seismology has lifted our notions about the interior of our planet from the realm of wild speculation to the stage of scientific measurement and well-reasoned inferences. Combined with geological information about surface rocks, laboratory experiments on rocks at high pressures and certain astronomical observations, it gives us a basis for learning something about the various conditions in the deep interior—its layered structure, the materials, their physical state, the pressures and so on.

The study of earthquakes is a fairly new science. In 1750 a writer on the subject in the *Philosophical Transactions* of the Royal Society of London apologized to "those who are apt to be offended at any attempts to give a natural account of earthquakes." But observations of earthquake effects accumulated, and late in the 19th century seismology began to emerge as a real quantitative science when the Englishman John Milne constructed in Japan a seismograph suitable for world-wide use. The seismograph was later developed further, notably by E. Wiechert in Germany, by Prince Galitzin in Russia and recently by Hugo Benioff of the California Institute of Technology.

The release of elastic strain-energy at the source, or "focus," of an earthquake produces waves which begin to radiate in all directions from the focus. In 1897 R. D. Oldham of England identified on seismograms three main types of seismic waves: (1) primary (P) waves, which are compression-and-expansion waves like those of sound; (2) secondary (S) waves, which vibrate at right angles to the direction of travel, as

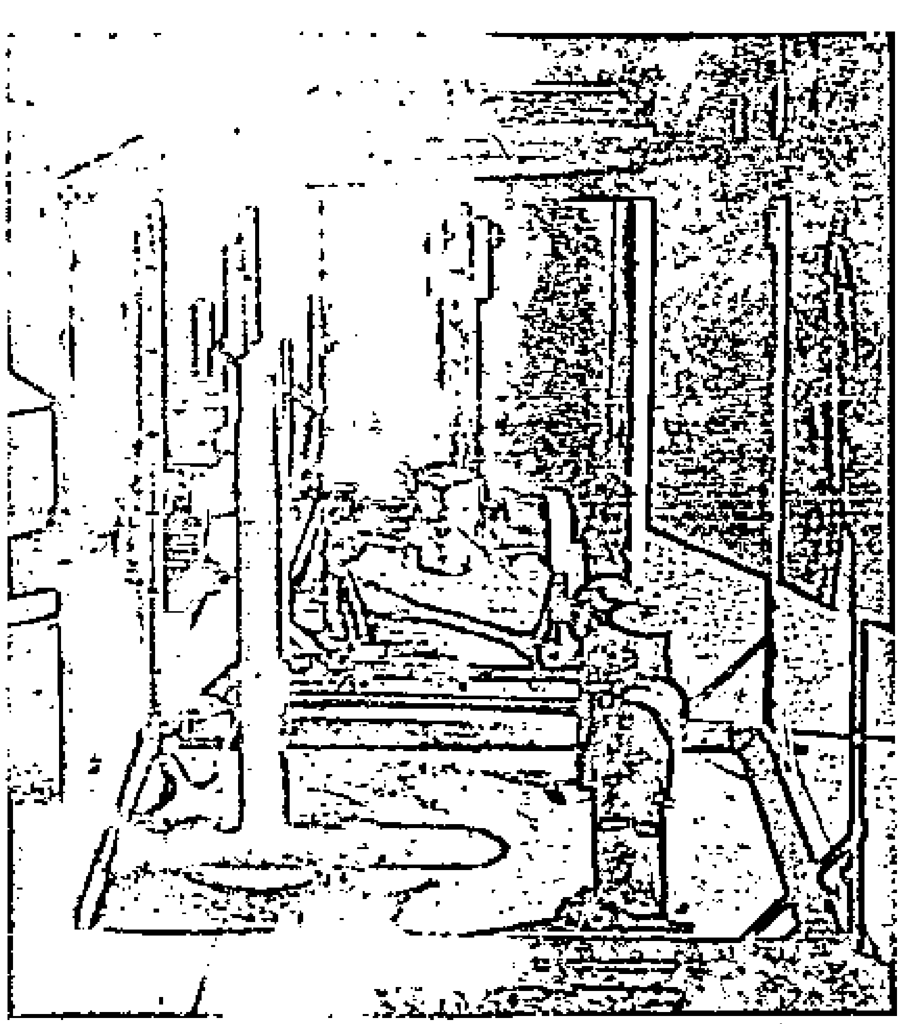

TWO SEISMOMETERS are photographed at the Lamont Geological Observatory of Columbia University. They consist essentially of three pendulums: one for each dimen-

light waves do; (3) surface waves, which appear in the upper 20 miles or so near the earth's surface. The P waves travel through both solid and liquid parts of the earth; the S waves only through solid.

S waves travel at about two thirds of the speed of P waves. The speed of both varies with depth in the earth; for example, the P waves travel at 8½ miles per second, their maximum speed, at a depth of 1,800 miles and at about three miles per second in rocks near the earth's surface. Because of the change of speed, the path of the waves' travel usually curves upward. When they arrive at a boundary between layers they may be refracted or reflected, and on reaching the earth crust they are reflected downward again. At a boundary either a P or an S wave may give rise to both P and S waves. Thus any one seismogram from a particular earthquake may show many distinct phases, signifying the stages of the waves' routes and their changes of form. A typical seismogram illustrating several phases is shown on the next two pages.

With this kind of evidence Oldham proved in 1906 that the earth has a large central core, and in 1914 Beno Gutenberg, then in Germany, located the boundary of the core at 1,800 miles below the earth's surface. Since the radius of the whole earth is about 3,960 miles, the central core has a radius of some 2,160 miles.

The discovery of the core came about from the observation of shadow zones where relatively few P waves were recorded. Consider P waves issuing from a major earthquake with its focus at the South Pole. These waves would be observed at the surface throughout the Southern Hemisphere and up to 15 degrees above the equator (*i.e.*, the latitude of Guatemala) in the Northern Hemisphere. But between the latitudes of Guatemala and Winnipeg little indication of P waves would be received. Then, from a latitude of 52 degrees north to the North Pole, the waves would come in again strongly. The whole of the U. S. would thus be part of a "shadow zone" for that earthquake. On examination, it was seen that the existence of such shadow zones required the presence of a central core which would bend sharply downwards the seismic rays striking it from above, somewhat after the manner in which light rays from a stick in water are bent by the water surface.

One of the great labors of seismologists during the first 40 years of this century was to evolve reliable tables for the times of travel of P and S waves along the various phases of their routes. In 1930 Sir Harold Jeffreys of the University of Cambridge, suspecting that the existing "travel-time tables" contained large errors, began a long series of studies to correct them. The author of this article was associated with Jeffreys in this work from 1931 to 1939.

The Jeffreys-Bullen tables of 1940 are now used internationally. They agree closely, in the main, with travel times derived about the same time by Gutenberg and Charles F. Richter at the California Institute of Technology. The travel-time tables are of cardinal importance for charting the structure of the earth's

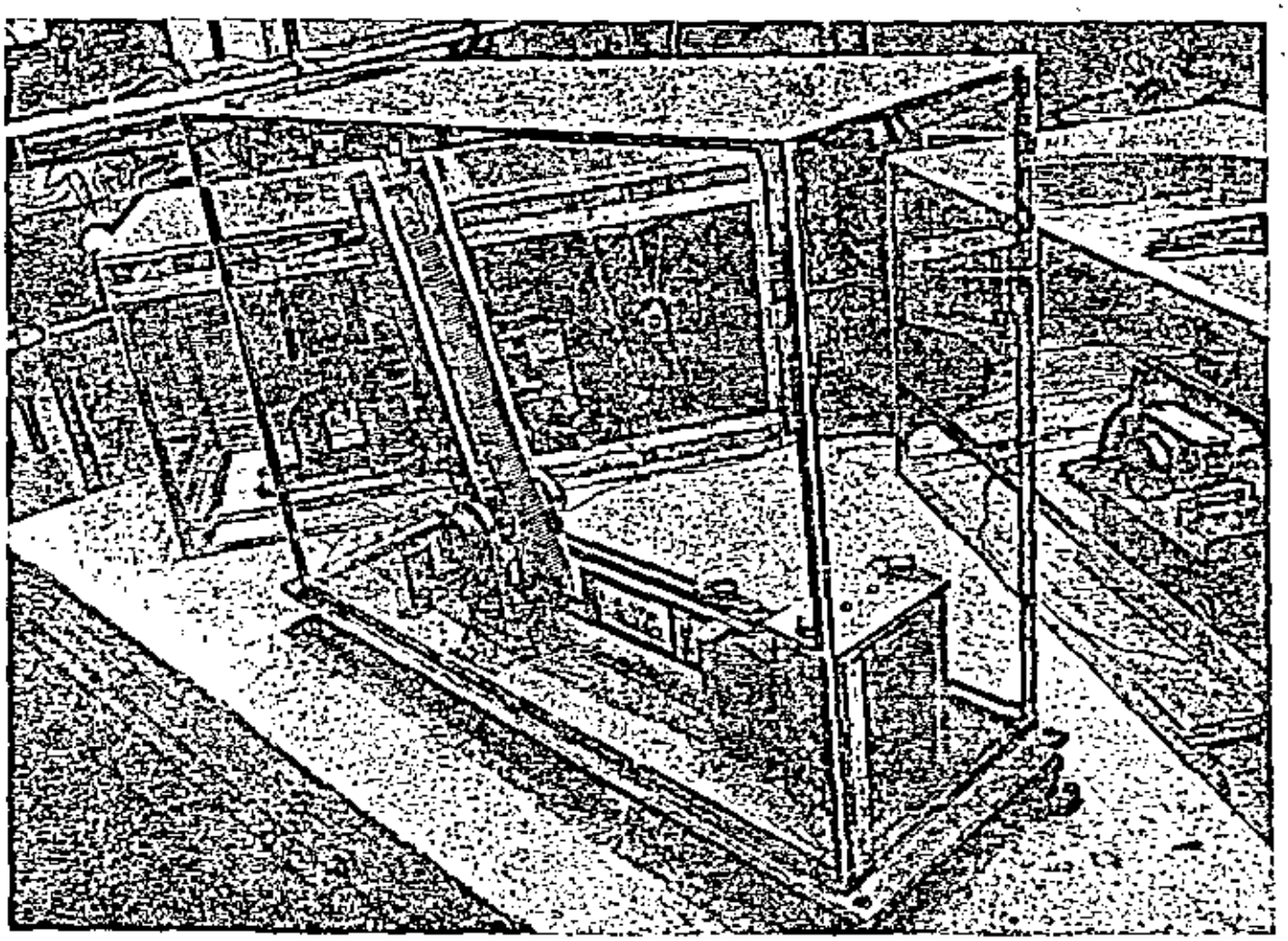

sion. When the earth shakes, the pendulums tend to stand still. Their apparent motion is then recorded by a pen or a beam of light. One of the pendulums, suspended by a horizontal arm and two diagonal wires, is visible at right in the photograph at left.

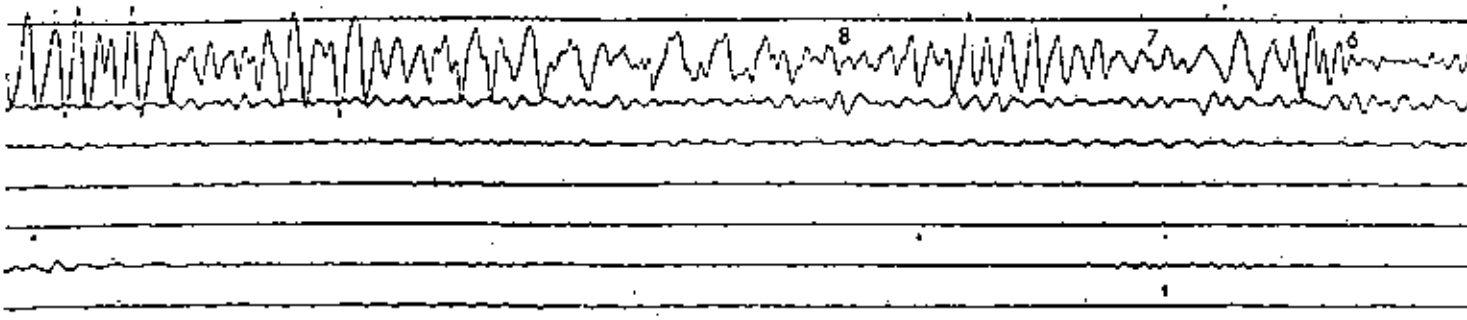

SEISMOGRAM of an earthquake on the Kamchatka Peninsula in Siberia was recorded at the Lamont Geological Observatory. The separate lines are actually part of a continuous spiral trace, going from right to left, on a circular drum. The interval between succes-

interior. It is possible to deduce from the tables the velocities of P waves and S waves in various parts of the interior. Studying the variations of velocity with depth, one can chart different layers and locate boundaries.

With the new tables Jeffreys calculated that Gutenberg's measurement, placing the boundary of the central core at 1,800 miles below the earth's surface, was correct within three or four miles. At least the outer part of the core is judged to be molten. S waves do not pass through it, and its fluid character is established by other evidence, including data on the tidal deformation of the solid earth and astronomical data on the movements of the earth's poles. H. Takeuchi of Japan has calculated that this region is at most one 300th as rigid as the next outward layer.

The use of the terms "solid" and "fluid" in connection with the huge pressures prevailing in the earth's interior is sometimes questioned. What a geophysicist means by the term "solid" in this context is simply that the elastic behavior of the material in question can be described by equations which match those applying to ordinary solids in normal laboratory conditions. These equations involve the use of two coefficients: "incompressibility," which is the measure of resistance to pressure, and "rigidity," signifying resistance to shearing stress. In the case of a fluid, the resistance to shear is much smaller than the resistance to compression. This is why a fluid does not transmit S waves.

All the earth outside the core is called the mantle. The whole of the mantle (apart from the oceans and pockets of magma in volcanic regions) is now known to be essentially solid: both S and P waves travel through every part of it.

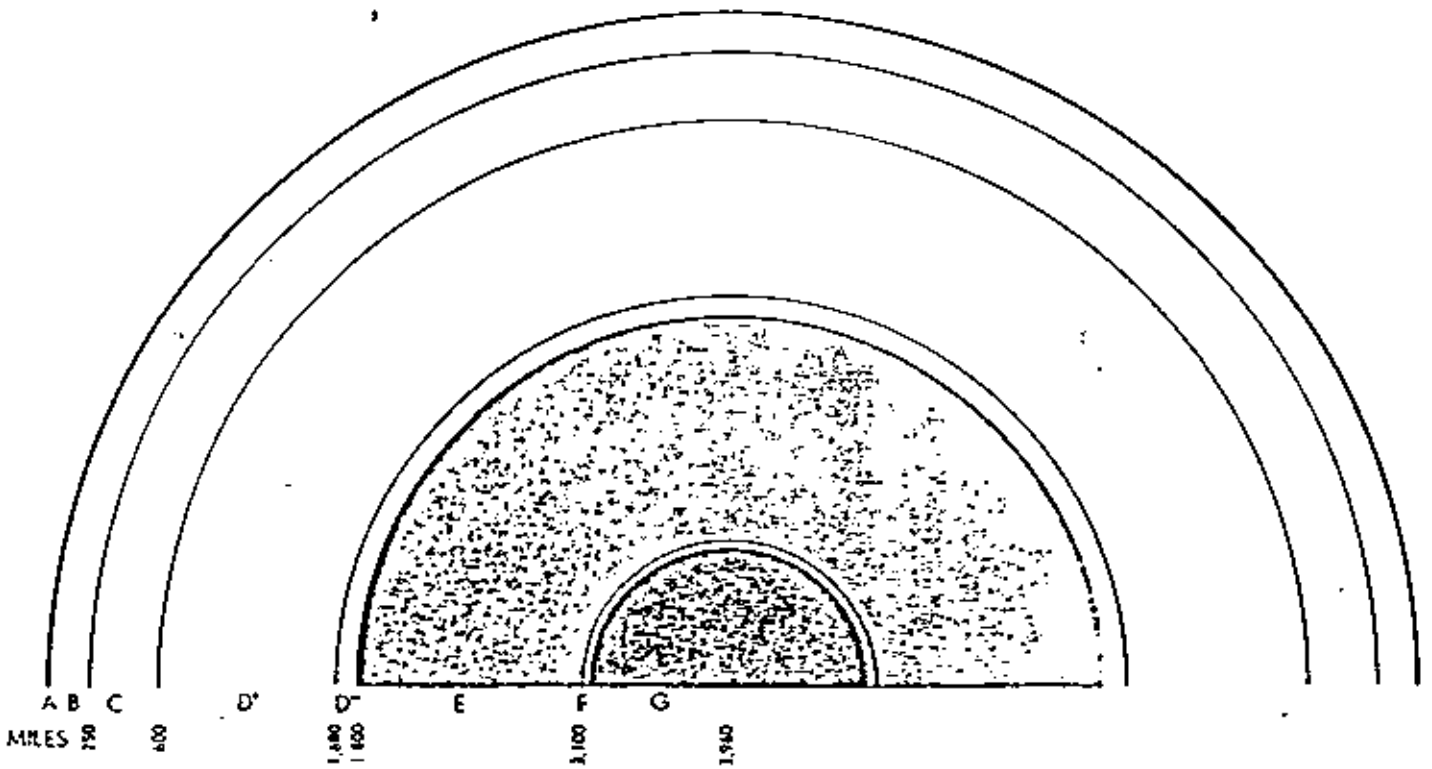

EARTH'S CROSS SECTION is divided into distinct layers through which seismic waves travel at different speeds. The outer core is indicated by the lighter tone of color; the inner core, by the darker tone of color. Layer A is the thin crust of the earth.

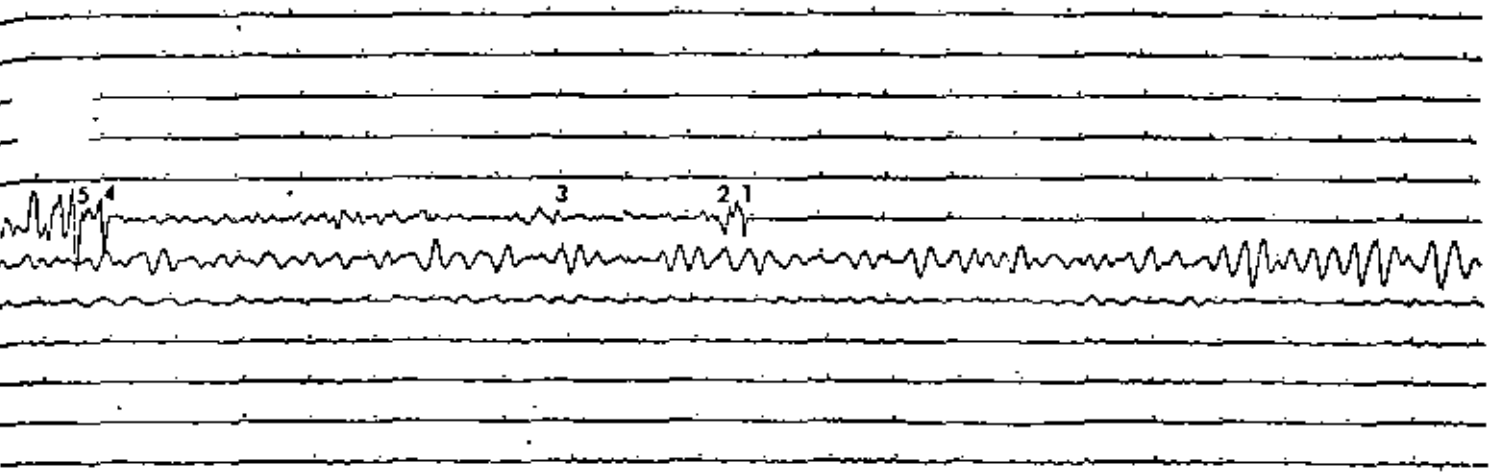

sive dots is one minute. The first disturbance recorded was the P wave designated by the number 1. Then followed the multiply reflected P waves 2 and 3. S waves begin at position 4, followed by multiply reflected waves at 5, 6 and 7. Surface waves start at 8.

In 1909 the Croatian seismologist A. Mohorovicic, studying the seismograph of a Balkan earthquake, discovered an important discontinuity (boundary) now known to be some 20 miles below the earth's surface. The part of the earth above the Mohorovicic discontinuity has come to be called the crust. But nowadays the term "crust" has only a conventional meaning. According to seismic evidence the crust is not more rigid than the material just below it.

Seismologically speaking, the crust differs from the underlying part of the mantle in the fact that P and S waves travel in it more slowly and with more variable speed. This irregularity of travel velocity makes detailed charting of the crust difficult. The work is being pursued vigorously, however, by the study of surface waves, of P and S waves from near earthquakes (near the recording station), of waves from large man-made explosions (such as the one on Helgoland in 1947) and by seismic probings with dynamite, as in oil prospecting. One important discovery has been that the crust is much thinner under the oceans than under the continents.

Seven distinct regions or shells have now been identified in the earth. In 1936 Miss I. Lehmann of Denmark discovered that the core was not uniform but seemed to consist of at least two different parts. Looking closely at the relatively minor P waves that emerge in the shadow zone on the surface, she concluded that these waves might come to the surface because they were bent sharply upward by an inner core where P waves traveled faster than in the outer core. Her proposal later received support from work by Gutenberg, Richter and Jeffreys. The inner core has a radius of some 800 miles, so the thickness of the

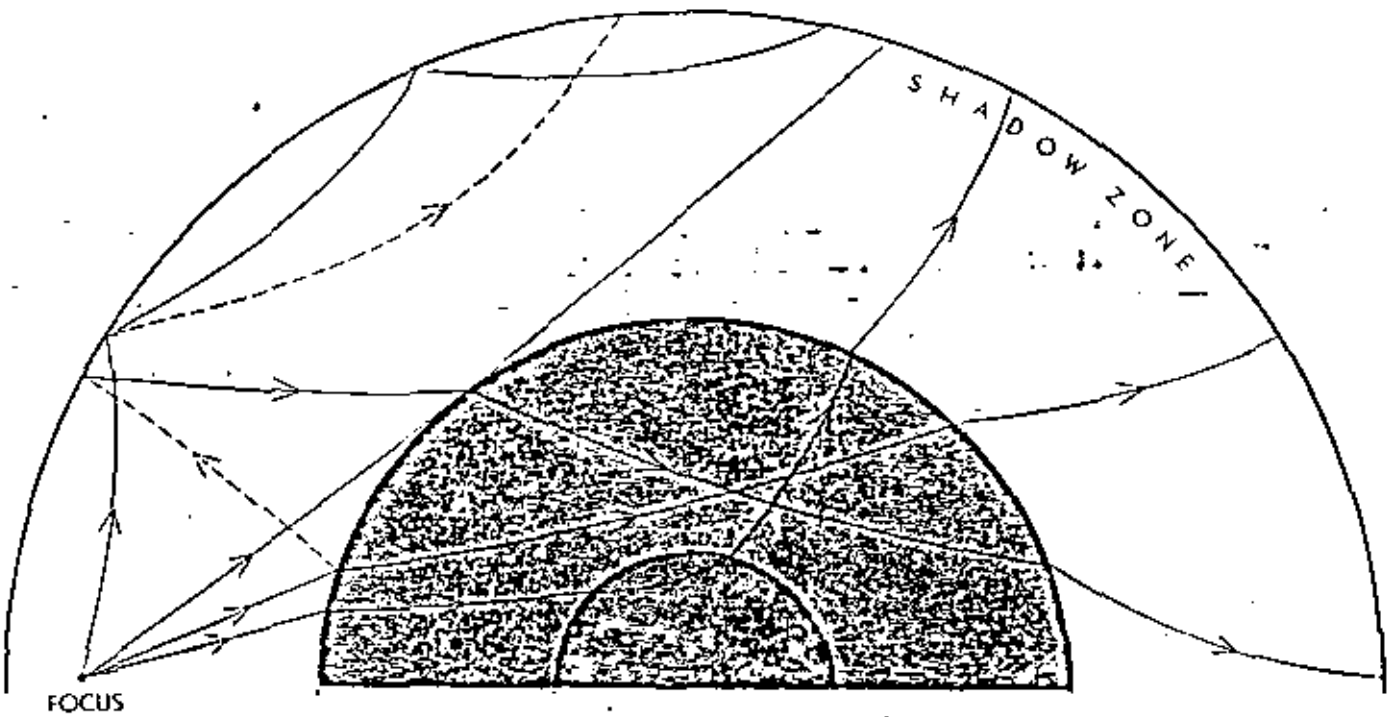

EARTHQUAKE WAVES are bent and reflected as they travel from their source. Solid lines represent P waves, dotted lines are S waves formed by reflection. The only P waves that can get into the shadow zone are those which enter the inner core and are sharply bent.

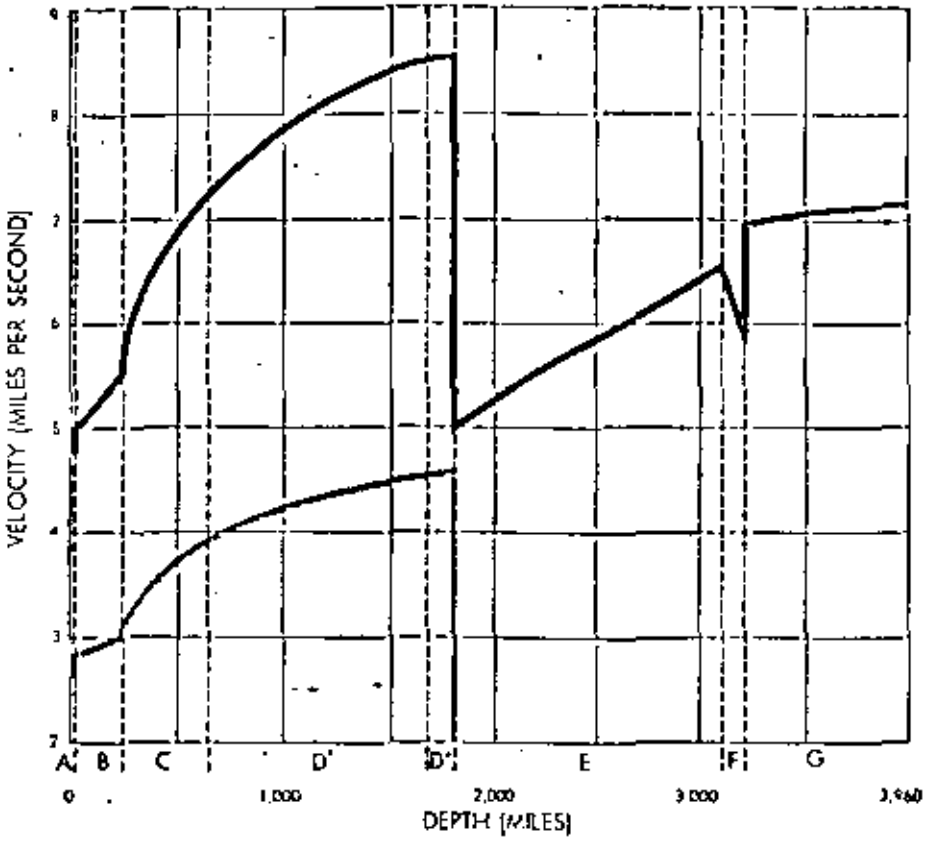

SEISMIC WAVE SPEEDS vary with depth. The black line gives velocities of P waves; the gray line, of S waves. Both change abruptly at core, or E layer, and the S wave disappears.

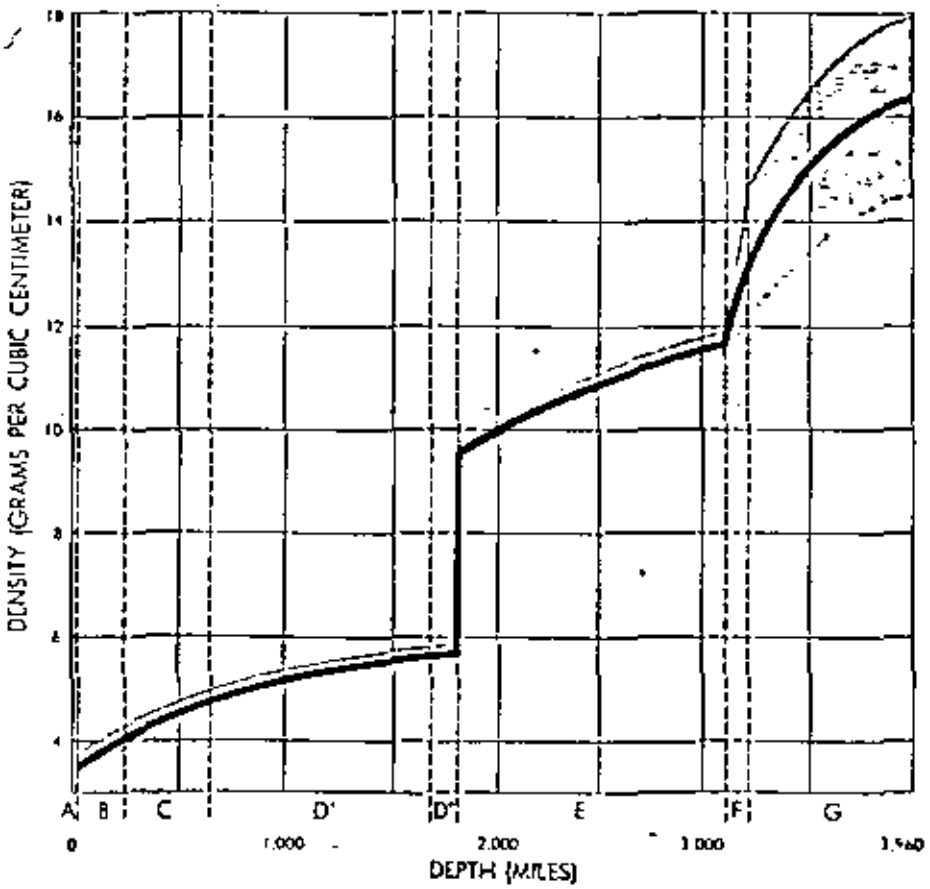

DENSITY of the earth's material increases with depth. The solid line shows the most probable value at each depth and the gray region outlines the probable range of uncertainty.

outer core would be about 1,300 miles.

On the basis of density variations the writer has divided the body of the earth into seven regions, called A, B, C, D, E, F and G [*see diagram on page 24*]. The A region is the crust. The rest of the mantle below is divided into B, C and D, with D subdivided into D' and D''. These divisions are still tentative because of certain uncertainties in estimates of velocity gradients. The outer part of the core is called E, and the inner part, G. Between the inner and outer core Jeffreys finds a layer F, some 80 miles thick, where the velocity of P waves declines sharply. Gutenberg has not found this layer, but has said that his data do not exclude its existence.

How can we estimate the pressures and physical characteristics of matter at these various depths in the body of the earth? The velocities of P and S waves are determined by the density, compressibility and rigidity of the material through which they pass, but they do not provide enough information to solve exact equations for those values. There are, however, indirect clues which help us to arrive at estimates—information on the earth's mass and moment of inertia, field observations and laboratory experiments on rocks, mathematical theories of elasticity and gravitational attraction.

By such means the writer has estimated that the earth's density increases gradually from 3.3 grams per cubic centimeter just below the crust to 5½ grams per c.c. at the bottom of the mantle, then jumps suddenly to 9¾ grams at the top of the core and thereafter increases steadily to 11¾ grams at the bottom of the outer core.

A related calculation gave the increase in pressure with depth in the earth. At the bottom of the Pacific Ocean the pressure is about 800 atmospheres. Only 200 miles down in the mantle the pressure is already 100,000 atmospheres—as great as the highest pressure Percy W. Bridgman of Harvard University has been able to produce in the laboratory. At the base of the mantle, 1,800 miles down, the pressure reaches the immense figure of 1½ million atmospheres, and at the center of the earth it is nearly four million atmospheres.

Next the calculations yielded the surprising finding that the rigidity of the material in the mantle increases with depth until, at the mantle's base, it is nearly four times that of steel in ordinary conditions. Below this, in the outer core, the seismic evidence shows that the rigidity sinks to practically zero, meaning that the material is essentially fluid.

Perhaps the most important fruits of this series of calculations have been the findings on compressibility. In spite of the sharp changes in density and in rigidity at the boundary between the mantle and the core, the compressibility of the material does not change substantially at the boundary, according to the calculations. This finding led the writer to examine the theoretical effect of pressures of a million atmospheres or more on materials likely to be present in the core. Taking into account a variety of evidence, the conclusion was that bounds could be set to the compressibilities of materials in the core.

Following this line of argument, it seems highly probable that the inner core, unlike the outer core, is solid in the sense defined. The idea that the inner core is solid, suggested by the writer in 1948 and since developed, would explain the speeding up of P waves when they penetrate into the inner core. Calculation indicates that the inner core is probably at least twice as rigid as steel at ordinary pressures.

On the same line of evidence we can also estimate, as we could not before, the density of the inner core. Apparently at the center of the earth the density is between 14½ and 18 grams per cubic centimeter. Yet another inference is that the increase of density with depth in the inner core (and at the base of the mantle) is greater than average, implying some variability in the composition of that region.

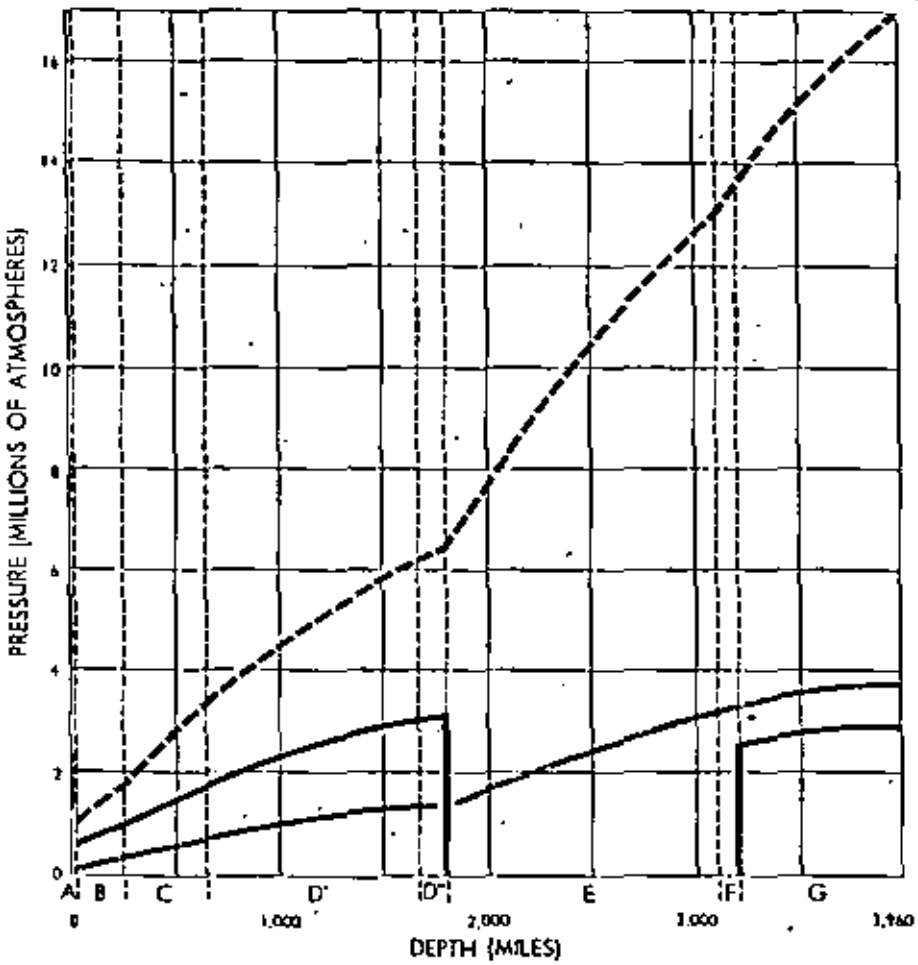

ELASTICITY of the earth's interior is shown graphically above. The gray line measures pressure. Incompressibility is indicated by dotted black line; rigidity, by solid black line.

What is the deep interior of the earth made of? For many years there have been good grounds for believing that much of the mantle below the crust consists of ultrabasic rock such as magnesium-iron silicate. The region B seems to be composed of a material like the known mineral olivine. C appears to be a transition region where the composition changes, perhaps only from one geometric form of olivine to another. The region D' may contain several distinct phases, such as silica, magnesia and iron oxide. The bottom of the mantle, D'', is probably of variable composition, but there is as yet no widely accepted agreement on what materials would have gravitated to this depth.

The composition of the central core has lately become the subject of extremely interesting new conjectures. It had long been assumed that the core consists largely of iron or nickel-iron, and this view was supported by analysis of meteorites, believed to be pieces of an exploded planet resembling the earth. But in 1941 W. Kuhn and A. Rittmann of Germany put forward the radical idea that compressed hydrogen made up the core. This theory, while contradicted by weighty arguments, gave rise to new investigations based on the idea that under increasingly high pressures the material at the base of the earth's mantle might suddenly jump in density. Thus the outer core may consist not of uncombined iron or nickel but of a high-density modification of the rocky material in the mantle just above it. This theory is highly controversial. On balance of probability the present evidence appears to favor a compromise; namely, that the outer core contains both uncombined iron and some material of appreciably smaller atomic number.

An interesting aspect of the new theory is that it makes plausible the idea that the planets Mars, Venus, Mercury and Earth are all of the same primitive over-all composition. Jeffreys has shown that the earth cannot have the same elemental composition as the other planets if its core is completely different from the mantle in composition. According to calculations by W. H. Ramsey of England and the writer, the observed masses and diameters of Mars and Venus, and the oblateness of Mars, would be accounted for fairly well by the theory that they are composed of terrestrial materials modified by pressure at depth.

As regards the earth's inner core, it probably consists of nickel and iron with perhaps some denser materials as well.

Estimates of the temperatures in the interior of the earth are much less certain than estimates of pressure. In deep mines the temperature rises at the rate of about 30 degrees Centigrade per mile as one descends. If it rose at this rate all the way down to the core the temperature in the center of the earth would exceed 100,000 degrees. Actually it is practically certain that the rate of increase is very much less in the depths of the earth. Present estimates are that the temperature at the center is no more than 2,000 to 6,500 degrees. In any case, it is fairly clear that the increase of temperature in the earth's interior is dwarfed by the increase in pressure.

5

THE PLASTIC LAYER OF THE EARTH'S MANTLE

DON L. ANDERSON

July 1962

Earth scientists have often pointed out that physical conditions inside our own planet are less well understood than those in stars light-years away. Even more paradoxical is the fact that the region within a few hundred miles of the surface presents more problems and gives rise to more technical controversy than the region below. One long-standing item of debate is the zone called the low-velocity layer.

In 1926 the seismologist Beno Gutenberg suggested that earthquake waves slow down when they travel through a zone roughly 100 to 200 kilometers (60 to 120 miles) below the surface. He attributed the effect to a decrease in the rigidity of the material in the zone compared with that above and below it. Most authorities considered his evidence to be dubious at best, and for 30 years they largely ignored his proposal. Recently a mass of data has accumulated that strongly supports the concept of a low-velocity, low-rigidity layer. Its existence has important implications for all theories concerned with structural changes in and near the earth's surface.

The idea that the earth becomes plastic—if not, indeed, liquid—at moderate depths goes back to the earliest days of geology. Volcanic lava flows pointed to a molten interior not too far below the surface. Observations on the rate of increase of temperature in deep mines indicated that if the temperature continues to increase at the same rate, rocks should be molten at depths of less than 100 kilometers. The enormous cracks and folds found in the earth's crust suggested upheavals in a mobile substratum. All this agreed with prevailing views of the origin of the solar system, which held that the earth and other planets had been torn loose from the sun and had had time to solidify only at the surface.

One of the most compelling arguments for some degree of fluidity in the interior came from the principle of isostatic equilibrium. As long ago as 1854 gravity measurements led geologists to suspect that the earth's crust floats on a denser material. Like other floating bodies, the crust seeks an equilibrium, riding deeper where it is heavier and rising higher where it is lighter. Subsequent studies, of both the strength of gravity and the propagation of earthquake waves, confirmed the notion, indicating that mountains have deep roots that support them just as the submerged portion of an iceberg supports the part above water, whereas plains resemble ice floes, having smooth upper and lower surfaces. Moreover, when the load on a part of the crust changes suddenly (on the geological time scale), the surface can be observed to respond by rising or sinking to restore equilibrium. For example, land covered by ice during the last glaciation is still rising at the rate of about a meter per century. Obviously this behavior implies that the material under the crust can flow, if only slowly.

On the other hand, several facts appeared to rule out the idea of widespread fluid material anywhere near the surface. From the tidal distortions of the solid earth in response to the pulls of the sun and moon, Lord Kelvin calculated that the earth is more rigid than steel. Studies of earthquake waves indicated that at depths down to thousands of kilometers the earth transmits not only compression waves (P waves) but also transverse, or shear, waves (S waves). Shear waves, which oscillate at right angles to their direction of motion, cannot propagate through liquids because liquids have no shear strength. When liquids are subjected to shearing forces, they simply flow. Finally, seismologists discovered that earthquakes originate as deep as 700 kilometers below the surface. Since an earthquake represents the abrupt yielding of rock to accumulated stress, it characterizes brittle, not plastic, material.

The answer to this apparent contradiction is suggested by the properties of noncrystalline materials such as glass and pitch, which behave like solids in

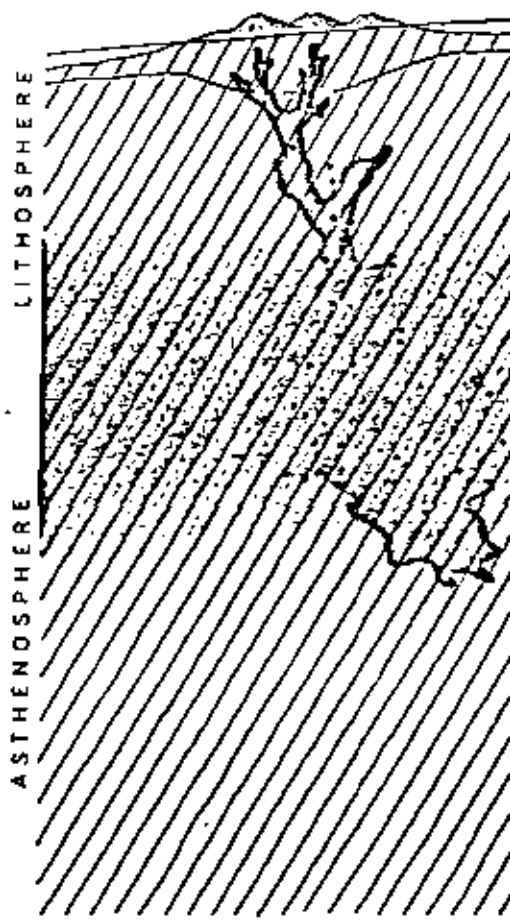

PLASTIC ZONE of earth's mantle (*color*) occupies an ill-defined region some 60 to perhaps 250 kilometers below the surface. In the plastic or low-velocity zone the tem-

the short run and like fluids over longer periods. They transmit shear waves and can support loads for a short time, but under a steady, long-lasting force they are plastic; that is, they flow and change their shape permanently. Under conditions of high temperature and high pressure the rock under the crust could also behave plastically. It would respond like a rigid solid to the relatively short-lived stresses that build up to cause earthquakes and the even briefer stresses involved in earthquake waves, while flowing slowly to adjust to the long-term stresses caused by changes in the weight of overlying material. Some geologists believe that the plastic substance under the crust is a glassy basalt. Recent evidence suggests, however, that it is crystalline. At high temperature even a crystalline material can flow easily, because melting at the boundaries of individual crystal grains allows them to slide over one another.

In 1909 the Yugoslav seismologist Andrija Mohorovičić proposed that at some distance below the surface there is a discontinuity where the velocity of earthquake waves jumps from about seven kilometers per second to eight. Subsequent measurements placed the Mohorovičić discontinuity, or Moho, at an average depth of 35 kilometers below the surface of the continents and only about five kilometers below the ocean floor. Under high mountains the Moho is as deep as 65 kilometers. Geologists saw in the Moho the lower boundary of the rigid, floating crust. The material between the Moho and the presumably liquid core of the earth they named the mantle. Yet the fact that seismic waves travel faster below the Moho than they do above it implies a greater rigidity at the top of the mantle than in the crust. It now seems clear that the Moho marks a change in chemical composition or crystal structure rather than an abrupt transition from strong to weak material.

The first seismic evidence for this transition was not forthcoming until Gutenberg announced the low-velocity zone. Actually what he had found was a decrease in the amplitude of compressional waves reaching the surface at a distance between 100 and 1,000 kilometers from an earthquake. At 1,000 kilometers the amplitudes were only a hundredth as great as they were at 100 kilometers. Beyond 1,000 kilometers the amplitudes increased sharply.

Gutenberg explained the effect by assuming a subsurface layer in which the earthquake waves travel slower than they do in the regions above or below. A wave entering this layer obliquely from above would be refracted downward, away from the surface, as light is bent downward when it passes from air to water. On leaving the bottom of the layer the wave would be refracted upward again [*see illustration on page 31*]. The result is that the wave would arrive at the surface farther away from its source than it would if there had been no decrease in velocity. Hence a gap would appear between the last "ray" that had missed the low-velocity layer and the first one to enter it. As the illustration shows, the gap, or shadow zone, is great-

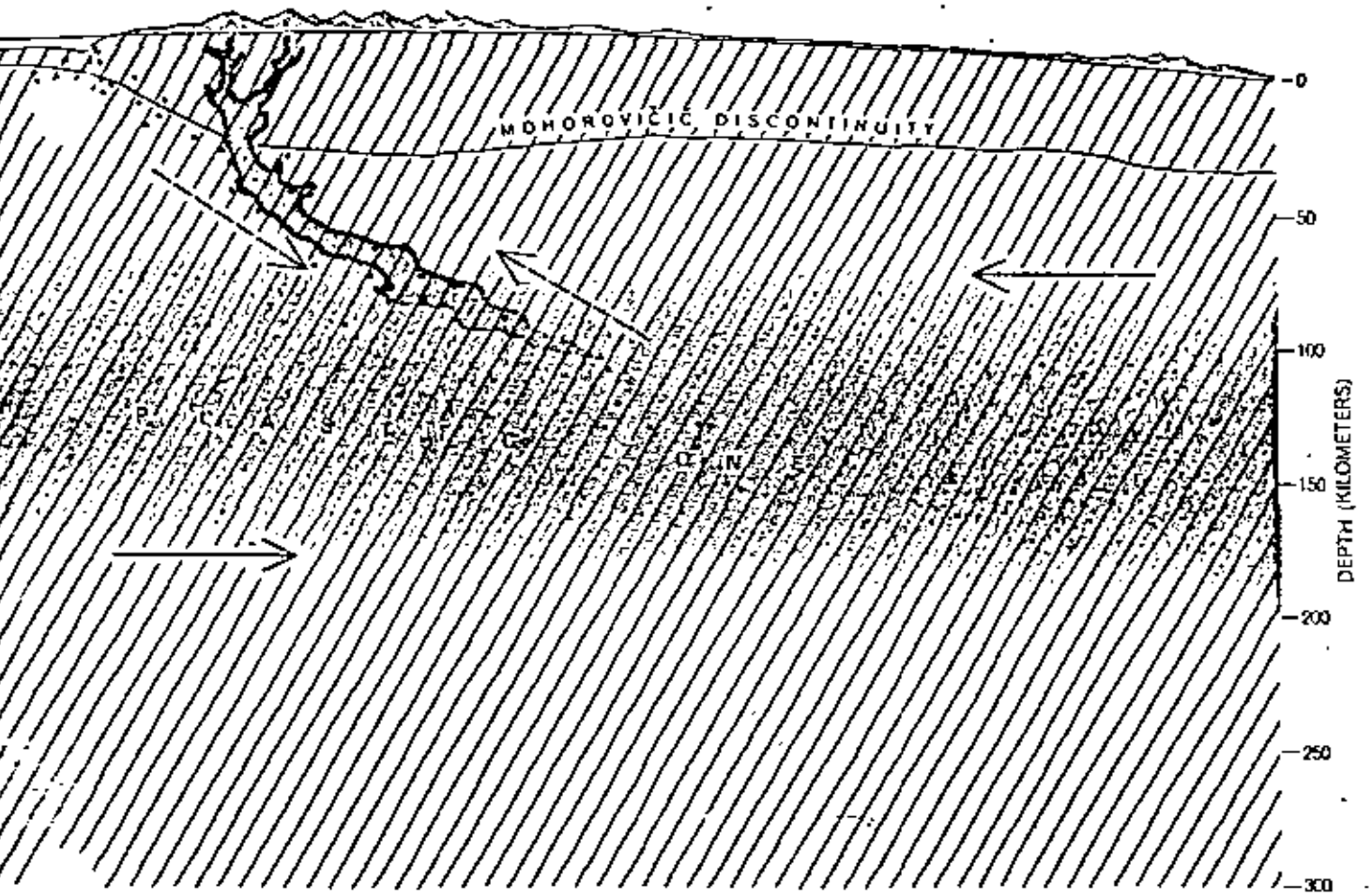

perature approaches the melting point of the rock. The lithosphere is very elastic or brittle rock; the asthenosphere, extending down to earth's core, can flow and relieve stress. In this highly schematic cross section of upper portion of earth, ocean and islands are at left. Dots denote earthquake foci. Broken arrows indicate possible movement of continents over ocean basin. Solid arrows mark hypothetical slippage of whole lithosphere over asthenosphere. The two solid-color regions represent magma, or molten rock.

est for an earthquake originating just above the top of the layer. Those coming from deeper levels evince no gap. From the extent of the shadow zone for different earthquakes, Gutenberg calculated that the layer is centered at a depth of about 150 kilometers, and that between 100 and 200 kilometers the velocity is some 6 per cent less than it is just under the Moho. Such a decrease in velocity means that the rock within the layer must be substantially less rigid than the material above and below it. The velocity does not reach the value it had at the base of the crust until some 250 or 300 kilometers below the surface.

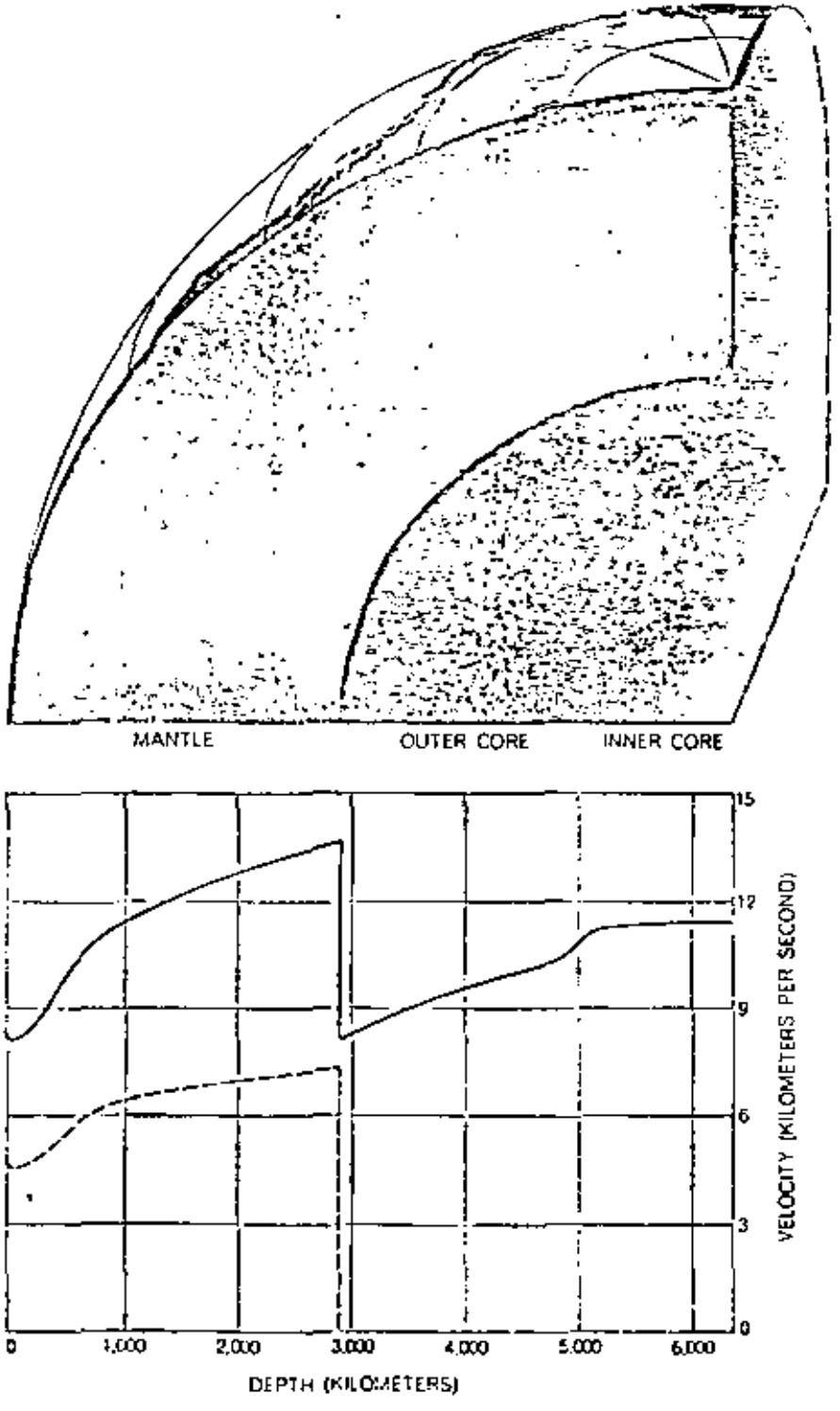

INTERNAL STRUCTURE OF THE EARTH is deduced from travel times of seismic waves. Solid line represents compressional, or P, waves; broken line represents shear, or S, waves. The latter disappear entirely at the outer core, indicating that this region is liquid. Low-velocity zone causes dip in curves at far left. Hatching on block diagram near surface marks low-velocity zone. It also marks transition zone above inner core at depth of 5,000 kilometers.

If the low-velocity layer were perfectly uniform, and if the waves really traveled as rays, the shadow zone at the surface would be completely "black." No waves at all would emerge within its limits. Actually the layer is full of inhomogeneities, and seismic waves do not travel strictly along classical ray paths. Like all waves, they bend around corners by diffraction, thereby leaking into shadowed regions. Both effects contribute to the energy that is found in the shadow zone.

It was partly this energy leak that made other workers reluctant to accept Gutenberg's conclusion. In those days seismologists paid little attention to the comparative amplitudes of earthquake waves. They were primarily interested in travel times, and they tended to accept any signal, weak or strong, if it appeared in their records at a time when readings at other seismographic stations led them to expect it.

Moreover, the evidence for the low-velocity layer was by no means clear-cut. The statistics were assembled from many earthquakes, large and small, shallow and deep. The data came from seismographs of different designs. In his calculations Gutenberg could make only approximate corrections for these variations as well as for the local irregularities, mostly unmapped, in the rock through which different waves traveled.

Underground nuclear explosions finally made possible a controlled experimental test of Gutenberg's analysis. The time, strength and location of these events is known so precisely that a single blast provides excellent data. Furthermore, seismographs today are more numerous, more sensitive and more standardized than they were in 1926. Studies of several explosions have confirmed the conclusions Gutenberg extracted so tediously from earthquake records [*see illustration on page* 33]. Seen in sharper detail, the low-velocity layer extends from about 60 kilometers to about 250 kilometers. (It is interesting to note that the layer damps blast waves so effectively that many seismologists think it poses a major difficulty for the detection of underground nuclear tests.)

Several independent pieces of evidence now support the idea of a low-velocity plastic layer. One is furnished by surface waves. These are seismic disturbances that follow the curved surface of the earth [*see bottom illustration on page* 32] instead of passing through its body. Although the waves travel along the surface, they "feel" the elastic properties of the underlying material to a

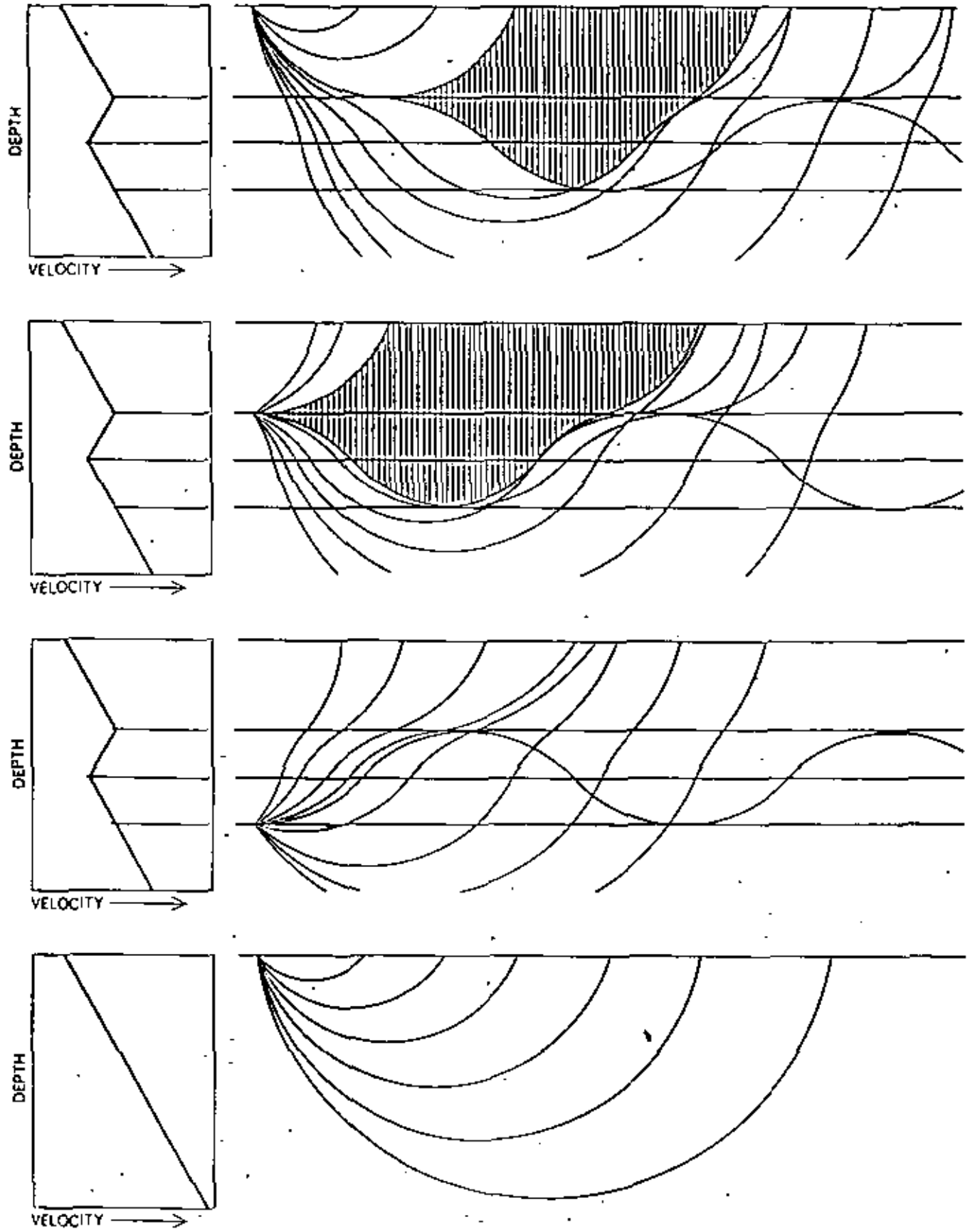

PATHS OF EARTHQUAKE WAVES bend in various ways in response to the low-velocity zone, depending on whether the earthquake occurs at the surface of the earth (*top*), at the top of the low-velocity zone (*second from top*) or below the zone (*third from top*). In the first two cases, refraction of waves by the zone creates a "shadow zone" (*hatching*), where direct waves from the earthquake do not appear. The bottom diagram shows how waves from an earthquake at the surface would travel if there were no low-velocity zone to bend them down. The graphs at left show changes in the velocity of earthquake waves with increasing depth.

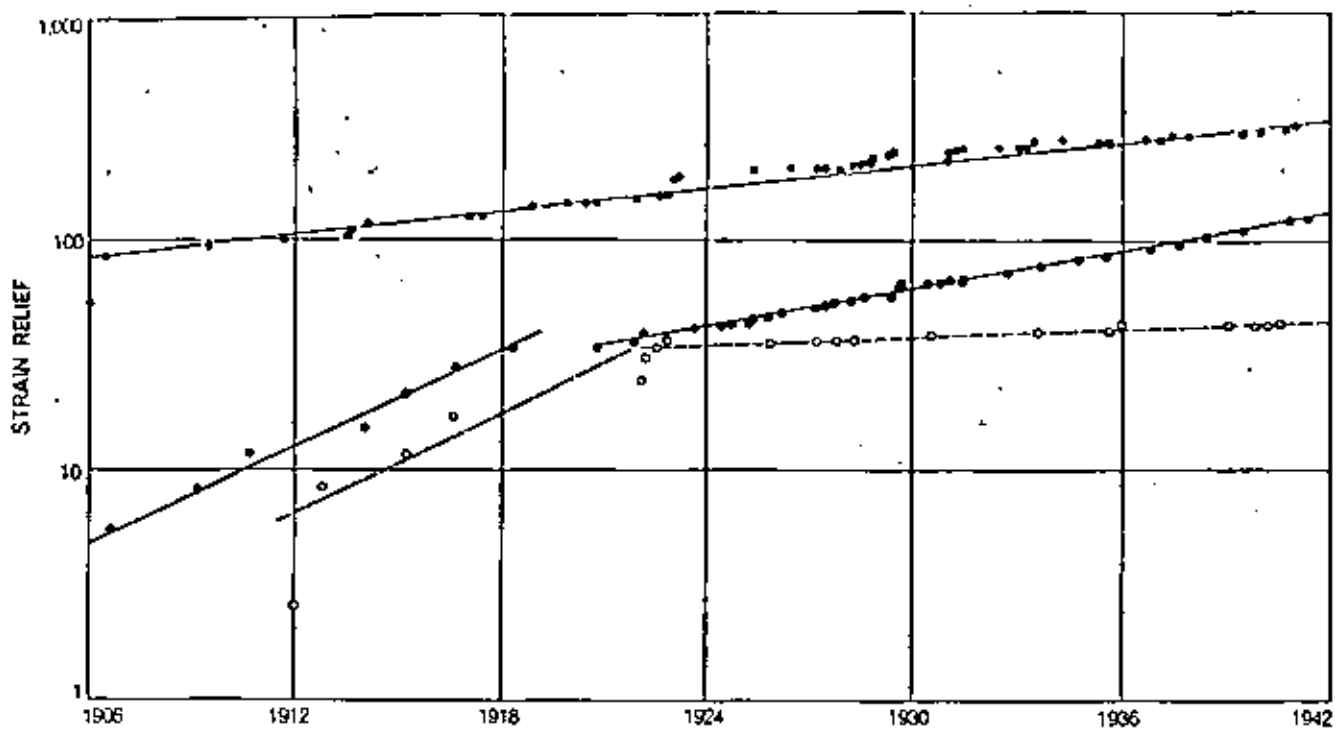

SEQUENCE OF EARTHQUAKES between 1906 and 1942 along west coast of South America falls into three groups: those occurring down to a depth of 70 kilometers (*colored dots, colored line*), those from 70 to 250 or 300 kilometers (*black dots, black line*) and those from 300 to 600 kilometers (*open dots, broken line*). The vertical scale shows relative amount of strain relieved by the quakes. Break in two lower groups around 1921 shows that they are mechanically coupled and are quite separate from the upper group.

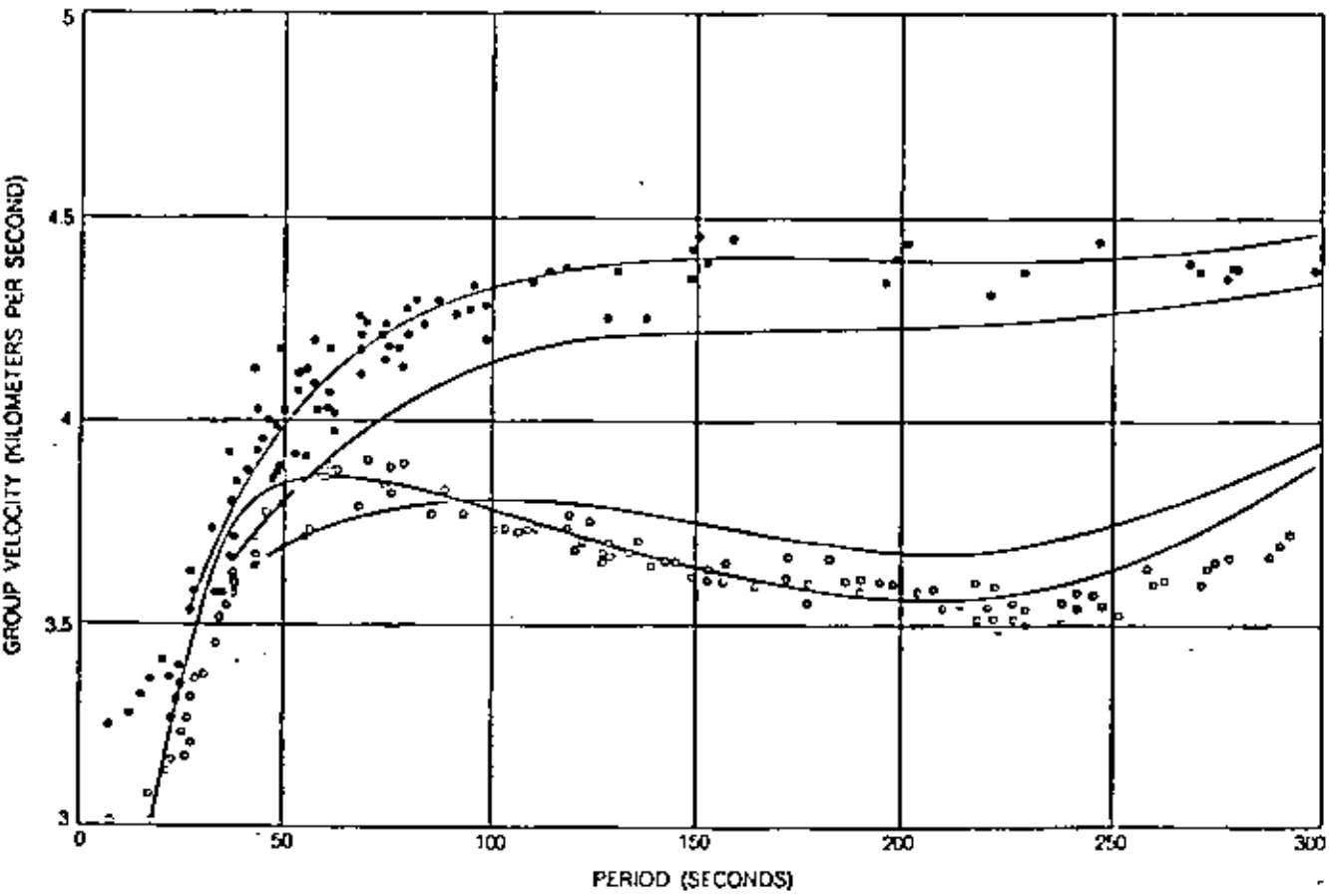

SURFACE-WAVE DATA reflect existence of low-velocity zone. The two types of dot represent actual observations of velocity of two kinds of surface waves plotted against wave period or length. Theoretical curves for an earth with a low-velocity zone (*colored lines*) fit observational data far more closely than do theoretical curves for an earth without a low-velocity zone (*black lines*).

depth that depends on their wavelength; the longer the wave, the deeper it feels (see "Long Earthquake Waves," by Jack Oliver; SCIENTIFIC AMERICAN Offprint 827). Since in general elasticity increases with depth, longer waves travel faster than shorter ones, and waves that start out together are dispersed, or spread out. Detailed analyses of the dispersion patterns show that elasticity does not increase continuously with depth but falls off in the region of the low-velocity layer.

Body waves, which pass through the deep interior, provide only a point-by-point sampling of the outer regions of the earth. Surface waves, on the other hand, contain information about these regions over their entire path. Recent studies of surface waves in our laboratory at the California Institute of Technology and at Columbia University have demonstrated for the first time that the low-velocity layer is present below the oceans as well as below the continents. Some of the waves used in the analysis had traveled around the earth as many as seven times. They indicate that the layer is in fact a world-wide phenomenon. Comparison of oceanic and continental paths shows that the waves are slowed more under the oceans. Evidently the geological differences between ocean basins and land masses are not limited to the crust but extend several hundred kilometers into the mantle.

Conclusive proof of the world-wide extent of the low-velocity layer came from the great Chilean earthquake of May 22, 1960. It was so violent that it set the earth as a whole into vibration, making it "ring" like a bell. The tone of a bell—that is, the frequencies at which it vibrates—depends on its elastic properties; a steel and a bronze bell emit different sounds. From records of the free vibrations following a big earthquake it is possible, with enormous mathematical labor, to deduce the elastic structure of the earth. The labor has been performed. It shows that the low-velocity zone is necessary to account for the observed frequencies.

In an attempt to construct a model of the earth that fits the current seismic data, I have been obliged to conclude that the low-velocity zone transmits the horizontal and vertical vibrations in shear waves at different speeds. A crystalline material in which the crystal grains were aligned in one direction would behave this way. One mechanism that could bring about such an alignment is a flow of the material. Others are directional heat flow and differential stress.

In addition to the purely seismic data, several other phenomena attest to a lowered rigidity in the material near the top of the mantle. Variations in atmospheric pressure cause measurable deflections of the earth's surface. The amount of deflection is much greater than it would be if the crust and mantle had the same strength. By assuming a weak layer in the upper mantle the observations can be explained quite well. Moreover, most earthquakes originate in the first 60 kilometers below the surface, at an average depth of 25 kilometers. At a depth of more than 60 kilometers the number falls abruptly, indicating a sudden drop in the strength of the rock.

From 60 kilometers down the frequency of earthquakes decreases steadily, dying away to zero at about 700 kilometers. This distribution implies that the rock becomes less brittle all the way from 60 to 700 kilometers and that it does not regain its strength at any deeper

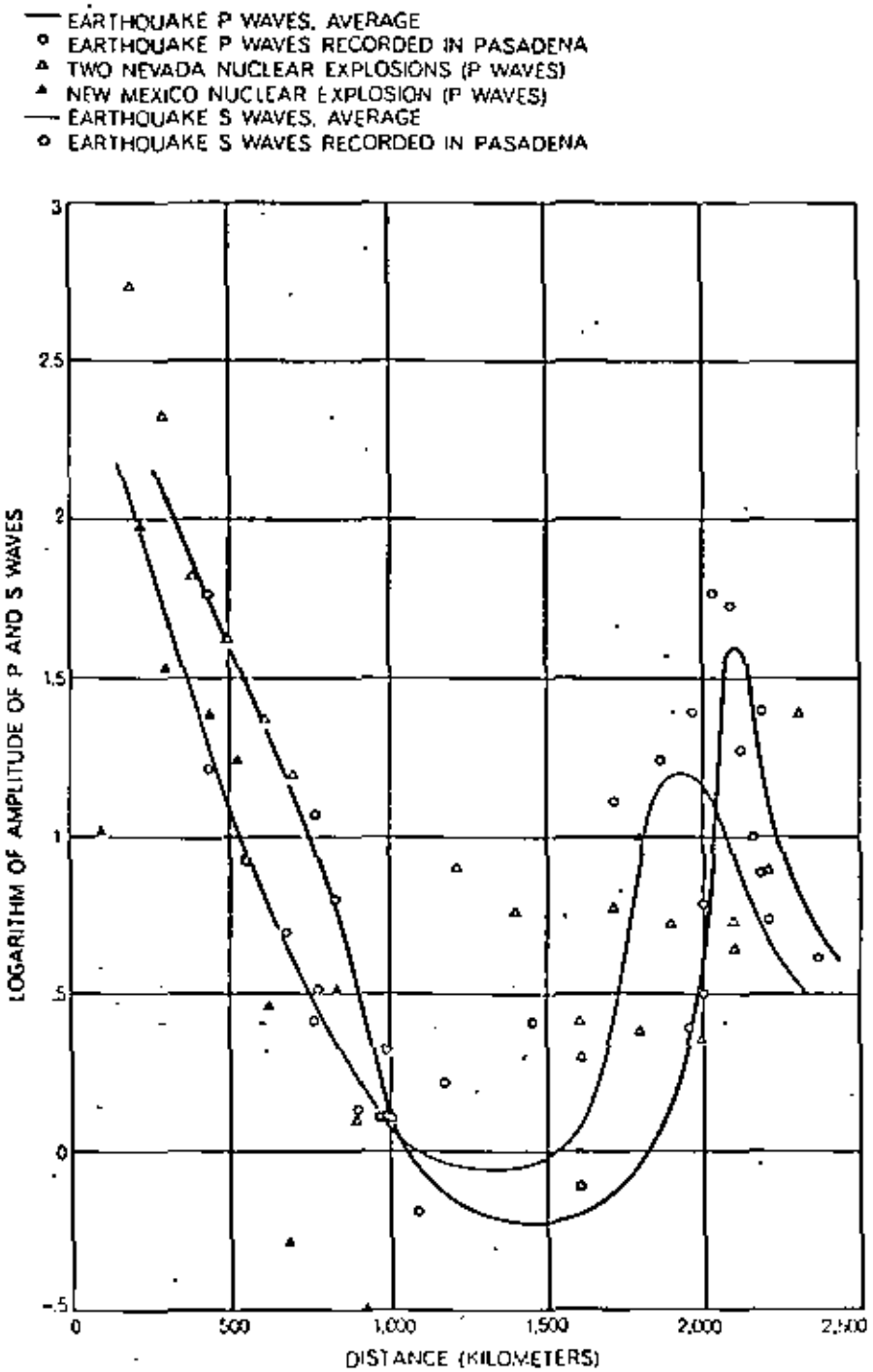

SHARP DROP IN AMPLITUDE of earthquake and nuclear-explosion waves between about 100 kilometers and 1,000 kilometers from the event is caused by low-velocity zone. The two curves of averages for earthquake P and S waves were drawn by Beno Gutenberg on basis of data from many earthquakes and observatories and represent world-wide averages.

level. The picture agrees with a nomenclature first proposed in 1914 by the U.S. geologist Joseph Barrell. He spoke of an upper, rigid "lithosphere" (from the Greek word *lithos*, meaning stone) and a lower, more plastic "asthenosphere" (from the Greek word *asthenes*, meaning weak). Barrell placed the boundary between the two at a depth of 100 kilometers. Now it appears to be not a sharp boundary but a transition zone starting at some 60 kilometers.

The concept of strength and weakness in the foregoing discussion applies to the time in which stresses build up to cause earthquakes. Viewed on this temporal scale the mantle undergoes a transition from a brittle to a plastic state at about 60 kilometers and thereafter increases in plasticity. On the much shorter time scale of earthquake-wave vibrations, however, the material reverts to a stronger, or more elastic, condition at a depth of more than 250 kilometers. The decrease in velocity at the top of the mantle is gradual; it is not yet clear whether the base of the low-velocity zone is characterized by a gradual or an abrupt increase in velocity.

Almost certainly the short-term properties that set apart the low-velocity layer are determined by the temperature and pressure of the mantle in relation to its melting point at different depths. In general the elasticity of any material decreases as its temperature approaches the melting point. But an increase in pressure raises the melting point and elasticity. Below the surface of the earth both temperature and pressure increase with depth, and so the two have opposing effects on the proximity to the melting point as well as on the elastic strength of rock. Presumably at a depth of about 60 kilometers temperature takes the upper hand and the rock begins to approach its melting point, growing weaker as the depth increases. This trend continues down to some 200 kilometers, where it reverses. Then pressure raises the melting point faster than the temperature increases and the material becomes more elastic (until the liquid outer core is reached). A few laboratory experiments on rock under high temperature and pressure seem to confirm this picture. Extrapolating the rather scanty data indicates a very low strength at a depth of somewhat more than 100 kilometers.

Hugo Benioff of the California Institute of Technology has discovered a remarkable indication of discontinuity at the level of the top of the low-velocity zone. In studying a large number of earthquakes in the Pacific Ocean earthquake belt he was able to connect certain sequences of earthquakes to single fault structures. One sequence that occurred in South America between 1906 and 1942 delineates a great fault off the west coast of the continent. The fault is some 4,500 kilometers long and goes down 600 kilometers—a tenth of the distance to the center of the earth. The earthquakes related to the fault fall naturally into three groups: (1) those shallower than 70 kilometers, (2) those from 70 to 250 or 300 kilometers and (3) those from 300 to 600 kilometers [*see top illustration on page 32*]. Analysis of the earth motions in the quakes showed a marked similarity between the intermediate and deep groups but no resemblance of these to the shallower group. In particular the motions of the two deeper groups changed suddenly, and in the

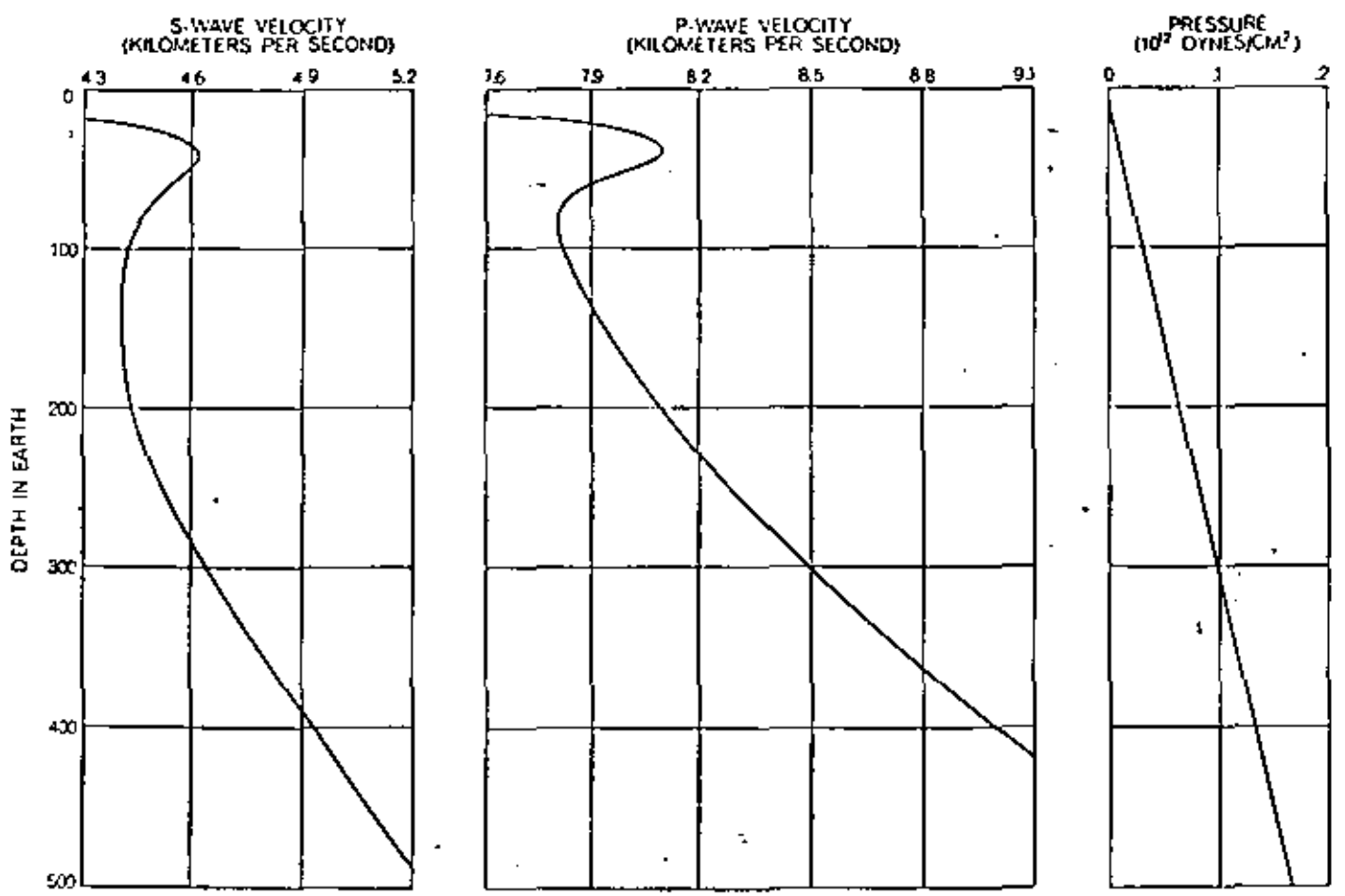

DATA FOR UPPER MANTLE reflect existence of plastic or low-velocity zone. The seismic-wave velocities and the number of earthquakes are the only curves made from direct measurements in the earth. Pressure is derived directly from depth. Temperature curve

same way, in 1921. There was no corresponding change in the shallower earthquakes. Evidently there is some mechanical coupling between the lower layers, but these are sharply decoupled from the region above 70 kilometers. Other areas of the circum-Pacific tectonic belt show similar phenomena.

When the earthquake foci are plotted in three dimensions, those down to 250 kilometers fall in a plane about 900 kilometers wide, dipping about 33 degrees under the continents with respect to the surface of the earth. The deep earthquakes, on the other hand, are on a plane tilted at 60 degrees. Thus, although they are mechanically connected, the intermediate and deep layers are spatially discontinuous. The dimensions and location of the intermediate layer correspond closely to those of the low-velocity zone.

An interesting clue to the state of the material in the upper mantle was furnished by the Soviet volcanologist G. S. Gorshkov in 1957. He found that shear waves from Japanese earthquakes do not reach the Kamchatka Peninsula when their paths cross the volcanic belt between Japan and the peninsula. Gorshkov concluded that there must be pockets of liquid magma at a depth of 55 kilometers that absorb the waves. Apparently in certain regions the temperature not only approaches the melting point but even exceeds it. Many seismologists have remarked on the fact that the average wavelength of shear waves is many times longer than that of compressional waves. The observation could be accounted for by a weak, perhaps partially molten, layer that absorbs the shorter S waves more than the longer S waves.

Volcanoes are concentrated in parts of the world where earthquakes are most common, and the earthquakes actually associated with volcanism mostly originate at depths between 60 and 200 kilometers. This suggests that volcanoes are connected with disturbances in the region of the low-velocity zone. Therefore the distribution of volcanoes constitutes direct evidence for the temperature–melting point relation inferred from laboratory measurements and suggests that the low-velocity layer may be the source of primary basaltic magma.

Volcanism and the postglacial uplift of the crust constitute the only dynamic, as opposed to static, geological "experiments." Both indicate fluidity, and some degree of actual flow, in the material below the crust. Moreover, they are consistent with the idea of a layer of maximum plasticity in the upper mantle.

Almost all present theories of isostasy and tectonics, including those concerned with mountain building, faulting and the possible drifting of the continents, focus attention on the Mohorovičić discontinuity, which divides the crust of the earth from the mantle. If the picture I have tried to outline in this article is correct, the important discontinuity is farther down, at the ill-defined boundary of the rigid lithosphere and the weaker asthenosphere. Most of the activity responsible for the broad-scale features of the earth's surface probably takes place in a low-velocity or plastic layer at the top of the asthenosphere, extending roughly from 60 to 250 kilometers in depth. In particular the existence of such a plastic layer makes the idea of continental drift much more plausible than it has seemed heretofore.

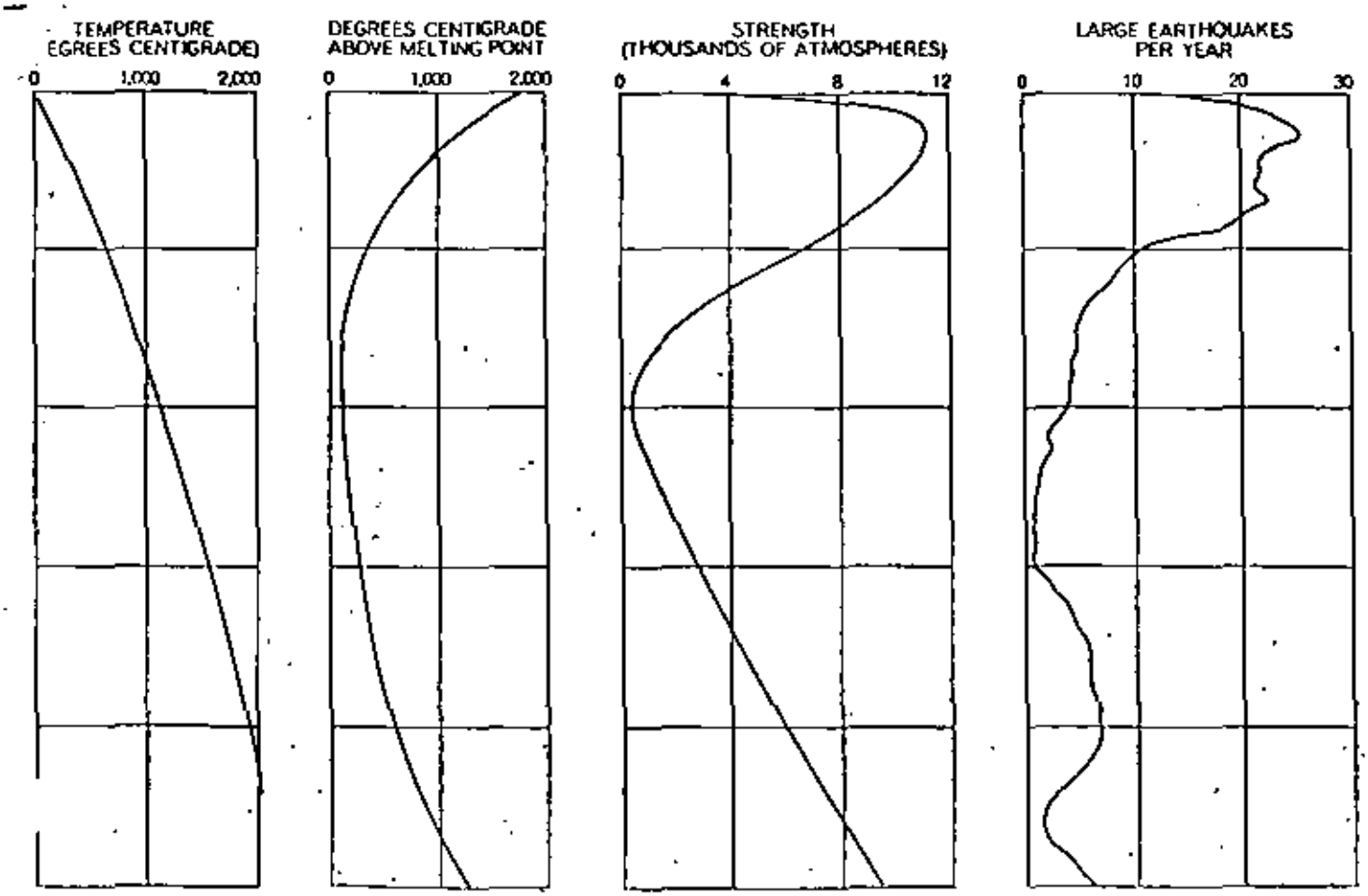

is based largely on theoretical considerations. Temperature above melting point is calculated from pressure and temperature curves. Strength, down to 50 kilometer depth, is derived indirectly from laboratory measurements; below that it is an extrapolation.

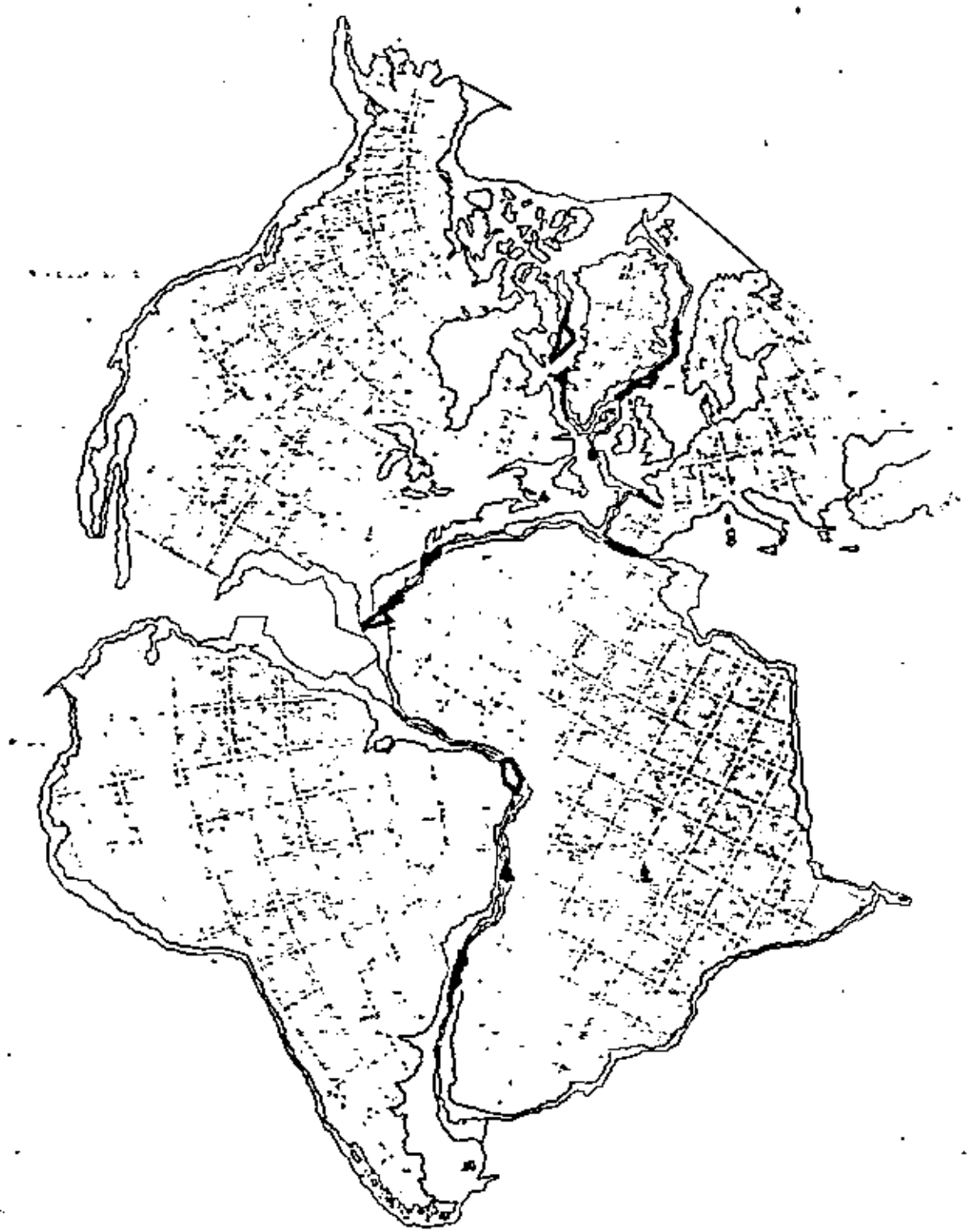

THE CONFIRMATION OF CONTINENTAL DRIFT

PATRICK M. HURLEY

April 1968

As recently as five years ago the hypothesis that the continents had drifted apart was regarded with considerable skepticism, particularly among American investigators. Since then, as a result of a variety of new findings, the hypothesis has gained so much support that its critics may now be said to be on the defensive. The slow acceptance of what is actually a very old idea provides a good example of the intensive scrutiny to which scientific theories are subjected, particularly in the earth sciences, where the evidence is often conflicting and where experimental demonstrations are usually not possible.

As long ago as 1620 Francis Bacon discussed the possibility that the Western Hemisphere had once been joined to Europe and Africa. In 1668 P. Placet wrote an imaginative memoir titled *La corruption du grand et du petit monde, où il est montré que devant le déluge, l'Amérique n'était point séparée des autres parties du monde* ("The corruption of the great and little world, where it is shown that before the deluge, America was not separated from the other parts of the world"). Some 200 years later Antonio Snider was struck by the similarities between American and European fossil plants of the Carboniferous period (about 300 million years ago) and proposed that all the continents were once part of a single land mass. His work of 1858 was called *La Création et Ses Mystères Dévoilés* ("The Creation and Its Mysteries Revealed").

By the end of the 19th century geology had come seriously into the discussion. At that time the Austrian geologist Eduard Suess had noted such a close correspondence of geological formations in the lands of the Southern Hemisphere that he fitted them into a single continent he called Gondwanaland. (The name comes from Gondwana, a key geological province in east central India.) In 1908 F. B. Taylor of the U.S. and in 1910 Alfred L. Wegener of Germany independently suggested mechanisms that could account for large lateral displacements of the earth's crust and thus show how continents might be driven apart. Wegener's work became the center of a debate that has lasted to the present day.

Wegener advanced a remarkable number of detailed correlations, drawn from geology and paleontology, indicating a common historical record on the two sides of the Atlantic Ocean. He proposed that all the continents were joined in a single vast land mass before the start of the Mesozoic era (about 200 million years ago). Wegener called this supercontinent Pangaea. Today the evidence favors the concept of two large land masses: Gondwanaland in the Southern Hemisphere and Laurasia in the Northern.

In the Southern Hemisphere an additional correlation was found in a succession of glaciations that took place in the Permian and Carboniferous periods. These glaciations left a distinctive record in the southern parts of South America, Africa, Australia, in peninsular India and Madagascar and, as has been discovered recently, in Antarctica. The evidence of glaciations is compelling: Beds of tillite—old, consolidated glacial rubble—have been studied in known glaciated regions and are unquestioned evidence of the action of deep ice cover. In addition many of the tillites rest on typically glaciated surfaces of hard crystalline rock, planed flat and grooved by the rock-filled ice moving over them.

This kind of evidence has been found throughout the Southern Hemisphere. In all regions the tillites are found not only in the same geological periods but also in a sequence of horizontal beds bearing fossils of identical plant species. This sequence, including the geological periods from the Devonian to the Triassic, is called the Gondwana succession. The best correlations are apparent in the Permocarboniferous beds, where two distinctive plant genera, *Glossopteris* and *Gangamopteris*, reached their peak of development. These plants were so abundant that they gave rise to the Carboniferous coal measures, which are commonly interbedded in the Gondwana succession [*see top illustration on next two pages*].

The South African geologist Alex L. du Toit and others have sought out and mapped these Gondwana sequences so diligently that today they provide the strongest evidence not only that these continental areas were joined in the past but also that they once wandered over or close to the South Pole. It is inconceivable that the complex speciation of the Gondwana plants could have evolved in the separate land masses we see today. It takes only a narrow strip of water, a few tens of miles wide at the most, to stop the spread of a diversified plant regime. The Gondwana land mass was apparently a single unit until the Mesozoic era, when it broke into separate parts. Thereafter evolution proceeded on divergent paths, leading to the biological diversity we observe today on the different continental units.

Wegener and Du Toit published their work in the 1920's and 1930's. The de-

FIT OF CONTINENTS (*opposite page*) was optimized and error-tested on a computer by Sir Edward Bullard, J. E. Everett and A. G. Smith of the University of Cambridge. Over most of the boundary the average mismatch is no more than a degree. The fit was made along the continental slope (*light gray*) at the 500-fathom contour line. The regions where land masses, including the shelf, overlap are black; gaps are white.

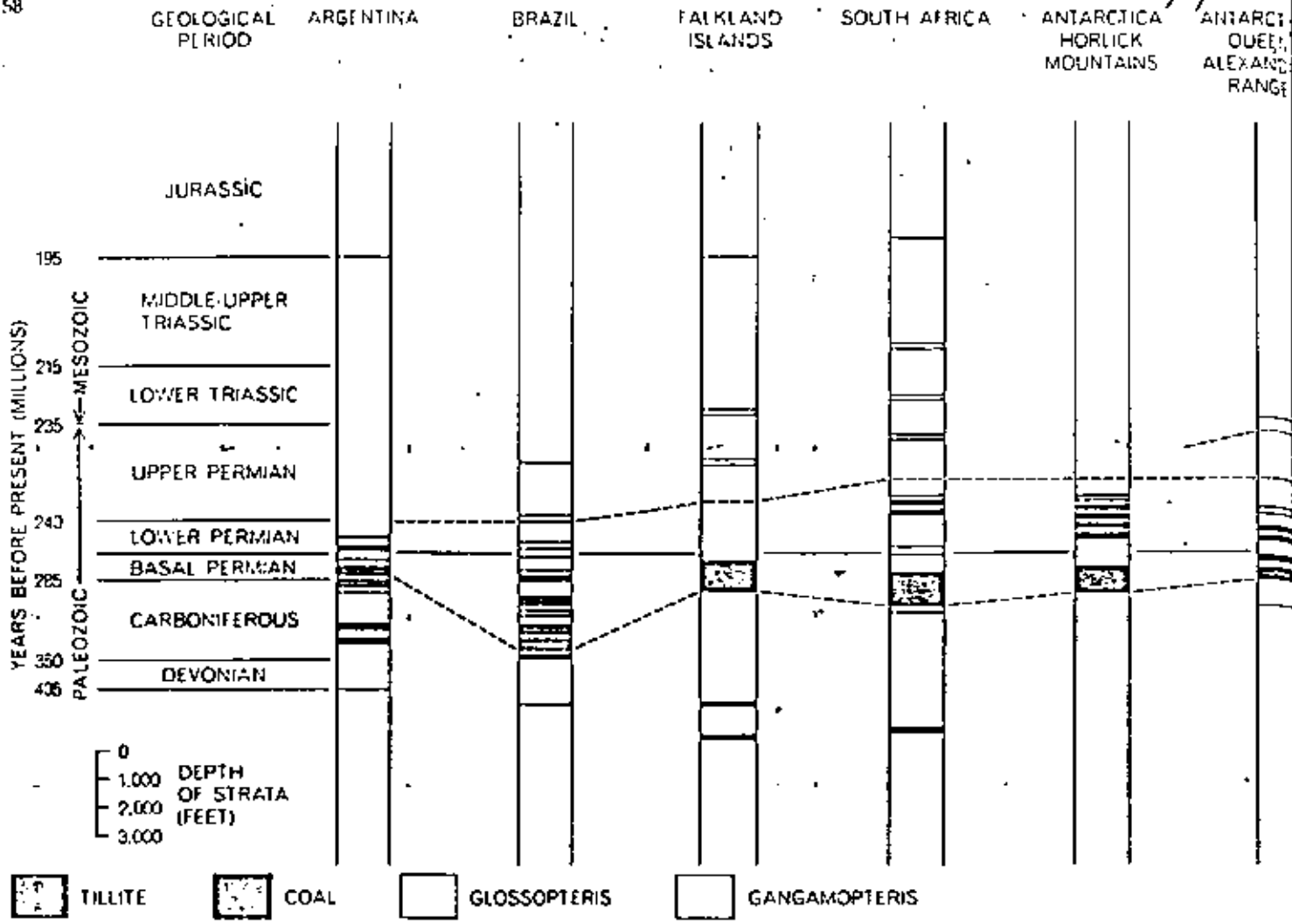

GONDWANA SUCCESSION is the name given to a late Paleozoic succession of land deposits found in South America, Africa, Antarctica, India and Australia. The succession contains beds of tillite (glacial rubble), coal deposits and a diversity of plants arranged in such a way that perhaps 200 million years ago the different areas must have been a single land mass known as Gondwanaland, or at

bate for and against drift became polarized largely between geologists of the Southern Hemisphere and the leaders of geophysical thought in the Western Hemisphere. Eminent geophysicists such as Sir Harold Jeffreys of the University of Cambridge voiced strong opposition to the hypothesis on the grounds that the earth's crust and its underlying mantle were too rigid to permit such large motions, considering the limited energy thought to be available.

Not all felt this way, however. In the late 1930's the Dutch geophysicist F. A. Vening Meinesz proposed that thermal convection in the earth's mantle could provide the mechanism. His ideas were supported by his gravity surveys over the deep-sea trenches and the adjacent island arcs of the western Pacific. The results implied that some force was maintaining the irregular shape of the earth's surface against its natural tendency to flatten out. Presumably the force was somehow related to thermal convection. Arthur Holmes of the University of Edinburgh added his weight to the argument in favor of the hypothesis, and he was followed by S. W. Carey of Tasmania, Sir Edward Bullard and S. K. Runcorn of Britain, L. C. King of South Africa, J. Tuzo Wilson of Canada and others [see the article "Continental Drift," by J. Tuzo Wilson, beginning on page 41]. The historical and dynamical characteristics of the earth now engaged the attention of many more geophysicists, and today the interplay of all branches of geology and geophysics generates the excitement of a new frontier area.

Continents and Oceans

Although the general nature of the earth's crust is familiar to most readers of *Scientific American*, it is worth reviewing and summarizing some of its major features while asking: How do these features look in the context of continental drift? The earth's topography has two principal levels: the level of the continental surface and the level of the oceanic plains. The elevations in between represent only a small fraction of the earth's total surface area. What maintains these levels? Left alone for billions of years, they should reach equilibrium at an average elevation below the present sea level, so that the earth would be covered with water. Instead we see sharp continental edges, new mountain belts, deep trenches in the oceans—in short, a topography that appears to have been regularly rejuvenated.

The continental areas are a mosaic of blocks that are roughly 1,000 kilometers across and have ages ranging from about 3,000 million years to a few tens of millions. In Africa there appear to be several ancient nuclear areas, or cratons, surrounded by belts of younger rocks. Most of the younger belts have an age of 600 million years or less, contrasting sharply with an age of 2,000 million to 3,000 million years for the cratons.

A closer look at the younger belts tells us that although much of the material is

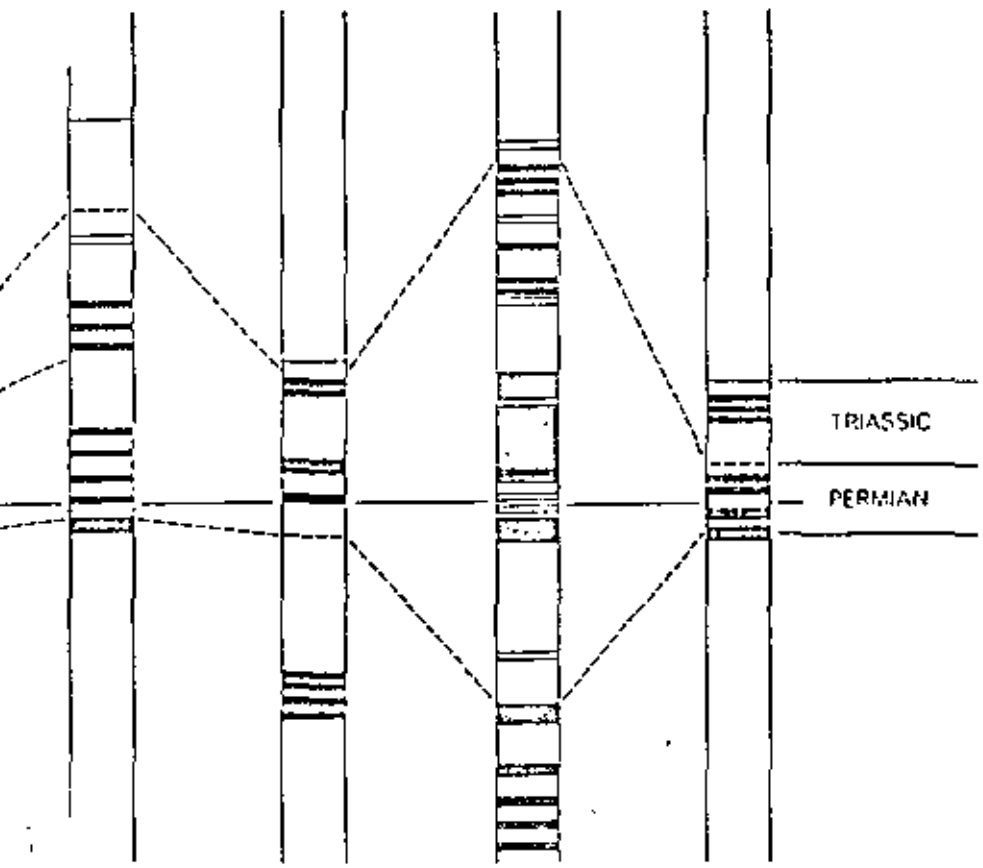

the very least a closely associated mass connected by land bridges. Only two of several major plant genera are plotted here: *Glossopteris* and *Gangamopteris*. The depths of the various deposits have been arbitrarily aligned between the lower and the basal Permian.

apparently new, there are large blocks that have the same age as the cratons. It looks as if the earth's surface has been warped and folded around the ancient continental masses, catching up segments of the crust and intruding younger igneous rocks into the folds. In some places the ancient material has been altered beyond recognition, but elsewhere it has been left fairly undisturbed and its antiquity can be determined by radioactive-dating methods. These composite belts are termed zones of rejuvenation. When they are eroded down to sea level, all we see, as far as topography is concerned, is another part of the continental platform. Geological mapping, however, reveals the belt structure clearly. A closer look at the cratons shows us that they too have the structure of preexisting mountain belts that have been carved into segments, with the younger material always cutting across the older structural pattern.

We see the process in action today. Our young mountain belts have not been eroded to sea level but show high elevations that are clearly apparent; we do not need geological surveys to observe them. It is only when we see the global distribution of these mountain belts on land areas, together with the distribution of rifts and their associated ridges under the oceans, that we begin to perceive the possibility that vast motions of the earth's surface may be their cause [*see illustration on next two pages*].

The earth is also encircled by belts of geological activity in the form of volcanoes, earthquakes and high heat flow, and observable motions in the form of folded rocks and the large displacements known as faults. In recent years the direction of displacements that are not observable on the surface has been deduced by the study of seismic waves arriving at various points on the earth's surface from earthquakes. It is now possible to tell the direction of slippage in the zones of rupture within the solid rocks of the earth's near-surface regions, so that the directions of the forces can be obtained.

If one looks at a map such as the one on the next two pages, one is immediately struck by the large scale and systematic distribution of these lines of geologic activity. Some of the systems are coherent over distances of several thousand kilometers. This immediately suggests the large-scale motion of material in the earth's interior. It does not, however, necessarily imply motions extending a similar distance into the interior. It is

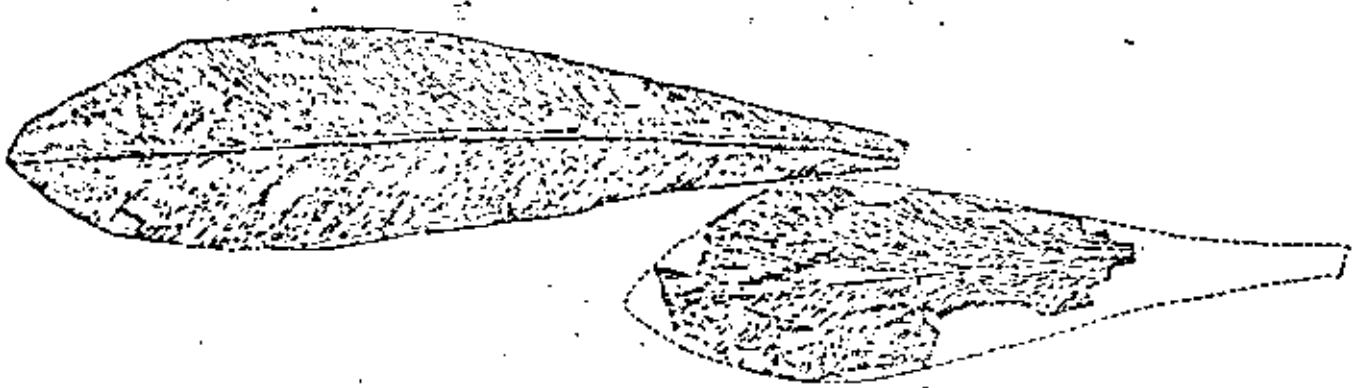

TYPICAL GONDWANA FLORA are *Glossopteris communis* (*leaf at left*) and *Gangamopteris cyclopteroides* (*right*), two species of fern that are identified in the Gondwana succession illustrated at the top of these two pages. The fossils from which these drawings were made were uncovered in the central part of Antarctica in 1961-1962 by William E. Long of Alaska Methodist University.

possible to have sheets of rigid material supporting stresses and fracturing over great distances if the underlying material is less rigid.

The topography of the ocean floors has been rapidly revealed in the past two decades by the sonic depth recorder. The principal systems of ridges and faults have been mapped in considerable detail by such oceanographers as Bruce C. Heezen and Maurice Ewing of Columbia University and H. W. Menard of the Scripps Institution of Oceanography. The layers of sediment on the sea floor have also been explored by such methods as setting explosive charges in the water and recording the echoes. It became a great puzzle how in the total span of the earth's history only a thin veneer of sediment had been laid down. The deposition rate measured today would extend the process of sedimentation back to about Cretaceous times, or 100 to 200 million years, compared with a continental and oceanic history that goes back at least 3,000 million years. How could three-quarters of the earth's surface be wiped clean of sediment in the last 5 percent of terrestrial time? Furthermore, why were all the oceanic islands and submerged volcanoes so young? The new oceanographic investigations were presenting questions that were awesome to contemplate.

In the early 1960's Harry H. Hess of Princeton University and Robert S. Dietz of the U.S. Coast and Geodetic Survey independently proposed that the oceanic ridge and rift systems were created by rising currents of material which then spread outward to form new ocean floors. On this basis the ocean floors would be rejuvenated, sweeping along with them the layer of sedimentary material. If such a mechanism were at work, no part of the ocean basins would be truly ancient. Although this radical hypothesis had much in its favor, it appeared farfetched to most.

Tracking the Shifting Poles

During this time a group of physicists and geophysicists were studying the directions of magnetism "frozen" into rocks in the hope of tracing the history of the earth's magnetic field. When an iron-bearing rock is formed, either by crystallization from a melt or by precipitation from an aqueous solution, it is

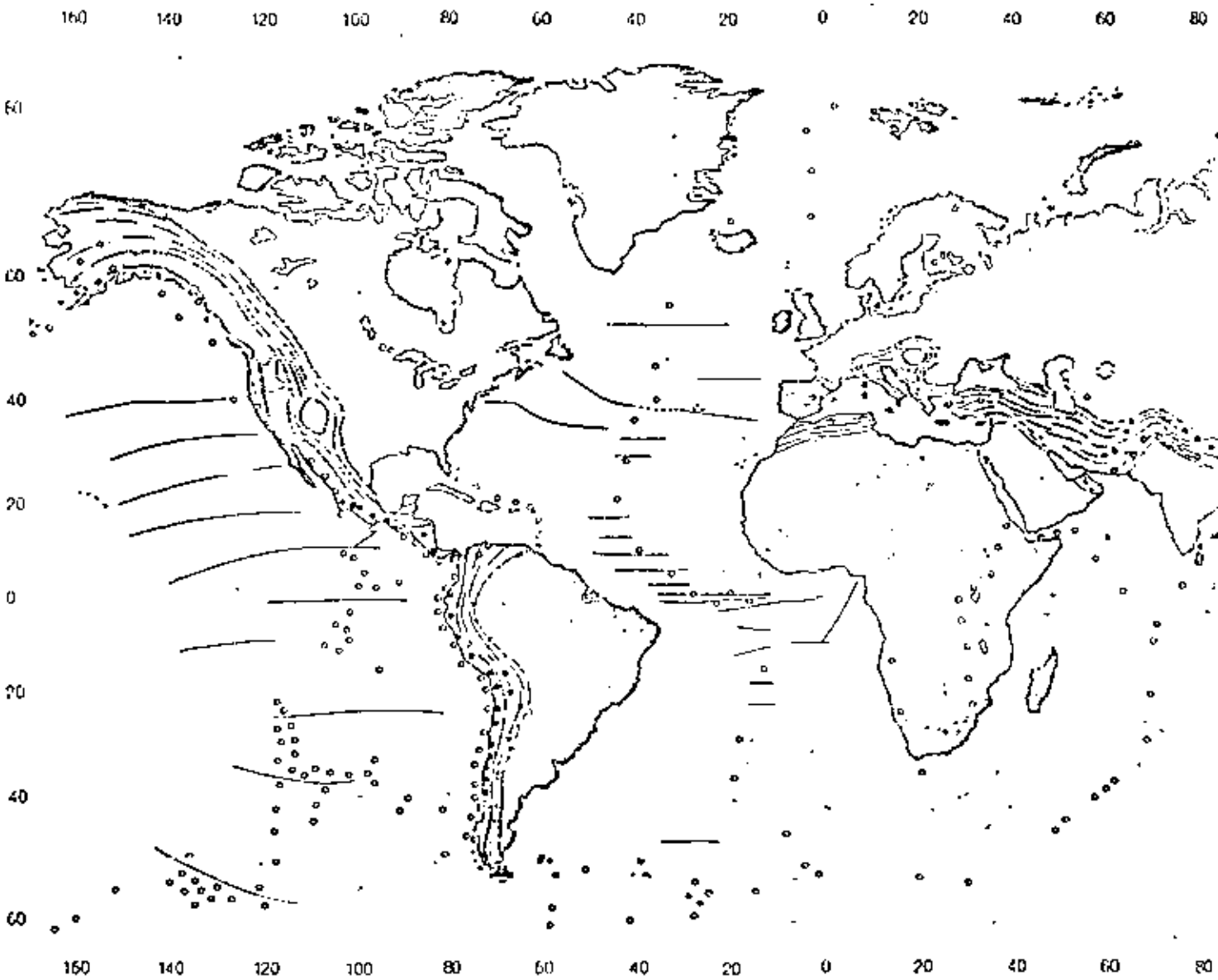

WORLDWIDE GEOLOGICAL PATTERNS provide evidence that the major land masses have been driven apart by a slow convection process that carries material upward from the mantle below the earth's crust. The dark-colored lines identify the crests of oceanic ridges that are now believed to coincide with upwelling regions. These ridges are crossed by large transcurrent fracture zones. The broken lines show the approximate limits of the oceanic rises. The light gray areas identify the worldwide pattern of recent mountain belts, island arcs, deep trenches, earthquakes and volcanism that apparently mark the downwelling of crustal material. The

slightly magnetized in the direction of the earth's magnetic field. Unless this magnetism is disturbed by reheating or physical distortion it is retained as a permanent record of the direction and polarity of the earth's magnetic field at the time the rock was formed. By measuring the magnetism in rocks of all ages from different continents, it has been possible to reconstruct the position of the magnetic pole in the past history of the earth. Great impetus was given to this study by P. M. S. Blackett and Runcorn, who with others soon found that the position of the pole followed a path going backward in time that was different for each continent [*see top illustration on next page*].

The interpretation of this effect was that the continents had moved with respect to the present position of the magnetic pole, and that since the paths were different for each land mass, they had moved independently. Because it was unlikely that the magnetic pole had wandered very far from the axis of the earth's rotation, or that the axis of rotation had changed position with respect to the principal mass of the earth, it was concluded that the continents had moved over the surface of the earth. Moreover, since the shift in latitude of the southern continents was generally southward going backward in time, the motions were in accord with the older evidence pointing toward a Gondwanaland in the south-polar regions. In short, the magnetic evidence supported not only the notion of continental drift but also the general locations from which the continents had moved within the appropriate time span.

downwelling seems to coincide with the occurrence of deep earthquakes (*triangles*) and earthquakes of intermediate depth (*solid dots*). Upwelling zones seem to coincide only with shallow earthquakes (*open dots*).

This was still not enough to sway the preponderance of American scientific opinion. Finally, at the annual meeting of the Geological Society of America in San Francisco in 1966, came the blows that broke the back of the opposition. Several papers put forward startling new evidence that related the concepts of ocean-floor spreading and continental drift, the curve of the oceanic ridge and fault systems and the direction and time scale of the drift motions. In addition, the development of new mechanisms explaining displacement along faults brought into agreement some of the formerly contradictory seismic evidence.

In the study of rock magnetism it was observed that the earth's magnetic field not only had changed direction in the past but also had reversed frequently. In order to study how frequently and when the reversals occurred three workers in the U.S. Geological Survey—Allan Cox, G. Brent Dalrymple and Richard R. Doell—carefully measured the magnetism in samples of basaltic rocks that they dated by determining the amount of argon-40 in the rocks formed by the decay of radioactive potassium-40. They noted a distinct pattern of reversals over some 3.0 million years [see "Reversals of the Earth's Magnetic Field," by Allan Cox, G. Brent Dalrymple and Richard R. Doell; SCIENTIFIC AMERICAN, February, 1967]. Their finding was soon confirmed when Neil D. Opdyke and James D. Hays of Columbia University found the same pattern in going downward into older layers in oceanic sediments. It was thus established that the polarity of the magnetic field had universally reversed at certain fixed times in the past.

Meanwhile an odd pattern of magnetism in the rocks of the ocean floors had been detected by Ronald G. Mason and Arthur D. Raff of the Scripps Institution of Oceanography. Using a shipborne magnetometer, they found that huge areas of the ocean floor were magnetized in a stripelike pattern. Putting together these patterns, the discovery of magnetic reversals and Hess's idea that the oceanic ridges and rifts were the site of rising and spreading material, F. J. Vine, now at Princeton, and D. H. Matthews of the University of Cambridge proposed that the hypothesis of the continuous creation of new ocean floors might be tested by examining the magnetic pattern on both sides of an oceanic ridge. The extraordinary discovery that the pattern was symmetrical with the ridge was demonstrated by Vine and Tuzo Wilson, who studied the two sides of a ridge next to Vancouver Island.

The history of the magnetic field going back into the past was laid out horizontally in the magnetism of the rocks of the sea floor going away from the ridge in both directions. It appeared that new hot material was rising from the rift in the center of the ridge and becoming magnetized in the direction of the earth's field as it cooled; it then moved outward, carrying with it the history of magnetic reversals. Since the dates of the reversals were known, the distance to each reversed formation gave the rate of spreading of the ocean floor [*see bottom illustration on next page*].

This important piece of work was quickly followed up by James R. Heirtzler, W. C. Pitman, G. O. Dickson and Xavier Le Pichon of Columbia, who have now shown that the ridges of the Pacific, Atlantic and Indian oceans all exhibit similar patterns. In fact, these workers have detected recognizable points in the history of magnetic reversals back about 80 million years, or in the Cretaceous period, and have drawn isochron lines, or lines of equal age, over huge strips of the ocean floors. Hence it is now possible to date the ocean floors and perceive the direction and rate of their lateral motion simply by conducting a magnetic survey over them. The implications for the study of drifting continents are immediately apparent.

These and other new findings do not unequivocally call for continental drift. It might be possible to have sea-floor spreading without drifting continents. Nonetheless, the directions and rates of motion for both sea-floor spreading and continental drift are entirely compatible. Above all, the principal objection to a hypothesis of continental movement has been removed.

Looking back, it is interesting to ob-

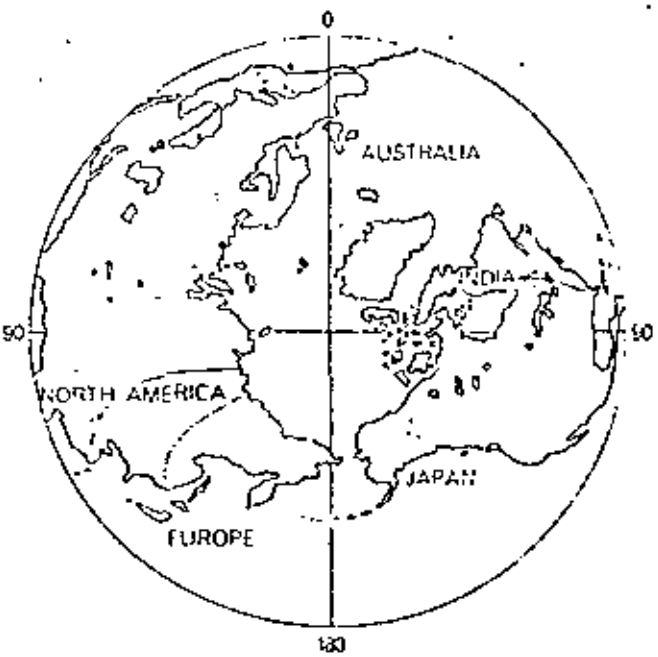

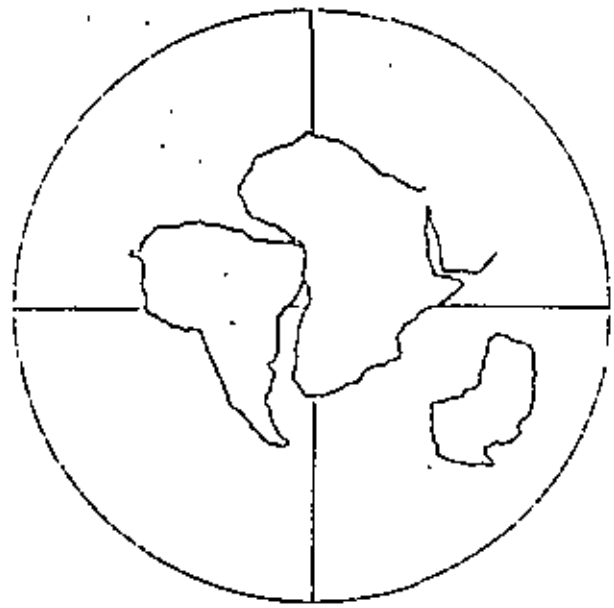

NORTH MAGNETIC POLE would appear to have wandered inexplicably during the past few hundred million years (*colored lines at left*), on the basis of "fossil" magnetism measured in rocks of various ages in various continents. The diagram is based on one by Allan Cox and Richard R. Doell of the U.S. Geological Survey. The pole could hardly have followed so many different tracks simultaneously; evidently it was the continents that wandered. K. M. Creer of the University of Newcastle upon Tyne found that the tracks could be brought together if South America, Africa and Australia were grouped in the late Paleozoic as shown at the *right*.

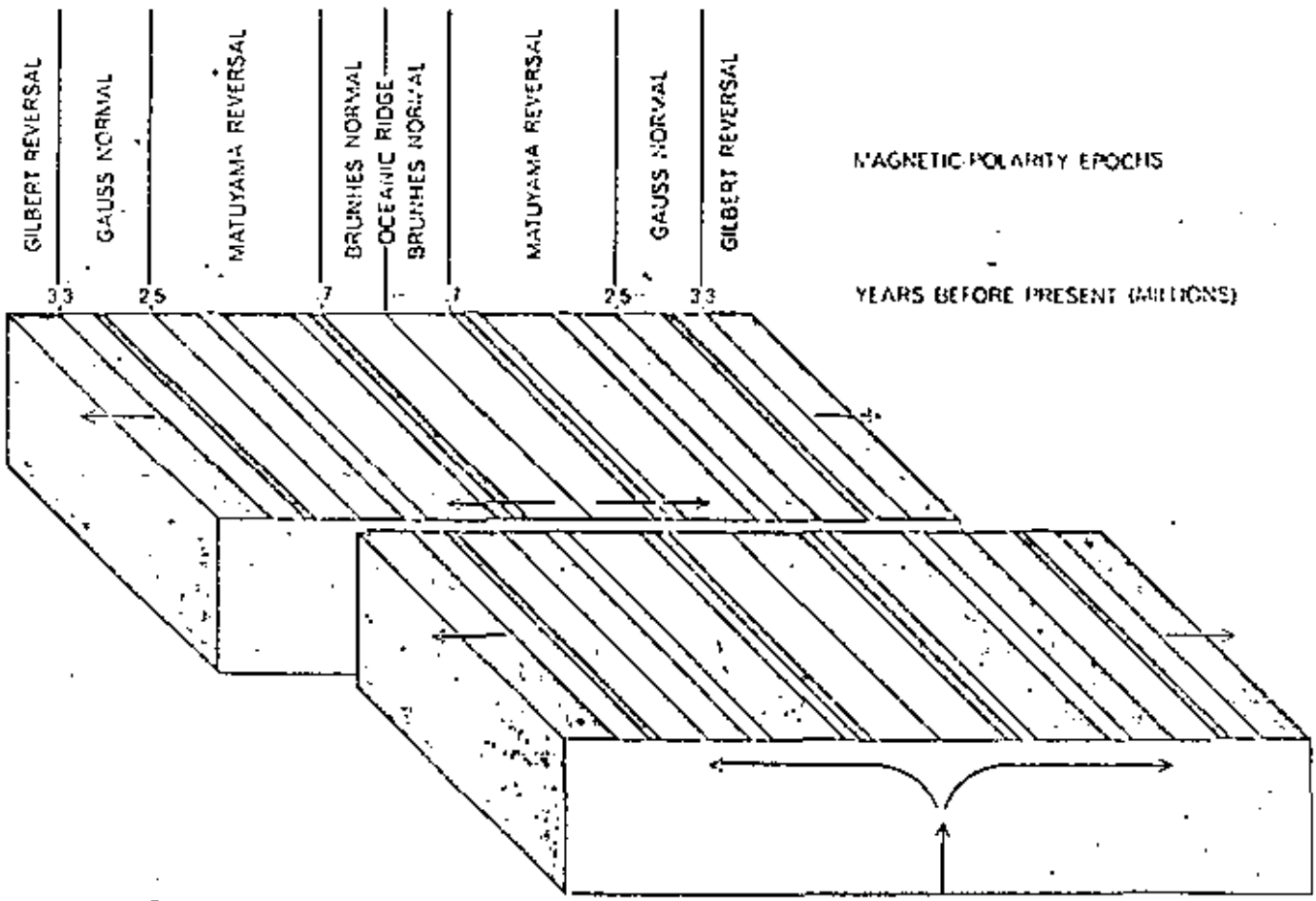

EVIDENCE FOR SEA-FLOOR SPREADING has been obtained by determining the polarity of fossil magnetism in rocks lying on both sides of oceanic ridges. In the diagram rocks of normal, or present-day, polarity are shown in color; rocks of reversed polarity are in gray. The displacement of the two blocks represents a transcurrent fracture zone. The symmetry suggests that the rocks welled up in a molten or semimolten state and gradually moved outward. The diagram is based on studies by a number of workers.

serve how each new piece of evidence presented in the past was met by counterevidence. Wegener's reconstruction, for example, was countered by numerous geologists who took exception to his detailed arguments. The arguments for the Permocarboniferous Gondwana glaciations were countered by Daniel I. Axelrod of the University of California at Los Angeles and others in this country. They contended that most species of fossil plant tend to be restricted to zones of latitude that hold for the continents in their present position, a fact that is hard to reconcile with the presumed pattern of glaciation. The idea that the great Gondwana land masses drifted in latitude has also been opposed by F. C. Stehli of Case Western Reserve University; his studies suggest that ancient fauna were most diverse at the Equator, and that the Equator defined in this way has not shifted.

Another Test of the Hypothesis

Any hypothesis must be tested on all points of observational fact. The balance of evidence must be strongly in its favor before it is even tentatively accepted, and it must always be able to meet the challenge of new observations and experiments. My own interest in the problem of continental drift was stimulated at a 1964 symposium in London sponsored by the Royal Society and arranged by Blackett, Bullard and Runcorn. At that time Bullard and his University of Cambridge associates J. E. Everett and A. G. Smith presented an elegant study of the geographic matching of continents on both sides of the North and South Atlantic. They had employed a computer to produce the best fit by the method of least squares. Instead of using shorelines, as had been done in earlier attempts, they followed the lead of S. W. Carey; he had chosen the central depth of the continental slope as representing the true edge of the continent.

The fit was remarkable [*see illustration on page 56*]. The average error was no greater than one degree over most of the boundary. My colleagues and I at the Massachusetts Institute of Technology now began to think of further testing the fit by comparing the sequence and age of rocks on opposite sides of the Atlantic.

Radioactive-dating techniques for determining the absolute age of rocks had reached a point where much could be learned about the age and history of both the ancient cratonic regions and the younger rejuvenated ones. For such purposes two techniques can be used in combination: the measurement of strontium 87 formed in the radioactive decay of rubidium 87 in a total sample of rock, and the measurement of argon 40 formed in the decay of potassium 40 in minerals separated from the rock. A collaborative effort was arranged between our geochronology laboratory and the University of São Paulo in Brazil (in particular with G. C. Melchet and U. Cordani of that institution). We also enlisted the aid of field geologists who had been working on the west coast of Africa (in Nigeria, the Ivory Coast, Liberia and Sierra Leone) and on the east coast of Brazil and Venezuela. The São Paulo group made the potassium-argon measurements of the Brazilian rock samples; we did the rubidium-strontium analyses on samples from all locations.

European geochronologists (notably M. Bonhomme of France and N. J. Snelling of Britain) had done pioneering work on the Precambrian geology of former French and British colonies and protectorates in West Africa. Of special interest to us at the start was the sharp boundary between the 2,000-million-year-old geological province in Ghana, the Ivory Coast and westward from these countries, and the 600 million-year-old province in Dahomey, Nigeria and east. This boundary heads in a southwesterly direction into the ocean near Accra in Ghana. If Brazil had been joined to Africa 600 million years ago, the boundary between the two provinces should enter South America close to the town of São Luis on the northeast coast of Brazil. Our first order of business was therefore to date the rocks from the vicinity of São Luis.

To our surprise and delight the ages fell into two groups: 2,000 million years on the west and 600 million years on the east of a boundary line that lay exactly where it had been predicted. Apparently a piece of the 2,000-million-year-old craton of West Africa had been left on the continent of South America.

In subsequent work on both sides we have found no incompatibilities in the age of many geological provinces on both sides of the South Atlantic [*see illustration on next page*]. Furthermore, the structural trends of the rocks also agree, at least where they are known. Minerals characteristic of individual belts of rocks are also found in juxtaposition on both sides; for example, belts of manganese, iron ore, gold and tin seem to follow a matching pattern where the coasts once joined.

Can such comparisons be made elsewhere? To some extent, yes. Unfortunately the rifting process by which a continent breaks up seems to be guided by zones of rejuvenation between cratons, as if these zones were also zones of weakness deep in the crust. It is necessary for the break to have transected the structure of the continent, cutting across age provinces, if one is to get a close refitting of the blocks. In the North Atlantic this is not the case, but the continental areas on both sides were simultaneously affected by an unmistakable oblique crossing of a Paleozoic belt of geological activity [*see illustration on page 65*]. Actually the belt covers the region of the Appalachian Mountains and the Maritime Provinces of North America, with an overlap along the coast of West Africa, and then splits into two principal belts: one extending through the British Isles and affecting the Atlantic coast of Scandinavia and Greenland and the other turning eastward into Europe. There is a superposition of at least four periods of renewed activity affecting the various parts of this complex. All four are represented on both sides of the North Atlantic, making this correlation extremely difficult to explain unless the continents were once together.

My colleagues H. W. Fairbairn and W. H. Pinson, jr., and I, as well as other workers, have made age measurements in the northern Appalachians and Nova Scotia for many years, and we have found all four periods well represented in New England. The earliest period of activity (which Fairbairn has named Neponset) is dated about 550 million years ago; it is seen in some of the large rock bodies in eastern Massachusetts and Connecticut, in the Channel Islands off the northern coast of France, in Normandy, Scotland and Norway. The next-oldest period (the Taconic) was about 450 million years ago and is found on the western edge of New England and in parts of the British Isles. The next period, going back about 360 million years, is strongly represented in the entire span of the Appalachians and Nova Scotia (where it is called the Acadian) and in England and Norway (where it is called the Caledonian). Finally, about 230 million years ago, the activity seemed to move into southern Europe and North Africa, where it has been called the Hercynian. This activity, however, also extended into New England; much of southern Maine, eastern New Hampshire, Massachusetts and Connecticut show rocks of this age. Here the event is called the Appalachian.

Farther south the Lower Paleozoic section of the northwest coast of Africa (Senegal) appears to continue under the younger coastal sediments of Florida,

23

This African belt shows large rock units with ages equivalent to the Neponset, and also evidence of the younger events.

The Fitting of Antarctica

The recent extensive geological surveys in Antarctica have been highly rewarding in reconstructing Gondwanaland. Prior to the end of the Permian period the younger parts of western Antarctica were not yet formed. Only eastern Antarctica was present, including the great belts of folded rocks that form the Transantarctic Mountains. These consist of two geosynclines, or sediment-filled troughs: the inner Eopaleozoic and the outer Paleozoic [*see illustration on page 66*]. The inner belt includes late Precambrian and early Cambrian sediments, which were folded and invaded by igneous rocks during late Cambrian or early Ordovician times (about 500 million years ago). Thus the inner belt is similar in age to the widespread event in the rest of Gondwanaland. It is marked by the Cambrian fossil Archaeocyatha, an organism that formed barrier reefs. These coral-like structures are found transecting sediments in bodies known as bioherms. The outer belt, farther within western Antarctica, is a geosyncline filled with Lower Paleozoic sediments. Like the northern Appalachians, it was deformed and invaded by igneous rocks in the middle and late Paleozoic. Later it was covered with a quite representative Gondwana succession, with its glacial deposits, coal and diverse plants.

There seems to be a similar record of events in eastern Australia. The bioherms of the Cambrian Archaeocyatha are found in a belt extending northward from Adelaide and mark the edge of an early geosyncline filled with sediments including late Precambrian and Cambrian ones. Later in time, and farther to the east, great thicknesses of Silurian and Lower Devonian sediments accumulated in the Tasman trough. Compression and igneous intrusion occurred in this Tasman geosyncline mostly in the late Lower Devonian period to the middle Devonian (about 350 million years

TENTATIVE MATCHING of geological provinces of the same age shows how South America and Africa presumably fitted together some 200 million years ago. Dark-colored areas represent ancient continental blocks, called cratons, that are at least 2,000 million years old. Light-colored areas are younger zones of geological activity: mostly troughs filled with sediments and volcanic rocks that were folded, compressed and intruded by hot materials, forming granites and other rock bodies. Much of this activity was 450 million to 650 million years ago, but some of it goes back 1,100 million years. The data show the sites of rocks dated by many laboratories, including the author's at the Massachusetts Institute of Technology. Solid dots denote rocks older than 2,000 million years; open dots denote younger rocks. The region near São Luís is part of an African craton left stranded on the coast of Brazil.

ago). The later cover of sediments includes a Gondwana succession similar to the one in Antarctica.

There is also strong evidence for a juncture between Australia and India, particularly in the Permian basins of sedimentation of the two continental blocks and in Gondwana sequences of coal and plants. Limestone beds containing the same Productid shells are found in the upper layers of the sequence on both sides. A correlation also exists between the banded iron ores of Yampi Sound in northwestern Australia and the similar ores of Singhbhum in India.

The illustration on page 66 is a reconstruction of Gondwanaland based on the evidence we have discussed so far. The three land masses—Antarctica, Australia and India—have been fitted together not at their present shorelines but where the depth of the surrounding ocean reaches 1,000 meters. As can be seen, the fit of the edges is good. The detailed fit of this assemblage into the southeastern part of Africa is still debated because most of the edges lack structures that cut across them. Nevertheless, I have included the edge of Africa in the map to show how it might possibly fit on the basis of limited age data from Antarctica.

This arrangement of land masses in the late Paleozoic is extremely tentative. It is now up to the geochronologists to test each juncture more closely for correlations in geologic age, and up to the field geologists to match structure and rock type. One particularly interesting fit may be forthcoming in a study of the boundaries of shallow and deep marine glacial deposits, and of the land tillites around what appears to be the start of an oceanic basin at the time Antarctica was breaking away. This attempt to establish the former position of Antarctica, which is being made by L. A. Frakes and John C. Crowell of the University of California at Los Angeles, may set in place the key piece in the puzzle. A detailed correlation of fossil plants in Antarctica with those of the adjacent land masses, which has been undertaken by Edna Plumstead of the University of Witwatersrand, is similarly limiting the possible position of the blocks.

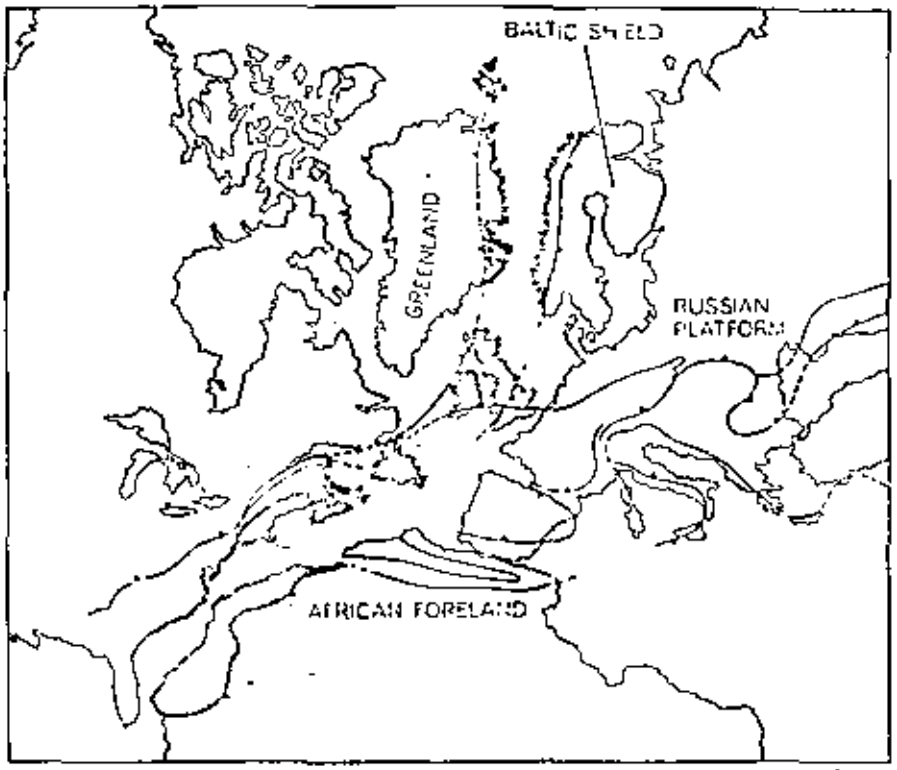

MATCHING OF NORTH ATLANTIC REGIONS is more difficult than in the South Atlantic. This tentative, prerift reconstruction of a portion of Laurasia depends on matching ancient belts of similar geological activity. The dark gray belt represents the formation of sediment-filled troughs and folded mountains in the early and middle Paleozoic (470 million to 350 million years ago). The medium gray belt was formed in the late Paleozoic (350 million to 200 million years ago). The latter belt overlapped the region of the former in the northern Appalachians and in southern Ireland and England, but diverged eastward in Europe. Four distinct and superimposed periods of geological activity occur on both sides of the present North Atlantic, providing strong evidence for a previous juncture.

The Age of the Atlantic

When did Gondwanaland begin to break up? One of the best pieces of evidence for the start of the opening of the South Atlantic is the age of offshore sediments along the west coast of Africa. Drilling through these sediments down to the ancient nonsedimentary rocks shows that the layer of sediments is quite young: not older than the middle Mesozoic (about 160 million years ago). If the South Atlantic had been in existence for a major part of geologic time, the continent of Africa would unquestionably have developed a large shelf of sediments along the entire length of its western margin. The continental shelf would consist of sediments dating all the way back to the time of the ancient cratons. This is not the case. It looks as though the rift started from the northern edge of western Africa in the middle Triassic and slowly opened to the south until the final separation occurred in the Cretaceous. The east coast of Africa, on the other hand, apparently started to open earlier, in the Permian.

With the acceptance of sea-floor spreading and continental drift the global problems of geology are beginning to be solved. Although the train of thought on such matters is not universally accepted in detail, it is something like the following. Continental areas appear to have greater strength, to a depth of 100 kilometers or so, than ocean basins do, so that they tend to maintain themselves as buoyant masses that are not destroyed by sinking motions. They can, however, be ruptured. Rising material pushes the surface apart; sinking material pulls the surface together and toward the region of sinking. Therefore if a sinking zone is established in an oceanic region, the continents will move toward the zone, and if a rising zone is established under a continent, the continent will split apart and the parts will move away from the zone. When the ocean floor moves toward a sinking zone in an oceanic region, it forms a deep trench bordered by volcanoes, chains of islands or elongated land masses such as the Philippines and Japan. When an ocean floor moves toward a continent, it appears to pass under the continental border, forming a great mountain chain. The mountain chain may be in part piled-up material that was already present and in part volcanic material that rose as the ocean swept its load of sediment, underlying volcanic rock and the continental shelf itself toward and under the edge of the continent. The process leads to a melting of underlying rock and to the intrusion of new volcanic material. The west coast of South America is a good example.

Another example is the thrust of India into Eurasia that formed the Himalayas. It has long been known that there was a large body of water between Africa and Eurasia and that a great thickness of sediments was deposited there at some time during the past 200 million years. This body is known as the Tethys Sea. It was located north of Arabia and extended from the former location of the Atlas Mountains to east of the Himalayas. As I have mentioned, it appears that Gondwanaland not only broke up but also moved northward, with India and Africa pushing up into Eurasia. This motion apparently caused the buckling up of sediments in the Tethys Sea, giving rise to the mountain ranges that now form a contorted chain from the western Atlas range through the Mediterranean, the western Alps, the Caucasus and the Himalayas.

The way the present mountain systems of the earth fall along great circles suggests that the motions in the earth's interior have a large-scale coherence, of the order of the dimensions of the earth itself. The prevailing explanation stems from a new lead in seismology: a zone in the earth at a depth of 100 or 200 kilom-

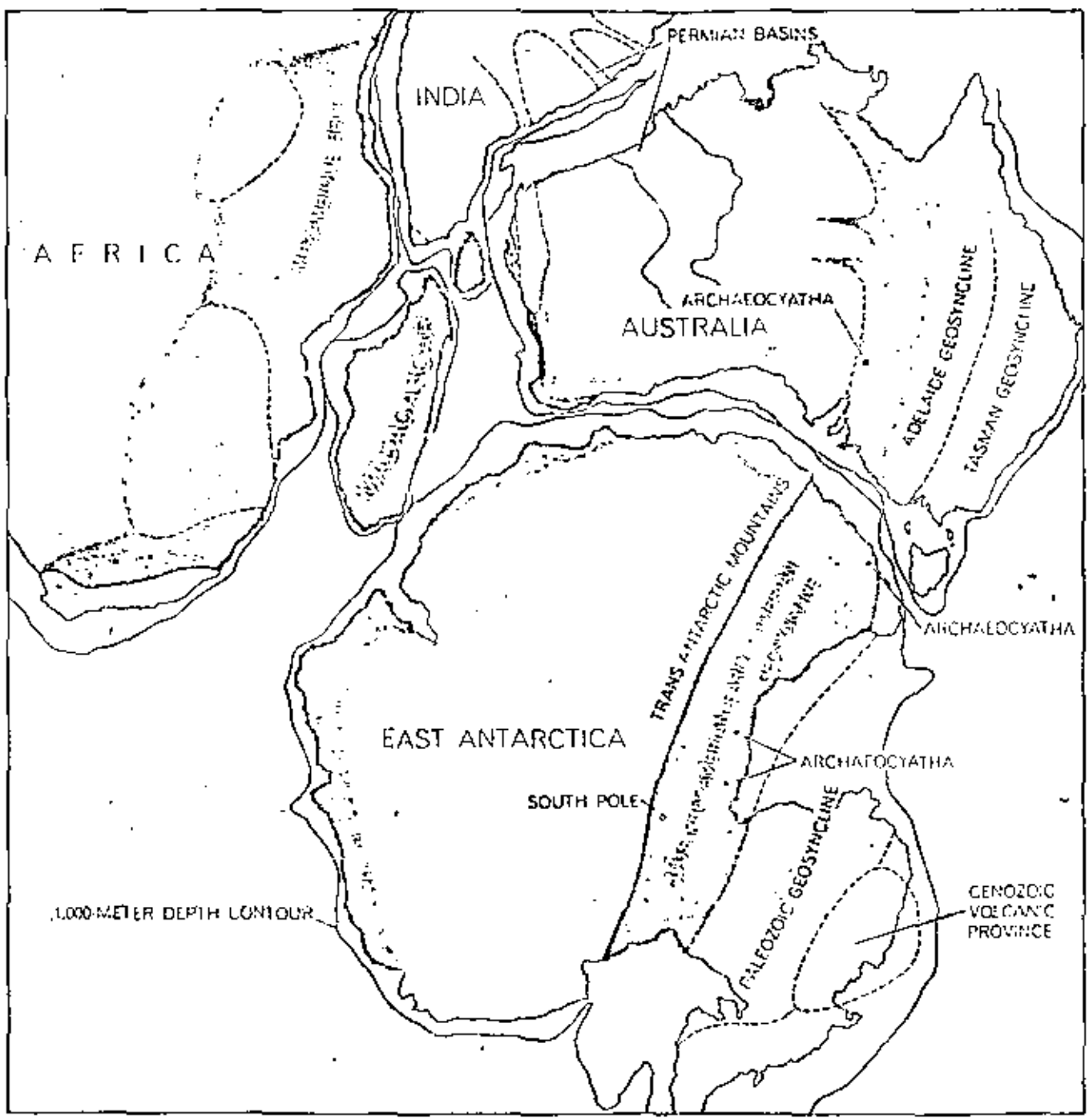

PART OF GONDWANALAND, tentatively reconstructed, brings together East Antarctica, Africa, Australia, Madagascar, India. The fit is at the 1,000-meter depth contour of the continental slope. Late Precambrian and Paleozoic geosynclines, or sediment-filled troughs, in eastern Australia are correlated in age and location with similar troughs along the Transantarctic Mountains. The deep Permian basins of northwest Australia match those of India. Glacial deposits, fauna and metal ores provide other correlations.

eters has been found to transmit seismic waves more slowly than the layers above and below it and to absorb seismic energy more strongly. This low-velocity zone is generally thought to consist of a material whose strength is reduced because a small amount of it is molten or because its temperature is approaching the melting point. The surface of the earth may therefore move around on this low-strength layer like the skin of an onion. It is believed the earth loses heat partly by conduction outward and partly by convection currents in the relatively thin layer above the weak zone. These currents, as they have been depicted by Walter M. Elsasser of Princeton and Egon Orowan of M.I.T., form rather flat convection cells.

A hypothesis that is currently popular is that the mechanism of spreading at the oceanic ridges involves the intrusion of hot material into ruptures near the surface. This material is the same as that in the low-velocity zone, lubricated by partly molten rock. A small proportion of the intruded material actually loses some of its melted fraction upward, giving rise to volcanoes and creating a thin layer (about five kilometers thick) of volcanic rock at the surface. The masses of intruded material cool as they move sideways from the central ridge, which is overlain by the thin layer of volcanic rock. This results in the observed distribution of seismic velocities at various depths, helps to explain why the flow of heat to the surface decreases with distance from the ridge and accounts for the pattern of magnetic reversals. At the sinking end of the convection cell this relatively rigid block of mantle material with its thin cover of basalt (plus a thin cover of new sediment) moves downward on an inclined plane.

It is clear where these concepts will lead. If folded mountain belts are the "bow waves" of continents plowing their way through ocean floors and ramming into other continents, we can use them to show us the relative directions of motion prior to the last great drift episode. If we look at the pre-drift Paleozoic mountain belts, such as the Appalachian belt of North America, the Hercynian of Europe and the Ural of Asia, we find that they are located *internally* in the great continental masses of Gondwanaland and Laurasia. This suggests that these pre-drift supercontinents had been formed by the inward motion of several separate blocks, which came together before they broke apart. Geologists have a new game of chess to play, using a spherical board and strange new rules.

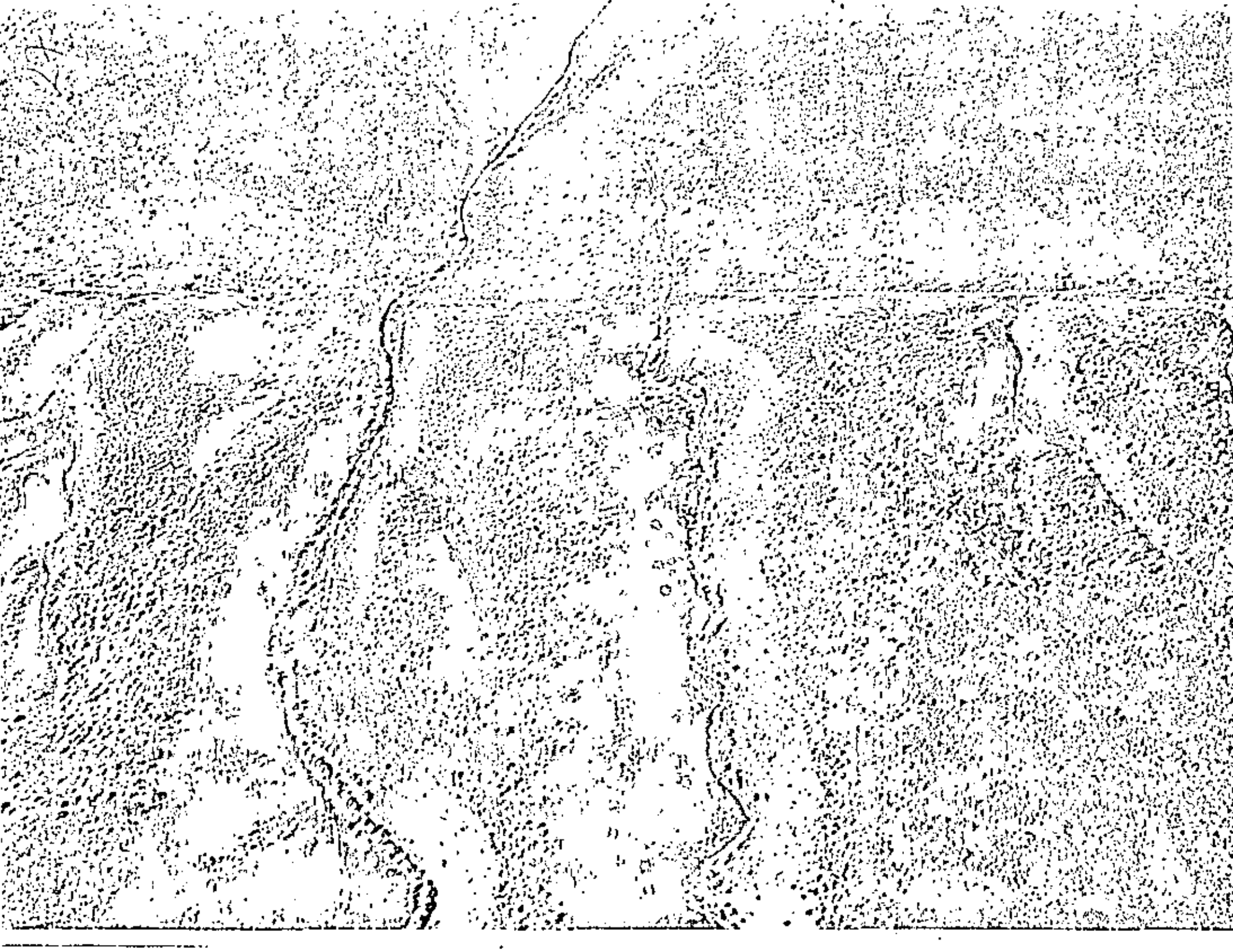

THE SAN ANDREAS FAULT

DON L. ANDERSON

November 1971

The San Fernando earthquake that occurred at sunrise on February 9, 1971, jolted many southern Californians into acute awareness that California is earthquake country. Although it was only a moderate earthquake (6.6 on the Richter scale), it was felt in Mexico, Arizona, Nevada and as far north as Yosemite National Park, more than 250 miles from San Fernando. It was recorded at seismic stations around the world. In spite of its relatively small size the San Fernando earthquake was extremely significant because it happened near a major metropolis and because its effects were recorded on a wide variety of seismic instruments. Within hours the affected region was aswarm with geologists mapping faults and seismologists installing portable instruments to monitor aftershocks and the deformation of the ground. It was immediately clear from data telemetered to the Seismological Laboratory of the California Institute of Technology in Pasadena from the Caltech Seismic Network that the earthquake was not centered on the much feared San Andreas fault or, for that matter, on any fault geologists had labeled as active. The faults in the area, however, are all part of the San Andreas fault system that covers much of California.

The San Andreas fault system (and its attendant earthquakes) is part of a global grid of faults, chains of volcanoes and mountains, rifts in the ocean floor and deep oceanic trenches that represent the boundaries between the huge shifting plates that make up the earth's lithosphere. The concept of moving plates is now fundamental to the theory of continental drift, which was long disputed but is now generally accepted in modified form on the basis of voluminous geological, geophysical and geochemical evidence. The theory had received strong support from the discovery that the floors of the oceans have a central rise or ridge, often with a rift along the axis, that can be traced around the globe. Within the rift new crustal material is continuously being injected from the plastic mantle below, forming a rise or ridge on each side of the rift. The newly formed crustal material slides away from the ridge axis. Since the magnetic field of the earth periodically reverses polarity, the newly injected material "freezes" in stripes parallel to the ridge axis, whose north-south polarity likewise alternates. By dating these stripes one can estimate the rate of sea-floor spreading.

The San Andreas fault system forms the boundary between the North American plate and the North Pacific plate and separates the southwestern part of California from the rest of North America. In general the Pacific Ocean and that part of California to the west of the San Andreas fault are moving northwest with respect to the rest of the continent, although the continent inland at least as far as Utah feels the effects of the interactions of these plates.

The relative motion between North America and the North Pacific has been estimated in a variety of ways. Seismic techniques yield values between 1½ and 2½ inches per year. The ages of the magnetic stripes on the ocean floor indicate a rate of about 2½ inches per year. Geodetic measurements in California give rates between two and three inches per year. The ages of the magnetic anomalies off the coast of California indicate that the oceanic rise came to intersect the continent at least 30 million years ago. Geologists and geophysicists at a number of institutions (notably the University of Cambridge, Princeton University and the Scripps Institution of Oceanography) have proposed that geologic processes on a continent are profoundly affected when a continental plate is intersected by an oceanic rise. At the rates given above the total displacement along the San Andreas fault amounts to at least 720 miles if motion started when the rise hit the continent and if all the relative motion was taken up on the fault. Displacements this large have not been proposed by geologists, but the critical tests would involve correlation of geology in northern California with geology on the west coast of Baja California, an area that has only recently been studied in detail. One can visualize how the west coast of North America may have looked 33 million years ago by closing up the Gulf of California and moving central and northern California back along the San Andreas fault to fit into the pocket formed by the coastline of the northern half of Baja California. This places all of California west of the San Andreas fault south of

DISPLACEMENT ALONG SAN ANDREAS FAULT is clearly visible in this aerial photograph of a region a few miles north of Frazier Park, Calif., itself 65 miles northwest of Pasadena, where the fault runs almost due east and west. This east-west section of the San Andreas fault is part of the "big bend," where the fault appears to be locked. The photograph is reproduced with north at the right. The hilly region to the left (south) of the fault line is moving upward (westward) with respect to the flat terrain at the right, causing clearly visible offsets in the two largest watercourses as they flow onto the alluvial plain.

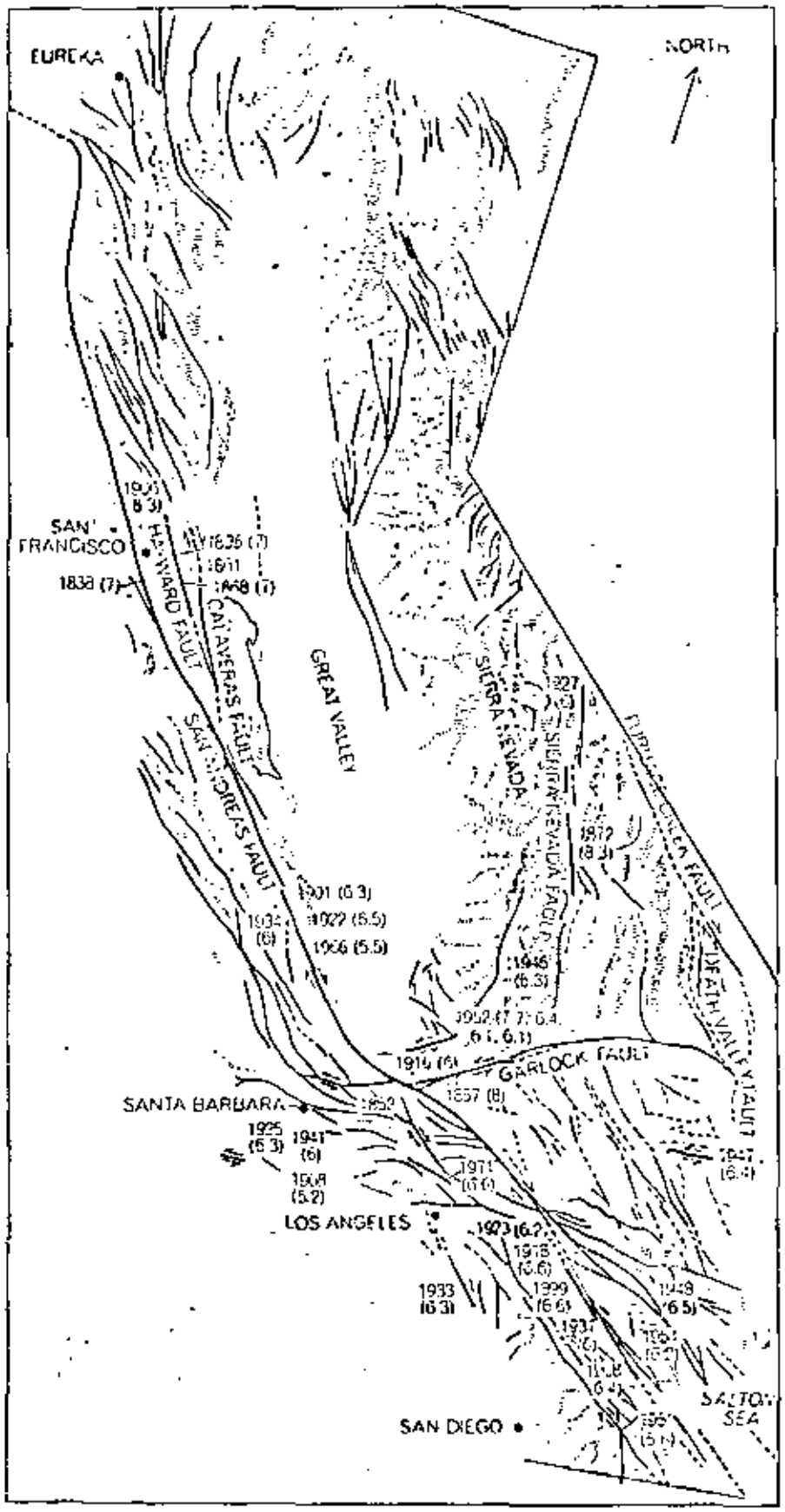

SIMPLIFIED FAULT MAP of California identifies in heavy black lines the faults that have given rise to major earthquakes since 1836. The magnitude of all but two of the earthquakes is given in parentheses next to the year of occurrence. For events that predated the introduction of seismological instruments the magnitudes are estimated from historical accounts. For two major events, the earthquakes of 1852 and 1861, information is too sparse to allow a magnitude estimate. Arrows parallel to the faults show relative motion.

the present Mexican border [*see illustration on page 150*].

California is riddled with faults, most of which trend roughly northwest-southeast, like most of the other tectonic and geologic features of California (such as the Sierra Nevada and the Coast Ranges). The prominent exceptions are the east-west-trending transverse ranges and faults that make up a band some 100 miles wide extending inland from between Los Angeles and Santa Barbara. The San Gabriel Mountains, which form the rugged backdrop to Los Angeles, are part of this complex geologic region, and it was here that the San Fernando earthquake struck. The northeast-trending Garlock fault and the Tehachapi Mountains, which separate the Sierra Nevada and the Mojave Desert, also cut across the general grain of California. The area to the west of most of the northwest-trending faults is moving northwest with respect to the eastern side. This is called right-lateral motion. If one looks across the fault from either side, the other side is moving to the right.

Motion on the Garlock fault is left-lateral, which, combined with the right-lateral motion on the San Andreas fault, means that the Mojave Desert is moving eastward with respect to the rest of California. Parts of the faults that have been observed or inferred to move as a result of earthquakes in historic times are shown in the illustration at the left. Also shown are the dates of the earthquakes and the magnitude of some of the more important ones. In general both the length of rupture and the total displacement are greater for the larger earthquakes. Horizontal displacements as great as 21 feet were observed along the San Andreas fault after the San Francisco earthquake of 1906, which had a magnitude of 8.3 on the Richter scale. (The Richter scale, devised by Charles F. Richter of Cal Tech, is logarithmic. Although each unit denotes a factor of 10 in ground amplitude, or displacement, the actual energy radiated by an earthquake is subject to various modifications.) The San Fernando earthquake produced displacements of six feet, whose direction was almost equally divided between the horizontal and the vertical.

The trend of the San Andreas fault system is roughly northwest-southeast from San Francisco to the south end of the Great Central Valley (the San Joaquin Valley) and again from the north of the Salton Sea depression to the Mexican border. The motion along the faults

in these areas is parallel to the fault and is mainly strike-slip, or horizontal. Between these two regions, from the south end of the San Bernardino Mountains to the Garlock fault, the faults bend abruptly and run nearly east and west, producing a region of overthrusting and crustal shortening [*see illustration below*]. The attempt of the southern California plate to "get around the corner" as it moves to the northwest is responsible for the complex geology in the transverse ranges, for the abrupt change in the configuration of the coastline north of Los Angeles and ultimately for the recent San Fernando earthquake. The big bend of the San Andreas fault is commonly regarded by seismologists as being locked and possibly as being the location of the next major earthquake. Much of the motion in this region, however, is being taken up by strike-slip motion along faults parallel to the San Andreas fault and by overthrusting on both sides of the fault. The displacements associated with the larger earthquakes in southern California in the vicinity of the big bend have averaged out to about 2¾ inches per year since 1800. The Kern County earthquake of 1952 (magnitude 7.7) apparently took care of most of the accumulated strain, at least at the north end of the big bend, that had built up since the Fort Tejon earthquake of 1857 (magnitude 8).

The San Andreas fault system cannot be completely understood independently of the tectonics and geology of most of the western part of North America and the northeastern part of the Pacific Ocean. This vast region is itself only a part of the global tectonic pattern, all parts of which seem to be interrelated. The earthquake, tectonic and mountain-building activities of western North America are intimately related to the relative motions of the Pacific and North American plates. Just as it is misleading to think of the San Andreas fault as an isolated mechanical system, so it is misleading to think of the entire San Andreas fault as a single system. The part of the fault that lies in northern California was activated earlier and has moved farther than the southern California section. The northern portion is less active seismically than the southern section and seems to have been created in a different way. It is also moving in a slightly different direction.

Measuring Displacements

There are several ways to measure displacements on major faults. Fairly recent displacements are reflected in offset stream channels [*see illustration on page 142*]. Many such offsets measured in thousands of feet are apparent across the San Andreas fault in central California, some of which can be directly related to earthquakes of historic times.

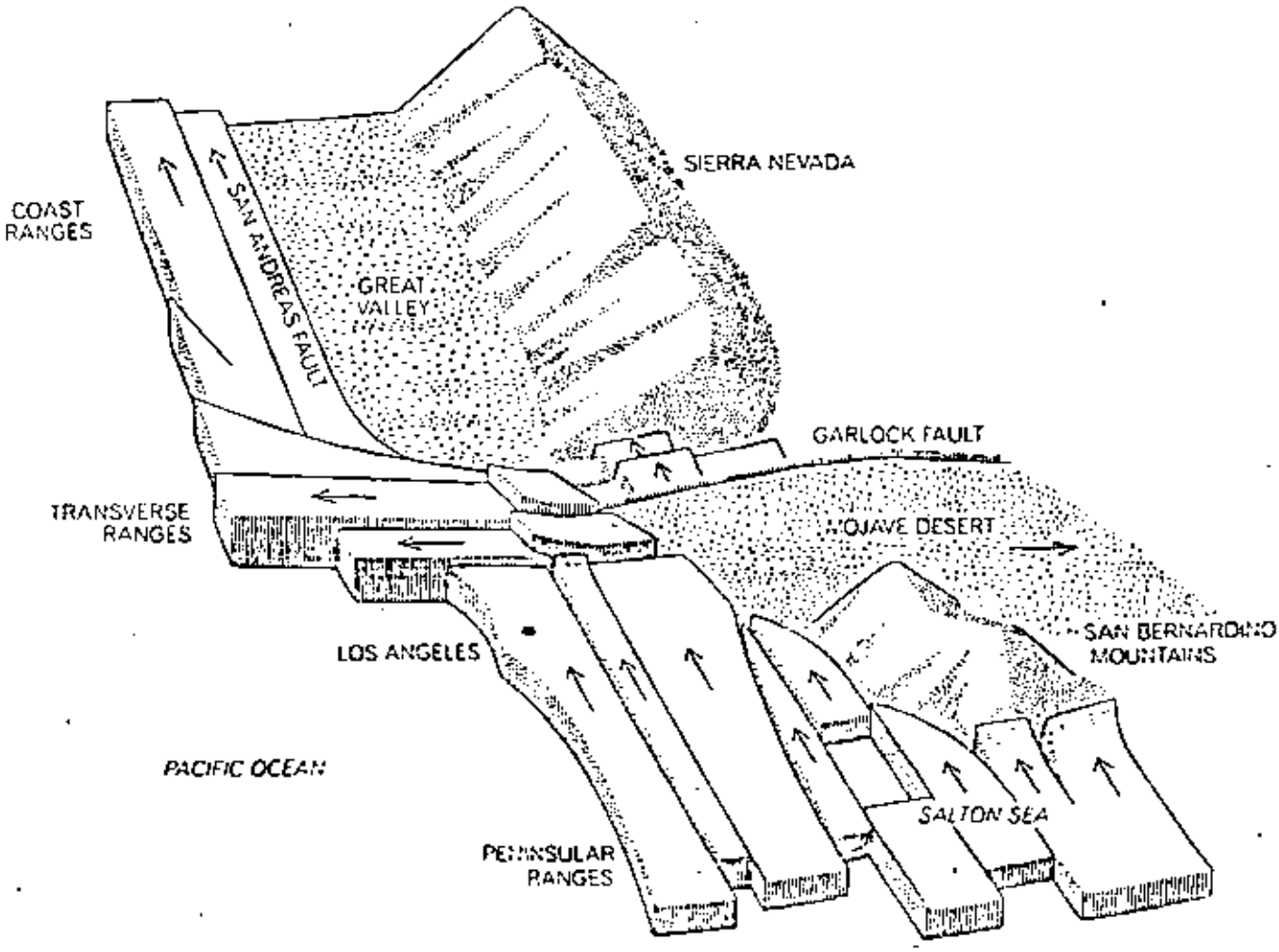

MOTION OF EARTH'S CRUST in southern California is generally northwest except where the lower group of blocks encounters the deep roots of the Sierra Nevada. At this point the blocks are diverted to the left (west), creating the transverse ranges and a big bend in the San Andreas fault system. Above the bend the blocks continue their northwesterly march, carrying the Coast Ranges with them. The Salton Sea trough at the lower right evidently represents a rift that has developed between two blocks.

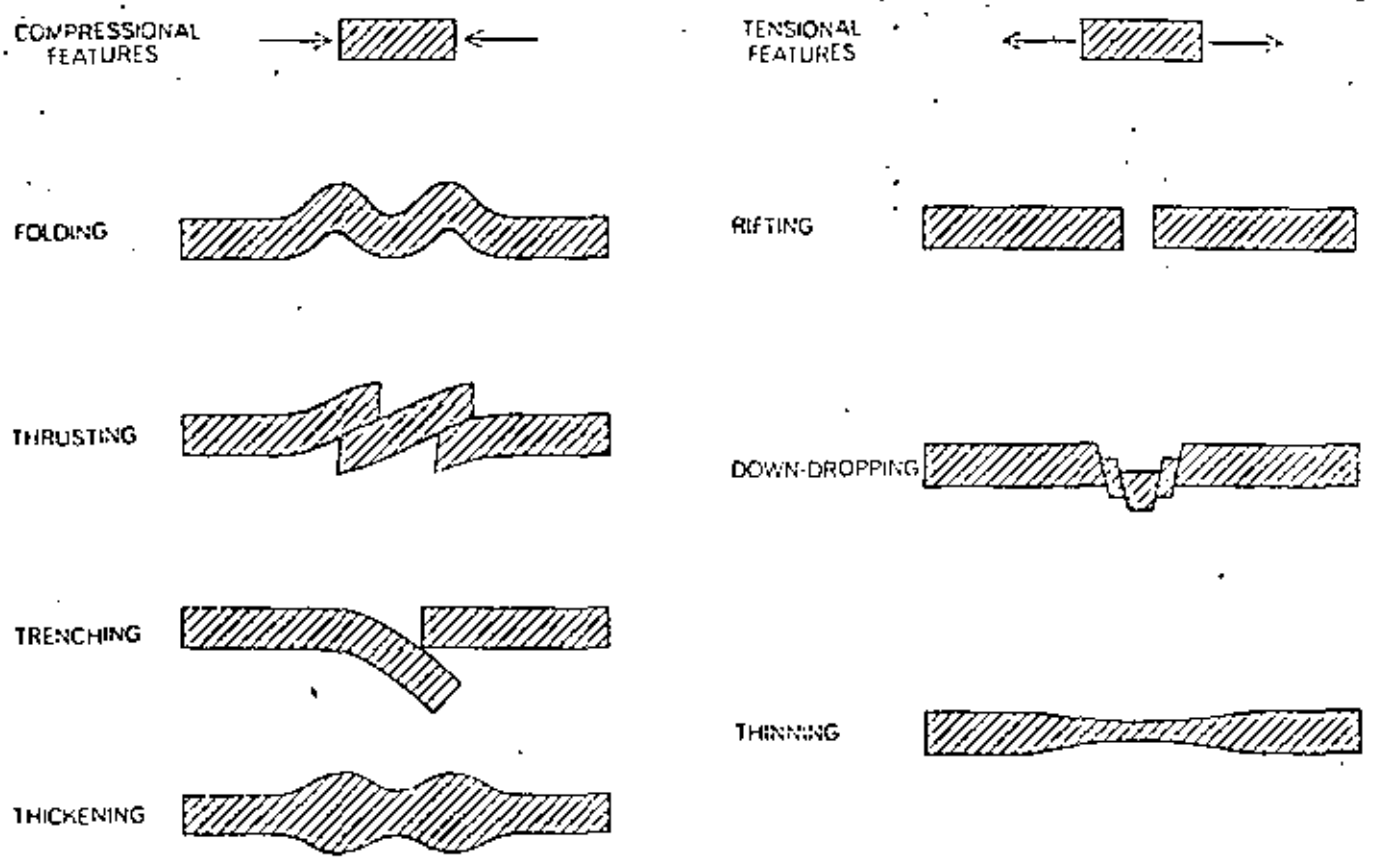

RESPONSE OF CRUSTAL PLATES to compression *(left)* and tension *(right)* accounts for most geologic features. According to the recently developed concept of plate tectonics, the earth's mantle is covered by huge, rigid plates that can be colliding, sliding past one another or rifting apart. The rifting usually occurs in the ocean floor. The San Andreas fault marks the location where two plates are sliding past each other. Plate tectonics helps to explain how the continents have drifted into their present locations.

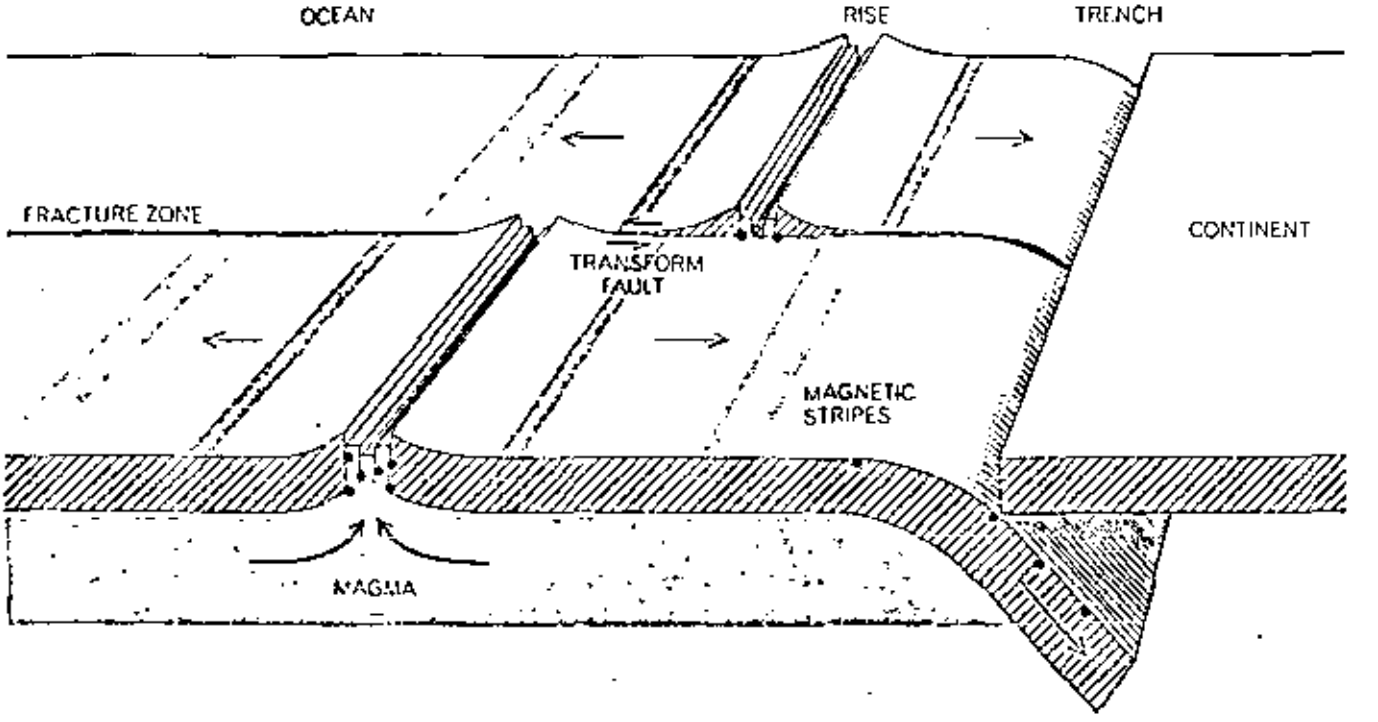

RIFT IN OCEAN FLOOR *(color)* initiates three major features of oceanic plate tectonics. The rift is bordered by a rise or ridge created by magma pushed up from the mantle below. The magma solidifies with a magnetic polarity corresponding to that of the earth. When, at long intervals, the earth's polarity reverses, the polarity of newly formed crust reverses too, resulting in a sequence of magnetic "stripes." A trench results when an oceanic plate meets a continental plate. A fracture zone and transform fault result when two plates move past each other. Earthquakes *(dots)* accompany these tectonic processes. The earthquakes in the vicinity of a rise and along a transform fault are shallow. Deep-focus earthquakes occur where a diving oceanic plate forms a trench.

Erosion destroys this kind of evidence very quickly. By matching up distinctive rock units that have been broken up and moved with respect to each other it is possible to document offsets of tens to hundreds of miles. A sedimentary basin often holds debris that could not possibly have been derived from any of the local mountains; matching up these basins with the appropriate source region on the other side of the fault can provide evidence of still larger displacements. When these various kinds of information are combined, one obtains a rate of about half an inch per year for motion on the San Andreas fault in northern and central California over the past several tens of millions of years.

This is much less than the 2½ inches per year that is inferred for the rate of separation of Baja California and mainland Mexico and the rate that is inferred from seismological studies in southern California. There are several possible explanations for the discrepancy. Northern and southern California may be moving at different rates; this seems unlikely since they are both attached to the same Pacific plate. On the other hand, part of the compression in the transverse ranges may result from a differential motion between the two parts of the state. Another possibility is that all of the relative motion between the North American plate and the Pacific plate is not being taken up by the San Andreas fault or even by the San Andreas fault system but extends well inland. The fracture zones of the Pacific seem to affect the geology of the continent for a distance of at least several hundred miles.

The Great Central Valley and the Sierra Nevada lie between two major fracture zones that abut the California coast: the Mendocino fracture zone and the Murray fracture zone. The transverse ranges, the Mojave Desert and the Garlock fault are all in line with the Murray fracture zone. Recent volcanism lines up with the extensions of the Clarion fracture zone and the Mendocino fracture zone. The basins and range geological province of the western U.S., a region of crustal tension and much volcanism, may represent a broad zone of deformation between the Pacific plate and the North American plate proper. Seismic activity is certainly spread over a large, diffuse region of the western U.S.

Although the subject has been quite controversial, most geologists are now willing to accept large horizontal displacements on the faults in California, particularly the San Andreas. Displacements as large as 450 miles of right-lat-

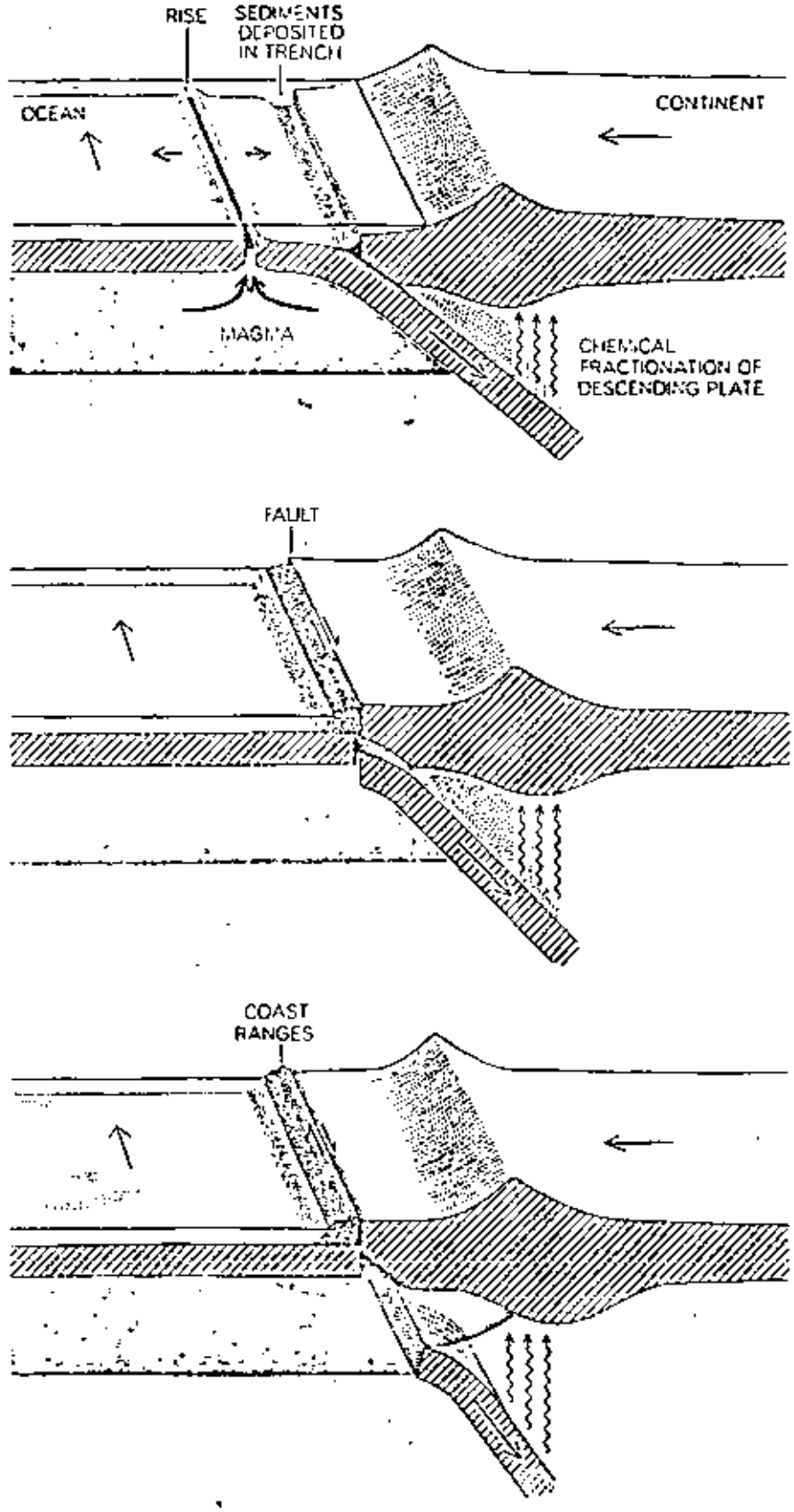

INTERACTION BETWEEN RISE AND TRENCH leads to mutual annihilation. The trench, formed as the oceanic plate dives under the continental plate, slowly fills with sediments carried by rivers and streams (*top*). Meanwhile the melting of the descending slab adds new material to the continent from below. When the axis of the rise reaches the edge of the continent, the flow of magma into the rift is cut off and trench sediments are scraped onto the western (that is, left) part of the oceanic plate (*middle*). The descending plate disappears under the continent and the sediments travel with the oceanic plate (*bottom*). The northern part of the San Andreas fault may have been formed in this way.

eral slip have been proposed for the northern segment of the fault. Displacements on the southern San Andreas fault are put at no more than 300 miles. This discrepancy has been puzzling to geologists. My own conclusion is that the part of northern and central California west of the San Andreas fault has moved northwest more than 700 miles and that the southern San Andreas fault has slipped about 300 miles, which makes the apparent discrepancy even worse. The discrepancy disappears if one drops the concept of a single San Andreas fault and admits the possibility that the two segments of the fault were initiated at different times.

The two-fault hypothesis is supported by straightforward extrapolation of the record on the ocean floor. The two San Andreas faults formed at different times, in different ways and may be moving at different rates. The record indicates that the western part of North America caught up with a section of the East Pacific rise somewhere between 25 million and 30 million years ago. Before the collision a deep oceanic trench existed off the coast such as now exists farther to the south off Central America and South America. The trench had existed for many millions of years, receiving sediments from the continent; subsequently the sediments were carried down into the mantle by the descending oceanic plate, which was diving under the continent. Based on what we know of trench areas that are active today one can assume that the plate sank to 700 kilometers and that the process was accompanied by earthquakes with shallow, intermediate and deep foci.

The Origin of Continents

Let us examine a little more closely what happens when an oceanic rise, the source of new oceanic crust, approaches a trench, which acts as a sink, or consumer of crust. Evidently the rise and the trench annihilate each other. The oceanic crust and its load of continental debris, which was formerly in the trench, rise because the crust is no longer connected to the plate that was plunging under the continent. The trench deposits are so thick they eventually rise above sea level and become part of the continent. The deposits are still attached to the oceanic plate, however, and travel with it [*see illustration on preceding page*].

In the case of the Pacific plate off California the deposits move northwest with respect to the continent. This is the stuff of coastal California north of Santa Barbara, particularly the Coast Ranges. According to this view, the northern segment of the San Andreas fault was born at the same time as northern California. The rise and the trench initially interacted near San Francisco, which then was near Ensenada in Baja California. Ensenada in turn was near the northern end of the Gulf of California, which was then closed.

The tectonics and geologic history of California, and in fact much of the western U.S., are now beginning to be understood in terms of the new ideas developed in the theories of sea-floor spreading, continental drift and plate tectonics. Many of the basic concepts were laid down by the late Harry H. Hess of Princeton and Robert S. Dietz of the Environmental Science Services Administration. Tanya Atwater of the University of California at San Diego and Warren Hamilton of the U.S. Geological Survey and their colleagues have made particularly important contributions by applying the concepts of plate tectonics to continental geology. We now know that the outer layer of the earth is immensely mobile. This layer, the lithosphere, is relatively cold and

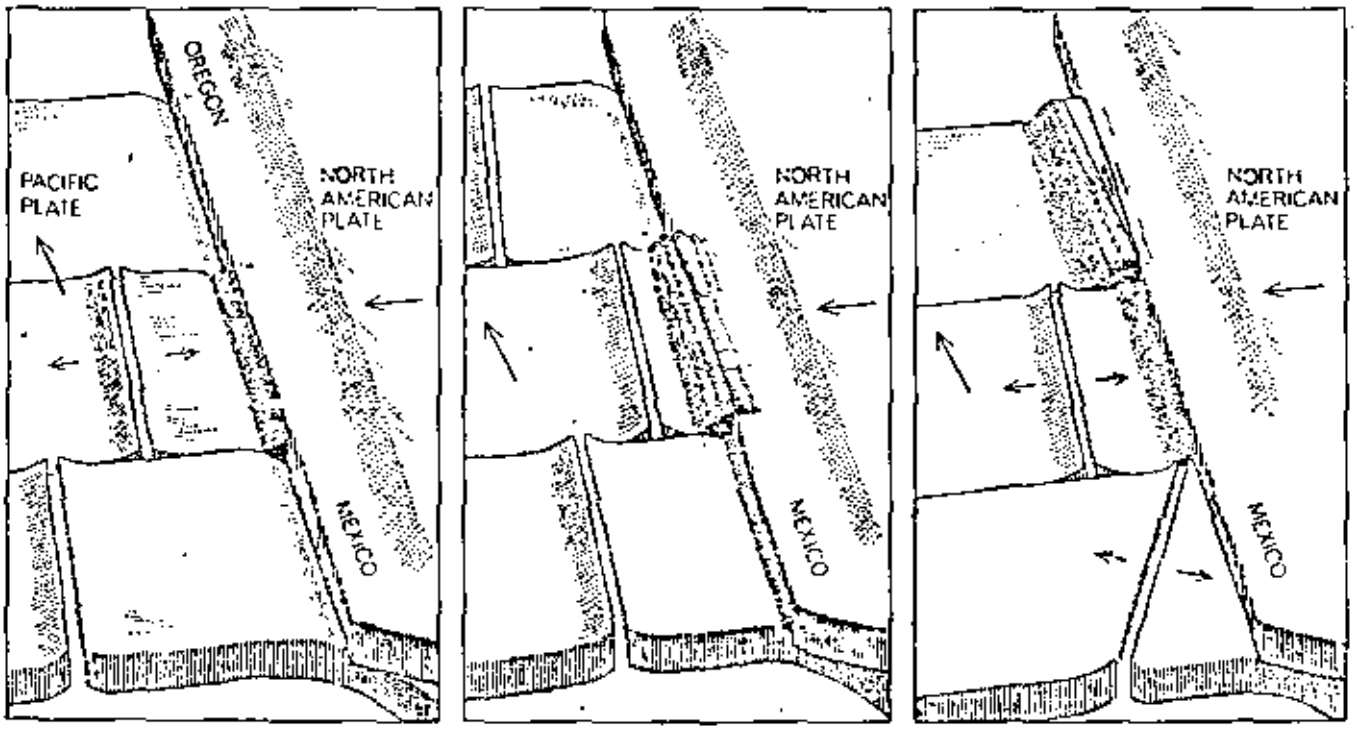

FORMATION OF SAN ANDREAS FAULT SYSTEM is depicted schematically in the six diagrams on these two pages. Some 30 million years ago (*left*) an oceanic rise system lay off the west coast of North America, which was carried by a plate moving toward the rise crests. The continental plate overrides the Pacific plate, producing a long trench. Meanwhile the entire Pacific plate is moving northwest. After a few million years (*right*) the rise nearest the continent is shut off. The trench by now has been filled with material eroded from the continent. These deposits will later become the California Coast Ranges. NORTHERN SECTION of San Andreas fault is created when the former trench deposits become attached to the northward-moving Pacific plate (*left*). The San Andreas fault lies between the two opposed arrows indicating relative plate motions. Meanwhile to the south a tilted rise crest

rigid and slides around with little resistance on the hot, partially molten asthenosphere.

Where the crust is thick, as it is in continental regions, the temperatures become high enough in the crust itself to cause certain types of crustal rocks to lose their strength and to offer little resistance to sliding. There is thus the possibility that the upper crust can slide over the lower crust and that the moving plate can be much thinner than is commonly assumed in plate-tectonic theory. The molten fraction of the asthenosphere, called magma, rises to the surface at zones of tension such as the mid-oceanic rifts to freeze and form new oceanic crust. The new crust is exposed to the same tensional forces (presumably gravitational) that caused the rift in the first place; therefore it rifts in turn and subsequently slides away from the axis of the rise. In addition to providing the magma for the formation of new crust, the melt in the asthenosphere serves to lubricate the boundary between the lithosphere and the asthenosphere and effectively decouples the two. The rise is one of the types of boundary that exist between lithospheric plates and is the site of small, shallow tensional earthquakes.

When two thin oceanic lithospheric plates collide, one tends to ride over the other, the bottom plate being pushed into the hot asthenosphere. The boundary becomes a trench. When the lower plate starts to melt, it yields a low-density magma that rises to become part of the upper plate; this magma becomes the rock andesite, which builds an island arc on what is to become the landward, or continental, side of the trench. (The rock takes its name from the Andes of South America. Mount Shasta in California is primarily andesite, as are the island arcs behind the trenches that surround the Pacific.) The thickness of the crust is essentially doubled as a result of the underthrusting. The material remaining in the lower plate is now denser than the surrounding material in the asthenosphere, both because it has lost a low-density fraction and because it is colder; thus it sinks farther into the mantle. In some parts of the world the downgoing slab can be tracked by seismic means to 700 kilometers, where it seems to bottom out. By this process new light material is added to the crust and new dense material is added to the lower mantle. A large part of what comes up stays up; a large part of what goes down stays down.

The introduction of chemical fractionation and a mechanism for "unmixing" makes the process different from the one customarily visualized, in which gigantic convection cells carry essentially the same material in a continuous cycle. The new process is able to explain in a convincing way how continents are formed and thickened. As the continent thickens and rises higher because of buoyancy, erosional forces become more effective and dump large volumes of continental sediments into the coastal trenches. A portion of the sediments is ultimately dragged under the continent to melt and form granite. The light granitic magma rises to form huge granitic batholiths such as the Sierra Nevada. A batholith is a large mass of granitic rock formed when magma cools slowly at great depth in the earth's crust. It is carried to the surface by uplifting forces and exposed by erosion.

The concept of rigid plates moving around on the earth's surface and interacting at their boundaries has been remarkably successful in explaining the evolution of oceanic geology and tectonics. The oceanic plates seem to behave rather simply. Tension results in a rise, compression results in a trench and lateral motion results in a transform fault

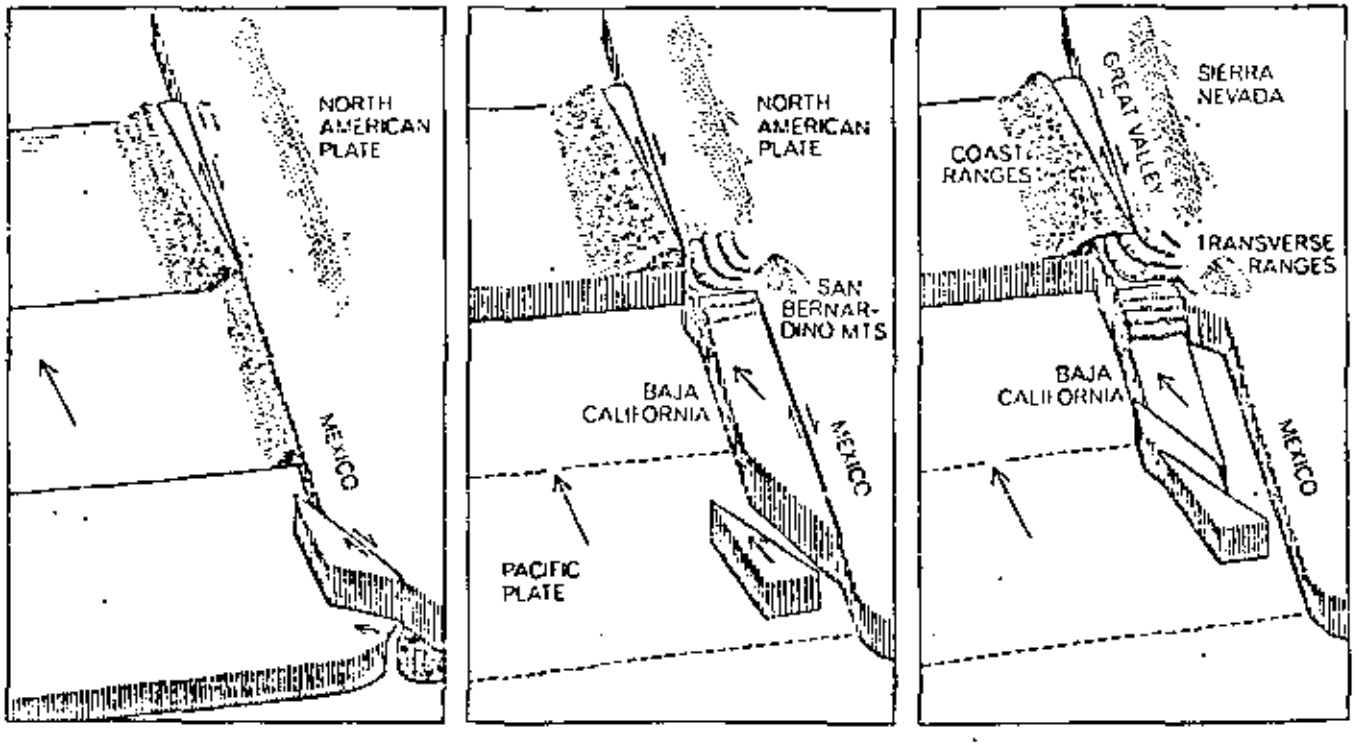

(not yet visible in the first pair of diagrams) is ready to encounter the continent end on at a break in the coastline south of Baja California. The collision (*right*) breaks off a part of the Baja California peninsula, which becomes attached to the Pacific plate and starts its journey to the northwest.

SOUTHERN SECTION of San Andreas fault is now fully activated (*left*) as the Baja California block begins sliding past the North American plate and collides with deeply rooted structures to the north, the Sierra Nevada and San Bernardino Mountains, which deflect the block to the west. More of Baja California breaks loose, opening up the Gulf of California. As Baja California continues to move northwestward (*right*) the Gulf of California steadily widens. The compression at the north end of the Baja California block creates the transverse ranges, which extend inland from the vicinity of present-day Santa Barbara.

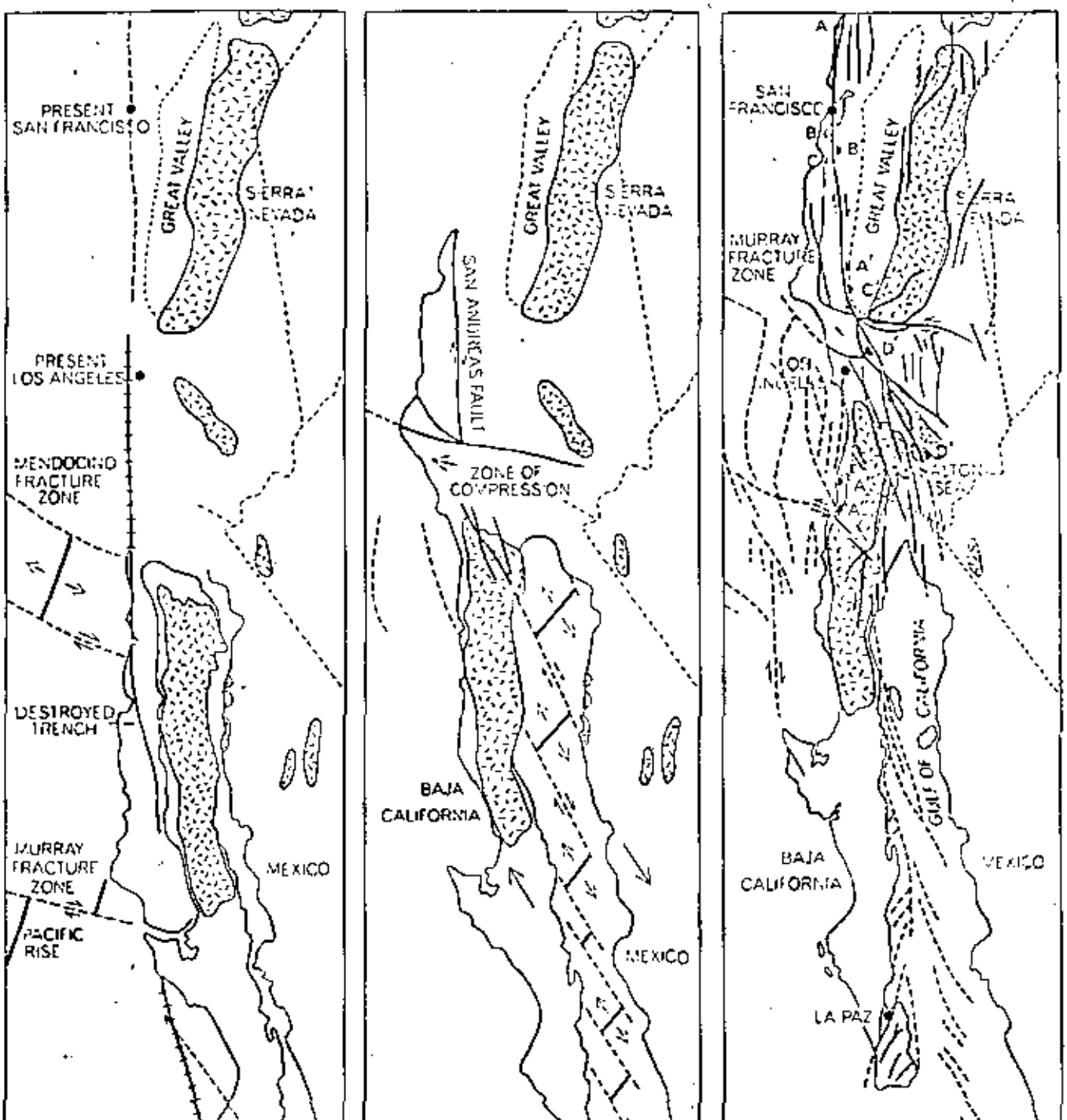

EARLY AND LATE STAGES in the history of the San Andreas fault are depicted. Twenty-five million years ago (*left*) Baja California presumably nestled against mainland Mexico. The first section of oceanic rise between the Murray fracture zone and the Pioneer fracture zone has just collided with the continent. Trench deposits are uplifted and become part of the Coast Ranges of California. The block containing the present San Francisco area (*dark color*) is about to start its long northward journey. A block immediately to the east (*light color*) becomes attached to the Pacific plate and eventually is jammed against the San Bernardino Mountains. Three million years ago (*middle*) the Gulf of California has started to open. As the peninsula moves away from mainland Mexico a series of rifts appear, fill with magma and are offset by numerous fractures. Baja California may have been torn off in one piece or in slivers. Southwest California and Baja California today (*right*) continue to slide northwest against the North American mainland. The illustration shows major fault systems and offshore fracture zones. On the basis of unique rock formations geologists infer that the Los Angeles area has moved northwest about 130 miles (*D'* to *D*) in the past 20 million years or less. Other studies indicate that the Palo Alto region has been carried about 200 miles (*C'* to *C*). Coastal rocks to the north of San Francisco have been displaced at least 300 miles (*B'* to *B*) and perhaps as much as 650 miles (*A''* to *A*) in the past 30 million years.

and a fracture zone [*see bottom illustration on page 146*]. The interaction of oceanic and continental plates or of two continental plates is apparently much more complicated, and this is one reason the new concepts were developed by study of the ocean bottom rather than continental geology.

The boundary between two oceanic plates can be a deep oceanic trench, an oceanic rise or a strike-slip fault depending on whether the plates are approaching, receding from or moving past each other. The forces involved are respectively compressional, tensional and shearing. When a thick continental plate is involved, compression can also result in high upthrust and folded mountain ranges. The Himalayas resulted from the collision of the subcontinent of India with Asia. I shall show that the transverse ranges in California were formed in a similar way. Tension can result in a wide zone of crustal thinning, normal faulting and volcanism; it can also create a fairly narrow rift of the kind found in the Gulf of California and the Red Sea [*see top illustration on page 146*].

The interaction of western North America with the Pacific plate has led to large horizontal motions along the San Andreas fault, to concentrated rifting as in the Salton Sea trough and the Gulf of California, to diffuse rifting and normal faulting accompanied by volcanism in the basins and range province of California, Nevada, Utah and Arizona, to large vertical uplift by overthrusting as in the transverse ranges north and west of Los Angeles, to the generation of large batholiths such as the Sierra Nevada and to the incorporation of deep-sea trench material on the edge of the continent. Ultimately the geology, tectonics and seismicity of California can be related to the collision of North America with the Pacific plate.

Most of the Pacific Ocean is bounded by trenches and island arcs. Trenches border Japan, Alaska, Central America, South America and New Zealand. Island arcs are represented by the Aleutians, the Kuriles, the Marianas, New Guinea, the Tongas and Fiji. The arcs are themselves bordered by trenches. All these arcs are characterized by andesitic volcanism and deep-focus earthquakes. Western North America is lacking a trench and has only shallow earthquakes, but the geology indicates that there was once a trench off the West Coast, and in fact there was once a rise. The present absence of a rise and a trench, the absence of deep-focus earthquakes and the existence of uplifted deep-sea sediments are all related.

Tracing back the history of the interaction of the Pacific plate with the North American plate, one is forced to conclude that the northern part and the southern part of the San Andreas fault originated at different times and in different ways. The northern part was evidently formed about 30 million years ago when a portion of rise between the Mendocino fracture zone and the Murray fracture zone approached an offshore trench bordering the southern part of North America. At that time the west coast of North America resembled the present Pacific coast of South America: there was a deep trench offshore, high mountains paralleled the coastline and large underthrusting earthquakes were associated with the downgoing lithosphere.

Origin of the Fault

As the rise approached the continent both the geometry and the dynamics of interaction changed [*see illustrations on pages 148 and 149*]. Depending on the spreading rate of the new crust generated at the rise and the rate at which the rise itself approaches the continent, the relative motion between the rise and the continental plate will decrease, stop or reverse when the rise hits the trench. The forces keeping the trench in existence will therefore decrease, stop or reverse, leading to uplift of the sedimentary material that has been deposited in the trench. In classical geologic terms these are known as eugeosynclinal deposits. Although they have been exposed to only moderate temperatures, they have been subjected to great pressures, both hydrostatic (owing to their depth of burial) and directional (owing to the horizontal compressive forces between the impinging plates). Eugeosynclinal sediments are therefore strongly deformed and become even more so as they are contorted and sheared during uplift. Much of the western edge of California and Baja California is underlain by this material, called the Franciscan formation. The formation is physically attached to the Pacific plate and is therefore moving northwest with respect to the rest of North America. The present boundary is the northern part of the San Andreas fault. Today this section of the San Andreas system extends from Cape Mendocino, north of San Francisco, to somewhere south and east of Santa Barbara, near the beginning of the great bend of the San Andreas fault, where the San Andreas and the Garlock faults intersect.

Meanwhile, 30 million years ago, another section of the rise south of the Murray fracture zone was still offshore, together with an active trench. Baja California was still attached to the mainland of Mexico and the Gulf of California had not yet opened up. The southern part of the San Andreas fault had not yet been formed.

The abrupt change in the direction of the coastline south of the tip of Baja California suggests that here the rise approached the continent more end on than broadside. A sliver of existing continent was welded onto the Pacific plate and rifted away from Mexico, thus forming Baja California and the Gulf of California. Thereafter Baja California participated in the northwesterly motion of the Pacific plate, with the result that the Gulf of California widened progressively with time.

About five million years were required for northern California, which had broken off from Baja California, to be carried about 200 miles to the northwest. At the end of that time the Gulf of California and the Salton Sea trough had not yet opened. The faults that delineate the major geologic blocks in southern California had not yet been activated. The block bearing the San Gabriel fault, now north of San Fernando, occupied the future Salton Sea trough. The transverse ranges will eventually be formed from the Santa Barbara, San Gabriel and San Bernardino blocks by strong compression from the south when Baja California breaks loose from mainland Mexico. This also opens up the Gulf of California and the Salton Sea trough.

As northern California is being carried away from Baja California by the Pacific plate another segment of oceanic rise south of the Murray fracture zone approaches the southern half of Baja California, where the situation described above is repeated except that the rise crest encounters a sharp bend in the coastline and the trench hits just south of the tip of the peninsula. Now instead of approaching the continent more or less broadside the rise approaches the continent end on. Mainland Mexico is still decoupled from that part of the Pacific plate to the west of the rise by the rise and the trench. Baja California, however, is now coupled to the northwestward-moving Pacific plate and Baja California is torn away from the mainland. This happened between four and six million years ago. Magma from the upper mantle wells up into the rift, forming a new rise that works its way north into the widening gulf. Alternatively, the entire peninsula of Baja California could have broken off from the mainland at the

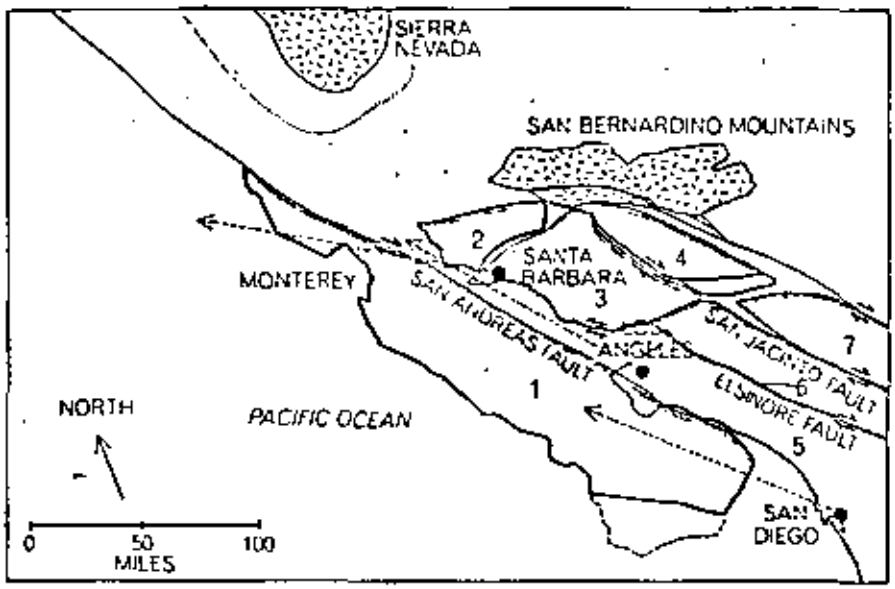

SEQUENCE OF SIMPLIFIED VIEWS shows the movement of major blocks in southern California over the past 12 million years. In the first view (*above*) the Gulf of California has not yet appreciably opened but the block carrying the Coast Ranges (1) has started to move rapidly northwest with activation of northern portion of San Andreas fault. Dots show origin and arrows show displacement of San Diego, Los Angeles and Santa Barbara.

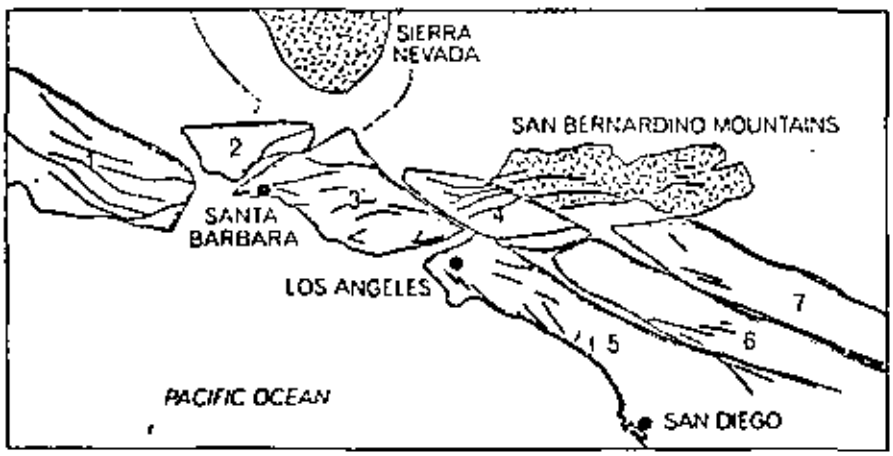

TWO MILLION YEARS AFTER ACTIVATION of the southern portion of the San Andreas fault four blocks (2, 3, 4, 7) have been forced against the deep roots of the Sierra Nevada and San Bernardino Mountains. Compressive forces create the transverse ranges. Meanwhile the block carrying the Coast Ranges (1) has been carried far to the northwest.

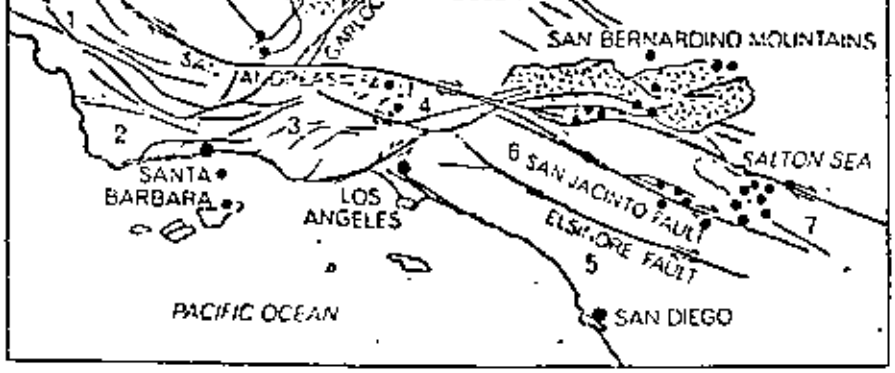

GEOLOGY OF SOUTHERN CALIFORNIA TODAY is dominated by compressive forces operating in the big bend of the San Andreas fault, which connects the southern and northern parts of the system. Colored dots show the location of earthquakes in the recent past.

same time. As the peninsula, including parts of southern California, moves north it collides with parts of the continent that are still attached to the main North American plate. This results in compression, overthrusting and shearing and the eventual formation of the transverse ranges.

The southern part of the San Andreas fault system was therefore formed by the rifting off of a piece of continent. Today it represents the boundary between two parts of the continental plate that are moving with respect to each other. This part of the San Andreas fault was formed well east, or inland, of the southward projection of the northern San Andreas.

The northerly march of southern California and Baja California seems to have been blocked when the moving plate encountered the thick continental crust to the north, particularly the massive granitic San Bernardino mountain range, which includes the 11,485-foot San Gorgonio Mountain. Since large and high mountain ranges have deep roots, the crust in this region is probably much thicker than normal, perhaps as thick as 50 kilometers. Earthquakes in this region are all shallower than 20 kilometers, which may be the thickness of the sliding plates. The blocks veer westward and are strongly overthrust as they attempt to get around the obstacle; this movement generates the big bend in the San Andreas fault system. The deflected blocks eventually join up with the northern California block.

Earthquake Country

From a social and economic point of view earthquakes are one of the most important manifestations of plate interaction. From a scientific point of view they supply a third dimension to the study of faults and the nature of the interactions between crustal blocks, including the stresses involved and the nature of the motions.

Seismologists at the University of California at Berkeley and at the Cal Tech Seismological Laboratory have been keeping track of earthquake activity in California for more than 40 years. Both groups have installed arrays of seismometers that telemeter seismic data to their laboratories for processing and dissemination to the appropriate public agencies. During the 36-year period 1934 through 1969 there were more than 7,300 earthquakes with a Richter magnitude of 4 or greater in southern California and adjacent regions [*see illustration on page 151*]. Many thousands more earthquakes of smaller magnitude are

routinely located and reported in the seismological bulletins. Although damage depends on local geological conditions and the nature of the earthquake, a rough rule of thumb is that a nearby earthquake of magnitude 3.5 or greater can cause structural damage. The average annual number of earthquakes of magnitude 3 or greater in southern California recorded since 1934 is 210, the number in any one year has varied from a low of 97 to a high of 391. The strongest earthquake in this period was the Kern County event of magnitude 7.7 in 1952. The aftershocks of that event increased the total number of events for several years thereafter.

In general the larger the earthquake, the greater the displacement across a fault and the greater the length of fault that breaks. The great earthquakes of 1906 and 1857 respectively caused large displacements across the northern and central parts of the San Andreas fault and relieved the accumulated strain in these areas. The accumulation of strain in southern California is relieved mainly by slip on a series of parallel faults and by overthrusting on faults at an angle to the main San Andreas system; that is what happened in the Kern County and San Fernando earthquakes. The unique east-west-trending transverse ranges were formed in this way. In the process deep-seated ancient rocks were uplifted and exposed by erosion.

Another seismically active area associated with major faults is south of the Mojave Desert near San Bernardino, where the faults show a sudden change in direction. The central part of the Mojave Desert is also moderately active. This is consistent with the idea that the sliding lithosphere is diverted by the San Bernardino Mountains. Faults and evidence of relatively recent volcanic events abound in the area. The northern part of Baja California is also quite active. An interesting feature of seismicity maps of southern California is the alignment of earthquakes in zones that trend roughly northeast-southwest, approximately at right angles to the major trend of the San Andreas system.

The map on the next page shows that the San Andreas fault itself has played only a small role in the seismicity of southern California over the past 30-odd years. One must not forget, however, that the great earthquake of 1857 probably broke the San Andreas fault for about 100 miles northwest and southeast from the epicenter. That epicenter is thought to have been near Fort Tejon, which is close to the projected intersection of the Garlock and San Andreas

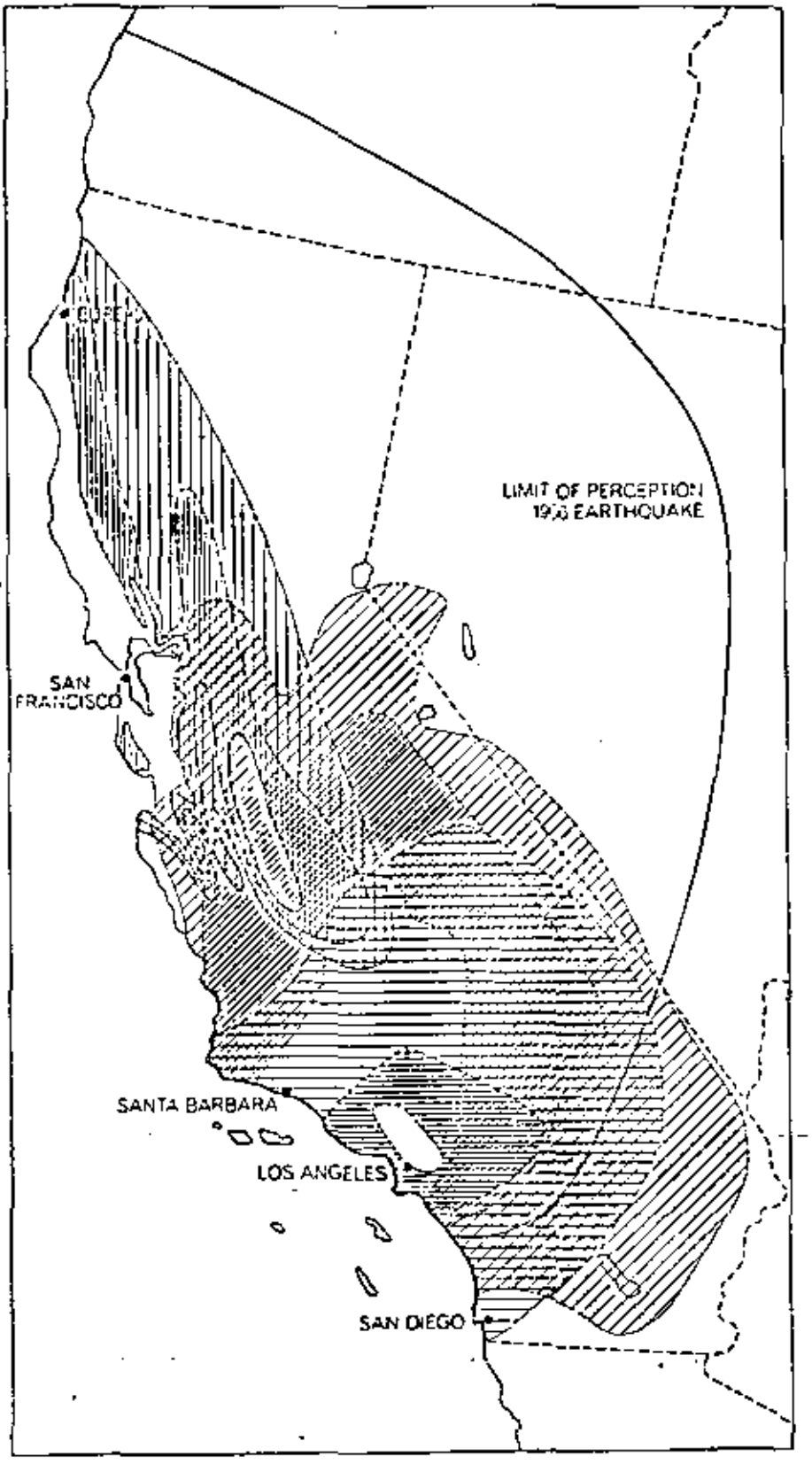

ISOSEISMAL CONTOUR MAP shows the pattern and intensity of ground-shaking produced by the 1906 San Francisco earthquake of magnitude 8.3, the 1952 Kern County earthquake of magnitude 7.7 and the 1971 San Fernando earthquake of magnitude 6.6. The Roman numerals indicate levels of perceived intensities as defined by the modified Mercalli scale. A short description of each level in the scale appears in the text on page 155.

faults; the actual location of the epicenter is uncertain by hundreds of miles because there were no seismic instruments in those days. Since that time this part of southern California has been remarkably quiet and seems to be locked, generating neither earthquakes nor creep. Activity along the San Andreas fault picks up near Coalinga, which is about midway between Bakersfield and San Francisco. Alignments of earthquakes are apparent along the San Jacinto and Imperial faults in the Salton Sea trough near the Mexican border. Although these faults lie west of the main San Andreas fault, they are part of the San Andreas system. The White Wolf fault, which is northwest of and parallel to the Garlock fault, has also been quite active, particularly after the Kern County earthquake, which occurred on this fault. The White Wolf fault lines up with the Santa Barbara Channel area, which has similarly been quite active.

One way to quantify the seismicity of southern California is to count the number of earthquakes per year per 1,000 square kilometers and compare this figure for the world as a whole. For example, southern California averages one earthquake of magnitude 3 or greater per year per 1,000 square kilometers. Thus within the entire region there are about 200 such earthquakes per year. The rate for earthquakes of magnitude 6.6, the size of the San Fernando earthquake, is about one every five or six years. The actual rates, however, vary considerably from year to year and depend somewhat on the time interval of the sample. The number of earthquakes decreases rapidly with size, and the average recurrence interval is not well established for the larger earthquakes. Southern California is about 10 times more active seismically than the world as a whole, which is simply to say that California is earthquake country.

Although certain areas in southern California are relatively free of earthquakes, none is immune from their effects. One of the largest quiet areas is the western part of the Mojave Desert wedge. This is surprising because the region is bounded on the northwest and southwest by areas that are obviously under large compression, as is shown by the upthrust mountains in the transverse and Tehachapi ranges and the large overthrust earthquakes that occurred in Kern County and San Fernando. It appears that the region is being protected from the northwesterly march of the southern California–Baja California block by the San Bernardino batholith and may represent a stagnation area in the lee of the mountains. Only a small number of earthquakes are centered near San Diego, although the larger earthquakes in northern Baja California and in the mountains between San Diego and the Salton Sea are felt in San Diego. The Great Central Valley north of Bakersfield and the eastern part of the Sierra Nevada are fairly inactive, as is a large area north of Santa Barbara in the Coast Ranges.

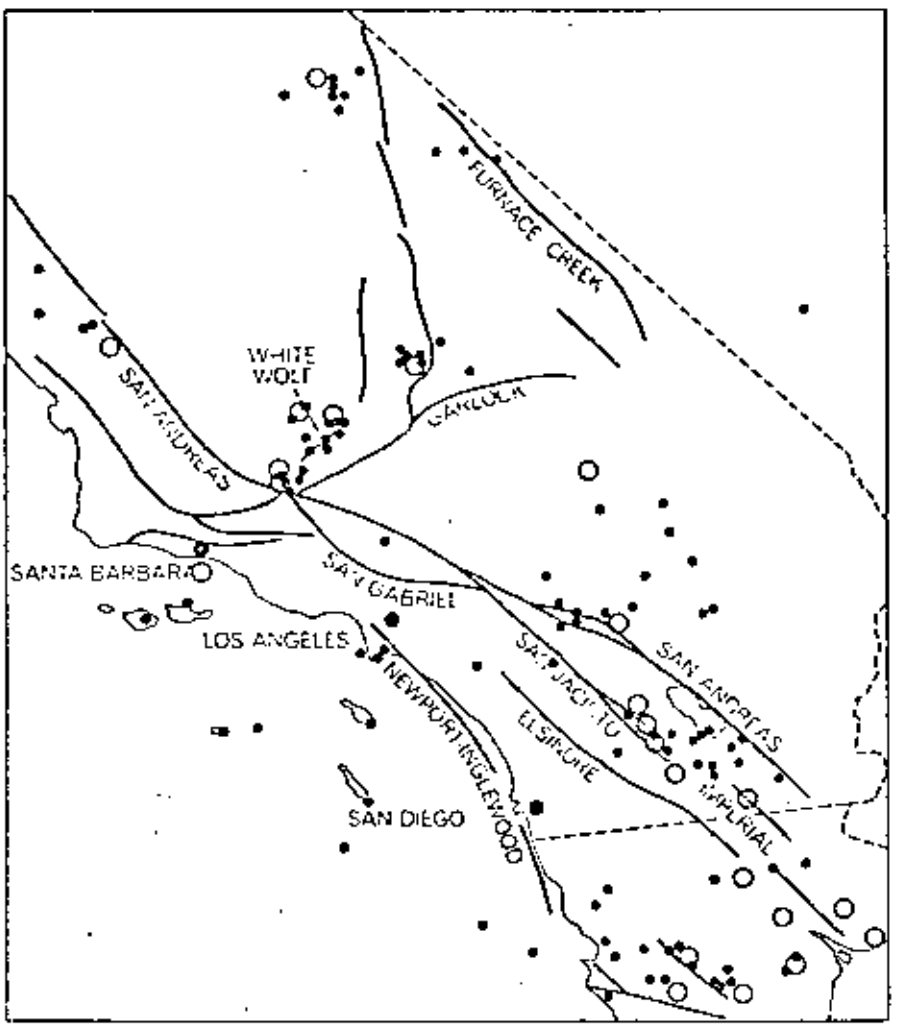

THIRTY-SIX-YEAR EARTHQUAKE RECORD shows the epicenters of all events of magnitude 5 or greater recorded in southern California and in the northern part of Baja California from 1934 through 1969. The epicenter is the point on the earth's surface above the initial break. Dots show earthquakes between 5 and 5.9 in magnitude. Open circles indicate earthquakes of magnitude 6 or greater. The hypocenter, the point of the initial break in the earth's crust, is often many miles below the surface in thrust-type earthquakes, a type frequently observed in this region. In the 36-year period southern California and adjacent regions experienced more than 7,300 earthquakes with a magnitude of 4 or more. Earthquakes are about 10 times more frequent in this area than they are in the world as a whole.

Magnitude and Intensity

It is somewhat deceptive to plot earthquakes as small points on a map. The points represent the epicenter: the point on the surface above the initial break. Once the break is started it can continue, if the earthquake is a major one, for hundreds of miles. Earthquakes of the thrust type, which result from a failure in compression, typically first break many miles below the surface; the surface break and maximum damage can be 10 miles or more from the epicenter. The distance over which strong shocks were felt during three large California earthquakes in this century (1906, 1952 and 1971) can be represented by plotting isoseismals: lines of equal intensity (*see illustration on preceding page*). The shape of the pattern varies with the type of earthquake and with the nature of the local geology; structures on deep sedimentary basins or on unconsolidated fill get a more intense shaking than structures on bedrock. The isoseismals of the

San Francisco earthquake are long and narrow, both because of the orientation of the fault and the length of the faulting and because of the northwest-southeast trend of the valleys. The orientation of the valleys in turn is controlled by the orientation of the San Andreas fault.

The public and the news media are confused about the various measures of the size of an earthquake. There are many parameters associated with an earthquake; they are usually regarded as fault parameters. They include the length, depth and orientation of the fault, the direction of motion, the rupture velocity, the radiated energy, the causal stresses and their orientation, the stress drop (which is related to the strength or the friction along the fault), the energy spectrum, the amount of offset or displacement and the time history of the motion. Most of these parameters can be estimated from seismic records, even from signals recorded several thousand kilometers from the earthquake. To obtain high precision, however, one needs records from many well-distributed seismic stations together with field observations at the site of the earthquake.

The magnitude on the Richter scale is a number assigned to an earthquake from instrumental readings of the amplitude of the seismic waves on a standard seismometer, the Wood-Anderson torsion seismometer. The amplitude must be suitably corrected for spreading and attenuation in the earth, and for instrumental response if a non-standard instrument is used. The magnitude is closely related to the energy of the earthquake, the single most important quantity by which earthquakes can be ranked one against another. If all the corrections are adequately made, a seismologist anywhere in the world will assign the same magnitude. In practice, because of the complicated radiation pattern of earthquakes and because of the distortion of the waves traveling through the earth, the initial magnitude assigned by various observatories may differ slightly. The magnitude scale is logarithmic and is open-ended at both ends. It is not a scale with a maximum value of 10, as is often reported in the press, and negative magnitudes are routinely measured by seismologists working on microearthquakes.

The intensity scale was developed for engineering purposes and is a qualitative measure of the intensity of ground vibration and structural damage. These qualitative assessments are assigned Roman numerals from I to XII. Unlike the magnitude of an earthquake, the intensity varies with distance and depends on the nature of the local ground. In general alluvial valleys, soft sediments and areas of uncompacted fill will magnify ground-shaking and will register higher intensities than adjacent areas on solid rock.

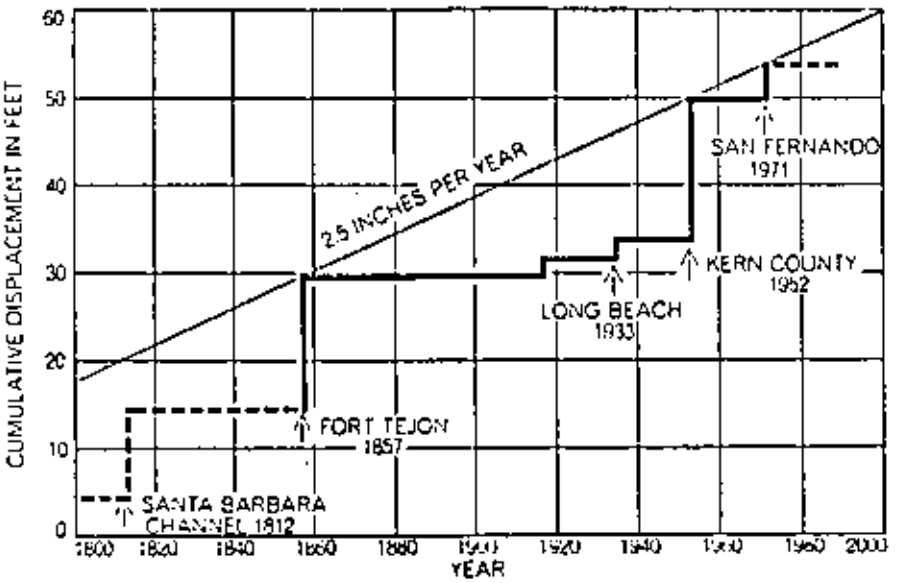

CUMULATIVE DISPLACEMENTS directly related to earthquakes indicate that southern California west of the San Andreas fault system is sliding northwestward at an average rate of 2½ inches per year. Major earthquakes relieve stresses that have built up over decades.

The intensity scale in common usage today is the Modified Mercalli Intensity Scale. The following characterizations of intensity, abridged from longer descriptions, indicate the kind of observations on which the Mercalli scale is based:

I. Not felt except by a very few under special circumstances. Birds and animals are uneasy; trees sway; doors and chandeliers may swing slowly.

II. Felt only by a few persons at rest, particularly on the upper floors of buildings.

III. Felt indoors, but many people do not recognize as an earthquake. Vibrations like the passing of light trucks. Duration of the shaking can be estimated.

IV. Windows, dishes and doors rattle. Walls make creaking sounds. Sensation like the passing of heavy trucks. Felt indoors by many, outdoors by few.

V. Felt by nearly everyone; many awakened. Small unstable objects are displaced or upset; plaster may crack.

VI. Felt by all; many are frightened and run outdoors. Some heavy furniture is moved; books are knocked off shelves and pictures off walls. Small church and school bells ring. Occasional damage to chimneys, otherwise structural damage is slight.

VII. Most people run outdoors. Difficult to stand up. Noticed by drivers of automobiles. Damage is negligible in buildings of good design and construction, slight to moderate in well-built ordinary structures, considerable in poorly built or badly designed structures. Waves on ponds and pools.

Intensity VII corresponds to the general experience within five or 10 miles of the surface faults associated with the San Fernando earthquake of last February. The following intensity levels were experienced in a small area of the northern San Fernando Valley and would be widely experienced in more severe earthquakes.

VIII. Steering of automobiles affected. Frame houses move on foundations if not bolted down; loose panel walls are thrown out. Some masonry walls fall. Chimneys twist or fall. Damage is slight in specially designed structures, great in poorly constructed buildings. Heavy furniture is overturned.

IX. General panic. Damage is considerable in specially designed structures; partial collapse of substantial buildings. Serious damage to reservoirs and underground pipes. Conspicuous cracks in the ground.

X. Most masonry and frame structures are destroyed with their foundations. Some well-built wooden structures are destroyed. Rails are bent slightly. Large landslides.

XI. Few, if any, masonry structures remain standing. Bridges are destroyed. Broad fissures in the ground. Rails are bent severely.

XII. Damage is nearly total. Objects are thrown into the air.

It is clear that the Mercalli intensity scale is people-oriented; anyone can ex-

timate the intensity from his own experience during an earthquake. The National Oceanic and Atmospheric Administration compiles information on intensities by mailing out questionnaires to a sample of the population living in an area that has experienced a sizable earthquake.

In order to obtain more exact information about the ground motions involved in earthquakes engineers have developed strong-motion accelerometers that automatically trigger and start to record when shaken severely. Most of these instruments are installed in the seismic areas of the U.S., with a particularly heavy concentration in and around Los Angeles. The instruments are expensive and must be located very close to an earthquake to provide useful data. More than 250 of the instruments were triggered during the San Fernando earthquake, and a wealth of engineering data will be provided by these records.

A strong-motion instrument records ground acceleration as a function of time. Accelerations are commonly reported as fractions of a g, the acceleration due to gravity at the earth's surface. One g is roughly 10 meters per second per second. In designing a building to withstand moderate earthquakes, engineers are concerned chiefly with the maximum accelerations, the period or frequency of shaking and the duration of shaking. Buildings in earthquake-hazard regions with stringent building codes are usually designed to withstand at least .1 g of acceleration; this corresponds to an intensity of about VII on the Mercalli scale.

Although there is no direct correlation between intensity and magnitude, the zone of destruction increases as the magnitude increases for shallow-focus earthquakes. In general the larger the magnitude of an earthquake, the longer the fault length, the larger the displacement across the fault and the longer the duration of shaking. The longer fault length alone accounts for much of the increased area of destruction. For example, the San Francisco earthquake of 1906 had an intensity of VII or greater out to a distance of 500 miles from the epicenter, and this may not have been the largest California earthquake in historic times. The San Francisco earthquake had a magnitude of 8.3. The 1952 Kern County earthquake (magnitude 7.7) had an intensity of VII or greater out to 50 miles. The recent San Fernando earthquake (magnitude 6.6) damaged older structures out to 25 miles. An earthquake of magnitude 5.5, the Parkfield earthquake of 1966, produced comparable damage to a distance of 10 miles.

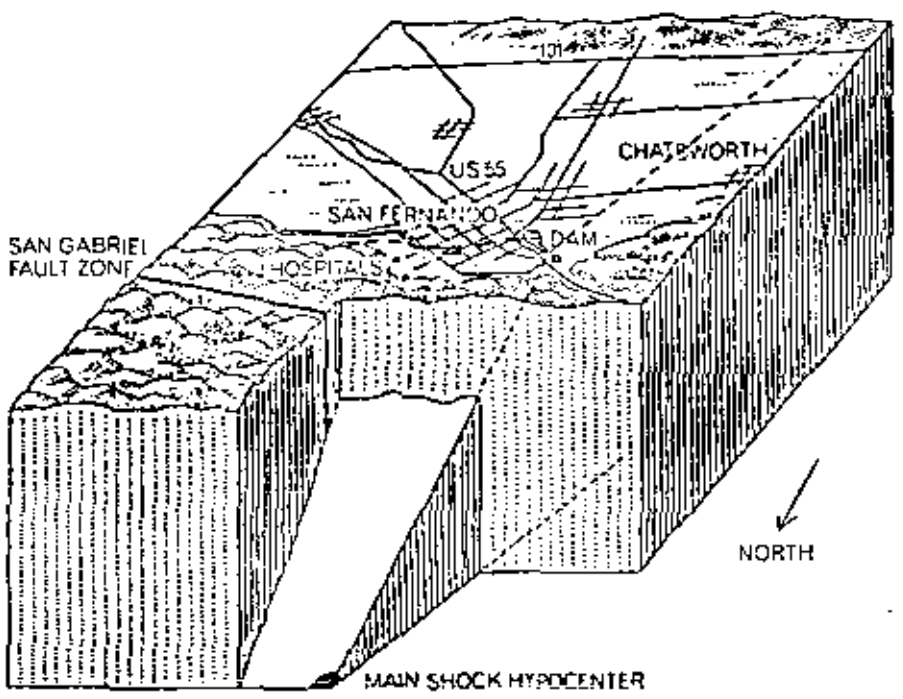

HYPOCENTER OF SAN FERNANDO EARTHQUAKE (*dark color*) of last February was 13 kilometers deep and 12 kilometers north of the area where the principal ground-shaking occurred. The earthquake collapsed sections of two hospitals in the San Fernando Valley, taking 64 lives, and so seriously weakened the earthen wall of the Van Norman Dam at the northern end of the San Fernando Valley that 80,000 people living below the dam had to leave their homes until the water level in the reservoir could be lowered. Total damage caused by the earthquake is estimated at $500 million to $1 billion. This three-dimensional view is based on a drawing prepared by two of the author's colleagues, Bernard Minster and Thomas Jordan, who worked with information supplied by geologists and geophysicists of the California Institute of Technology. The view is looking toward Los Angeles.

The February Earthquake

The San Fernando earthquake occurred in the San Gabriel Mountains just north of the San Fernando Valley, a densely populated northern suburb of Los Angeles. The San Gabriel Mountains are part of the structural province of the transverse ranges: the band of east-west-trending mountains, valleys and faults that is characterized by strong and geologically recent tectonic deformation. Geologists recognize that the region is one of recent crustal shortening caused by north-south compression. The mountains, produced by buckling and thrusting, are one result of this crustal shortening. They have been thrusting over the valleys to the south for at least five million years along fault planes that dip to the north or northeast.

Although many faults are known to have been active in this area in the past several thousand years, the San Fernando earthquake produced the first historic example of surface faulting. The San Gabriel Mountains rise abruptly some 5,000 feet above the San Fernando Valley and the Los Angeles basin to the south. During the earthquake of February 9 a wedge-shaped prism of the crystalline basement rock comprising the San Gabriel Mountains was thrust over the San Fernando Valley to the southwest, thereby raising the elevation of a section of the San Gabriel Mountains and sliding it slightly to the west. The displacement is consistent with the motions that have been occurring for millions of years, as one can infer from geologic offsets and uplifts. It also agrees with the general picture presented here, namely that the transverse ranges were formed by the collision of the southern and Baja California block with the central and northern California block, and with the concept that the southern California block is being diverted to the west by the massive San Bernardino batholith. One can infer that the thickening of the crust involved in the overthrusting and uplift of the San Gabriel Mountains made this region an additional obstacle to the northwesterly march of

the southern California block. If it did, this would lend additional support to the notion that the plates in California are only 15 to 20 kilometers thick. An intriguing possibility is that the upper part of the crust is sliding with relatively little friction on a layer of rock rich in the mineral serpentine.

The hypocenter, or point of initial rupture, of the San Fernando earthquake was at a depth of 13 kilometers under the San Gabriel Mountains. The fault motion was propagated to the surface along a fault inclined northward at an angle of 45 degrees and broke the surface near the cities of San Fernando and Sylmar, at the boundary between the crystalline rocks of the mountains and the sediments of the valleys [*see illustration on page 156*]. Two heavily damaged hospitals were between the epicenter and the surface break and were therefore on the upthrust, or elevated, block. The hundreds of aftershocks following the earthquake covered an area of approximately 300 square kilometers; the total volume of rock lifted up was about 2,500 cubic kilometers.

Even though the elevation difference between the peaks of the San Gabriel Mountains, such as Mount Wilson and Mount Baldy, and the floors of the adjacent valleys is impressive, it does not represent the total uplift. Erosion removes material from the mountains and deposits it in the valleys. The total amount of differential vertical motion probably exceeds two and a half miles, and horizontal displacements in the transverse ranges probably exceed 25 miles. Many thousands of earthquakes of the San Fernando type must have occurred in the area over the past several million years.

Seismic surveillance of the region with instruments dates back only four decades. In this period the northern San Fernando Valley was less active seismically than many other parts of the greater Los Angeles area, although it was comparable to the average for all southern California. On the basis of the seismic data there was no reason to believe the San Fernando area was any more or less likely than any other region of recent mountain-building in southern California to experience a large earthquake. On the other hand, the thrusting and bending associated with the geologic processes in the region, and the tilting that was associated with the earthquake and its aftershocks, suggest that a dense network of tiltmeters could provide a warning of the next large earthquake here.

DIVISION DE EDUCACION CONTINUA
FACULTAD DE INGENIERIA U.N.A.M.

VII CURSO INTERNACIONAL DE INGENIERIA SISMICA

SISMOLOGIA Y SISMICIDAD

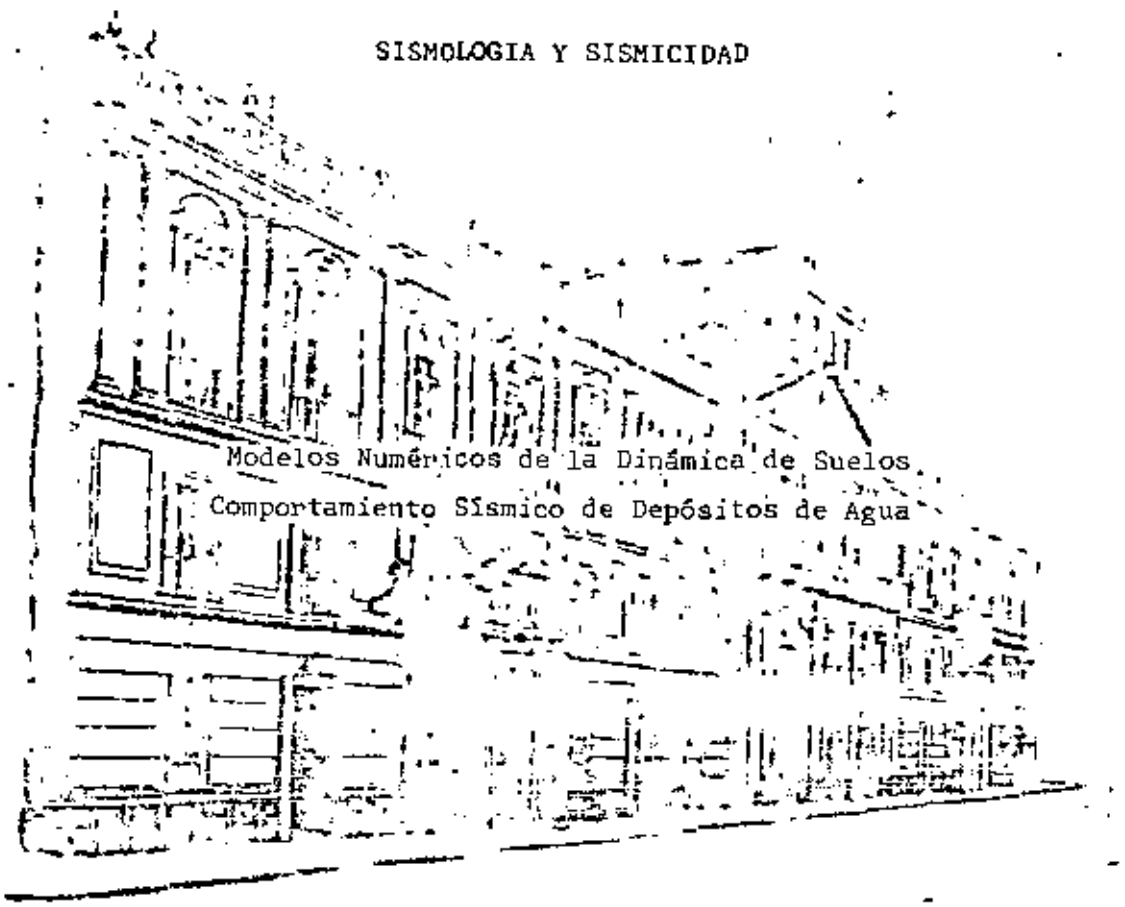

Modelos Numéricos de la Dinámica de Suelos. Comportamiento Sísmico de Depósitos de Agua

Ing. Abraham Díaz Rodríguez

Julio 1981

MODELOS NUMERICOS DE LA DINAMICA DE SUELOS - COMPORTAMIENTO SISMICO DE DEPOSITOS DE ARENA

Abrahnm Díuz Rodríguez
Román Cervantes Beltrán
Víctor Porras Silva

Profesores, División de Estudios de Posgrado, Facultad de Ingeniería, UNAM.

1. INTRODUCCION

La respuesta dinámica de los depósitos naturales es uno de los problemas de la dinámica de suelos que tiene gran interés en la ingeniería sísmica y, que debido a su complejidad, se hace necesario hacer uso de los métodos numéricos para llegar a soluciones apropiadas en aquellos problemas en los cuales las condiciones de frontera no son simples, y que dicho sea, son las situaciones que más frecuentemente se encuentran.

En este trabajo se discuten los modelos numéricos, y se presenta una breve descripción de las características más importantes que a juicio de los autores son los más representativos para cuantificar el fenómeno de licuación de arenas. También se presenta un ejemplo de aplicación para mostrar la versatilidad de la herramienta numérica.

2. MODELOS NUMERICOS EXISTENTES

Es objeto de esta sección hacer una breve descripción de las características de algunos de los modelos numéricos que se han utilizado en el análisis del fenómeno de licuación y que, de acuerdo con la experiencia de los autores, se consideran los más representativos.

La descripción de los modelos numéricos considerados se hará con base en la formulación de las ecuaciones de movimiento en el contexto de la teoría del medio continuo. Por tanto, se hará énfasis en las ecuaciones constitutivas del material, la magnitud de los desplazamientos considerados, la modelación de la generación de poro, así como el método de solución de las ecuaciones de movimiento.

Respecto al material, el enfoque que se ha seguido para su modelación consiste en definir por separado el comportamiento del esqueleto así como los cambios volumétricos que ocasiona la densificación. Los parámetros de las ecuaciones se definen básicamente de pruebas ante cargas cíclicas de amplitud constante.

2.1 *Modelos Desarrollados en la Universidad de California, Berkeley*

Las referencias 5 a 8, representan una bibliografía selecta que discute los modelos desarrollados en la Universidad de California, cuyas características principales son:

1) Establece las ecuaciones de movimiento en función de esfuerzos totales
2) Consideran el problema de desplazamientos pequeños
3) El comportamiento no-lineal de los suelos se trata ya sea mediante un procedimiento lineal equivalente o mediante un criterio tipo Masing(26), que puede ser un Ramberg-Osgood o un Martin-Davidenkov(7).
4) La generación de la presión de poro se calcula a partir de resultados de pruebas triaxiales cíclicas consolidadas-no drenadas(10), cuyas variables son:
   - σ'_0 , esfuerzo de consolidación
   - σ_{dp} , esfuerzo desviador cíclico
   - $(u_g)_N$, presión de poro generada para N ciclos
   - N_ℓ , número de ciclos para provocar la licuación

   Al representar las relaciones N/N_ℓ vs $\frac{u_g}{\sigma'_0}$ se obtiene una franja angosta de forma peculiar que se presenta mediante

$$\frac{N}{N_\ell} = \left[\frac{1}{2}\left(1 - \cos\frac{u_g}{\sigma'_0}\right)\right]^\alpha \qquad (2.1)$$

   α es un parámetro que depende del tipo de arena y de las condiciones de prueba(7). Al aplicar la expresión (2.1) para una historia irregular de ciclos de esfuerzos es necesario transformar dicha historia en un número de ciclos equivalente, de amplitud constante, según el criterio descrito en la referencia(27).
5) Las ecuaciones de movimiento se integran con el método del elemento finito ya sea con el criterio del método lineal equivalente o bien en forma incremental. La integración respecto al tiempo se lleva a cabo mediante un esquema que utilice el dominio de la frecuencia; o bien uno directo, paso a paso, en el dominio del tiempo.
6) El amortiguamiento considerado es el lineal equivalente como se define en la ref 22; o bien el que resulta de considerar un modelo histerético.
7) La disipación de la presión de poro se calcula con base en la generación de la presión de poro conocida y la teoría de Consolidación Unidimensional.

8) Para problemas bidimensionales la respuesta dinámica se cuantifica con el método lineal equivalente, mientras que para los problemas no lineales incrementales se considera únicamente el caso unidimensional.

2.2 *Modelo Desarrollado en la Universidad de British Columbia, Vancouver*

Este modelo se describe en las referencias 13 a 15, con las siguientes características:

1) Establece las ecuaciones de movimiento en función de esfuerzos efectivos
2) Considera el problema de desplazamientos pequeños
3) La curva esfuerzo-deformación para el esqueleto es del tipo hiperbólico

$$\tau = G_{mo}\,\gamma/(1 + G_{mo}\,\gamma/\tau_{mo}) \qquad (2.2)$$

donde

G_{mo} es el módulo tangente inicial máximo, y
τ_{mo} es el esfuerzo cortante máximo sin provocar la falla
G_{mo} y τ_{mo} se determinan según la ref 23 .

Las trayectorias de descarga y recarga se describen mediante el criterio tipo Masing(26).

$$\frac{\tau-\tau_r}{2} = \frac{G_m(\gamma-\gamma_r)}{2}\Big/\left(1 + \frac{G_m|(\gamma-\gamma_r)|}{2\tau_m}\right) \qquad (2.3)$$

donde

γ_r y τ_r son la deformación cortante y esfuerzo cortante del punto donde ocurre la inversión de esfuerzo
G_m y τ_m son el módulo al cortante y el esfuerzo cortante, respectivamente, para el ciclo N , expresados por:

$$G_m = G_{mo}\left[1 + \frac{\varepsilon_{vd}}{H_1+H_2\,\varepsilon_{vd}}\right]\left(\frac{\sigma'_v}{\sigma'_{vo}}\right)^{1/2} \qquad (2.4)$$

$$\tau_m = \tau_{mo}\left[1 + \frac{\varepsilon_{vd}}{H_3+H_4\,\varepsilon_{vd}}\right]\left(\frac{\sigma'_v}{\sigma_{vo}}\right)^{1/2} \qquad (2.5)$$

donde

ε_{vd} es la deformación volumétrica acumulada
H_1, H_2, H_3 y H_4 son constantes experimentales
σ'_v y σ'_{vo} son los esfuerzos verticales efectivos en el ciclo N e inicial, respectivamente

4) La generación de la presión de poro se calcula mediante el cambio de volumen acumulado, obtenido experimentalmente. La expresión del incremento del cambio de volumen es:

$$\Delta\varepsilon_{vd} = C_1(\gamma - C_2\varepsilon_{vd}) + \frac{C_3\,\varepsilon^2_{vd}}{\gamma + C_4\,\varepsilon_{vd}} \qquad (2.6)$$

C_1, C_2, C_3 y C_4 son constantes experimentales que toman en cuenta el tipo de arena y la compacidad relativa.

En condiciones no-drenadas y completa saturación, el incremento de la presión de poro durante cada intervalo de tiempo de integración se calcula mediante

$$\Delta u = \bar{E}_r\,\Delta\varepsilon_{vd} \qquad (2.7)$$

donde

$\bar{E}_r$ es el módulo de recuperación elástica unidimensional

5) Las ecuaciones de movimiento se resuelven con el método de diferencias finitas y la integración se lleva a cabo con el método beta de Newmark.
6) Además del amortiguamiento histerético, se puede incluir amortiguamiento viscoso, de acuerdo con el criterio de Rayleigh.
7) La disipación de la presión de poro se calcula con base en la Teoría de la Consolidación Unidimensional.
8) El modelo es unidimensional y las ecuaciones de movimiento y las de disipación de la presión de poro se integran en forma independiente.

2.3 *Modelo Desarrollado en la Universidad de Illinois, Urbana-Champaign*

En la ref 19 se presenta la formulación de este modelo, cuyas características se resumen a continuación:

1) Las ecuaciones de movimiento se formulan en función de los esfuerzos efectivos.
2) Considera el problema de desplazamientos pequeños.
3) Utiliza como ecuación constitutiva al modelo desarrollado por Ishihara y sus colaboradores, descrito en las referencias 20 y 21. La ecuación del esqueleto, válida hasta el inicio de la licuación, para representar la aplicación de la carga (tanto positiva como negativa) resulta ser

$$\left(\frac{q}{p'}\right) = \frac{\gamma\,G_o\,S_{max}}{\gamma\,G_o + S_{max}} \qquad (2.8)$$

donde

q es el esfuerzo cortante
p' la presión efectiva
γ la deformación angular
G_o el módulo de rigidez al cortante inicial
S_{max} es el valor de q/p' cuando γ tiende a infinito

Las trayectorias de descarga se consideran lineales, con pendiente G_o hasta que alcanza el valor máximo o mínimo previo de q/p', donde posteriormente se considera válida la ec 2.8 .

De acuerdo con las referencias 20 y 21, la licuación inicial ocurre cuando el esfuerzo se aproxima, sin llegar, a la línea de falla, denominada estado crítico, cuya ecuación se puede escribir como:

$$f_1 = q - p' \tan\phi = 0 \qquad (2.9)$$

Si p'_o es el esfuerzo efectivo inicial del material en condiciones no drenadas, la trayectoria de esfuerzos en el plano p'-q se modela como un cuarto de elipse, expresada por la ecuación siguiente:

$$f_2 = q^2 + \lambda^2\left[p'^2 - \left(\frac{2\lambda}{\lambda+\tan\psi}\right)p' p_o' + \left(\frac{\lambda-\tan\phi}{\lambda+\tan\phi}\right)p_o'^2\right] = 0 \quad (2.10)$$

$$\lambda = \frac{p_f'}{p_o' - p_f'} \tan\phi \quad (2.11)$$

donde

p_f' es la intersección de la trayectoria de esfuerzos en cuestión con la línea de falla.

Para el comportamiento después de la licuación inicial, Ishihara et al (ref 21) proponen una trayectoria diferente de la de falla.

4) La generación de presión de poro se considera al acoplar el movimiento del agua. El acoplamiento se base en la teoría de Biot (ref 24) al considerar el material constituido por dos fases.
5) Las ecuaciones de movimiento originalmente se establecieron en forma general para el problema lineal (ref 25) y se formularon para resolverse con el método del elemento finito. Posteriormente se consideraron válidas para el comportamiento no lineal del sólido (ref 18) y se establecieron en forma incremental. Para la integración respecto al tiempo se utiliza el método theta de Wilson.
6) La disipación de la presión de poro está implícita en la modelación del movimiento del agua.
7) El amortiguamiento implícito en el modelo es el histerético y el provocado por el movimiento del agua. También se puede adicionar el amortiguamiento del tipo viscoso.
8) El modelo se desarrolla en forma general para el caso lineal, sin embargo, para el problema no lineal se particularizó en uno unidimensional.

2.4 *Modelo Desarrollado en la Universidad de Michigan, Ann Arbor*

Las referencias 11 y 12 describen el procedimiento seguido para el desarrollo del modelo en cuestión, cuyas características principales son:

1) Las ecuaciones de movimiento se establecen en función de los esfuerzos efectivos.
2) Considera el problema de desplazamientos pequeños
3) Utiliza como ecuación constitutiva para el esqueleto un modelo Ramberg-Osgood modificado con ablandamiento por deformación, de la forma siguiente:

$$\gamma = \frac{\tau}{G_o(\bar{\sigma}_z)}\left[1 + \alpha\left|\frac{\tau}{\tau_1 \tau_R(\bar{\sigma}_z)}\right|^{R-1}\right] \quad (2.12)$$

donde

τ es el esfuerzo cortante
γ la deformación angular y
$\bar{\sigma}_z$ el esfuerzo vertical efectivo

Los valores de G_o y τ_R corresponden al módulo de rigidez al cortante para deformaciones infinitesimales y al esfuerzo cortante asociado, respectivamente y se calculan de acuerdo con la ref 23, para el problema unidimensional. Los parámetros del modelo de Ramberg-Osgood en cuestión son α, C_1 y R. Para definir las trayectorias de carga y descarga se utiliza el criterio de Masing(ref 26).

4) La generación de presión de poro se considera al acoplar el movimiento del agua. El acoplamiento se efectúa al considerar el flujo vertical del agua y utilizar la ley de Darcy.
5) Las ecuaciones de movimiento se establecen en forma de ecuaciones de ondas de cortante y de compresión. La solución de las ecuaciones de movimiento se obtienen con el método de las características y el acoplamiento de las ecuaciones se establece en el proceso de solución.
6) La disipación de la presión de poro se considera en forma implícita al modelar el movimiento del agua.
7) El amortiguamiento implícito en el modelo es el histerético y el provocado por el movimiento del agua.
8) El modelo es unidimensional.

2.5 *Modelo Desarrollado en la Universidad de Sussex, Wales*

Este método se describe en la ref 16 y sus características se resumen a continuación:

1) Establece las ecuaciones de movimiento en función de los esfuerzos efectivos.
2) Considera el problema de los desplazamientos grandes.
3) El comportamiento del sólido se modela con la ecuación constitutiva de la elastoplasticidad. La superficie de fluencia utilizada corresponde al criterio de falla de Mohr-Coulomb con una regla de fluencia no asociativa.
4) La generación de la presión de poro se considera al cuantificar la compactación ε_o, debida a cargas cíclicas. La deformación volumétrica, ε_o, la cuantifican con base en pruebas de cortante simple, cíclicas, de amplitud constante, no drenadas, con medición de presión de poro. Las variables experimentales $\theta = \tau/\sigma_{mo}'$,

donde

τ es el esfuerzo cortante
σ_{mo}' el esfuerzo medio inicial, efectivo,
γ la amplitud de deformación angular
p la presión de poro y
N el número de ciclos, son la base para construir la expresión siguiente:

$$\varepsilon_o = f(\kappa) \quad (2.13)$$

$$d\kappa = g(\theta)\, d\xi \quad (2.14)$$

$$d\xi = \sqrt{de_{ij}\, de_{ij}}, \quad i,j = 1,2,3 \quad (2.15)$$

donde

de_{ij} es el incremento del tensor de deformaciones desviador, correspondiente al tensor de deformaciones finitas dE_{ij}.

Para los datos experimentales que se utilizaron en esta formulación, se obtuvo la expresión siguiente:

$$d\varepsilon_o = \frac{A}{1+B\kappa}\, d\kappa \quad (2.16)$$

Los valores experimentales de los coeficientes A y B se cuantifican para las dos etapas en que se divide el fenómeno. Antes y después de la licuación inicial definida por la relación $p/\sigma_{mo}' = 0.6$.

5) Las ecuaciones de movimiento se resuelven con el

método del elemento finito y la integración respecto al tiempo se lleva a cabo mediante un método paso a paso basado en un esquema explícito de diferencias centrales.

6) Además del amortiguamiento histerético, se considera el amortiguamiento viscoso con el criterio de Rayleigh.
7) No considera el efecto de la disipación de la presión de poro.
8) La formulación presentada, aunque general, se desarrolla para el problema bidimensional. En los ejemplos considerados supone que el amortiguamiento conduce a una matriz diagonal y es donde resulta más efectivo el esquema de diferencias centrales que es condicionalmente estable (ref 17).

3. EJEMPLO DE APLICACION

Para ilustrar la utilización de los modelos numéricos descritos, se presenta la respuesta dinámica del depósito arenoso mostrado en la fig 1.

El modelo utilizado corresponde al desarrollado en la Universidad de British Columbia, Vancouver, mediante el programa de computadora DESRA-1 (ref 29).

El sismo considerado corresponde a los diez primeros segundos del acelerograma de El Centro de 1940, componente N-S, escalado convenientemente.

Los conceptos de mayor interés que se cuantifican en el depósito, para varias aceleraciones del sismo, son las siguientes:

a) Acelerograma calculado en la superficie
b) Historia de la generación de presión de poro
c) Historia de las deformaciones angulares
d) Curvas esfuerzo-deformación.

Con el análisis dinámico efectuado se determinan los elementos necesarios para estimar la potencialidad de licuación del depósito en cuestión. Tal estimación se hace al cuantificar la aceleración máxima del temblor que provoca el inicio de la licuación, en alguno de los estratos del depósito, al final o durante el sismo. Con esta información se puede aseverar que el fenómeno de licuación se propaga cuando ocurra un sismo de mayor intensidad o duración o ambos.

3.1 *Características del Depósito Considerado*

3.1.1 Estratigrafía

Los depósitos de suelos granulares de la costa del Pacífico de la República Mexicana pueden ser caracterizados como: depósitos de suelos granulares finos de estructura suelta como arenas finas y limos. Además, tienen una alta compresibilidad y susceptibilidad a grandes cambios volumétricos ante solicitaciones cíclicas.

Los depósitos de arena, que en general son de varios metros de espesor, provienen de transportación-sedimentación eólica, marina y fluvial. Su granulometría es relativamente uniforme, aunque los depósitos pueden ser heterogéneos según haya sido la historia de su formación.

La fig 1 representa un perfil estratigráfico de las características señaladas arriba.

En términos generales el depósito consiste de: un relleno de 1.5 m de espesor, formado por boleos, gravas, arenas y limos. Subyacente al relleno se encuentra un estrato de arcilla de 1.0 m de espesor; sigue, al estrato de arcilla, un estrato de arena fina con un espesor de 7.0 m. En seguida se presenta un estrato de gravas arenosas de 2.0 m de espesor. Le sigue un estrato de arena fina limosa de 10.0 m de espesor. Por último se tiene una capa de arenas y gravas mezcladas de 3.5 m de espesor.

El nivel de aguas freáticas (NAF) se localiza a 1.0m de profundidad.

3.1.2 Propiedades mecánicas de los estratos

Para utilizar el modelo numérico seleccionado es necesario definir las propiedades mecánicas de los estratos que forman al depósito. Con base en la estratigrafía mostrada en la fig 1, la idealización seleccionada del depósito se muestra en la fig 2. En tal figura se puede observar que el relleno de 1.5 m y el estrato de arcilla se sustituyen por una sobrecarga de 3.25 t/m^2 y el efecto del estrato de arcilla se considera además como una frontera impermeable. El depósito se subdividió en once estratos. La ecuación constitutiva para cada estrato queda definida mediante las curvas esqueleto inicial y subsecuentes. La curva esqueleto inicial queda definida mediante los parámetros σ_{mo} y τ_{mo}, y se obtuvieron de acuerdo con el criterio dado por la ref 23. Las curvas esqueleto subsecuentes quedan definidas mediante σ_{mt} y τ_{mt} que, a su vez, quedan definidas mediante las constantes H_1, H_2, H_3 y H_4; y se obtienen de acuerdo con el criterio especificado en la ref 30.

La generación de presión de poro, Δu, queda definida mediante la cuantificación de la deformación volumétrica producida por la compactación, $\Delta\varepsilon_{vd}$, y el módulo de recuperación elástica, E_r. La deformación volumétrica se determina mediante los parámetros C_1, C_2, C_3 y C_4, y se seleccionan de acuerdo con la ref 30. El módulo de recuperación elástica queda definido mediante los parámetros K_2, m y n. Para tomar en cuenta la disipación de la presión de poro es necesario conocer los valores de la permeabilidad, k.

Además del amortiguamiento histerético, implícito en la formulación del modelo numérico, se consideró un amortiguamiento del tipo viscoso del dos porciento mediante los parámetros α y β que definen el criterio de Rayleigh.

Los valores de los parámetros que se utilizaron en el análisis del depósito se muestran en la fig 2.

3.2 *Respuesta del Depósito con Frontera Superior Impermeable*

Al efectuar el análisis dinámico del depósito se encontró que el acelerograma del sismo que provoca el inicio de la licuación es el que se muestra en la fig 3, con aceleración máxima de 0.104 g (1.01 m/s^2) donde g es la aceleración de la gravedad. El

acelerograma calculado en la superficie se muestra en la fig 4 .

En este caso el estrato licuado es el superficial, identificado con el número uno. Tal conclusión se puede obtener al observar en la fig 5, la variación de la relación de presión de poro u/σ_{ov} (incremento de presión de poro, u , y presión vertical efectiva inicial, σ_{ov}). Este fenómeno también se refleja en el incremento excesivo de la deformación, como se puede observar en las figs 7 y 9 .

Para tener una idea objetiva de la zona afectada por la licuación, en la fig 26 se muestra la variación de la presión de poro generada en el instante en que se inicia la licuación. En tal figura se observa que el daño se localiza únicamente en la parte superior del depósito. A fin de efectuar comparaciones posteriores, en las figs 6, 8 y 10 se presenta la información correspondiente al estrato nueve.

3.3 *Respuesta del Depósito con Frontera Superior Permeable*

Ante la posibilidad de transformar la frontera impermeable en permeable, mediante remoción o drenaje, es necesario cuantificar el efecto de tal solución en función de la potencialidad de licuación del depósito.

Al calcular la respuesta del depósito con frontera permeable ante el sismo que provoca la licuación del depósito con frontera impermeable, se concluye que no se presenta el fenómeno de licuación como puede observarse en las figs 11, 17 y 26.

El acelerograma del sismo que provoca el inicio de la licuación del depósito en cuestión se muestra en la fig 18, con aceleración máxima de 0.198 g (1.94 m/s^2) y el correspondiente acelerograma calculado en la superficie se indica en la fig 19 .

La licuación del depósito se inicia en el estrato nueve, a los 6.02 segundos, como puede observarse en las figs 21, 23, 25 y 26. El incremento de la presión de poro en el estrato superficial es prácticamente despreciable como se muestra en las figs 20, 22, 24 y 26 .

3.4 *Análisis de la Potencialidad de Licuación del Depósito*

Debido al número de factores que gobiernan al fenómeno de licuación (ref 31) es conveniente aclarar que las conclusiones son aplicables únicamente al ejemplo utilizado y no es recomendable su extrapolación a otras condiciones que difieren de las consideradas.

En el depósito con frontera superior impermeable la licuación se inicia en el estrato superior, lo que provoca que su influencia se propague al segundo y tercer estrato (fig 26). El efecto de la reducción de la presión efectiva en el material del estrato superficial ocasiona que el módulo de rigidez al cortante se reduzca sensiblemente, pero sin ocasionar lazos de histéresis significativos (fig 9); lo cual no sucede a partir del tercer estrato (fig 10). La respuesta de aceleraciones en la superficie se amplifica continuamente durante el sismo (ver figs 3 y 4).

Si se considera que el depósito se encuentra a una distancia epicentral de 30 km, la magnitud del sismo que ocasionaría la licuación es: M = 5.6 (ref 32) .

Al considerar el caso de que sea permeable la frontera superior del depósito, la respuesta ante el sismo de magnitud 5.6 cambia radicalmente y no existen indicios de licuación, según se observa en las figs 12, 14, 16 y 26. El material del estrato No. 1 no sufre ablandamiento y prácticamente su comportamiento es lineal (ver fig 16). La respuesta de aceleración en la superficie es prácticamente la misma que se obtiene en el caso de frontera superior impermeable.

De acuerdo con el acelerograma que ocasione la licuación del depósito con frontera permeable, la magnitud del sismo correspondiente sería igual a: M = 6.6 (ref 32). La licuación se inicia en el estrato 9, a una profundidad de 15.25 m (ver fig 21) y por esta razón su influencia se refleja en la mayoría de los estratos, según se observa en la fig 26. La respuesta de aceleraciones en la superficie se amplifica durante el tiempo en que se alcanza una relación de presión de poro (u/σ_{ov}) del orden del 85 porciento, y a partir de ese instante existe una reducción notable (ver figs 19 y 21). El comportamiento del material en la zona licuada es altamente no lineal (ver fig 25). Los dos estratos superiores prácticamente no son influenciados por el fenómeno de licuación.

4. CONCLUSIONES Y RECOMENDACIONES

4.1 *Conclusiones*

Las conclusiones generales que se pueden derivar de este trabajo son:

a. Se ha demostrado la eficacia de los métodos numéricos para cuantificar la potencialidad de licuación de un depósito cuando las ecuaciones de movimiento se establecen en función de los esfuerzos efectivos.

b. La redistribución y disipación de la presión de poro generada tiene una gran influencia en la estabilidad del depósito.

4.2 *Recomendaciones*

El comportamiento dinámico de los suelos granulares constituye, dentro de la dinámica de suelos, uno de los problemas que actualmente está lejos de ser comprendido totalmente y es mucho lo que falta por dilucidar en torno a ello y, por tanto, constituye un campo fértil de investigación. En esta línea se pueden hacer las siguientes recomendaciones:

a. Continuar con el desarrollo teórico de las ecuaciones constitutivas que reproduzcan con mayor aproximación el comportamiento de medios de dos fases.

b. Es necesario desarrollar técnicas experimentales en el laboratorio para la determinación de los parámetros que intervienen en modelos numéricos bidimensionales, así como la calibración de tales modelos para cargas diferentes a las cíclicas de amplitud constante.

c. Se necesita la comprobación de los resultados obtenidos con modelos numéricos, con los obtenidos en mediciones de campo en modelos a escala natural debidamente instrumentados.

5. RECONOCIMIENTO

Los autores agradecen al Centro de Estadística y Cálculo del Colegio de Posgraduados de Chapingo, por su valiosa colaboración en el procesamiento de los programas de computadora y en especial al grupo de graficación. Asimismo agradecen al profesor W.A. Liam Finn, de la Universidad de British Columbia, Vancouver, las facilidades brindadas.

6. REFERENCIAS

1. Marsal, R.J., 1961
"*Behavior of a Sandy Uniform Soil During the Jalitpan Earthquake, Mexico*", Proc. 5th Internal Conf. on Soil Mech. and Foundation Eng., Vol 1

2. Seed, H.B., 1969
"*The Influence of Local Soil Conditions on Earthquake Damage*", Soil Dynamics Speciality Conference, 7th Internal. Conf. on Soil Mech. and Foundation Eng., Mexico

3. Seed, H.B. and Lee, K.L., 1966
"*Liquefaction of Saturated Sands During Cyclic Loading*", J. Soil Mech. Found. Div., Proc. ASCE, Vol 92, No. SM6

4. Seed, H.B. and Idriss, I.M., 1967
"*An Analysis of the Soil Liquefaction in the Niigata Earthquake*", J. Soil Mech. Found. Div., Proc. ASCE, Vol 93, No. SM3

5. Schnabel, P.B., Lysmer, J., and Seed, H.B., 1972
"*SHAKE: A Computer Program for Earthquake Response Analysis of Horizontally Layered Sites*", Report No. EERC 72-12, Earthquake Engineering Research Center, University of California, Berkeley, Calif.

6. Seed, H.B., Martin, P.P., and Lysmer, J., 1975
"*The Generation and Dissipation of Pore Water Pressures During Soil Liquefaction*", Report EERC 75-26, Earthquake Engineering Research Center, University of California, Berkeley, Cal.

7. Martin, P.P., 1975
"*Non-Linear Methods for Dynamic Analysis of Ground Response*", PhD. Thesis, University of California, Berkeley, Calif.

8. Booker, J.R., Rahman, M.S., and Seed, H.B., 1976
"*GADFLEA: A Computer Program for the Analysis of Pore Pressure Generation and Dissipation During Cyclic or Earthquake Loading*", Report No. EERC 76-24, Earthquake Engineering Research Center, University of California, Berkeley, Cal.

9. Martin, G.R., Finn, W.D., and Seed, H.B., 1975
"*Fundamentals of Liquefaction Under Cyclic Loading*", J. Geotech. Eng. Div., Proc. ASCE, Vol 101, No. GT5

10. Lee, K.L. and Albaisa, A., 1974
"*Earthquake Induced Settlements in Saturated Sand*", J. Geotech. Eng. Div., Proc. ASCE, Vol 100, No. GT4

11. Wylie, E.B. and Streeter, V.L., 1976
"*Characteristics Methods for Liquefaction of Soils*", 2nd. Internal. Conf. Num. Meth. Geomech Blacksburg, Va.

12. Liou, C.P., Streeter, V.L., and Richart, F.E., 1977
"*Numerical Model for Liquefaction*", J. Geotech. Eng. Div., Proc. ASCE, Vol 103, No. GT6

13. Lee, K.W., 1975
"*Mechanical Model for the Analysis of Liquefaction of Horizontal Soil Deposits*", PhD. Thesis, The University of British Columbia, Vancouver

14. Finn, W.D.L., Byrne, P.M., and Martin, G.R., 1976
"*Seismic Response and Liquefaction of Sands*", J. Geotech. Eng. Div., Proc. ASCE, Vol 102, No. GT8

15. Finn, W.D.L., Lee, K.W., and Martin, G.R., 1977
"*An Effective Stress Model for Liquefaction*", J. Geotech. Eng. Div., Proc. ASCE, Vol 103, No. GT6

16. Zienkiewicz, O.C., Chang, C.T., and Hinton, E., 1978
"*Non-Linear Seismic Response and Liquefaction*", Int. J. Numer. Anal. Meth. Geomech., Vol 2

17. Wilson, E.L., 1978
"*Numerical Methods for Dynamic Analysis*", Chap. 6: "Numerical Methods in Offshore Engineering", Edited by O.C. Zienkiewicz, K.W. Lewis and K.G. Stagg, John Wiley

18. Ghaboussi, J. and Wilson, E.L., 1973
"*Liquefaction Analysis of Saturated Granular Soils*", Proc. VWCEF, Vol 1, Rome

19. Ghaboussi, J. and Umit Dikmen, S., 1978
"*Liquefaction Analysis of Horizontally Layered Sands*", J. Geotech. Eng. Div., Proc. ASCE, Vol 104, No. GT3

20. Ishihara, K., Yatsuoka, F., and Yasuda, S., 1975
"*Undrained Deformation and Liquefaction and Sand Cyclic Stress*", Soils and Foundations, Vol 15, No. 1

21. Ishihara, K., Lysmer, J., Yasuda, S., and Hirao, H., 1976
"*Prediction of Liquefaction in Sand Deposits During Earthquakes*", Soils and Foundations, Vol 16, No. 1

22. Seed, H.B. and Idriss, I.M., 1970
"*Soil Moduli and Damping Factor for Dynamic Response Analysis*", Report No. EERC 70-10,

Earthquake Eng. Research Center, University of California, Berkeley, Calif.

23. Hardin, B.O. and Drnevich, V.P., 1972
"*Shear Modulus and Damping in Soils: Design Equations and Curves*", J. Soil Mech. Found Div., Proc. ASCE, Vol 98, No. SM7

24. Biot, M.A., 1961.
"*Mechanics of Deformations and Acoustic Propagation in Porous Media*", J. Appl. Phycs., Vol 33, No. 4

25. Ghaboussi, J. and Wilson, E.L., 1972
"*Variational Formulation of Dynamics of Fluid-Saturated Porous Elastic Solids*", J. Eng. Mech. Div., Proc. ASCE, Vol 98, No. EM4

26. Pyke, R., 1979
"*Nonlinear Soil Models for Irregular Cyclic Loading*", J. Geotech. Eng. Div., Proc. ASCE, Vol 105, No. GT6

27. Seed, H.B., Idriss, I.M., Makdesi, F., and Banerjee, N., 1975
"*Representation of Irregular Stress Time Histories by Equivalent Uniform Stress Series in Liquefaction Analysis*", Report No. EERC 75-29, Earthquake Eng. Research Center, University of California, Berkeley, Cal.

28. Mondkar, D.P., and Powell, G.H., 1975
"*Static and Dynamic Analysis of Nonlinear Structures*", Report No. EERC 75-10, Earthquake Engineering Research Center, University of California, Berkeley, Cal.

29. Lee, K.K.W. and Finn, W.D.L., 1978
"*DESRA-1: Program for the Dynamic Effective Stress Response Analysis of Soil Deposits Including Liquefaction Evaluation*", Department of Civil Engineering, Soil Mechanics Series No. 36, The University of British Columbia, Vancouver, Canada

30. Bhatia, S., 1979
"*Determination of Constants for DESRA-1 and DESRA-2 from Laboratory Data*", University of British Columbia

31. Seed, H.B., 1979
"*Soil Liquefaction and Cyclic Mobility Evaluation for Level Ground During Earthquakes*", J. Geotech. Eng. Div., Proc. ASCE; Vol 105, No. GT2

32. Schnabel, P.B. and Seed, H.B., 1972
"*Accelerations in Rock for Earthquakes in the Western United States*", Report No. EERC 72-2, Earthquake Engineering Research Center, University of California, Berkeley, Cal.

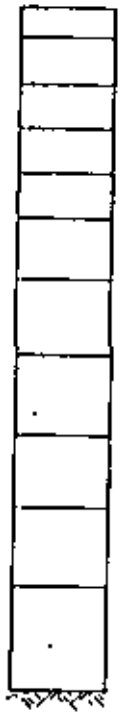

ESTRATOS	d_i (m)	Zi (m)	G_{mo} (kg/cm²)	τ_{mo}	k (cm/s)
1	1.0	0.5	415	0.285	0.065
2	1.5	1.75	464	0.318	0.065
3	1.5	3.25	498	0.341	0.065
4	1.5	4.75	985	0.676	0.065
5	1.5	6.25	1225	0.859	0.065
6	2.0	8.0	1323	0.907	0.050
7	2.5	10.25	1409	0.968	0.065
8	2.5	12.75	1584	1.072	0.065
9	2.5	15.25	1694	1.162	0.065
10	2.5	17.75	1794	1.230	0.065
11	3.5	20.75	1903	1.305	0.150

a) Constantes para G_{mo} y τ_{mo}

$K_1 = 0.734$

$K_2 = 0.426$

$K_3 = 0.550$

$K_4 = 0.300$

b) Constantes para $\Delta\varepsilon_{vd}$

$C_1 = 0.734$

$C_2 = 0.7900$

$C_3 = 0.5625$

$C_4 = 0.7500$

c) Constantes para E_r

$k_2 = 0.0025$

$n = 0.43$

$a = 0.62$

d) Constantes para amortiguamiento viscoso

$\alpha = 0$

$\beta = 0.005$

Fig. 2 PROPIEDADES DE LOS ESTRATOS DEL DEPOSITO

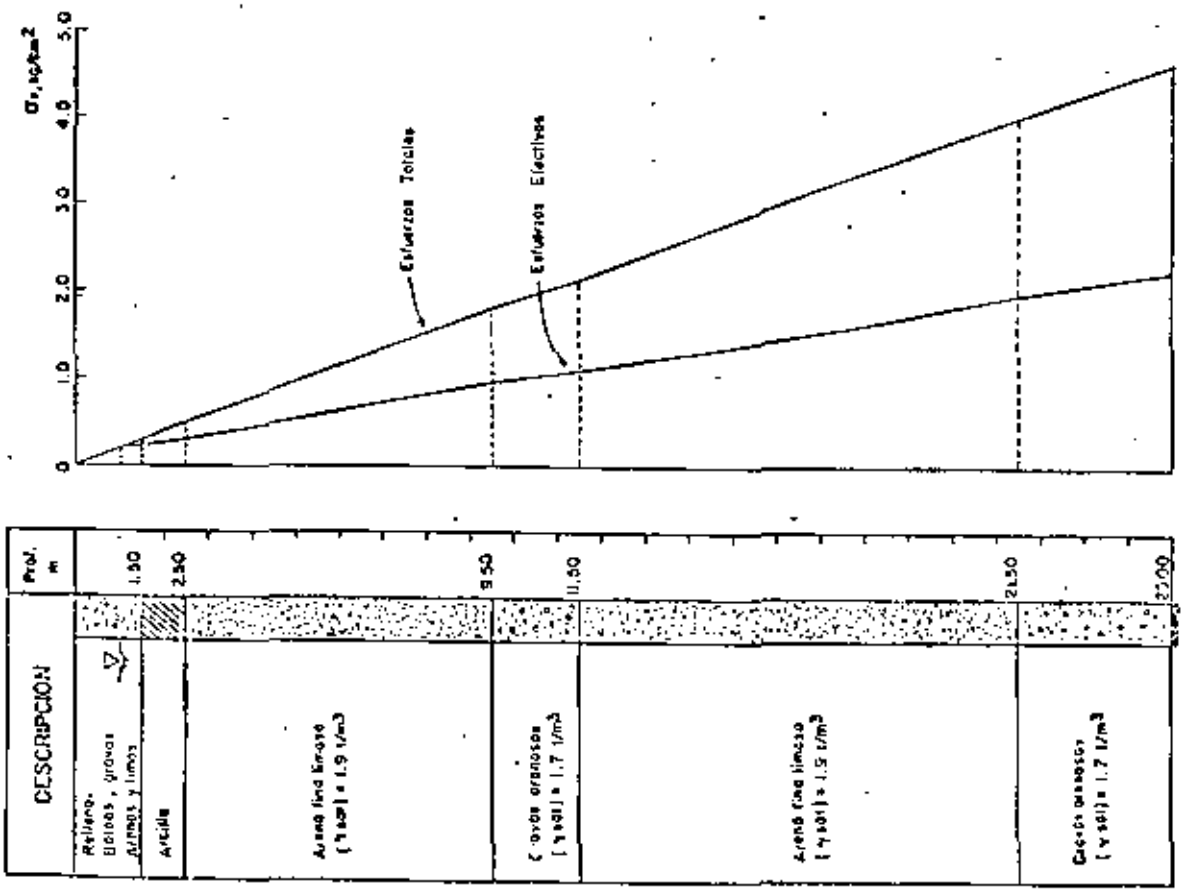

Fig. 1 ESTRATIGRAFIA DEL DEPOSITO

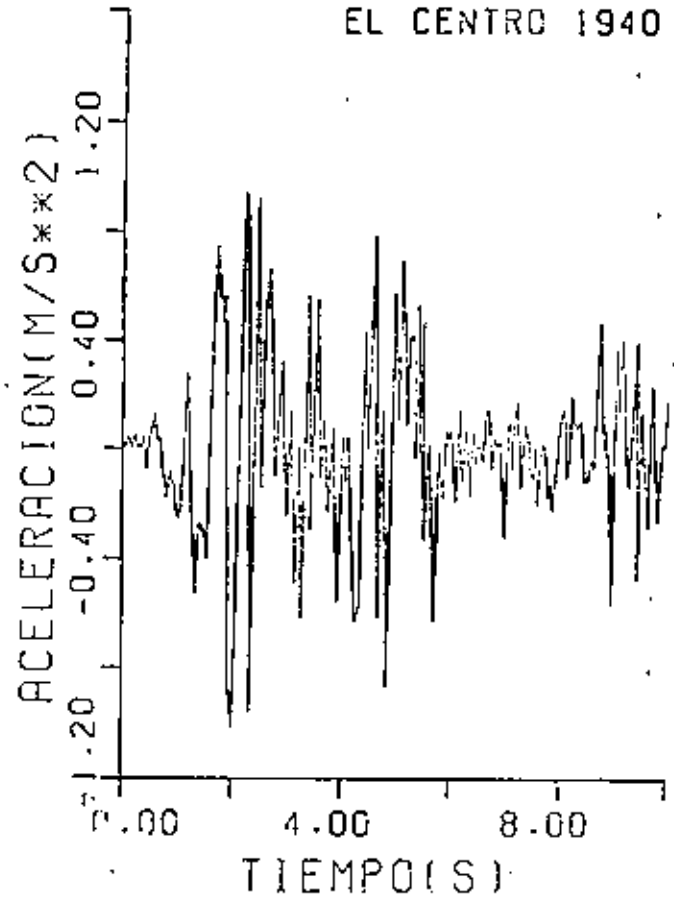

Fig. 3 DEPOSITO LICUADO CON FRONTERA SUPERIOR IMPERMEABLE. ACELEROGRAMA DEL SISMO (a_{gmax}=0.104g)

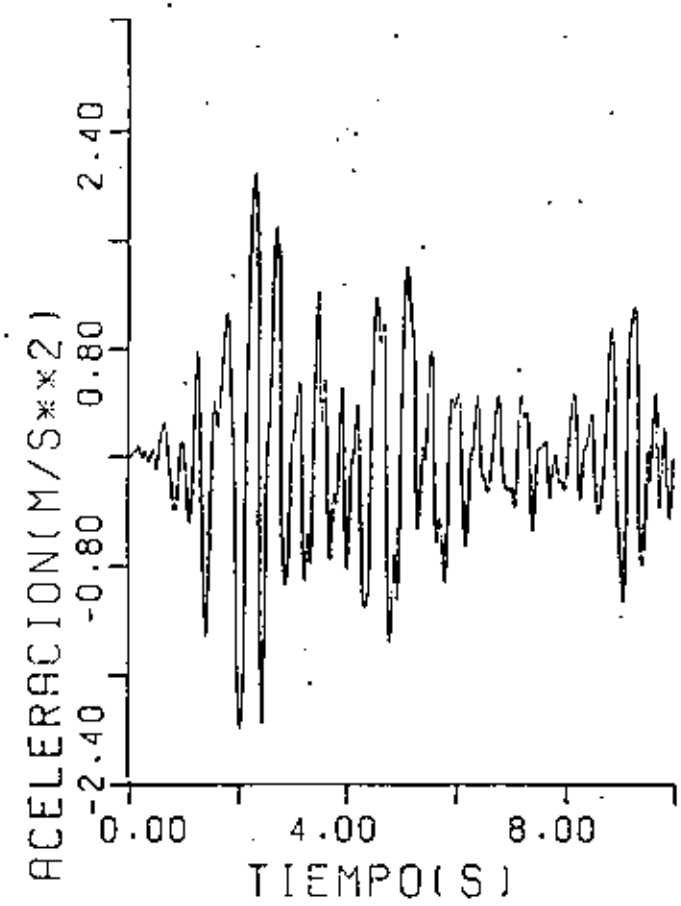

Fig. 4 DEPOSITO LICUADO CON FRONTERA SUPERIOR IMPERMEABLE. ACELEROGRAMA CALCULADO EN LA SUPERFICIE

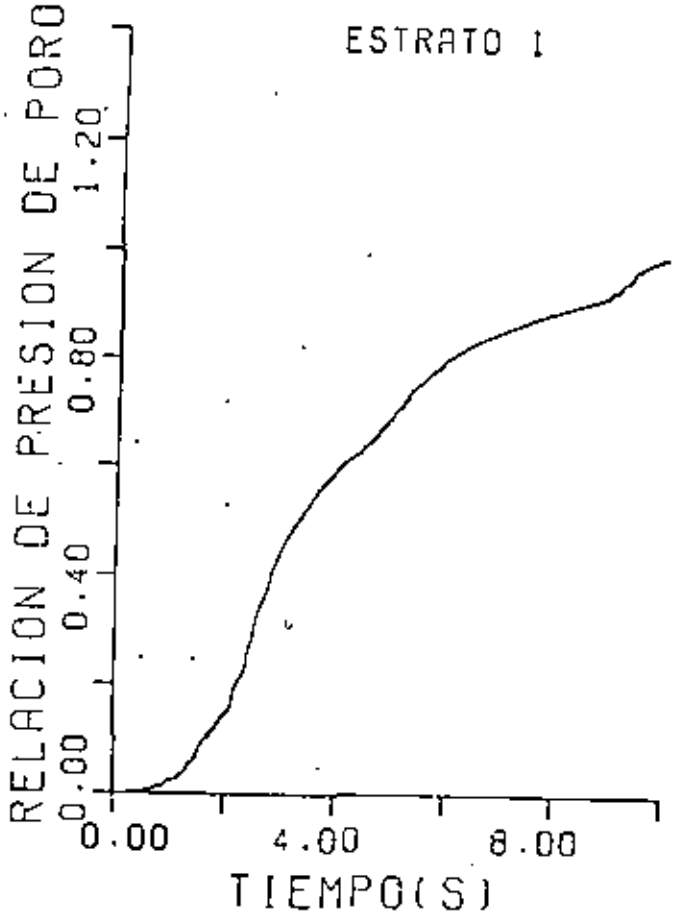

Fig. 5 DEPOSITO LICUADO CON FRONTERA SUPERIOR IMPERMEABLE. HISTORIA DE LA GENERACION DE PRESION DE PORO A LA PROFUNDIDAD DE 0.5 m

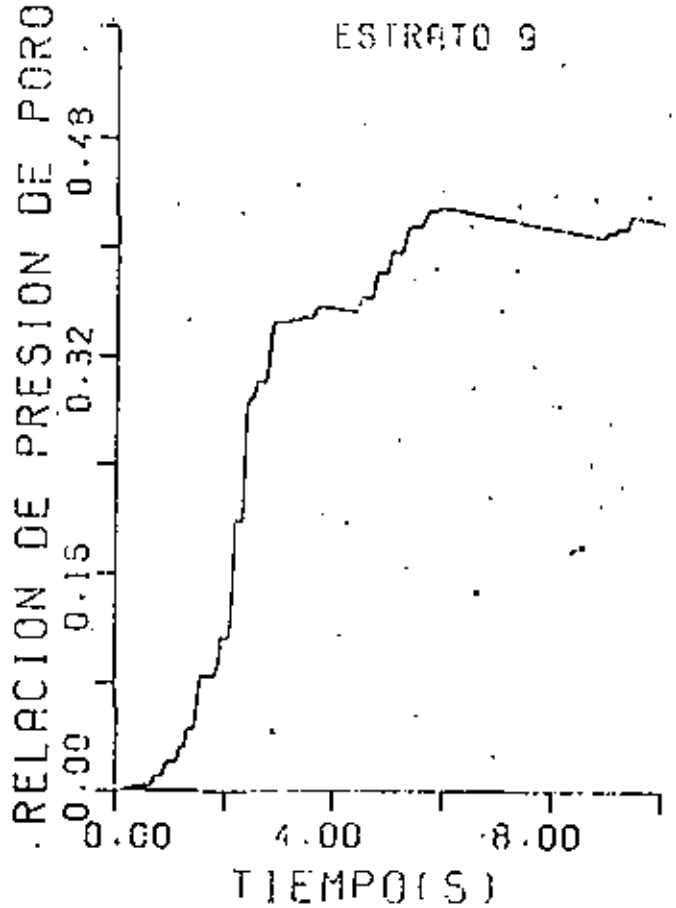

Fig. 6 DEPOSITO LICUADO CON FRONTERA SUPERIOR IMPERMEABLE. HISTORIA DE LA GENERACION DE PRESION DE PORO A LA PROFUNDIDAD DE 15.25 m

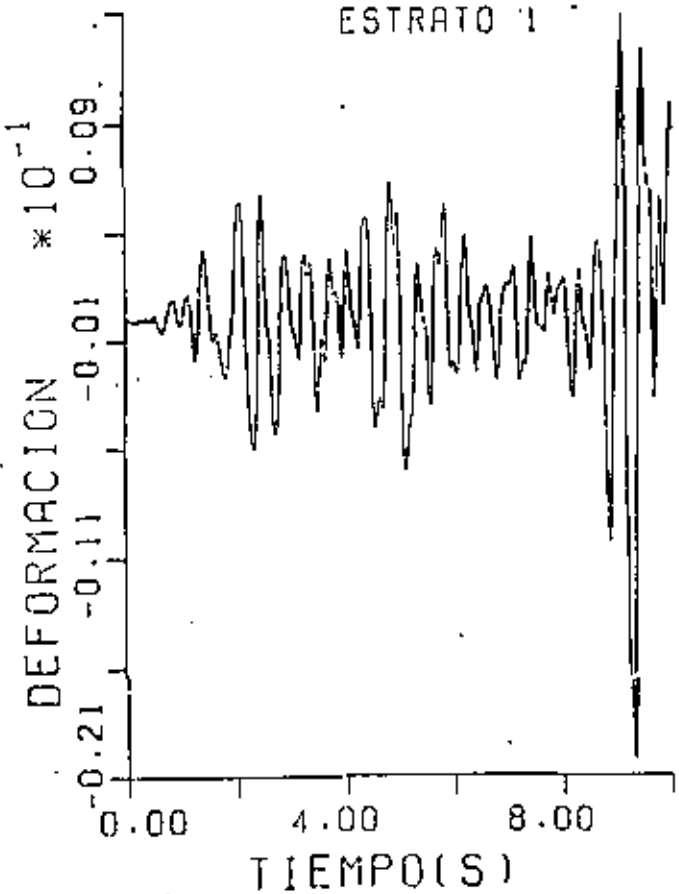

Fig. 7 DEPOSITO LICUADO CON FRONTERA SUPERIOR IMPERMEABLE. HISTORIA DE LAS DEFORMACIONES ANGULARES A LA PROFUNDIDAD DE 0.5 m

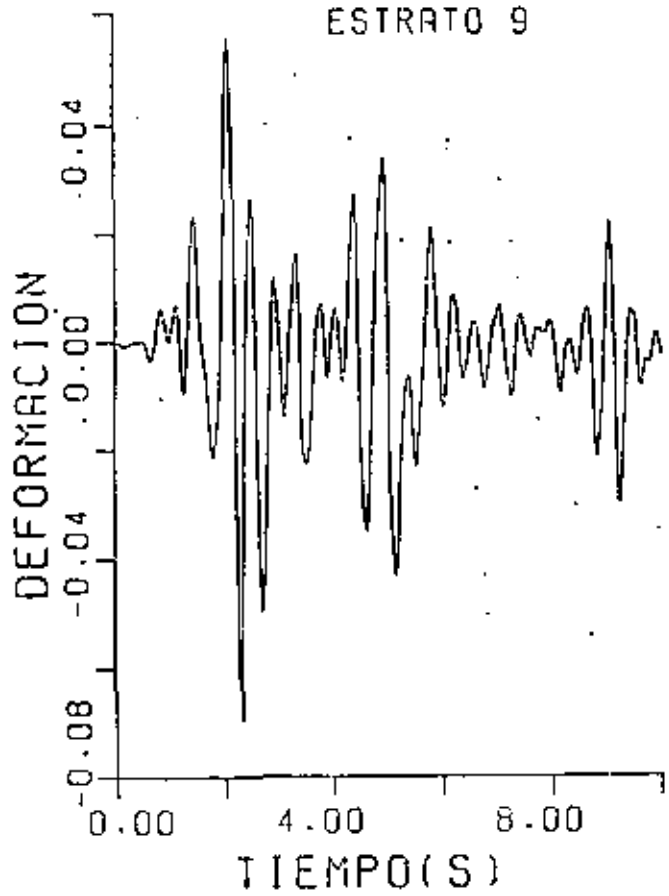

Fig. 8 DEPOSITO LICUADO CON FRONTERA SUPERIOR IMPERMEABLE. HISTORIA DE LAS DEFORMACIONES ANGULARES A LA PROFUNDIDAD DE 15.25 m.

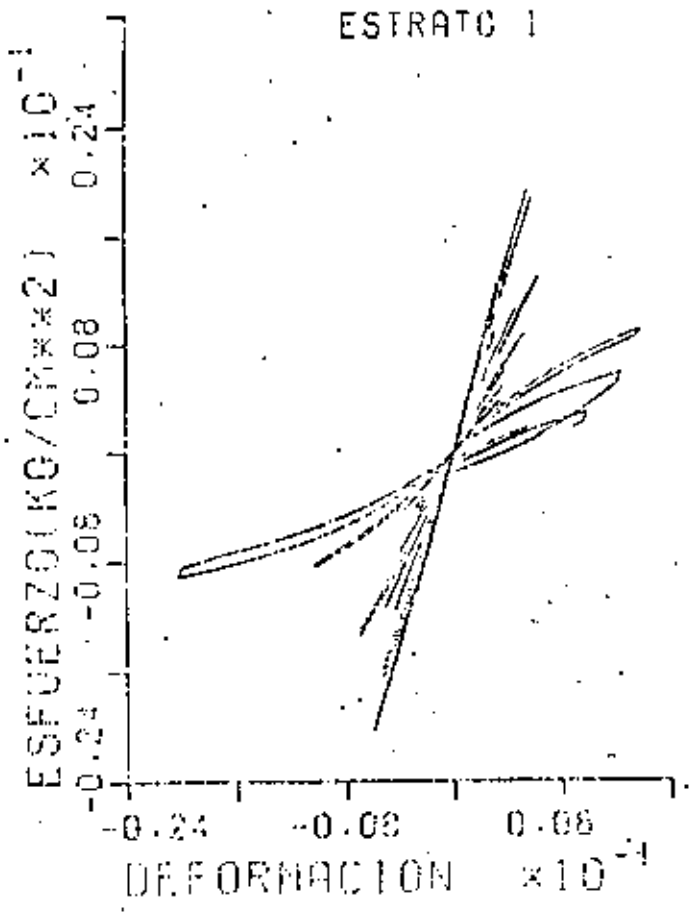

Fig. 9 DEPOSITO LICUADO CON FRONTERA SUPERIOR IMPERMEABLE. RELACION ESFUERZO DEFORMACION A LA PROFUNDIDAD DE 0.5 m.

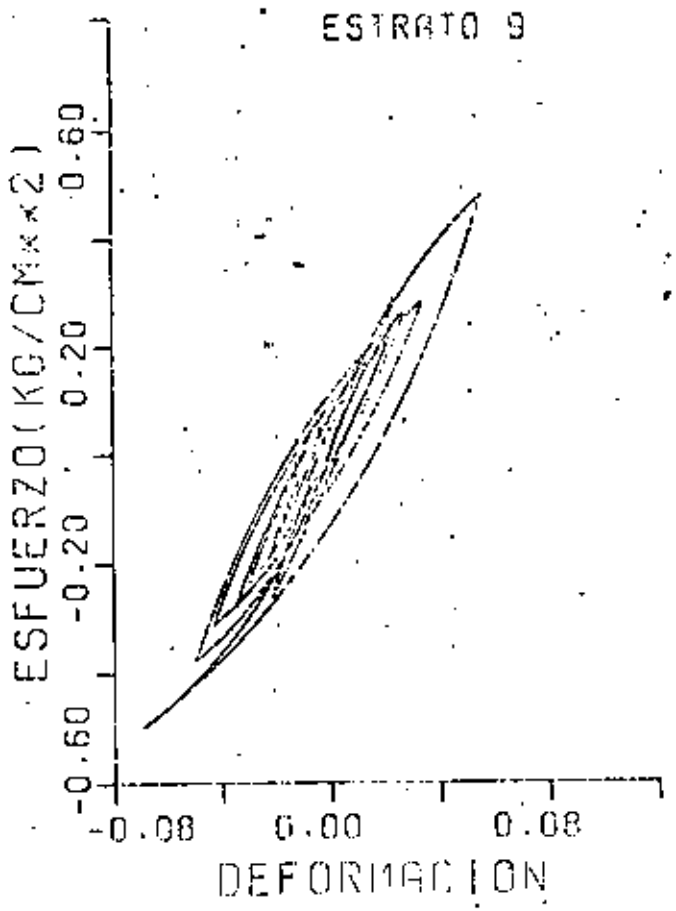

Fig.10 DEPOSITO LICUADO CON FRONTERA SUPERIOR IMPERMEABLE. RELACION ESFUERZO DEFORMACION A LA PROFUNDIDAD DE 15.25 m

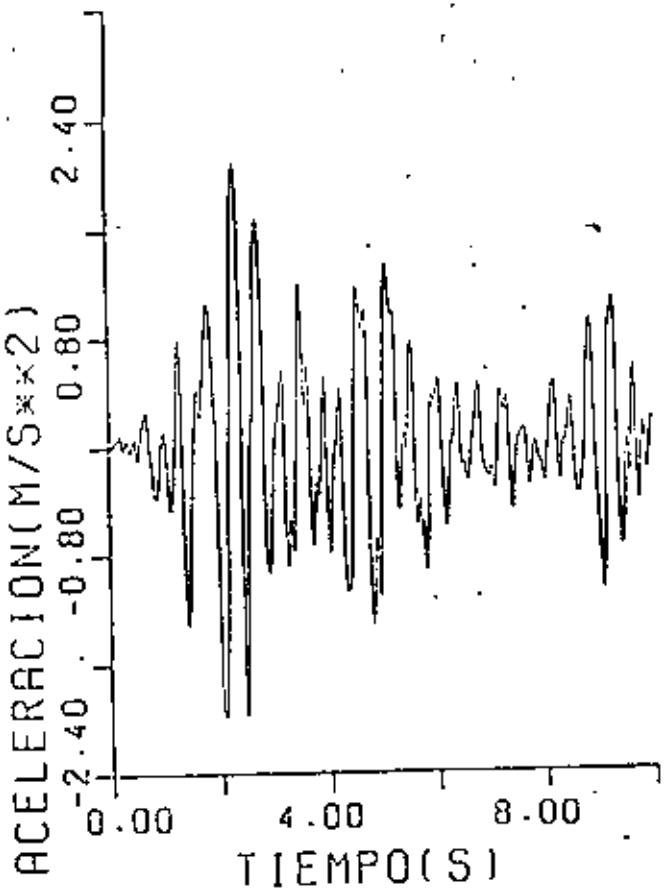

Fig. 11. DEPOSITO NO LICUADO CON FRONTERA SUPERIOR PERMEABLE. ACELEROGRAMA CALCULADO EN LA SUPERFICIE, CORRESPONDIENTE AL SISMO (QUE PROVOCA LICUACION EN EL DEPOSITO CON FRONTERA SUPERIOR IMPERMEABLE)

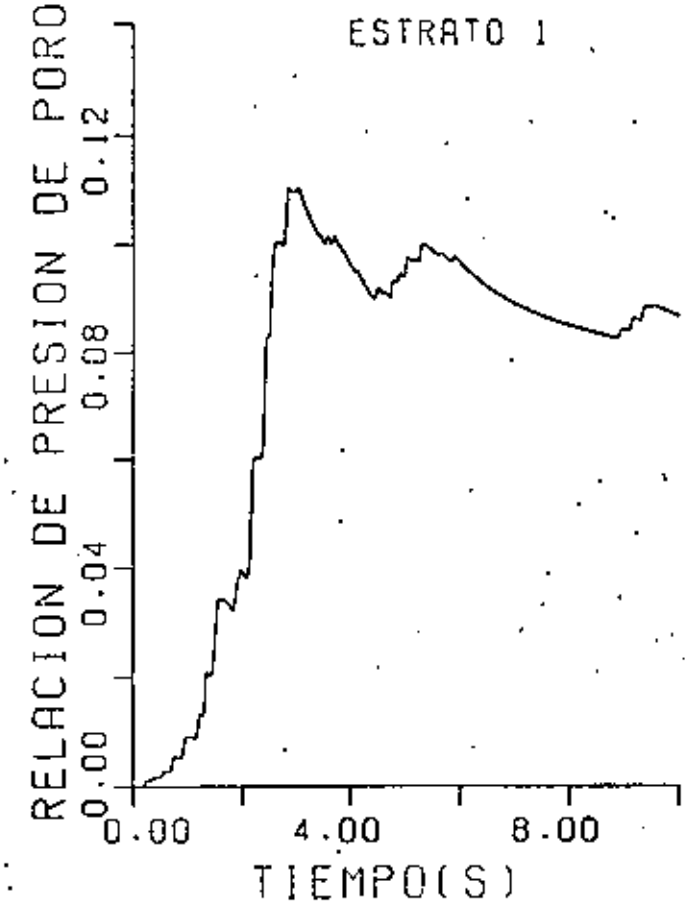

Fig. 12 DEPOSITO NO LICUADO CON FRONTERA SUPERIOR PERMEABLE. HISTORIA DE LA GENERACION DE PRESION DE PORO A LA PROFUNDIDAD DE 0.5 m

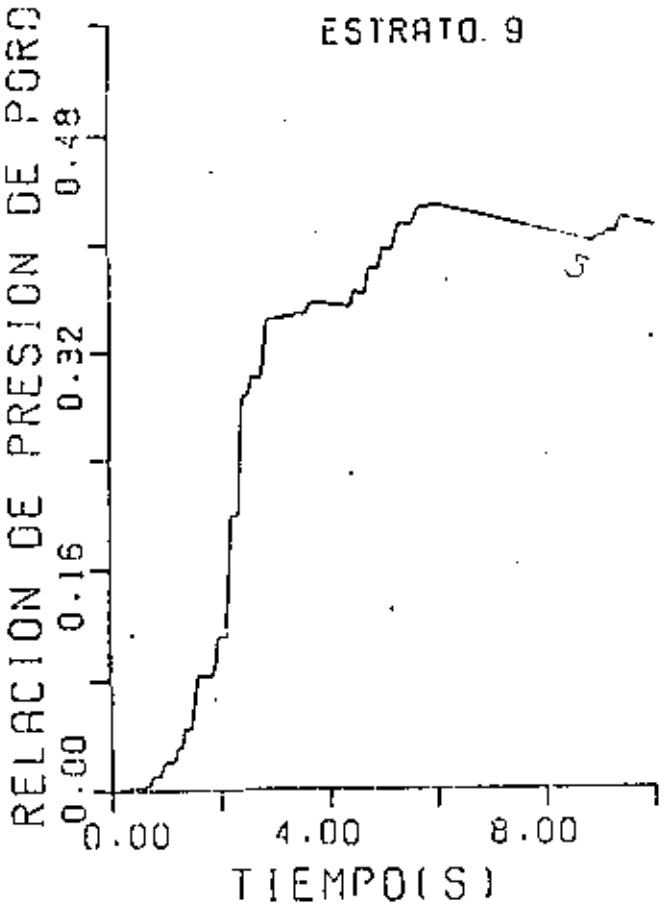

Fig. 13 DEPOSITO NO LICUADO CON FRONTERA SUPERIOR PERMEABLE. HISTORIA DE LA GENERACION DE PRESION DE PORO A LA PROFUNDIDAD DE 15.25m

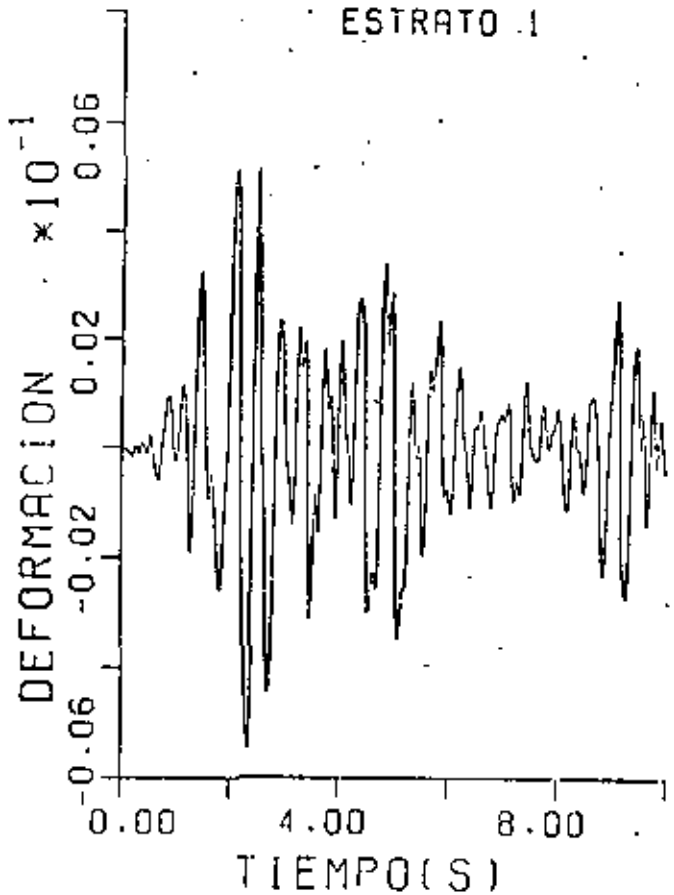

Fig.14 DEPOSITO NO LICUADO CON FRONTERA SUPERIOR PERMEABLE. HISTORIA DE LAS DEFORMACIONES ANGULARES A LA PROFUNDIDAD DE 0.5 m.

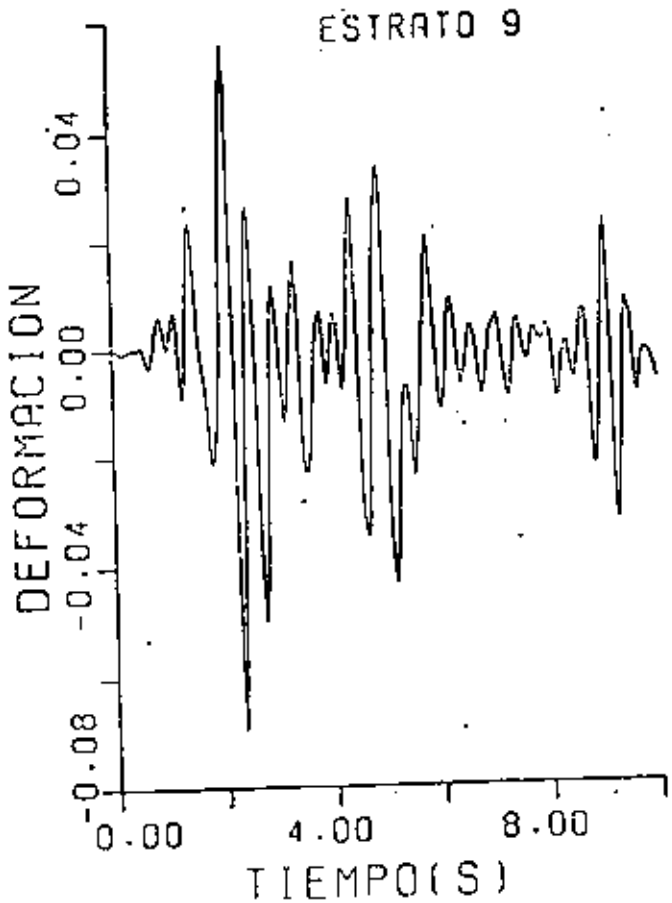

Fig. 15 DEPOSITO NO LICUADO CON FRONTERA SUPERIOR PERMEABLE. HISTORIA DE LAS DEORMACIONES ANGULARES A LA PROFUNDIDAD DE 15.25 m

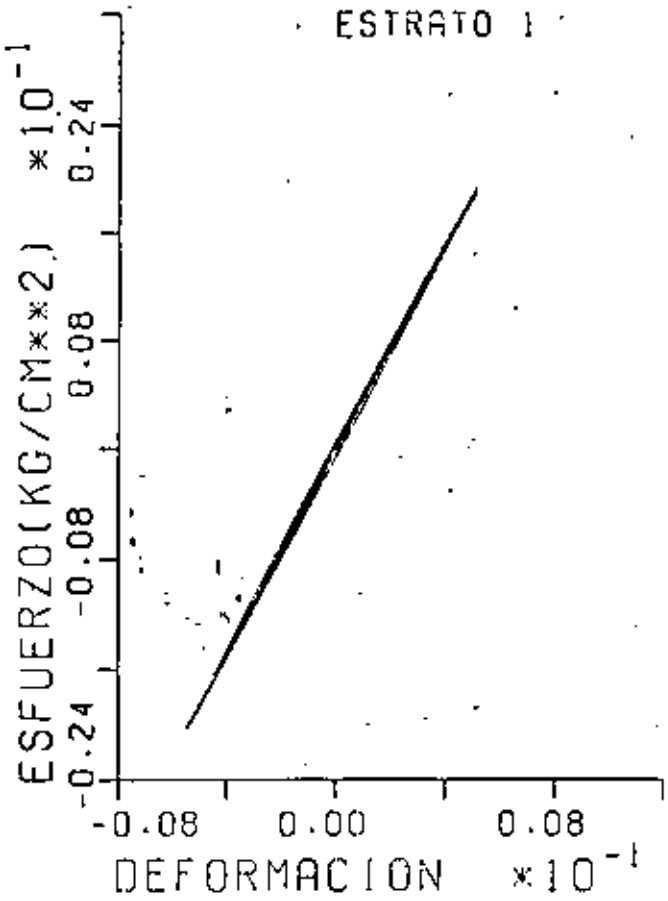

Fig. 16 DEPOSITO NO LICUADO CON FRONTERA SUPERIOR PERMEABLE. RELACION ESFUERZO DEFORMACION A LA PROFUNDIDAD DE 0.5 m

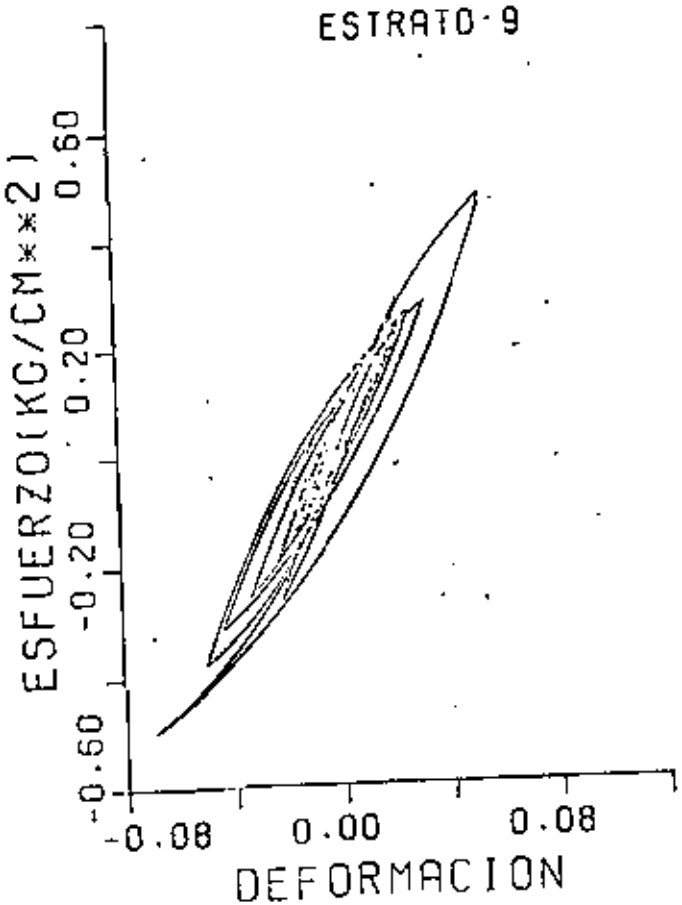

Fig.17 DEPOSITO NO LICUADO CON FRONTERA SUPERIOR PERMEABLE. RELACION ESFUERZO-DEFORMACION A LA PROFUNDIDAD DE 15.25 m

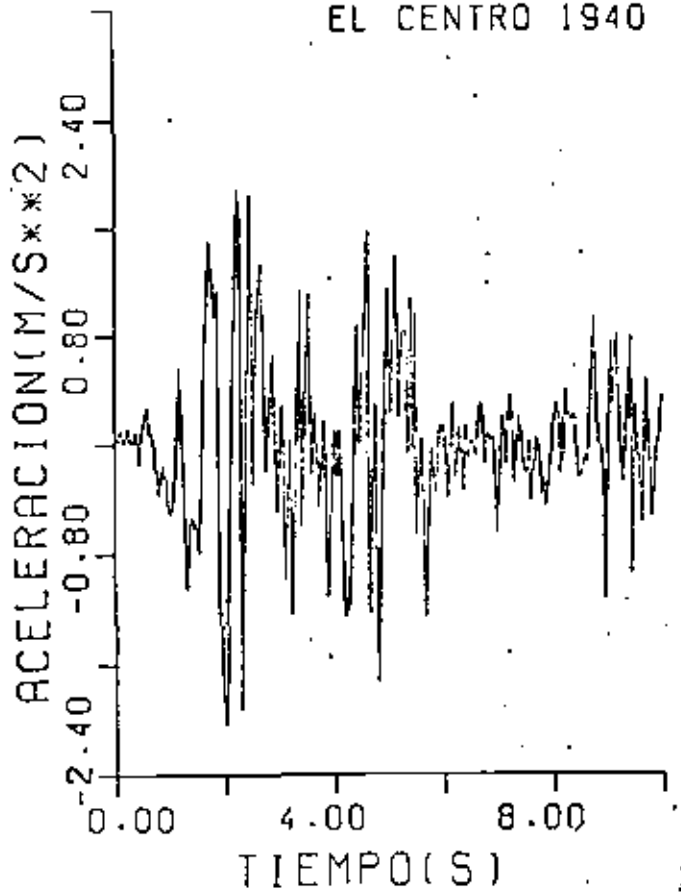

Fig.18 DEPOSITO LICUADO CON FRONTERA SUPERIOR PERMEABLE. ACELERO - GRAMA DEL SISMO (Ogmax 0.198 g)

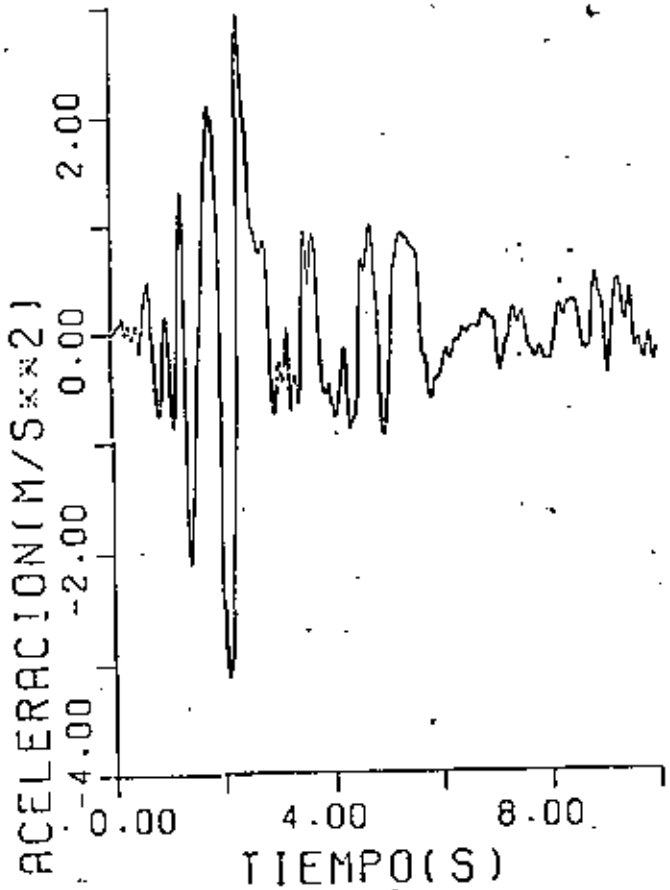

Fig.19 DEPOSITO LICUADO CON FRONTERA SUPERIOR PERMEABLE. ACELEROGRAMA CALCULADO EN LA SUPERFICIE

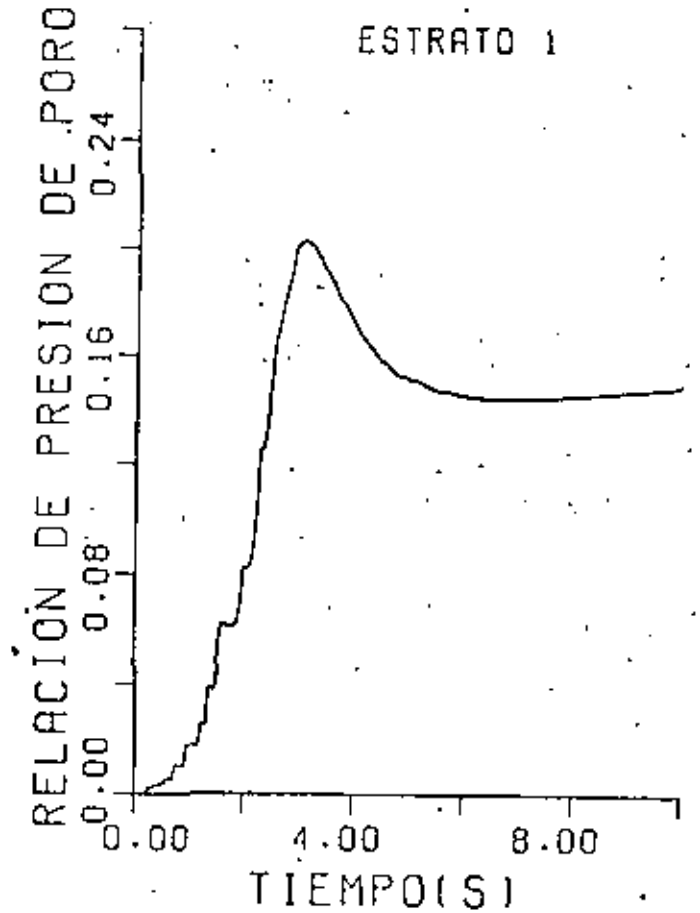

Fig. 20 DEPOSITO LICUADO CON FRONTERA SUPERIOR PERMEABLE. HISTORIA DE LA GENERACION DE PRESION DE PORO A LA PROFUNDIDAD DE 0.5 m.

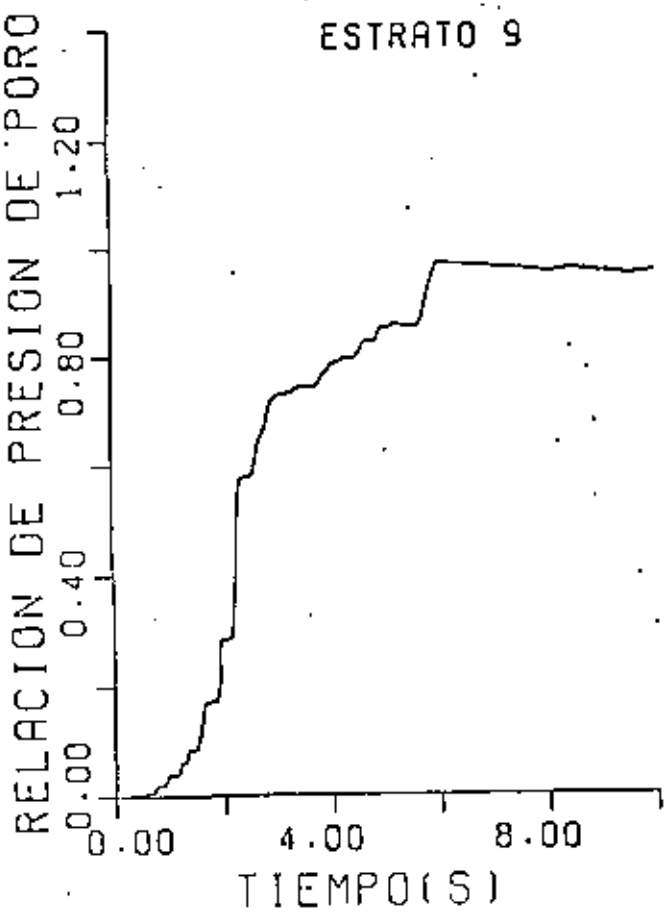

Fig. 21 DEPOSITO LICUADO CON FRONTERA SUPERIOR PERMEABLE. HISTORIA DE LA GENERACION DE PRESION DE PORO A LA PROFUNDIDAD DE 15.25 m.

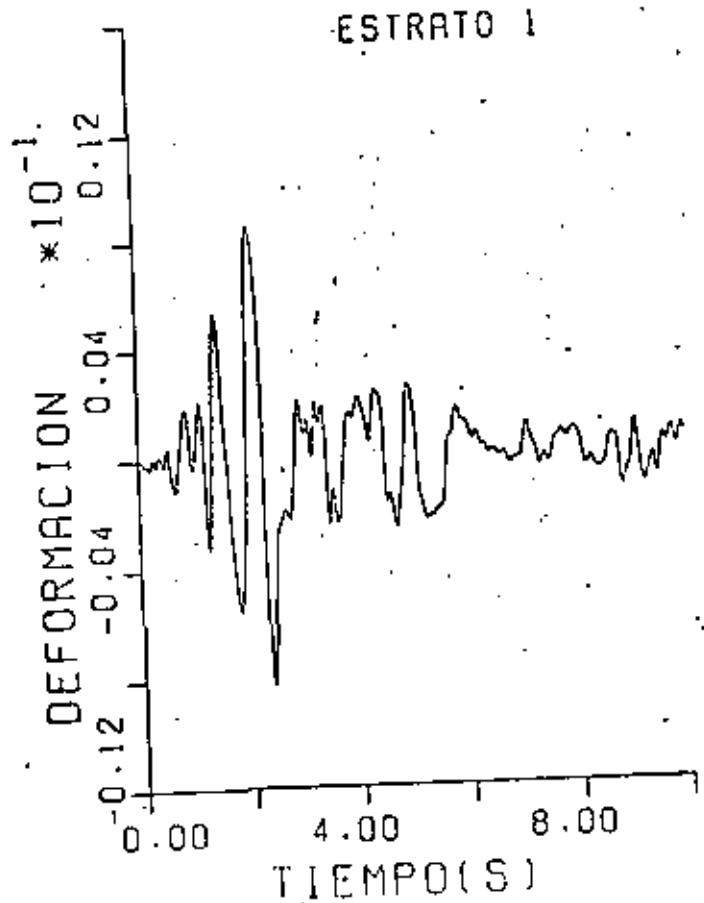

Fig. 22 DEPOSITO LICUADO CON FRONTERA SUPERIOR PERMEABLE HISTORIA DE LAS DEFORMACIONES ANGULARES - A LA PROFUNDIDAD 0.5 m.

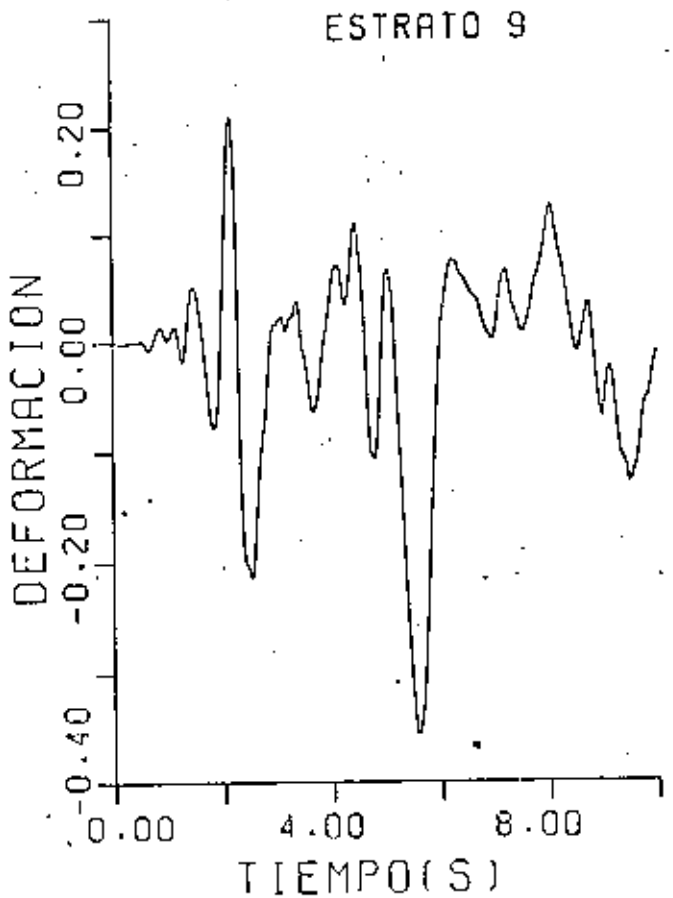

Fig. 23 DEPOSITO LICUADO CON FRONTERA SUPERIOR PERMEABLE. HISTORIA DE LAS DEFORMACIONES ANGULARES - A LA PROFUNDIDAD 15.25 m.

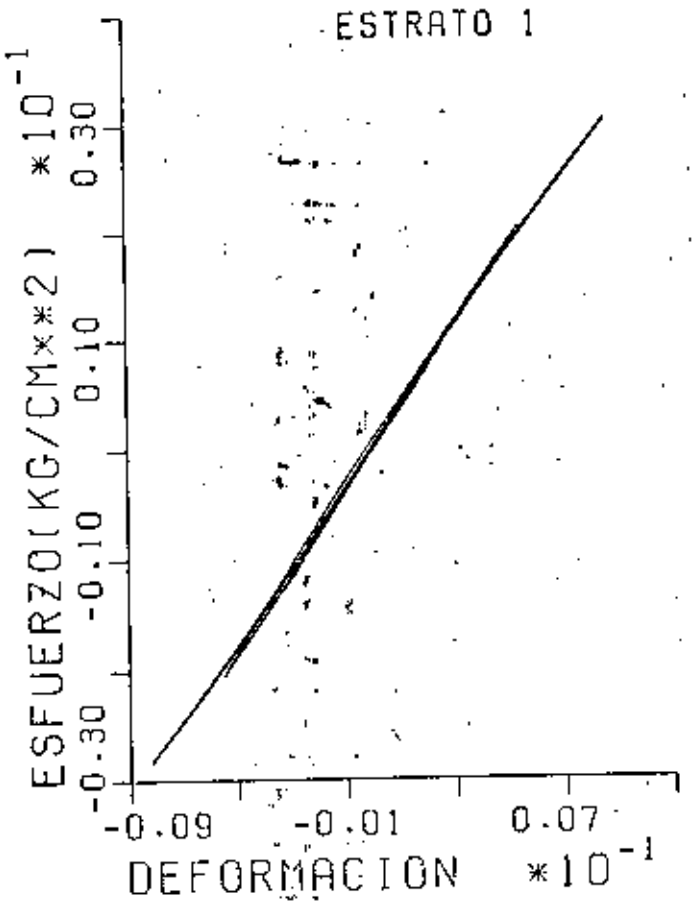

Fig.24 DEPOSITO LICUADO CON FRONTERA SUPERIOR PERMEABLE. RELACION ESFUERZO DEFORMACION A LA PROFUNDIDAD DE 0.5 m.

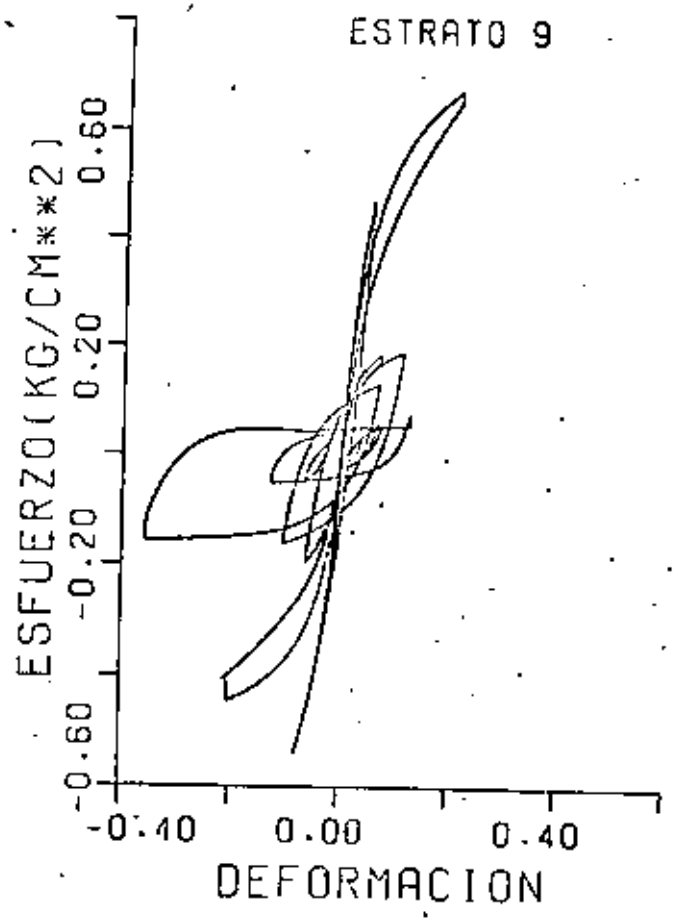

Fig.25 DEPOSITO LICUADO CON FRONTERA SUPERIOR PERMEABLE. RELACION ESFUERZO DEFORMACION A LA PROFUNDIDAD DE 15.25 m.

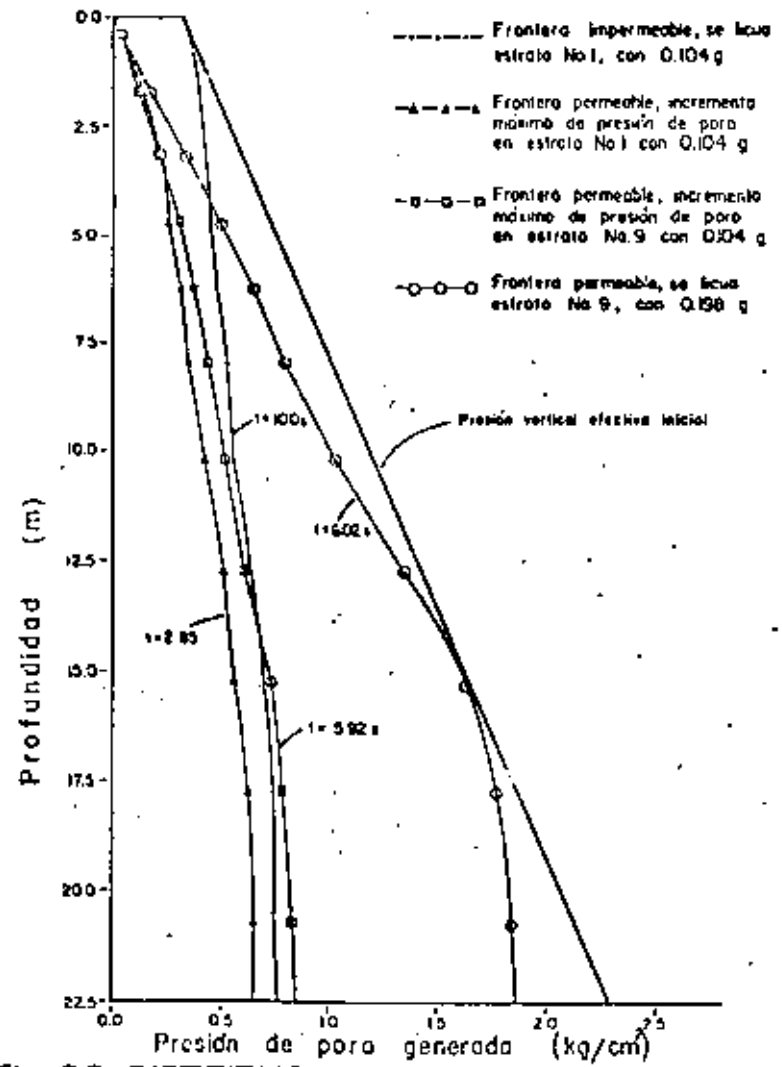

Fig. 26 DISTRIBUCION DE LA GENERACION DE PRESION DE PORO EN EL DEPOSITO PARA LAS INTENSIDADES DEL SISMO Y CONDICIONES DE FRONTERA CONSIDERADAS